MODELING CERTAIN COMPLEX PHENOMENA THAT OCCUR WITHIN RESERVOIR FLUID MOVEMENTS

by

Shabbir Mustafiz

Submitted
in partial fulfillment of the requirements
for the degree of

DOCTOR OF PHILOSOPHY

Major Subject: Civil Engineering
at

DALHOUSIE UNIVERSITY

Halifax, Nova Scotia December, 2006

Your file Votre référence
ISBN: 978-0-494-27649-5
Our file Notre référence
ISBN: 978-0-494-27649-5

DALHOUSIE UNIVERSITY

To comply with the Canadian Privacy Act the National Library of Canada has requested that the following pages be removed from this copy of the thesis:

Preliminary Pages
- Examiners Signature Page
- Dalhousie Library Copyright Agreement

Appendices
- Copyright Releases (if applicable)

DEDICATION

"The scenes of our life resemble pictures in rough mosaic; they are ineffective from closeup, and have to be viewed from a distance if they are to seem beautiful"
(Arthur Schopenhauer: On the Vanity of Existence)

To

THE PEOPLE

Who view from a distance and find beauty in roughness of the big-picture of life

TABLE OF CONTENTS

LIST OF TABLES

LIST OF FIGURES

ACKNOWLEDGEMENTS

I would like to express my sincere gratitude and thanks to Dr. M.R. Islam for his supervision and endless guidance throughout the period of this study. His creativity, interest and inspiration contributed remarkably towards the successful completion of this dissertation. I am also grateful to Dr. L. Liu for his advice and constant encouragement in various phases of this study. I would also like to thank Dr. E. Shakshuki and Dr. S. Hussain for their keen interest and participation in the petroleum engineering research conducted at Dalhousie University. My appreciation also goes to Dr. G. Coşkuner of Husky Energy for his interest in the Adomian decomposition method, which is used to solve the nonlinear Buckley-Leverett problem.

I would like to thank Dr. S.H. Mousavizadegan for his countless hours with me in discussing topics related to nonlinearity, multiple solutions and advanced mathematics. His knowledge and intellect has enriched me and this research tremendously. Appreciation goes to Dr. F. Ma and Dr. K. Agha for their assistance in numerical modeling of non-Darcy flow and laser drilling respectively. The suggestions by Dr. M. Satish, Dr. C. Ketata and Dr. H. Belhaj have helped in preparing the state-of-the-art chapter of this dissertation. I am also grateful to G. Zatzman and R. Shapiro for sharing their insights on socio-economic issues, a nutrient in the state-of-the-art of reservoir simulation chapter. The collaboration work with Dr. A.Y. Zekri of United Arab Emirates University is profoundly acknowledged for conducting the laboratory experiments and plotting the traced front movements in the first-contact miscible displacement study. Appreciation also goes to N. Bjorndalen for the microwave experiments.

I would also like to mention the friendly environment of Dr. Islam's research team. In particular, Mehedi, Monir and David Prior have offered unparalleled support whenever needed. I gratefully acknowledge the unconditional caring of Serperi, Hassan bhai,

Bhabee, Sunnyda, Doly Boudi, Setar bhabee, Saroj and Era bhabee. Their hospitality during my graduate studies will always be freshly remembered.

I would have never pursued the doctoral degree if Baba did not ignite the passion for knowledge in me. In times of disappointment and despair of conducting this research, I have always found hope and strength listening to Ammu. My sister's insurmountable expectation has always been a source of motivation in my life. Most importantly, I would have never dreamt of finishing this dissertation unless Nancy, my wife, had given me continuous mental support. No word would suffice to measure her sacrifice and belief in me. Nancy would never let me feel we are living few thousands kilometers away.

Finally, I would like to thank the Killam Foundation for its support in the form of pre-doctoral scholarship. The research grants from the Atlantic Innovation Fund (AIF) and the faculty of graduate studies (FGS) scholarships are also gratefully acknowledged.

ABSTRACT

The most important objective of any petroleum scheme is to extract more petroleum fluids, which are the blood line to the petroleum industries. The objective would be achieved more efficiently if the industry had the luxury of launching a 'reservoir shuttle' or a 'petroleum balloon' to roam around the reservoir. Since such is not the case, it makes the task of modeling most daunting. This dissertation addresses a number of complex phenomena such as nonlinearity in reservoir problems, non-Darcy flow, multiple solutions to natural phenomena, laser drilling, microwave irradiation for improved horizontal well performance etc. through theoretical, numerical or experimental investigations.

This dissertation presents the state-of-the-art of reservoir simulation, which shows that in the Information Age, the salient features of the Science of Intangibles are important and necessary to be considered in the simulators. New, simple and explicit equations are developed for interblock geometric factors and bulk volumes that can reduce complicated logic in programming and source of confusion in reservoir simulation. The study on linearization of single-phase fluid flow problem shows that linearization during formulation can affect pressure results more than that caused by linearization during numerical evaluation. The fluid viscosity and formation volume factor are found to demonstrate weak nonlinearity in single-phase fluid flow problems. Several nonlinear problems including the Buckley-Leverett equation (with capillary) are solved by the Adomian Decomposition Method. The solution demonstrates that neither frontal shock nor multiple saturation values are the true representation of the displacement process. In another numerical study, the *engineering approach* eliminates the conventional notion of giving preference to point-distributed grid over the block-centred grid in treating constant pressure boundary problems. This dissertation also finds that theoretically multiple solutions of any natural phenomenon are possible, although, some solutions may not be readily recognizable as meaningful or even 'real'. The complexity is attributed further to non-Darcy condition in well-simulation involving constant production and non-flow boundary. It is shown that the pressure drop predicted by the Forchheimer model is higher than that predicted by the Darcy model at high-velocity and the pseudo-steady velocity is also higher for the Forchheimer model than that for the Darcy model. The numerical results provide comparable accuracy with the results provided by a recent scheme reported to be Δx^4 and Δt^4 accurate. Results of a linear displacement study show that the frontal movement is faster for Forchheimer model than Darcy model in an accumulating reservoir. The effects of depletion or accumulation of fluid in a reservoir on mixing length, displacement efficiency are also reported. Besides, a number of miscible displacement runs are conducted to obtain correlations of areal sweep efficiency as functions of mobility ratio and water-alternating-gas ratio. A comprehensive review on the prospects of laser and modeling of laser-drilling in sandstone and limestone indicate the technology to be *the wave* in future-drilling. The effects of microwave irradiation phenomenon on immiscible fluids are also studied for temperature profiles and a reasonable accuracy is found between the experimental and numerical results.

Chapter 1

1 INTRODUCTION

The terms 'modeling' and 'reservoir fluid movements' are frequently used together in petroleum engineering, sometimes in various technical terms, e.g., modeling of miscible or immiscible displacement, modeling enhanced oil recovery schemes and others, depending on the conditions, processes or schemes that take place in petroleum reservoirs. With the ubiquitous presence of computers and computer technology, the current petroleum era is enjoying some of the most advanced and sophisticated applications of technologies and science. However, the nature of technological progress is such that the more there are solutions the more challenges surface. We often hear about that the medical research doubles its knowledge in every seven years. Even the growth in computer technology that sees doubling of capacity every 12-18 months (Moore's law) cannot keep up with the growth in knowledge. This growth in knowledge cannot be accomplished without continuous research and innovation.

1.1. Objectives

1.1.1. Global Objective

Reservoir fluids are the blood line for the entire petroleum industry. Similar to the general objective of any petroleum scheme, the various features of this dissertation are also aimed to ensure extraction of more petroleum fluids either through direct or indirect contributions. In terms of simulation, it is the prediction of recovery of petroleum fluids as accurately as possible. Accuracy is the most desirable feature as it is close to reality or

the truth. However, results with better accuracy may involve lots of complexity, and often such complexity is avoided.

The complexity in reservoirs is not just a matter of geological challenges or difficulties associated with a recovery schemes, it is also a matter of limitations of underlying assumptions behind numerous theories and laws that are used to describe fluid flow in porous media. Because any petroleum reservoir is naturally occurring, its behavior is non-linear and most often characterized as chaotic. Dealing with such a process with engineering approaches, which mostly deal with idealized and linearized systems, is a formidable challenge. In addition, the fact that monitoring reservoir, let alone accessing it, is far from being an established technology makes it even a greater challenge because one cannot validate the theory with experimental data.

The complexity of a phenomenon can be counterbalanced by the advantages gained out of it. Such advantages include both tangible and intangible features, e.g.

1. less time requirement;
2. reduced cost, and
3. increased convenience (without losing any information that might be achieved as a result of complexity) etc.

In addition, features such as-

4. advancements and/or refinement in theory;
5. new and advanced mathematical techniques, and
6. innovative and state-of-the-art technologies

can have tremendous impact in petroleum engineering research. The investigation of these features remains one of the most important global goals of this dissertation.

In this dissertation, a number of complex phenomena associated with petroleum reservoir fluids are addressed through modeling, which refers to theoretical, numerical or experimental studies.

1.1.2. Specific Objectives

The primary specific objectives of this dissertation are as follows:

1. The effects of nonlinearity in reservoir problems;

2. Development of new, simple equations useful in reservoir problems;

3. Utilization of new and advanced mathematical method;

4. Modeling (numerical) of non-Darcy flow phenomenon in the reservoir;

5. Modeling (experimental) of first contact miscible water-alternating-gas displacement system;

6. Modeling (numerical) of novel drilling phenomenon;

7. Modeling (experimental and numerical) of irradiation phenomenon on immiscible fluids.

Besides secondary specific objectives, which are also relevant and important in achieving the global goals, are presented in this dissertation:

1. Description of the state-of-the-art of reservoir simulation;

2. Handling of Dirichlet boundary condition with *Engineering Approach*;

3. Investigation of possible multiple solutions in natural phenomena;

4. Use of the new mathematical method in solving nonlinear partial differential equations including the Buckley-Leverett equation with capillary effects (note that nonlinearity is an indicator of a complex process in the reservoir);

5. Preparation of diffusivity equations in accordance with the decomposition technique;

6. Comparison of pressure and velocity profiles based on Darcy and non-Darcy flow in the reservoir using an advanced numerical scheme (note that the movement of reservoir fluids may not be adequately described by Darcy's law alone);

7. Prediction of pressure profiles analytically and numerically in accumulating and depleting linear reservoirs, and

8. To study the effects of reservoir type, e.g., accumulating or depleting on the movement of tracer front, the length of tracer mixing zone and displacement efficiency.

1.2. Organization of the thesis

Chapter 1 introduces the thesis and its layout. This chapter also outlines the global and specific objectives both primary and secondary and shows how these objectives are to be met in this dissertation.

To meet the specified objectives, it is important to have a general knowledge of the state-of-the-art of reservoir simulation although each following chapter independently reviews literature on the concerned topic of that particular chapter. ***Chapter 2*** elucidates the

state-of-the-art of modeling of various fields, e.g., flow through fractures, coupled fluid flow and mechanical deformation of the medium, fluid flow under the influence of thermal stress, etc. The chapter also identifies the potential research areas.

One of the important aspects in any solution process is how suitably and easily the governing equation can be handled without the loss of any significant information and preferably without the loss of any information. The calculation of geometric factor and bulk volume are needed in reservoir simulation when the reservoir is divided in many gridblocks. ***Chapter 3*** elucidates development of more user-friendly and simple equations for the calculation of geometric factor and bulk volume that make use of the presently available equations.

A number of factors affect fluid flow in petroleum reservoir and the dependence of various factors on each other are nonlinear. However, to avoid the complexity, often linearization on the flow equation is imposed. In ***Chapter 4***, the effects of linearization in the flow equation is investigated (*Section 4.1*). It may be added here that the suggested equations in *Chapter 3* are useful in calculating the geometric factor and bulk volume in *Chapter 4*.

The most conventional practice is to use the finite difference concept when writing the flow equations of gridblocks of a petroleum reservoir. However, the same exercise can be accomplished by using the *engineering approach* (Abou-Kassem et al., 2006), which is followed in *Section 4.1* of *Chapter 4*. Since *engineering approach* is a recent addition to reservoir simulation studies, *Section 4.2* is included in *Chapter 4*. *Section 4.2* is offered to investigate the treatment of Dirichlet type boundary condition by engineering approach in compare to the current practices.

The nonlinearity involved in *Chapter 4* also raises a question if there can be more than a single solution of any nonlinear process. In ***Chapter 5***, several polynomials and

simultaneous equations of two variables as a model for a natural phenomenon is presented in search of finding the complete spectrum of solutions. This Chapter introduces the concept of inherently multiple solutions and the Knowledge dimension. Even though concrete examples of this Knowledge dimension from petroleum reservoir applications is a matter of significant future research, it is alluded that such dimension exists and one must include the prospect of multiple solutions, including those that can be best characterized as intangibles.

The content of *Chapter 4* and *Chapter 5* opens up the scope to employ advanced numerical method in treating nonlinear problems. Some recent success of utilizing the Adomian decomposition method (ADM) worked as the driving force to investigate the method on several nonlinear problems in ***Chapter 6***. The decomposition technique is implemented on equations such as the Burgers equation, which is the simplest model for one-dimensional turbulence in fluid flow or the Korteweg-de Vries (KdV) equation that describes the motion of nonlinear wave in shallow water under gravity. This equation is useful for geophysical applications and realtime reservoir monitoring. In absence of the entire set of governing equations in reservoir flow, this equation serves as a valid example, the generalization of which can shed light to the discovery of the Knowledge dimension.

The Adomian decomposition technique is further applied in ***Chapter 7*** to the Buckley-Leverett (1942) analysis including the effects of capillary pressure. Features such as multiple-valued saturation points and shock front are discussed during implementing the mathematical investigation. In another application, the decomposition method is used only to formulate the well-test equations as appear in ***Chapter 8***.

In ***Chapter 9***, complexity is assumed by considering non-Darcy flow is taking place in the reservoir. The pressure analyses based on the Forchheimer flow equation is presented in this chapter and compared with that based on Darcy's equation.

The non-Darcy flow condition is further investigated into another miscible displacement study in ***Chapter 10***. In this chapter, results of frontal displacement features in accumulating and depleting reservoirs as well as in a uniform, steady reservoir are presented. The chapter also demonstrates analytical and numerical results of transient pressure and velocity profiles in accumulating and depleting reservoirs in which non-uniform flow is taking place.

The study of miscible displacement is extended to another application in ***Chapter 11***. It demonstrates an experimental investigation of solvent flooding using the water-alternating-gas technique.

An indispensable part of the petroleum recovery process is drilling of wells and a complete drilling activity costs huge amount of money. Any improvement in drilling activities can save millions of dollars to the industries and understanding such fact, ***Chapter 12*** *(including Sections 12.1 and 12.2)* of this thesis is organized to examine a novel drilling method using laser technology. In *Section 12.1*, the potential of laser as a drilling option is reviewed. In *Section 12.2*, numerical studies are conducted using the same technology to investigate its effects on limestone and sandstone samples.

The use of horizontal wells facilitates the recovery of petroleum fluids. For example, horizontal wells are found to be beneficial in steam assisted gravity drainage (SAGD) applications in Northern Alberta where land use is restricted as a result of growing environmental concern. However, the benefits can be offset by precipitation of crude oil components or plugging of wells. ***Chapter 13*** demonstrates the microwave irradiation technique to remove these precipitates. The chapter also includes experimental and numerical models that predict transient temperature of petroleum fluids when irradiated by microwave technology.

1.3. Research contribution

The most important contributions of this research are:

1. Experimental and numerical modeling of petroleum fluids (immiscible) under microwave irradiation for improved horizontal well performance;

2. Mathematical modeling (using the Adomian decomposition method) of nonlinear Bukcley-Leverett equation and avoiding unrealistic multiple saturation values;

3. Mathematical modeling of the effects of linearization on solutions of reservoir engineering problems;

4. Numerical modeling of laser technology as a novel drilling method;

5. Developing new equations for geometric factor and bulk volume, which are derived from those available in the literature, but are simple and avoid making estimations;

6. Flexibility in using the grid system in the engineering approach when treating Dirichlet type boundary condition;

7. Mathematical modeling of the existence of multiple solutions in natural phenomenon;

8. Numerical modeling of frontal displacement features, such as, concentration profile, displacement front mixing length, displacement efficiency of accumulating and depleting reservoirs;

9. Analytical and numerical modeling of transient pressure and velocity profiles of accumulating and depleting reservoirs using Darcian and non-Darcian (Forchheimer) flow equations;

10. Developing new correlations of areal sweep efficiency as function of mobility ratio at various water alternating gas ratios.

Publications

Chapter 2:

Chapter 2 highlights Secondary Specific Objective 1.

This chapter is accepted for publication in the *Journal of Petroleum Science and Technology*, September, 2006.

Chapter 3:

Chapter 3 highlights Primary Specific Objective 2.

This chapter is accepted for publication in the *Journal of Petroleum Science and Technology*, 2005, *in press*.

Chapter 4:

Chapter 4.1 highlights Primary Specific Objective 1.

This chapter is accepted for publication in the *Journal of Petroleum Science and Technology*, August, 2006.

Chapter 4.2 highlights Secondary Specific Objective 2.

This chapter is a part of Chapter 5 of the book 'A handbook of knowledge-based petroleum reservoir simulation', Gulf Publishing Company, Houston, TX, to be published in 2006.

Chapter 5:

Chapter 5 highlights Secondary Specific Objective 3.

This chapter is accepted for publication in the *Journal of Nature Science and Sustainable Technology,* August, 2006.

Chapter 6:

Chapter 6 highlights Secondary Specific Objective 4.

This chapter is published in the *Journal of Nature Science and Sustainable Technology,* vol. 1, no. 1, July, 2006.

Chapter 7:

Chapter 7 highlights Primary Specific Objective 3.

This chapter is submitted for publication in the *Journal of Petroleum Science and Technology,* August, 2006.

Chapter 8:

Chapter 8 uses the mathematical technique associated with Primary Specific Objective 3. It also highlights Secondary Specific Objective 5.

This chapter is published in the proceedings of the 4^{th} *International Conference on Computational Heat and Mass Transfer,* Paris-Cachan, May 17-20, 2005.

Chapter 9:

Chapter 9 highlights Primary Specific Objective 4. It also highlights Secondary Specific Objective 6.

This chapter is submitted for publication in the *Journal of Petroleum Science and Engineering*, September, 2006.

Chapter 10:

Chapter 10 highlights Primary Specific Objective 4. It also highlights Secondary Specific Objectives 7 and 8.

This chapter is submitted for publication in the *Journal of Petroleum Science and Engineering*, June, 2006.

Chapter 11:

Chapter 11 highlights Primary Specific Objective 5.

This chapter is submitted for publication in the *Journal of Petroleum Science and Technology*, September, 2006.

Chapter 12:

Chapter 12.1 highlights first part of Primary Specific Objective 6.

This chapter is published in the *Journal of Petroleum Science and Technology*, vol. 22, no. 9-10, pp. 1187-1198, 2004.

Chapter 12.2 highlights last part of Primary Specific Objective 6.

This chapter is published in the *Journal of Petroleum Science and Technology*, vol. 22, no. 9-10, pp. 1173-1186, 2004.

Chapter 13:

Chapter 13 highlights Primary Specific Objective 7.

This chapter appears in the proceedings of the *ASME International Mechanical Engineering Conference and Exposition*, Orlando, Florida, USA, November 6-11, 2005.

Chapter 2

2 STATE-OF-THE-ART OF PETROLEUM RESERVOIR SIMULATION

2.1. Abstract

Today, practically all aspects of reservoir engineering problems are solved with a reservoir simulator. The use of the simulators is so extensive that it will be no exaggeration to describe them as 'the standard'. The simulators enable us to predict reservoir performance, although this task becomes immensely difficult when dealing with complex reservoirs. The complexity can arise from variation in formation and fluid properties. The complexity of the reservoirs has always been handled with increasingly advanced approaches. This paper presents some of the latest advancements in petroleum reservoir simulation. Also discussed is the framework of a futuristic reservoir simulator.

It is predicted that in near future, the coupling of 3D imaging with comprehensive reservoir models will enable one to use drilling data as input information for the simulator creating a real-time reservoir monitoring system. Time is also not far when a virtual reservoir will be a reality and will be able to undergo various modes of production schemes. The coupling of ultra-fast data acquisition system with digital/analog converters transforming signals into tangible sensations will make use of the capability of virtual reality incorporated into the state-of-the-art reservoir models. In their finest form, the reservoir simulators must be intelligent enough to integrate environmental impacts of enhanced oil recovery (EOR) processes into the technical and economical feasibility of different EOR's. The economics, however, should respect both short-term and long-term impacts of oil production in order to claim technical accuracy as well as rendering petroleum production schemes truly sustainable.

2.2. Introduction

The Information Age is synonymous with Knowledge. However, if proper science is not used, information alone cannot guarantee transparency, which is the pre-condition to Knowledge. Proper science requires thinking or imagination with conscience, the very essence of humanity. Imagination is necessary for anyone wishing to make decisions based on science. Imagination always begins with visualization – actually, another term for simulation (Abou-Kassem et al., 2006). Even though there is a commonly held misconception that physical experimentation precedes scientific analysis, the truth is simulation is the first one that has to be worked out even before designing an experiment. This is why the petroleum industry puts so much emphasis on simulation studies. The petroleum industry is known to be the biggest user of computer models. More importantly, unlike other big-scale simulation, such as space research and weather models, petroleum models do not have an option of verifying with real data. Because petroleum engineers do not have the luxury of launching a 'reservoir shuttle' or a 'petroleum balloon' to roam around the reservoir, the task of modeling is the most daunting. Indeed, from the advent of computer technology, the petroleum industry pioneered the use of computer simulations in virtually all aspects of decision-making. From the golden era of petroleum industries, very significant amount of research dollars have been spent to develop some of the most sophisticated mathematical models ever used. Even as the petroleum industry transits through its "middle age" in a business sense and the industry no longer carries the reputation of being the 'most aggressive investor in research', oil companies continue to spend liberally for reservoir simulation studies and even for developing new simulators.

2.3. The Essence of Reservoir Simulation

Today, practically all aspects of reservoir engineering problems are solved with reservoir simulators, ranging from well testing to prediction of enhanced oil recovery. For every

application, however, there is a custom-designed simulator. Even though, quite often, 'comprehensive', 'All-purpose', and other denominations are used to describe a company simulator, every simulation study is a unique process, starting from the reservoir description to the final analysis of results. Simulation is the art of combining physics, mathematics, reservoir engineering, and computer programming to develop a tool for predicting hydrocarbon reservoir performance under various operating strategies. Figure 2.1 depicts the major steps involved in the development of a reservoir simulator (Odeh, 1982). In this figure, the *formulation* step outlines the basic assumptions inherent to the simulator, states these assumptions in precise mathematical terms, and applies them to a control volume in the reservoir. Newton's approximation is used to render these control volume equations into a set of coupled, nonlinear partial differential equations (PDE's) that describe fluid flow through porous media (Ertekin et al., 2001). These PDE's are then discretized, giving rise to a set of non-linear algebraic equations. Taylor series expansion is used to discretize the governing PDE's. Even though this procedure has been the standard in the petroleum industry for decades, only recently Abou-Kassem et al. (2006) pointed out that there is no need to go through this process (expression in PDE, followed by discretization). In fact, by setting up the algebraic equations directly, one can make the process simple and yet maintain accuracy (Mustafiz et al., 2006a). The PDE's derived during the *formulation* step, if solved analytically, would give reservoir pressure, fluid saturations, and well flow rates as continuous functions of space and time. Because of the highly nonlinear nature of the PDE's, analytical techniques cannot be used and solutions must be obtained with numerical methods. In contrast to analytical solutions, numerical solutions give the values of pressure and fluid saturations only at discrete points in the reservoir and at discrete times. *Discretization* is the process of converting PDE's into algebraic equations. Several numerical methods can be used to discretize the PDE's; however, the most common approach in the oil industry today is the finite-difference method. To carry out discretization, a PDE is written for a given point in space at a given time level. The choice of time level (old time level, current time level, or the intermediate time level) leads to the explicit, implicit, or Crank-Nicolson formulation

method. The discretization process results in a system of nonlinear algebraic equations. These equations generally cannot be solved with linear equation solvers and linearization of such equations becomes a necessary step before solutions can be obtained. *Well representation* is used to incorporate fluid production and injection into the nonlinear algebraic equations. *Linearization* involves approximating nonlinear terms in both space and time. Linearization results in a set of linear algebraic equations. Any one of several linear equation solvers can then be used to obtain the *solution*. The solution comprises pressure and fluid saturation distributions in the reservoir and well flow rates. *Validation* of a reservoir simulator is the last step in developing a simulator, after which the simulator can be used for practical field applications. The validation step is necessary to make sure that no errors were introduced in the various steps of development and in computer programming.

There are three methods available for the discretization of any PDE: the Taylor series method, the integral method, and the variational method (Aziz and Settari, 1979). The first two methods result in the finite-difference method, whereas the third results in the variational method. The "Mathematical Approach" refers to the methods that obtain the nonlinear algebraic equations through deriving and discretizing the PDE's. Developers of simulators relied heavily on mathematics in the mathematical approach to obtain the nonlinear algebraic equations or the finite-difference equations. A new approach that derives the finite-difference equations without going through the rigor of PDE's and discretization and that uses fictitious wells to represent boundary conditions has been recently presented by Abou-Kassem et al. (2006). This new approach is termed the "Engineering Approach" because it is closer to the engineer's thinking and to the physical meaning of the terms in the flow equations. Both the engineering and mathematical approaches treat boundary conditions with the same accuracy if the mathematical approach uses second order approximations. The engineering approach is simple and yet general and rigorous. In addition, it results in the same finite-difference equations for any hydrocarbon recovery process. Because the engineering approach is

independent of the mathematical approach, it reconfirms the use of central differencing in space discretization and highlights the assumptions involved in choosing a time level in the mathematical approach.

2.4. Assumptions behind Various Modeling Approaches

2.4.1. Conventional approach

Reservoir performance is traditionally predicted using three methods, namely, 1) Analogical; 2) Experimental, and 3) Mathematical. The mathematical method, however, is the most commonly used by the modern petroleum community. Methods, such as: 1) material balance; 2) decline curve; 3) statistical; and 4) analytical are the predominant techniques that are used in the mathematical model. Ertekin et al. (2001) discussed each of the methods including their assumptions:

2.4.1.1. Mathematical method

2.4.1.1.1. Material balance

Material balance equations are known to be the classical mathematical representation of the reservoir. According to the principle, the amount of material remaining in the reservoir after a production time interval is equal to the amount of material originally present in the reservoir minus the amount of material removed from the reservoir due to production plus the amount of material added to the reservoir due to injection. This equation describes the fundamental physics of the production scheme of the reservoir. There are several assumptions in the material balance equation

1. Rock and fluid properties do not change in space;
2. Hydrodynamics of the fluid flow in the porous media is adequately described by Darcy's law;
3. Fluid segregation is spontaneous and complete;
4. Geometrical configuration of the reservoir is known and exact;
5. PVT data obtained in the laboratory with the same gas-liberation process (flash vs. differential) are valid in the field;
6. Sensitive to inaccuracies in measured reservoir pressure. The model breaks down when no appreciable decline occurs in reservoir pressure, as in pressure maintenance operations.

2.4.1.1.2. Decline curve

The rate of oil production decline generally follows one of the following mathematical forms: exponential, hyperbolic and harmonic. The following assumptions apply to the decline curve analysis

1. The past processes continue to occur in the future;
2. Operation practices are assumed to remain same.

2.4.1.1.3. Statistical method

In this method, the past performance of numerous reservoirs is statistically accounted for to derive the empirical correlations, which are used for future predictions. Ertekin et al. (2001) described it as a 'formal extension of the analogical method' and mentioned about the following assumptions, which belong to this method

1. Reservoir properties are within the limit of the database;
2. Reservoir symmetry exists;

3. Ultimate recovery is independent of the rate of production.

In addition, Zatzman and Islam (2006) recently pointed out a more subtle, yet far more important shortcoming of the statistical methods. Practically, all statistical methods assume that two or more objects based on a limited number of tangible expressions makes it legitimate to comment on the underlying science. It is equivalent to stating if effects show a reasonable correlation, the causes can also be correlated. As Zatzman and Islam (2006) pointed out, this poses a serious problem as, in absence of time space correlation (pathway rather than end result), anything can be correlated with anything, making the whole process of scientific investigation spurious. They make their point by showing the correlation between global warming (increase) with a decrease in the number of pirates. The absurdity of the statistical process becomes evident by drawing this analogy. Shapiro et al. (in press) pointed out another severe limitation of the statistical method. Even though they commented on the polling techniques used in various surveys, their comments are equally applicable in any statistical modeling. They wrote: "Frequently, opinion polls generalize their results to a U.S. population of 300 million or a Canadian population of 32 million on the basis of what 1,000 or 1,500 "randomly selected" people are recorded to have said or answered. In the absence of any further information to the contrary, the underlying theory of mathematical statistics and random variability assumes that the individual selected "perfectly" randomly is no more nor less likely to have any one opinion over any other. How perfect the randomness may be determined from the "confidence" level attached to a survey, expressed in the phrase that describes the margin of error of the poll sample lying plus or minus some low single-digit percentage "nineteen times out of twenty", *i.e.*, a confidence level of 0.95. Clearly, however, assuming *in the absence of any knowledge otherwise* a certain state of affairs to be the case, *viz.*, that the sample is random and no one opinion is more likely than any other, seems more useful for projecting horoscopes than scientifically assessing public opinion."

2.4.1.1.4. Analytical method

Analytical methods can only apply to linear equations. Most approaches simplify boundary conditions and apply to single-phase flow in order to solve the governing equations.

2.4.2. Differential calculus

The history of differential calculus dates back to the time of Leibnitz and Newton. In this concept, the derivative of a continuous function is related to the function itself. In the core of differential calculus is Newton's formula, which has the following approximation attached to it: the magnitude and direction change independently of one another. There is no problem in having separate derivatives for each component of the vector or in superimposing their effects separately and regardless of order. That is what mathematicians mean when they describe or discuss Newton's derivative being used as a "linear operator". Following this, comes Newton's difference-quotient formula. When the value of a function is inadequate to solve a problem, the rate at which the function changes, sometimes, becomes useful. Therefore, the derivatives are also important in reservoir simulation. In Newton's difference-quotient formula, the derivative of a continuous function is obtained. This method relies implicitly on the notion of approximating instantaneous moments of curvature, or infinitely small segments, by means of straight lines. This alone should have tipped everyone off that this derivative is a linear operator precisely because, and to the extent that, it examines change over time (or distance) within an already established function (Islam, 2006). This function is applicable to an infinitely small domain, making it non-existent. When, integration is performed, however, this non-existent domain is assumed to be extended to finite and realistic domain, making the entire process questionable.

2.4.2.1. Taylor series expansion

The Taylor series expansion is a very important tool in numerical analysis. By this method of expansion, most well-behaved functions are converted to simple polynomials. When the Taylor series expansion is carried out for a finite number of terms and the remainder is ignored, the series becomes an approximation of the function.

2.4.2.2. Finite difference method

Finite difference calculus is a mathematical technique, which is used to approximate values of functions and their derivatives at discrete points, where they are not known. The following assumptions are inherent to the finite difference method.

1. The relationship between derivative and the finite difference operators, e.g., forward difference operator, backward difference operator and the central difference operator is established through the Taylor series expansion. In other word, it assumes that a relationship between the operators for discrete points and the operators of the continuous functions is acceptable.

2. The relationship involves truncation of the Taylor series of the unknown variables after few terms. Such truncation leads to accumulation of error. Mathematically, it can be shown that most of the error occurs in the lowest order terms.

a) The forward difference and the backward difference approximations are the first order approximations to the first derivative.

b) Although the approximation to the second derivative by central difference operator increases accuracy because of a second order approximation, it still suffers from the truncation problem.

c) As the spacing size reduces, the truncation error approaches to zero more rapidly. Therefore, a higher order approximation will eliminate the need of same number of

measurements or discrete points. It might maintain the same level of accuracy; however, less information at discrete points might be risky as well.

3. The solutions of the finite difference equations are obtained only at the discrete points. These discrete points are defined either according to block-centered or point distributed grid system. However, the boundary condition, to be specific, the constant pressure boundary, may appear important in selecting the grid system with inherent restrictions and higher order approximations.

4. The solutions obtained for gridpoints are in contrast to the solutions of the continuous equations.

5. In the finite difference scheme, the local truncation error or the local discretization error is not readily quantifiable because the calculation involves both continuous and discrete forms. Such difficulty can be overcome when the mesh-size or the time step or both are decreased leading to minimization in local truncation error. However, at the same time the computational operation increases, which eventually increases the round-off error.

2.4.3. Darcy's law

Because most reservoir simulation studies involve the use of Darcy's law, it is important to understand the assumptions behind this momentum balance equation. The following assumptions are inherent to Darcy's law and its extension

1. The fluid is homogenous, single-phase and Newtonian;

2. No chemical reaction takes place between the fluid and the porous medium;

3. Laminar flow condition prevails;

4. Permeability is a property of the porous medium, which is independent of pressure, temperature and the flowing fluid;

5. There is no slippage effect; e.g., Klinkenberg phenomenon;

6. There is no electro-kinetic effect.

2.5. Recent Advances in Reservoir Simulation

2.5.1. Improving quality of the reservoir model prediction: *speed and accuracy*

Advances have been made in many fronts. As the speed of computers increased following Moore's law (doubling every 12 to 18 months), the memory also increased. For reservoir simulation studies, this translated into the use of higher accuracy through inclusion of higher order terms in Taylor series approximation as well as great number of grid blocks, reaching as many as billion blocks. The greatest difficulty in this advancement is that the quality of input data did not improve at par with the speed and memory of the computers. As Fig. 2.2 shows, the data gap remains possibly the biggest challenge in describing a reservoir. Note that the inclusion of great number of grid blocks makes the prediction more arbitrary than that predicted by fewer blocks, if the number of input data points is not increased proportionately. This point is elucidated in Fig. 2.3. Figure 2.3 also shows the difficulty associated with modeling with either too small or too large grid blocks. The problem is particularly acute when fractured formation is being modeled. The problem of reservoir cores being smaller than the representative elemental volume (REV) is a difficult one, which more accentuated for fractured formations that have a higher REV. For fractured formations, one is left with a narrow band of grid blocks, beyond which solutions are either meaningless (large grid blocks) or unstable (too small grid blocks).

2.5.2. New fluid flow equations

The fundamental question to be answered in modeling fracture flow is the validity of the governing equations used. The conventional approach involves the use of dual-porosity, dual permeability models for simulating flow through fractures. Choi et al. (1997) demonstrated that the conventional use of Darcy's law in both fracture and matrix of the fractured system is not adequate. Instead, they proposed the use of the Forchheimer

model in the fracture while maintaining Darcy's law in the matrix. Their work, however, was limited to single-phase flow. In future, the present status of this work can be extended to a multiphase system. It is anticipated that gas reservoirs will be suitable candidates for using Forchheimer extension of the momentum balance equation, rather than the conventional Darcy's law. Similar to what was done for the liquid system (Cheema and Islam, 1995); opportunities exist in conducting experiments with gas as well as multiphase fluids in order to validate the numerical models. It may be noted that in recent years several dual-porosity, dual-permeability models have been proposed based on experimental observations (Tidwell and Robert, 1995; Saghir et al., 2001).

2.5.3. Modeling coupled fluid flow and geomechanical stress

Coupling different flow equations has always been a challenge in reservoir simulators. In this context, Pedrosa et al. (1986) introduced the framework of hybrid grid modeling. Even though this work was related to coupling cylindrical and Cartesian grid blocks, it was used as a basis for coupling various fluid flow models (Islam and Chakma, 1990; Islam, 1990). Coupling flow equations in order to describe fluid flow in a setting, for which both pipe flow and porous media flow prevails continues to be a challenge (Mustafiz et al., 2005a).

Geomechanical stresses are very important in production schemes. However, due to strong seepage flow, disintegration of formation occurs and sand is carried towards the well opening. The most common practice to prevent accumulation as followed by the industry is take filter measures, such as liners and gravel packs. Generally, such measures are very expensive to use and often, due to plugging of the liners, the cost increases to maintain the same level of production. In recent years, there have been studies in various categories of well completion including modeling of coupled fluid flow and mechanical deformation of medium (Vaziri et al., 2002). Vaziri et al. (2002) used a finite element analysis developing a modified form of the Mohr–Coulomb failure

envelope to simulate both tensile and shear-induced failure around deep wellbores in oil and gas reservoirs. The coupled model was useful in predicting the onset and quantity of sanding. Nouri et al. (2006) highlighted the experimental part of it in addition to a numerical analysis and measured the severity of sanding in terms of rate and duration. It should be noted that these studies (Nouri et al., 2002; Vaziri et al., 2002 and Nouri et al., 2006) took into account the elasto-plastic stress-strain relationship with strain softening to capture sand production in a more realistic manner. Although, at present both studies lag validation with field data, they offer significant insight into the mechanism of sanding and have potential in smart-designing of well-completions and operational conditions.

Recently, Settari et al. (2006) applied numerical techniques to predict subsidence induced by gas production in the North Adriatic. Due to the complexity of the reservoir and compaction mechanisms, Settari (2006) took a combined approach of reservoir and geomechanical simulators in modeling subsidence. As well, an extensive validation of the modeling techniques was undertaken, including the level of coupling between the fluid flow and geomechanical solution. The researchers found that a fully coupled solution had an impact only on the aquifer area, and an explicitly coupled technique was good enough to give accurate results. On gridding issues, the preferred approach was to use compatible grids in the reservoir domain and to extend that mesh to geomechanical modeling. However, it was also noted that the grids generated for reservoir simulation are often not suitable for coupled models and require modification.

In fields, on several instances, subsidence delay has been noticed and related to overconsolidation, which is also termed as the threshold effect (Merle et al., 1976; Hettema et al., 2002). Settari et al. (2006) used the numerical modeling techniques to explore the effects of small levels of overconsolidation in one of their studied fields on the onset of subsidence and the areal extent of the resulting subsidence bowl.

The same framework that Settari et al. (2006) took can be introduced in coupling the multiphase, compositional simulator and the geomechanical simulator in future.

2.5.4. Modeling fluid flow under thermal stresses

The temperature changes in the rock can induce thermo-elastic stresses (Hojka et al., 1993), which can either create new fractures or can alter the shapes of existing fractures, changing the nature of primary mode of production. It can be noted that the thermal stress occurs as a result of the difference in temperature between injected fluids and reservoir fluids or due to the Joule Thompson effect. However, in the study with unconsolidated sand, the thermal stresses are reported to be negligible in comparison to the mechanical stresses (Chalaturnyk and Scott, 1995). Similar trend is noticeable in the work by Chen et al. (1995), which also ignored the effect of thermal stresses, even though a simultaneous modeling of fluid flow and geomechanics is proposed.

Most of the past research has been focused only on thermal recovery of heavy oil. Modeling subsidence under thermal recovery technique (Tortike and Farouq Ali, 1987) was one of the early attempts that considered both thermal and mechanical stresses in their formulation. There are only few investigations that attempted to capture the onset and propagation of fractures under thermal stress. Recently, Zekri et al. (2006) investigated the effects of thermal shock on fractured core permeability of carbonate formations of UAE reservoirs by conducting a series of experiments. Also, the stress-strain relationship due to thermal shocks was noted.

Apart from experimental observations, there is also the scope to perform numerical simulations to determine the impact of thermal stress in various categories, such as water injection, gas injection/production etc.

Gas injection is the most important form of enhanced oil recovery. More recently, the prospect of CO_2 sequestration has increased the appeal of gas injection scheme. Any gas injection scheme (miscible or immiscible) goes through significant temperature change (Joule-Thompson effect), which can be beneficial or detrimental to the process depending on the reservoir characteristics. This effect is particularly significant for fractured formations similar to the ones found in the Atlantic region. However, few researchers have addressed this problem.

Cheema and Islam (1995) suggested that a dual-permeability, dual-porosity approach might not be necessary for modeling naturally fractured formations. Instead, the average anisotropy values could be assigned based on the direction of the rose diagram of the formation. There is the potential to test this methodology for reservoir applications. Saghir et al. (2001) used a finite element model in order to assess the role of natural fractures as well as thermal stresses in determining fluid flow in a reservoir. However, future opportunities lie in scaling up the proposed fracture flow model to a 3-D, multiphase and compositional simulator. This model will be able to include various thermal applications, such as miscible displacement in a thermally active fractured formation. However, to translate this expectation into reality, a number of experimental and numerical tasks need to be addressed:

2.5.4.1. Experimental challenges

The need of well designed experimental work in order to improve the quality of reservoir simulators cannot be over-emphasized. Most significant challenge in experimental design arise from determining rock and fluid properties. Even though, progress has been made in terms of specialized core analysis and PVT measurements, numerous problems persist due to difficulties associated with sampling techniques and core integrity. Recently, Belhaj et al. (2006) used a 3-D spot gas permeameter to measure permeability at any spot on the surface of the sample, regardless of the shape and size. Moreover, a mathematical

model was derived to describe the flow pattern associated with measuring permeability using the novel device.

In a reservoir simulation study, all relevant thermal properties including coefficient of thermal expansion, porosity variation with temperature, and thermal conductivity need to be measured in case such information are not available. Experimental facilities e.g., double diffusive measurements, transient rock properties; point permeability measurements can be very important in fulfilling the task. In this regard, the work of Belhaj et al. (2006) is noteworthy.

In order to measure the extent of 3-D thermal stress, a model experiment is useful to obtain temperature distribution in carbonate rock formation in the presence of a heat source. Examples include microwave heating water-saturated carbonate slabs with in order to model only conduction and radiation. An extension to the tests can be carried out to model thermal stress induced by cold fluid injection for which convection is activated. The extent of fracture initiation and propagation can be measured in terms of so-called damage parameter. Time-dependent crack growth still is an elusive topic in petroleum applications (Kim and van Stone, 1995). The methodology outlined by Yin and Liu (1994) can be considered to measure fracture growth. The mathematical model can be developed following the numerical method developed by Wang and Maguid (1995).

Young's modulus, compressive strength, and fracture toughness are important for modeling the onset and propagation of induced fracture for the selected reservoir. Incidentally, the same set of data is also useful for designing hydraulic fracturing jobs (Rahim and Holditch, 1995).

2.5.4.2. Numerical challenges

2.5.4.2.1. Theory of onset and propagation of fractures due to thermal stress

Fundamental work needs to be performed in order to develop relevant equations for thermal stresses. Similar work has been initiated by Wilkinson et al. (1997), who used finite element modeling to solve the problem. There has been some progress in the design of material manufacturing for which in situ fractures and cracks are considered to be fatal flaws. Therefore, formulation of complete equations is required in order to model thermal stress and its effect in petroleum reservoirs. It is to be noted that this theory deals with only transient state of the reservoir rock.

2.5.4.2.2. 2-D and 3-D solutions of the governing equations

In order to determine fracture width, orientation, and length under thermal stresses as a function of time, it is imperative to solve the governing equations first in 2-D. The finite difference is the most accepted technique to develop the simulator. An extension of the developed simulator to the cylindrical system is useful in designing hydraulic fractures in thermally active reservoirs. The 3-D solutions are required to determine 3-D stresses and the effects of permeability tensor. Such simulation will provide with the flexibility of determining fracture orientation in the 3-D mode and guide as a design tool for hydraulic fracturing. Although the 3-D version of the hydraulic fracturing model will be in the framework put forward earlier (Wilkinson et al., 1997), however, differences of opinion exist as to how thermal stress can be added to the in situ stress equations.

2.5.4.2.3. Viscous fingering during miscible displacement

Viscous fingering is believed to be dominant in both miscible and immiscible flooding and of much importance in a number of practical areas including secondary and tertiary

oil recovery. However, modeling viscous fingering remains a formidable task. Only recently, researchers from Shell have attempted to model viscous fingering with the chaos theory. Islam (1993) has reported in a series of publications that periodic and even chaotic flow can be captured properly by solving the governing partial differential equations with improved accuracy (Δx^4, Δt^2). This needs to be demonstrated for viscous fingering. The tracking of chaos (and hence viscous fingering) in a miscible displacement system can be further enhanced by studying phenomena that onset fingering in a reservoir. It eventually will lead to developing operating conditions that would avoid or minimize viscous fingering. Naami et al. (1999) conducted both experimental and numerical modeling of viscous fingering in a 2-D system. They modeled both the onset and propagation of fingers by solving governing partial differential equations. Recent advances in numerical schemes (Aboudheir et al., 1999; Bokhari and Islam, 2005) can be suitably applied in modeling of viscous fingering. The scheme proposed by Bokhari and Islam (2005) is accurate in the order of Δx^4 in space and Δt^2 in time. Similar approach can be extended for tests in a 3-D system in future. Modeling viscous fingering using finite element approach has been attempted as well (Saghir et al., 2000).

2.5.5. Improvement in remote sensing and monitoring ability

One of the most coveted features in present reservoir studies is to develop advanced technologies for real-time data transmission for both down-hole and wellhead purposes (chemical analysis of oil, gas, water, and solid) from any desired location. This study can lead to conducting real-time control of various operations in all locations, such as in the wellbore, production string and pipelines remotely. However, several subtasks need to be addressed to make advances in remote sensing and monitoring:

2.5.5.1. Monitoring reservoirs and tubular

This task will improve the ability to capture phenomena occurring at three levels: reservoir, wellbore, and wellhead/pipelines. The conventional seismic technology has a resolution of 20m for the reservoir region. While this resolution is sufficient for exploration purposes, it falls short of providing meaningful results for petroleum field development, for which 1m resolution is necessary to monitor changes (with 4-D seismic) in a reservoir. For the wellbore, a resolution of 1 mm is necessary. This can also help detect fractures near the wellbore. The current technology does not allow one to depict the reservoir, the wellbore, or the tubular with acceptable resolution (Islam, 2001a). In order to improve resolution within a wellbore, acoustic response need to be analyzed. In addition, fiber-optic detection of multiphase flow can be investigated. Finally, it will be possible to develop a data acquisition system that can be used as a real-time monitoring tool, once coupled with a signal processor. Recently, Zaman et al. (2006) used a laser spectroscope to detect paraffin in paraffin-contaminated oil samples. After passing through the oil sample, the laser light was detected by a semi-conductor photodiode, which, in turn, converted the light signal into electric voltage. In their study, the paraffin concentrations ranged between 20% and 60% wt and a thickness of 1 and 10 mm. They developed a 1-D mathematical model to describe the process of laser radiation attenuation within the oil sample based on energy balance. Further the problem was numerically solved, which were found to be in correlation with those obtained from the experiments. Their model can be used to predict the net laser light and the amount of light absorbed per unit volume at any point within the oil sample. The mathematical model was extended to different types of oil products to determine the local rate of absorption in an oil layer under different working environments. The effects of the angle of incidence, bottom reflectivity, and layer depth were discussed in this regard.

It is true that there is skepticism about the growing pace of applying 4-D seismic for enhanced monitoring (Feature-*First break*, 1997), yet the advancement in the last decade

assures that the on-line monitoring of reservoirs is not an unrealistic dream (Islam, 2001a). Strenedes (1995) reported that the average recovery factor from all the fields in the Norwegian sector increased from 34-39% over 2-3 years, due to enhanced monitoring. The needs for an improved technique was also emphasized to face the challenge of decine production in North Sea.

2.5.5.2. Monitoring offshore structures

In order to remain competitive in today's global economic environment, owners of civil structures need to minimize the number of days their facilities are out of service due to maintenance, rehabilitation or replacement. Indicators of structural system performance are needed for the owner to allocate resources toward repair, replacement or rehabilitation of their structures. To quantify these system performance measures requires structural monitoring of large civil structures while in service (Mufti et al., 1997). It is, therefore, important to develop a structural monitoring system that will integrate

1. Fiber optic sensor systems;
2. Remote monitoring communication systems;
3. Intelligent data processing system;
4. Damage detection and modal analysis system and
5. Non-destructive evaluation system.

It will be more useful if the monitoring device is capable of detecting signs of stress corrosion cracking. A system of fiber optic-based sensor and remote monitoring communication will allow not only monitoring of the internal operating pressures but also the residual stress levels, which are suspected for the initiation and growth of near-neutral pH stress corrosion cracking. Finally, the technology can be applied in real-time in monitoring offshore structures. Along this line of research, the early detection of

precipitation of heavy organics such as paraffin, wax, resin, asphaltene, diamondoid, mercaptdans, and organometallic compounds, which can precipitate out of the crude oil solution due to various forces causing blockage in the oil reservoir, well, pipeline and in the oil production and processing facilities is worth mentioning (Zaman et al., 2004). Zaman et al. (2004) utilized solid detection system by light transmittance measurement for asphaltene detection, photodiode for light transmittance measurement for liquid wax, detection, and ultrasound and strain gauge solid wax detection. Such attempt, if effectively used, has a potential to reduce pigging (the common commercial term for cleaning the pipeline) and in turn, the maintenance cost considerably.

2.5.5.3. Development of a Dynamic Characterization Tool (based on seismic-while-drilling data)

It will use the inversion technique to determine permeability data. At present, cuttings need to be collected before preparing petrophysical logs. The numerical inversion requires the solution of a set of non-linear partial differential equations. Conventional numerical methods require these equations to be linearized prior to solution (discussed early in the paper). In this process, many of the routes to final solutions may be suppressed (Mustafiz et al., 2006a) while it is to be noted that a set of non-linear equations should lead to the emergence of multiple solutions. Therefore, it is important that a nonlinear problem is investigated for multiple-value solutions of physical significance.

The Adomian Decomposition Method (ADM) is relatively, a new mathematical approach in petroleum engineering. In recent years, the technique has emerged as an alternative method to solve various mathematical models including algebraic, differential, integral, integro-differential, partial differential equations (PDEs) and systems, higher-order ordinary differential equations, and others in physics and mathematics. Wazwaz (2001) and Wazwaz and El-Sayed (2001) reported that the ADM is useful in solving problems

without considering linearization, perturbation, or unjustified assumptions that may alter the nature of the problem under investigated. Further, El-Sayed and Abdel-Aziz (2003) noted that the ADM can be more useful than the numerical methods because of providing with analytic, verifiable and rapidly convergent approximations adding insight into the character and the behaviour of the solution as obtainable in the closed form solution. However, there have been only few publications relevant to petroleum research that utilized the Adomian technique (Mustafiz et al., 2006b; Rahman et al., in press; Mustafiz et al., 2005b; Mustafiz and Islam, 2005). Recent studies indicate that a broad avenue still remains open for the decomposition method to be investigated in nonlinear reservoir problems.

2.5.5.4. Use of 3-D Sonogram

This feature illustrates the possibility of using 3-D sonogram for volume visualization of the rock ahead of the drill bit. In order to improve resolution and accuracy of prediction ahead of the drill bit, the 3-D sonogram technique will be extremely beneficial. The latest in ultrasound technology offers the ability to generate images in 4-D (time being the 4^{th} dimension). In preparation to this task, a 3-D sonogram can be adopted to detect composition of fluid through non-invasive methods. Note that such a method is not yet in place in the market. Also, there is the potential of coupling 3-D sonogram with sonic while drilling in near future.

This coupling will allow one to use drilling data to develop input data for the simulator with high resolution. Availability and use of a sophisticated compositional 3-D reservoir simulator will pave the way to developing real-time reservoir modeling – a sought after goal in the petroleum industry for sometime.

2.5.6. Virtual reality (VR) applications

In the first phase of this task, the coupling of an existing compositional, geomechanical simulator with the VR machine is required. Time travel can be limited to selected processes with limited number of wells primarily. Later time travel can expand as the state-of-the-art in simulation becomes more sophisticated.

Indeed, reservoir engineers have the difficult task of conducting reservoir design without ever going for a site inspection. This research is aimed at creating a virtual reservoir that can undergo various modes of petroleum production schemes (including thermal, chemical, and microbial EOR). It is comprehended that in future the virtual reservoir, in its finished form, will be coupled with virtual production and separation systems. A virtual reservoir will enable one to travel through pore spaces at the speed of light while controlling production/injection schemes at the push of a button. Because time travel is possible in virtual system, one does not have to wait to see the impact of a reservoir decision (e.g. gas injection, steam huff-and-puff) or production problems (e.g. wellbore plugging due to asphaltene precipitation).

The use of virtual reality in petroleum reservoir is being discussed only in the context of 3-D visualization (Editorial, *Oil & Gas Journal*, 1996). A more useful utilization of the technique, of course, will be in reservoir management, offshore monitoring, and production control. While a full-fledged virtual reservoir is still considered to be a tool for the future, one must concentrate on physics and mathematics of the development in order to ensure that a virtual reservoir does not become a video game. Recently, several reports have appeared on the use of virtual reality in platform systems, and even production networking (Editorial, *Oil & Gas Journal*, 1996). An appealing application of virtual reality lies in the areas of replacing expensive laboratory experiments with computational fluid dynamics models. However, petroleum-engineering phenomena are still so poorly described (mathematically) that replacing laboratory experiments will lead

to gross misunderstanding of dominant phenomena. Recently, Statoil has developed a virtual reality machine that would simulate selected phenomena in the oilfield. Similarly, Norsk Hydro has reported the virtual modeling of a cave. The reservoir simulator behind the machine, however, is only packed with rudimentary calculations. More advanced models have been used in drilling and pipelines.

Even though the concept is novel, the execution of the described plan can be realistic in near future. The reservoir data (results as well as the reservoir description) will be fed into an ultra-fast data acquisition system. The key here is to solve the reservoir equations so fast that the delay between data generation and the data storage/distribution unit is not 'felt' by a human. The data acquisition system could be coupled with digital/analog converters that will transform signals into tangible sensations. These output signals should be transferred to create visual, thermal, acoustic, and piezometric effects. Therefore, this task should lead to coupling the virtual reality capability with a state-of-the-art reservoir model. When it becomes successful, it will not be mere dream to extend the model to vertical section of the well as well as surface facilities.

2.5.7. Intelligent reservoir management

Intelligent systems can be utilized effectively to help both operators and design engineers to make decisions. The major goal of this management program is to develop a novel Knowledge Based Expert System (KB ES) that helps design engineers to choose a suitable EOR method for an oil reservoir. It should be a comprehensive ES that integrates the environmental impacts of each EOR process into the technical and economical feasibility of different EOR's.

Most conventional reservoir management models are based on linear programing (Liu and Ramirez, 1994). Recenty, non-linear optimization has been added. However, nonlinearities are invoked as constraints and even then difficulties

persist in solving these problems in its non-linear forms (Sarma et al., 2006). In addition, true (human) intelligence is not incorporated.

Past intelligent reservoir management referred to computer or artificial intelligence. Recently, Islam (2006a) demonstrated that computer operates quite differently from how humans think. He outlined the need for new line of expert systems that are based on human intelligence, rather than artificial intelligence. Novel expert systems embodying pro-nature features are proposed based on natural human intelligences (Ketata et al., 2005a, 2005b). These experts system use human intelligence which is opposite to artificial intelligence. In these publications, authors attempted to include the knowledge of non-European races who had a very different approach to modeling. Also, based on Chinese abacus and quipu (latin American ancient tribe), Ketata et al. (2006a; 2006b) developed an expert system that can be characterized as the first expert system without using the conventional computer counting system. These expert systems provide the basis of an intelligent, robust, and efficient computing tool.

Because all natural phenomena are non-linear, we argued that any acceptable computational technique must produce multiple solutions. With this objective, Islam (2006b) developed a new computational method that finds dynamic derivatives of any function and also solves set of non-linear equations. More recently, Islam et al. (in press) and Mousavizadegan et al. (in press), proposed a new technique for finding invariably multiple solutions to every natural equation. These techniques essentially create a cloud of data points and the user can decide which ones are most relevant to a certain application.

Another significant aspect of 'intelligence' was addressed by Ketata et al. (2006a, 2006c). This aspect involves the redefining of zero and infinity. It is important to note that any discussion of human intelligence cannot begin without the mathematics of intangibles, which include proper understanding of these concepts.

Finally, a truly intelligent reservoir model should be able to model chaos. It is recognized that 'chaos' is the interrelated evolutionary order of nature elements. It is the science of objects and systems nature. A new chaos theory has been developed by Ketata et al. (2006d).

2.5.8. Economic models based on futuristic energy pricing policies

There is a distinct need to integrate energy pricing and economic models with a reservoir simulator. The energy pricing policy is one of the most complex and sensitive global issues. With growing worldwide concern about environment and conservation of nature, the economic models must reflect them through futuristic, green-energy policies. The economics models should have the following features, which are often ignored in economic models. They are (Khan and Islam, 2006; in press[1]):

1. Short-term and long-term impact of oil production on agriculture, livestock, fisheries and others affecting the food chain;
2. Intangible cost of groundwater and air pollution resulting from petroleum activities;
3. Clean-up cost of accidental oil spills;
4. Costs related to inherently deficient engineering design;
5. Costs related to political constraints on energy pricing.

The comprehensive economic model will allow one to evaluate a project based on its merit from economic as well as environmental and social values. Even though political constraints constitute a part of social models, it is well known that petroleum policies are more acutely dependent on world politics (Baade et al., 1990; Stickey, 1993). Therefore, political constraints should be identified as the primary variable in energy pricing (Zatzman and Islam, in press[1]).

The new model must also focus on the integration of pricing and qualitative controls in the abatement of cost-effective reductions in energy related CO_2 emissions. Worldwide demand for energy is increasing faster than ever (Dung and Piracha, 2000). The demand for oil and gas is increasing faster than the growth rates of GDP in developing and developed countries. Petroleum is used as inputs for manufacturing, construction, agriculture, power generating, and service sectors. This is also a final consumer product. As demand for goods and services increases, the demand for oil will also increase. As GDP increases, the demand for oil as a final consumer product will also increase. Therefore, inefficient supply and demand management policies on petroleum can impose severe constraints on output, employment, standard of living, the backward and forward linkage effects and the growth of other dependent sectors of the domestic and global economy. The new model must develop a pricing policy that will ensure sustainable development while allowing certain qualitative controls which will minimize the average emissions of energy related CO_2. Such policies are feasible and can be achieved at minimum social cost (Howarth and Winslow, 1994). The qualitative control can be achieved through the employment of green technologies (Islam, 2000).

Zatzman and Islam (in press[2]) investigated the possibilities about the true potential of a given resource in the process of collecting during actual production information about dynamic changes in reservoir conditions in situ. The idea would be to eliminate much of the guesswork built into current demand-based modeling of energy prices. In general, these models project costs well into the future to "take care" of the margin of error incorporated in the guesswork. It can be considered a shift from the demand-based to the supply-based modeling, from control exercised downstream over national production companies upstream to a profound challenge against such control. According to the proposal by Zatzman and Islam (in press[2]), it is less meaningful to speak of "future energy price", and more meaningful to think in terms of another energy pricing model. The correction of guesswork with actual knowledge gathered in situ during production has a number of implications. It renders moot, or irrelevant, any previous assumption of

resource scarcity or globally finite supply as a boundary condition, as the issue shift increasingly away from the price of energy to how this price and its trend are modeled.

The state-of-the-art model needs to be employed to predict the future oil price so that producers, consumers, firms, governments and other stakeholders in the industry are able to plan a sustainable growth of output, employment and income. Also the model should be able to decompose the effects of each of the variables in determining the oil price and computing the individual contribution. The behaviors of the following variables will determine equilibrium world price of oil:

1. Excess demand;
2. Market power;
3. World commodity price index;
4. Price expectations;
5. Political power;
6. Environmental cost;
7. Taxes and tariffs, and
8. Cost of political constraints.

2.5.9. Integrated system of monitoring, environmental impact and economics

Recently, there have been renewed efforts by the petroleum companies to integrate economics with reservoir simulation. As for example, Schlumberger has been conducting reservoir management and economic analysis through ECLIPSE and MERAK. MERAK can perform economic evaluation, decline analysis, and fiscal modeling that calculate the value of oil and gas properties in Canada, the United States and around the world. The merge of such package with a state-of-the-art reservoir simulator can be used as research tool for validation of various concepts, such as, cost of environmental impact, financial worth of bottom-line driven economy, and others. All

engineering, economical, environmental, and socio-political constraints should be integrated through a global optimization package (Finley et al., 1998).

It is also envisioned that a global optimization package, in its matured form, will initiate the development of solution to environmental problems, including risk analysis and decision support (Abdeh-Kolahchi et al., in press; Hossain et al., in press; Khan and Islam, in press[2]; Khan et al., in press). An exposure assessment of the airborne and waterborne pollutants during CO_2 and water injection processes respectively can be conducted to study their impact on marine environment and offshore workers (Khan and Islam, in press[1]). The study on the evaluation of pollutants in conjunction with fluid flow injection will be helpful in creating a multiple-response experimental design. The rationale for conducting experiments will be to introduce a non-bias approach from both the process operation and environmental aspects. Most importantly, the goal should be to introduce the principles of *pollution prevention* (P2) at the research level in order to reduce the need for "*end-of-pipe*" mitigation strategies during implementation. Also the exposure assessment and treatment mitigation phase can be incorporated into the virtual reservoir model, as described previously. Recently, Lakhal et al. (in press) outlined how petroleum operations can be rendered 'green' by following what they termed the 'olympic' model.

Finally, whenever the community in question could be viewed as having been marginalized, and left behind by economic events, there is a perception that little is being done to mitigate these contamination problems, in contrast to large cities where such problems receive close attention, leading to the perception of an "*environmental injustice*" regarding such pollution. However, with the increasing awareness of human rights and justice in all aspects of life, the general public seems to be committed to have such environmental injustice dealt with in a fair and equitable manner (Zatzman and Islam, in press[2]).

2.6. Conclusions

This paper presents descriptions of various features of a reservoir simulator including their limitations, present status and potentials. The results of a reservoir simulation studies have significant impact on environmental and socio-economic aspects of life. The strength of a simulator cannot be measured only by its capacity to handle billions of grid blocks, but also how closely it captures the science and mathematics of the reservoirs with careful consideration of the impacts on economic and social aspects. The paper also points out the scopes where the very latest knowledge can be implemented in a smart and intelligent way through a state-of-the-art knowledge.

2.7. References

Abdeh-Kolahchi, A., Satish, M.G., Ketata, C. and Islam, M.R., (in press) Sensitivity analysis of genetic algorithm parameters in groundwater monitoring network optimization for petroleum contaminant detection, International Journal of Risk Assessment and Management

Aboudheir, A., Kocabas, I. and Islam, M.R., (1999) Improvement of numerical methods in petroleum engineering problems. Proc. of the IASTED International Conference, Applied Modeling and Simulation, Cairns, Australia, September 1-3

Abou-Kassem, J.H., Farouq Ali, S.M., and Islam, M.R., (2006) Petroleum reservoir simulation: A basic approach, Gulf Publishing Company, Houston, 445 p.

Baade, H.W., Lopez-Portillo, G.M., and Guillermo, F., (1990) Texas International Law Journal, vol. 25, no.3, 381-387

Belhaj, H.A., Mousavizadegan, S.H., Ma, F. and Islam, M.R., (2006) Three-dimensional

permeability utilizing a new gas-spot permeameter, SPE 100428, SPE Gas Technology Symposium, Calgary, May 15-17

Bokhari, K., (2003) Experimental and numerical modeling of viscous fingering in liquid-liquid displacement, MASc thesis, Department of Chemical Engineering, Dalhousie University

Bokhari, K. and Islam, M.R., (2005) Improvement in the time accuracy of numerical methods in petroleum engineering problems – A new combination, Energy Sources, vol. 27, no. 1-2, 45-60

Bokhari, K., Mustafiz, S. and Islam, M.R., (2006) Numerical modeling of viscous fingering under combined effects of thermal, solutal and mixed convection in liquid-liquid miscible displacements, Journal of Petroleum Science and Technology, accepted for publication, May

Chalaturnyk, Rick, and Scot, J. D., (1995) Geomechanics issues of steam assisted gravity drainage, paper SPE 30280, presented at the International Heavy Oil Symposium held in Calgary, AB, Canada, June 19-21

Cheema, T.J. and Islam, M.R., (1995) A new modeling approach for predicting flow in fractured formations, In: El-Kady (Editor), Groundwater Models for Resources Analysis and Management, Lewis Publishers, Boca Raton, FL, pp. 327-338

Chen, H. Y., Teufel, L.W., Lee, R. L., (1993) Couple fluid flow and geomechanics in reservoir study-I, theory and governing equations, paper SPE 30752, paper presented at the SPE annual technical conference and exhibition, Dallas, USA., October

Choi, I., Cheema, T. and Islam, M.R., (1997) A new dual-porosity/dual permeability model with non-Darcian flow through fractures, Journal of Petroleum Science and Engineering, vol. 17, pp. 331-344

Dung, H.T. and Piracha, A.L., (2000) Journal of Energy and Development, vol. 25, no. 1, pp. 47-70

Editorial, (1996) Watching the world: tangible benefits of virtual reality, Oil & Gas Journal, vol. 94, no.13, p. 30

El-Sayed, S.M. and Abdel-Aziz, M.R., (2003) A comparison of Adomian's decomposition method and wavelet-Galerkin method for solving integro-differential equations, Applied Mathematics and Computation, vol. 136, pp. 151-159

Ertekin, T., Abou-Kassem, J.H., and King, G.R., (2001) Basic applied reservoir simulation, SPE textbook series, vol. 7, 406 p., SPE: Richardson, TX

Feature, (1997) Caution expressed over industry optimism on 4D seismic technology, First Break, vol. 15, no. 2, p. 51

Finley, J.R., Pinter, J.D., and Satish, M.G., (1998) Automatic model calibration applying global optimization techniques, Journal of Environmental Modeling and Assessment, vol. 3, no. 1-2, pp. 117-126

Hettema, M., Papamichos, E. and Schutjens, P., (2002) Subsidence delay: Field observations and analysis, Oil and Gas Science and Technology, Rev. IFP, vol. 57, no. 5, pp. 443-458

Hojka, K., Dusseault, M.B. and Bogobowicz, A.D., (1993) Analytical solutions for transient thermoplastic stress fields around a wellbore during fluid injection into permeable media, Journal of Canadian Petroleum Technology, vol. 32, no. 4, pp. 49-57

Hossain, M.E., Ketata, C., Khan, M.I. and Islam, M.R., (in press) Flammability and individual risk assessment for natural gas pipelines, International Journal of Risk Assessment and Management

Howarth, R.B. and Winslow, M.A., (1994) Energy use and CO_2 emissions reduction: Integrating pricing and regulatory policies, Energy – The International Journal, vol 19, pp. 855-867

Islam, M.R., (1993) Route to chaos in chemically enhanced thermal convection in porous media, Chemical Engineering Communications, vol. 124, pp. 77-95

Islam, M.R., (2000) Energy State of the Art 2000, Ed. C.Q. Zhou, Int. Sci. Serv., Charlottesville, VA, 21 pp.

Islam, M.R., (2001a) Emerging technologies in monitoring of oil and gas reservoirs, SPE paper no. 68804, Proc. SPE Western Regional Conference, Bakersfield, California, March 26-30

Islam, M.R., (2001b) Emerging technologies in subsurface monitoring of petroleum reservoirs, SPE 69440, SPE Latin America and Caribbean Petroleum Engineering Conference, Buenos Aries, Argentina, March 25 – 28

Islam, M.R., (2006a) Computing for the information age, Proc. of the 36th International Conference on Computers and Industrial Engineering, Keynote Speech, Taipei, Taiwan, June 20-23

Islam, M.R., (2006a) Comprehensive mathematical modelling of horizontal wells, paper no. 69, Proc. of the 2nd European Conference on the Mathematics of Oil Recovery, Latitudes Camargue, Arles, France, September 11-14

Islam, M.R. and Chakma, A., (1990) Comprehensive physical and numerical modeling of a horizontal well, SPE 20627, Proc. of the SPE Annual Conference and Exhibition, New Orleans.

Ketata, C., Satish, M., Islam, M.R., (2005a) Knowledge-based optimization of rotary drilling system, Proceedings of 2005 International Conference on Computational and Experimental Engineering and Science, Hyderabad, India, December 1-6

Ketata, C. Satish, M., Islam, M.R., (2005b) Stochastic evaluation of rock properties by sonic-while-drilling data processing in the oil and gas industry, Proceedings of 2005 International Conference on Computational and Experimental engineering and Science, Hyderabad, India, December 1-6

Ketata, C. Satish, M.G., and Islam, M.R., (2006a) The Meaningful zero, Proceedings of 36th Conference on Computer and Industries, June, Taiwan

Ketata, C. Satish, M.G., and M.R. Islam, (2006b) Cognitive work analysis of expert systems design and evaluation in the oil and gas industry, Proceedings of 36th Conference on Computer and Industries, June, Taiwan

Ketata, C., Satish, M.G., Islam, M.R., (2006c) The meaningful infinity, International Conference on Computational Intelligence for Modelling, Control and Automation-2006, Sydney, Australia, November 29–December 1

Ketata, C., Satish, M.G. and Islam, M.R., (2006d) Multiple Solution Nature of Chaos Number-Oriented Equations, International Conference on Computational Intelligence for Modelling, Control and Automation-2006, Sydney, Australia, November 29–December 1

Khan, M.I. and Islam, M.R., (2006) True sustainability in technological development and natural resources management, Nova Science Publishers, NY, USA

Khan, M.I. and Islam, M.R., (in press[1]) A handbook on sustainable oil and gas operations, Gulf Publishing Company, TX

Khan, M.I. and Islam, M.R., (in press[2]) Technological analysis and quantitative assessment of oil and gas development on the Scotian Shelf, Canada, International Journal of Risk Assessment and Management

Khan, M.I., Lakhal, S.Y., Satish, M., and Islam, M.R., (in press) Towards achieving sustainability: application of green supply chain model in offshore oil and gas operations, International Journal of Risk Assessment and Management

Kim, K.S. and van Stone, R.H., (1995) Hold time crack growth analysis at elevated temperatures, Engineering Fracture Mechanics, vol. 52, no. 3, pp. 433-444

Lakhal, S., H'mida, S., and Islam, M.R., (in press) Green supply chain parameters for a Canadian petroleum refinery company, Journal of Environmental Technology and Management

Liu, SW. and Ramirez, W.F., (1994) Optimal control of three-dimensional steam flooding process, Journal of Petroleum Science and Engineering, vol. 11, pp. 137-154

Merle, H.A., Kentie, C.J.P., van Opstal, G.H.C. and Schneider, G.M.G., (1976) The Bachaquero study - A composite analysis of the behavior of a compaction drive/solution gas drive reservoir, SPE Journal of Petroleum Technology, pp. 1107-1115, September

Mufti, A.A., Tadros, G., and Jones, P.R., (1997) Field assessment of fibre-optic Bragg grating strain sensors in the Confederation Bridge, Canadian Journal of Civil Engineering, vol. 24, no. 6, pp. 963–966

Mustafiz, S., Belhaj, H., Ma, F., Satish, M., Islam, M.R., (2005a) Modeling horizontal well oil production using modified Brinkman's model, Proc. ASME International Mechanical Engineering Congress and Exposition (IMEC*E)*, Orlando, Florida, USA, Nov. 5-11.

Mustafiz, S., Biazar, J. and Islam, M.R., (2005b) An Adomian decomposition solution to the modified Brinkman model (MBM) for a 2-dimensional, 1-phase flow of petroleum fluids, Proc. CSCE 33rd Annual Conference, Toronto, Canada, June 2-4

Mustafiz, S. and Islam, M. R., (2005) Adomian decomposition of two-phase, two-dimensional non-linear PDEs as applied in well testing, Proc. 4th International Conference on Computational Heat and Mass Transfer, Paris-Cachan, May 17-20

Mustafiz, S., Moussavizadegan, H., and Islam, M.R., (2006a) The effects of linearization on solutions of reservoir engineering problems, Journal of Petroleum Science and Technology, accepted for publication, July, 17 pg.

Mustafiz, S., Moussavizadegan, H., and Islam, M.R., (2006b) Adomian decomposition of Buckley-Leverett equation with capillary effects, Journal of Petroleum Science and Technology, submitted for publication, August

Naami, A.M., Catania, P., and Islam, M.R., (1999) Numerical and experimental modeling of viscous fingering in two-dimensional consolidated porous medium, CIM paper no. 118, CIM conference, Regina, October

Nouri, A., Vaziri, H. and Islam, M.R., (2002) A new theory and methodology for modeling sand production, Energy Sources, vol. 24, no. 11, pp. 995-1008

Nouri, A., Vaziri, H., Kuru, E. and Islam, R., (2006) A Comparison of Two Sanding Criteria in Physical and Numerical Modeling of Sand Production, Journal of Petroleum Science and Engineering, vol. 50, pp. 55-70

Pedrosa, Jr., Oswaldo A. and Aziz, K., (1986) Use of a Hybrid Grid in Reservoir Simulation, SPE 13507, *SPE Reservoir Engineering*, pp. 611-621, November.

Rahman, M. A., Mustafiz, S., Biazar, J., Koksal, M. and Islam, M. R., (in press) Investigation of a novel perforation technique in petroleum wells - perforation by drilling, Journal of the Franklin Institute

Saghir, M.Z., Chaalal, O. and Islam, M.R., (2000) Experimental and numerical modeling of viscous fingering, Journal of Petroleum Science and Engineering, vol. 26, no. 1-4, pp. 253-262

Saghir, M.Z., Vaziri, H. and Islam, M.R., (2001) Heat and mass transfer modeling of fractured formations, Journal of Computational Fluid Dynamics, vol. 15, no. 4, pp. 279-292

Sarma, P., Durlofsky, L.J., Aziz, K. and Chen, W.H., (2006) Efficient real-time reservoir management using adjoint-based optimal control and model updating, Computational Geosciences, vol. 10, pp. 3-36

Shapiro, R., Zatzman, G.M., Mohiuddin, Y. (in press) Towards understanding the science of disinformation, Journal of Nature Science and Sustainable Technology

Standenes, S., (1995) Seismic monitoring – a tool for improved reservoir management, SEISMIC 95, London

Stickey, D.C., (1993) New forces in international energy law: A discussion of political, economic, and environmental forces within the current international energy market, Tulsa Journal of Comparative and International Law, vol. 1, no. 1, p. 95.

Tidwell, V.C., and Robert, J.G., (1995) Laboratory investigation of matrix imbibition from a flow fracture, Geophysical Research Letters, vol. 22, pp. 1405-1408

Tortike, W.S. and Farouq Ali, S.M., (1987) A framework for multiphase nonisothermal fluid flow in a deforming heavy oil reservoir, SPE 16030, 9th SPE symposium on reservoir simulation, San Antonio, TX, February 1-4

Vaziri, H.H., Xiao, Y., Islam, R. and Nouri, A., (2003) Numerical modeling of seepage-induced sand production in oil and gas reservoirs, Journal of Petroleum Science and Engineering, vol. 36, pp. 71-86

Yin, X.C. and Liu, X.H., (1994) Investigations of fracture instability in crack growth for several metals- Part I: Experimental results, International Journal of Fracture, vol. 69, no. 2, pp.123-143

Wazwaz, A.M., (2001) A new algorithm for calculating Adomian polynomials for nonlinear operators, Applied Mathematics and Computation, vol. 111, no. 1, pp. 33–51

Wazwaz, A.M. and El-Sayed, S.M., (2001) A new modification of Adomian decomposition method for linear and nonlinear operators, Applied Mathematics and Computation, vol. 122, no. 3, pp. 393-405

Zaman, M., Bjorndalen, N. and Islam, M.R., (2004) Detection of precipitation in pipelines, Petroleum Science and Technology, vol. 22, no. 9-10, pp. 1119-1141

Zaman, M., Agha, K.R. and Islam, M.R., (2006) Laser based detection of paraffin in crude oil samples: Numerical and experimental study, Petroleum Science and Technology, vol. 24, no. 1, pp. 7-22

Zatzman, G.M., and Islam, M.R., (in press[1]) Natural gas pricing, in Mokhatab, S., Speight, J.G., and Poe, W.A., editors, Handbook of natural gas transmission and processing, Elsevier Inc.

Zatzman, G.M. and Islam, M.R., (in press[2]) Economics of intangibles: Nova Science Pulisher, NY, USA

Zekri, A.Y., Mustafiz, S., Chaalal, O. and Islam, M.R., (2006) The effects of thermal shock on homogenous and fractured carbonate formation, Journal of Petroleum Science and Technology, submitted for publication

2.8. Appendices

2.8.1. Appendix A: Figures

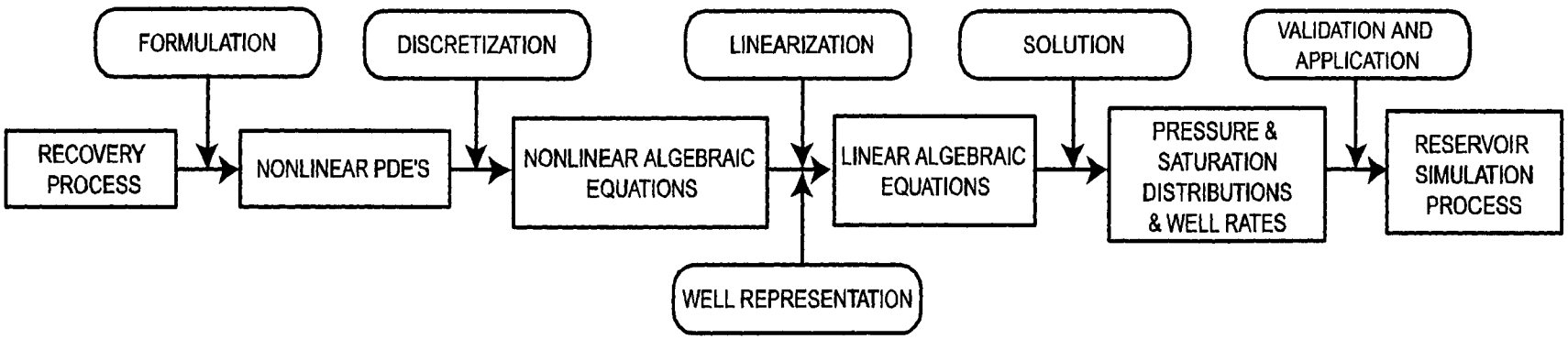

Fig. 2.1. Major steps used to develop reservoir simulators (redrawn from Odeh, 1982)

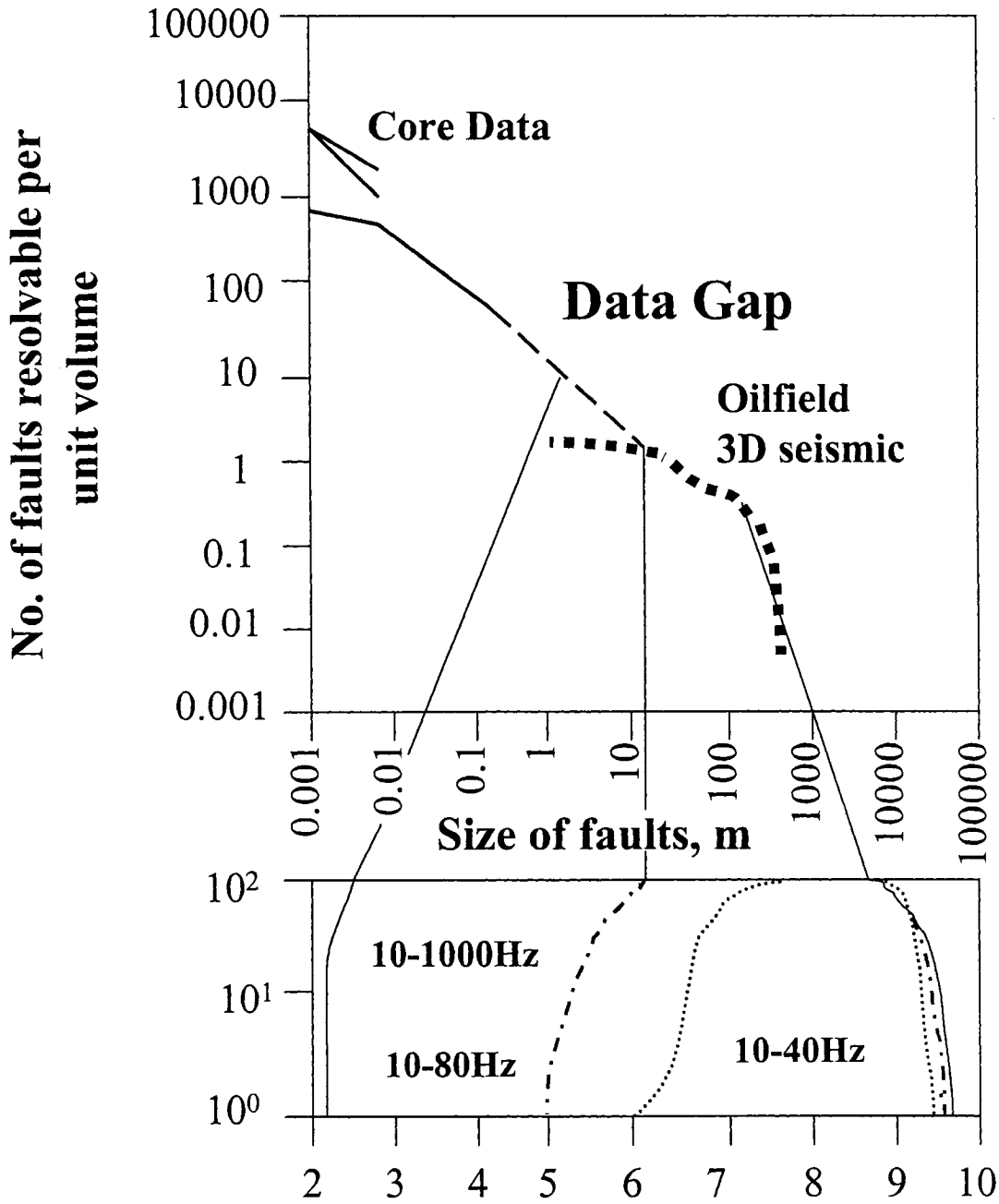

Fig. 2.2. Data gap in geophysical data (Islam, 2001a); reservoir simulators can now handle as many as billion grid blocks. However, monitoring technology has not been advanced enough to provide realistic data for those grid blocks

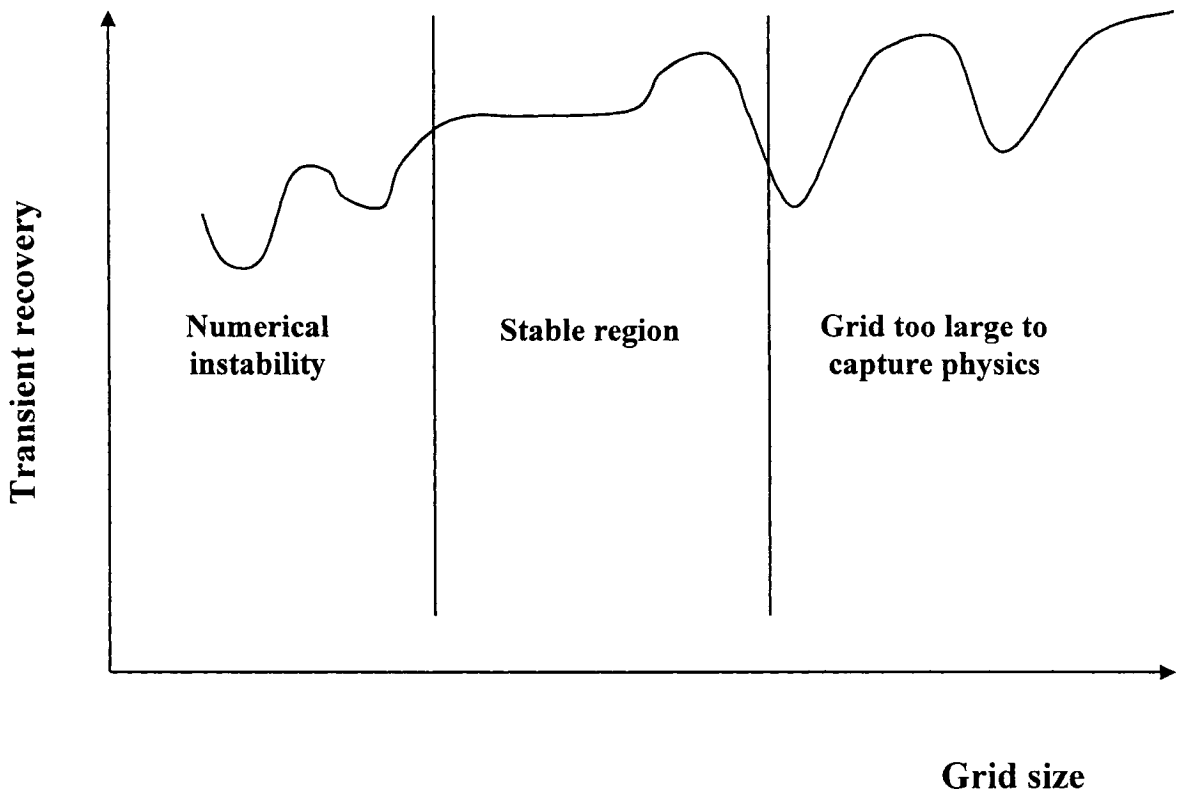

Fig. 2.3. The problem with the finite difference approach has been the dependence on grid size and the loss of information due to scaling up (Islam, 2001b).

Chapter 3

3 NEW SIMPLE EQUATIONS FOR INTERBLOCK GEOMETRIC FACTORS AND BULK VOLUMES IN SINGLE-WELL SIMULATION

3.1. Abstract

This paper presents new equations for the calculation of interblock geometric factors and bulk volume of blocks in radial-cylindrical coordinates for both block-centered grid and point-distributed grid. The new equations require the knowledge of logarithmic spacing constant (α_{lg}) only for interblock geometric factor calculations and both logarithmic spacing constant (α_{lg}) and radius of pressure points (r_i) for bulk volume calculations. The new equations are derived from those available in the literature, but are simple and do away with the estimation, in the radial direction, of one set of block boundaries for transmissibility calculations and another set of block boundaries for bulk volume calculations.

3.2. Introduction

Single-well simulation is often used to study water and gas conning in wells (MacDonald and Coats, 1970), to assess the effect of completion/production strategies of individual wells, to create well production pseudo functions to conduct 2D areal simulation runs (Chappelear and Hirasaki, 1976), and to aid in matching water-cut and Gas-Oil Ratio (GOR) of individual wells during history matching (Emmanuel and Cook, 1974). Gridblock dimensions in block-centered grid (or gridpoint spacing in point-distributed grid) in the θ- and z-directions and properties such as permeability, porosity, and elevation are required for each gridblock (or gridpoint). The location of gridpoints or the

points that represent gridblocks in the r-direction, bulk volumes, and interblock geometric factors are calculated internally in the simulator. Their calculation must satisfy certain conditions involving the estimation of the location in the r-direction of pressure points, block boundaries for transmissibility (or interblock geometric factor) calculations (logarithmic spacing in r), and block boundaries for bulk volume calculations (logarithmic spacing in r^2). This requires complicated logic in programming and is a source of confusion in reservoir simulation. Furthermore, such block boundaries in the r-direction are not needed in interpretation of simulation results. Therefore, the purpose of this paper is to develop simple and explicit equations for the calculation of interblock geometric factors and block bulk volumes for single-well simulation.

3.3. Current equations

The flow equations in radial-cylindrical coordinates have transmissibilities in the r-, θ-, and z-directions that are defined as:

$$T_{r_{i\pm1/2,j,k}} = G_{r_{i\pm1/2,j,k}} f_{r_{i\pm1/2,j,k}}, \tag{3.1a}$$

$$T_{\theta_{i,j\pm1/2,k}} = G_{\theta_{i,j\pm1/2,k}} f_{\theta_{i,j\pm1/2,k}}, \tag{3.1b}$$

and

$$T_{z_{i,j,k\pm1/2}} = G_{z_{i,j,k\pm1/2}} f_{z_{i,j,k\pm1/2}}, \tag{3.1c}$$

where G = geometric factor and f = a function of pressure for single-phase flow ($f = \frac{1}{\mu B}$) or a function of pressure and fluid saturation for multi-phase flow (e.g., $f = \frac{k_{rp}}{\mu_p B_p}$). The grid construction in the θ- and z-directions (gridblock dimensions or gridpoints spacing and block boundaries) is the same as that used in rectangular coordinates for both block-centered grid and point-distributed grid. In the r-direction,

however, points representing gridblocks and gridpoints are spaced such that pressure drops between neighboring points are equal, block boundaries for transmissibility calculations are spaced logarithmically in r to warrant that the radial flow rates between neighboring points using the integrated continuous and discretized forms of Darcy's law are identical, and block boundaries for bulk volume calculations are spaced logarithmically in r^2 to warrant that the actual and discretized bulk volumes of blocks are equal (Aziz and Settari, 1979; Ertekin et al., 2001). Therefore, the radii for the pressure points ($r_{i\pm1}$), transmissibility calculations ($r^L_{i\pm1/2}$), and bulk-volume calculations ($r_{i\pm1/2}$) are calculated as follows.

For pressure points,

$$r_{i+1} = \alpha_{lg} r_i = \alpha_{lg}^i r_1 \tag{3.2}$$

for $i = 1,2,3...n_r - 1$.

For interblock geometric factors,

$$r^L_{i+1/2} = \frac{r_{i+1} - r_i}{\log_e(r_{i+1}/r_i)} \tag{3.3}$$

for $i = 1,2,3...n_r - 1$

and

$$r^L_{i-1/2} = \frac{r_i - r_{i-1}}{\log_e(r_i/r_{i-1})} \tag{3.4}$$

for $i = 2,3...n_r$.

For block bulk volume,

$$r^2_{i+1/2} = \frac{r^2_{i+1} - r^2_i}{\log_e(r^2_{i+1}/r^2_i)} \tag{3.5}$$

for $i = 1,2,3...n_r - 1$

and

$$r_{i-1/2}^2 = \frac{r_i^2 - r_{i-1}^2}{\log_e(r_i^2 / r_{i-1}^2)} \tag{3.6}$$

for $i = 2,3...n_r$.

For block-centered grid, α_{lg}, r_1 and bulk volume of Gridblock (i, j, k) are calculated using-

$$\alpha_{lg} = \left(\frac{r_e}{r_w}\right)^{1/n_r}, \tag{3.7}$$

$$r_1 = [\alpha_{lg} \log_e(\alpha_{lg})/(\alpha_{lg} - 1)]r_w, \tag{3.8}$$

and

$$V_{b_{i,j,k}} = (r_{i+1/2}^2 - r_{i-1/2}^2)(\tfrac{1}{2}\Delta\theta_j)\Delta z_{i,j,k} \tag{3.9a}$$

for $i = 1,2,3...n_r - 1$, $j = 1,2,3...n_\theta$, $k = 1,2,3...n_z$;

and

$$V_{b_{n_r,j,k}} = (r_e^2 - r_{n_r-1/2}^2)(\tfrac{1}{2}\Delta\theta_j)\Delta z_{n_r,j,k} \tag{3.9b}$$

for $j = 1,2,3...n_\theta$, $k = 1,2,3...n_z$.

For point-distributed grid, α_{lg}, r_1 and bulk volume of Gridpoint (i, j, k) are calculated using-

$$\alpha_{lg} = \left(\frac{r_e}{r_w}\right)^{1/(n_r-1)}, \tag{3.10}$$

$$r_1 = r_w, \tag{3.11}$$

and

$$V_{b_{i,j,k}} = (r_{i+1/2}^2 - r_{i-1/2}^2)(\tfrac{1}{2}\Delta\theta_j)\Delta z_k. \tag{3.12a}$$

Note that $r_{i-1/2}^2 = r_w^2$ for $i = 1$ and $r_{i+1/2}^2 = r_e^2$ for $i = n_r$. That is to say, equation 3.12a applies for $i = 2,3...n_r - 1$.

$$V_{b_{1,j,k}} = (r_{1+1/2}^2 - r_w^2)(\tfrac{1}{2}\Delta\theta_j)\Delta z_k, \tag{3.12b}$$

for $i = 1$,

and

$$V_{b_{n_r,j,k}} = (r_e^2 - r_{n_r-1/2}^2)(\tfrac{1}{2}\Delta\theta_j)\Delta z_k, \tag{3.12c}$$

for $i = n_r$.

The geometric factors are calculated next using Table 3.1 for block-centered grid and Table 3.2 for point-distributed grid.

In Tables 3.1 and 3.2, r_i, $r_{i\pm1/2}$, and $r_{i\pm1/2}^L$ depend on the value of Subscript i only for $j = 1,2,3...n_\theta$ and $k = 1,2,3...n_z$; $\Delta\theta_j$ and $\Delta\theta_{j\pm1/2}$ depend on the value of Subscript j only for $i = 1,2,3...n_r$ and $k = 1,2,3...n_z$. Δz_k and $\Delta z_{k\pm1/2}$ in Table 3.2 depend on the value of Subscript k only for $i = 1,2,3...n_r$ and $j = 1,2,3...n_\theta$, whereas in Table 3.1, $\Delta z_{i,j,k}$ and $\Delta z_{i,j,k\pm1/2}$ depend on the value of Subscripts i, j, and k for $i = 1,2,3...n_r$; $j = 1,2,3...n_\theta$; and $k = 1,2,3...n_z$. This difference is a result of grid construction in block-centered and point-distributed grids.

3.4. Development of new equations

Abou-Kassem et al. (2006) have pointed out that equations 3.3 through 3.6 can be expressed in terms of r_i and α_{lg} only as shown in Appendix A:

$$r^{L}_{i+1/2} = \{(\alpha_{lg} - 1)/[\log_e(\alpha_{lg})]\} r_i \tag{3.13}$$

for $i = 1,2,3...n_r - 1$;

$$r^{L}_{i-1/2} = \{(\alpha_{lg} - 1)/[\alpha_{lg} \log_e(\alpha_{lg})]\} r_i \tag{3.14}$$

for $i = 2,3...n_r$;

$$r^{2}_{i+1/2} = \{(\alpha^2_{lg} - 1)/[\log_e(\alpha^2_{lg})]\} r^2_i \tag{3.15}$$

for $i = 1,2,3...n_r - 1$;

$$r^{2}_{i-1/2} = \{(\alpha^2_{lg} - 1)/[\alpha^2_{lg} \log_e(\alpha^2_{lg})]\} r^2_i \tag{3.16}$$

for $i = 2,3...n_r$.

In addition, the quotients: $r_i / r^{L}_{i-1/2}$, $r^{L}_{i-1/2} / r_{i-1}$, $r^{L}_{i+1/2} / r_i$, $r_{i+1} / r^{L}_{i+1/2}$, and $r^{L}_{i+1/2} / r^{L}_{i-1/2}$ are functions of the logarithmic spacing constant α_{lg} only as expressed in equations A-12, A-15, A-7, A-10, and A-17, respectively.

$$r_i / r^{L}_{i-1/2} = [\alpha_{lg} \log_e(\alpha_{lg})]/(\alpha_{lg} - 1), \tag{3.17}$$

$$r^{L}_{i-1/2} / r_{i-1} = (\alpha_{lg} - 1)/\log_e(\alpha_{lg}), \tag{3.18}$$

$$r^{L}_{i+1/2} / r_i = (\alpha_{lg} - 1)/\log_e(\alpha_{lg}), \tag{3.19}$$

$$r_{i+1} / r^{L}_{i+1/2} = [\alpha_{lg} \log_e(\alpha_{lg})]/(\alpha_{lg} - 1), \tag{3.20}$$

and

$$r^{L}_{i+1/2} / r^{L}_{i-1/2} = \alpha_{lg}. \tag{3.21}$$

Further more, equation 3.9 or 3.12 can be rearranged as-

$$(\tfrac{1}{2}\Delta\theta_j)(r^{2}_{i+1/2} - r^{2}_{i-1/2}) = V_{b_{i,j,k}} / \Delta z_{i,j,k}. \tag{3.22}$$

Substitution of equations 3.17 through 3.22 into the equations in Tables 3.1 and 3.2 results in Tables 3.3 and 3.4, respectively.

For block-centered grid, equation 3.9a can be expressed as equation A-22.

$$V_{b_{i,j,k}} = \{(\alpha_{lg}^2 - 1)^2 / [\alpha_{lg}^2 \log_e(\alpha_{lg}^2)]\} r_i^2 (\tfrac{1}{2}\Delta\theta_j)\Delta z_{i,j,k} \qquad (3.2A)$$

for $i = 1,2,3,...n_{r-1}$; and equation 3.9b becomes equation A-26,

$$V_{b_{n_r,j,k}} = \{1 - [\log_e(\alpha_{lg})/(\alpha_{lg} - 1)]^2 (\alpha_{lg}^2 - 1)/[\alpha_{lg}^2 \log_e(\alpha_{lg}^2)]\} r_e^2 (\tfrac{1}{2}\Delta\theta_j)\Delta z_{n_r,j,k} \qquad (3.23b)$$

for $i = n_r$.

For point-distributed grid, equations 3.12a, 3.12b, and 3.12c can be expressed as equations A-22, A-31, and A-29, respectively (for $j = 1,2,3,...n_\theta$ and $k = 1,2,3,...n_z$):

$$V_{b_{i,j,k}} = \{(\alpha_{lg}^2 - 1)^2 / [\alpha_{lg}^2 \log_e(\alpha_{lg}^2)]\} r_i^2 (\tfrac{1}{2}\Delta\theta_j)\Delta z_k, \qquad (3.24a)$$

for $i = 2,3,...n_{r-1}$;

$$V_{b_{1,j,k}} = \{[(\alpha_{lg}^2 - 1)/\log_e(\alpha_{lg}^2)] - 1\} r_w^2 (\tfrac{1}{2}\Delta\theta_j)\Delta z_k, \qquad (3.24b)$$

for $i = 1$;

and

$$V_{b_{n_r,j,k}} = \{1 - (\alpha_{lg}^2 - 1)/[\alpha_{lg}^2 \log_e(\alpha_{lg}^2)]\} r_e^2 (\tfrac{1}{2}\Delta\theta_j)\Delta z_k, \qquad (3.24c)$$

for $i = n_r$.

3.5. Calculation of pore volumes and interblock geometric factors

3.5.1. Block-centered grid

The procedure for the calculation can be simplified using the following algorithm:

1. Define $\alpha_{lg} = \left(\frac{r_e}{r_w}\right)^{1/n_r}$. (3.7)

2. Let $r_1 = [\alpha_{lg} \log_e(\alpha_{lg})/(\alpha_{lg} - 1)]r_w$. (3.8)

3. Set $r_{i+1} = \alpha_{lg} r_i = \alpha_{lg}^i r_1$, (3.2)

   where $i = 1,2,3,...n_r - 1$.

4. Estimate block bulk volume using-

   $V_{b_{i,j,k}} = \{(\alpha_{lg}^2 - 1)^2 / [\alpha_{lg}^2 \log_e(\alpha_{lg}^2)]\} r_i^2 (\frac{1}{2}\Delta\theta_j)\Delta z_{i,j,k}$ (3.2A)

   for $i = 1,2,3,...n_r - 1$; $j = 1,2,3,...n_\theta$; and $k = 1,2,3,...n_z$;

   and

   $V_{b_{n_r,j,k}} = \{1 - [\log_e(\alpha_{lg})/(\alpha_{lg} - 1)]^2 (\alpha_{lg}^2 - 1)/[\alpha_{lg}^2 \log_e(\alpha_{lg}^2)]\} r_e^2 (\frac{1}{2}\Delta\theta_j)\Delta z_{n_r,j,k}$ (3.23b)

   for $i = n_r$;; $j = 1,2,3,...n_\theta$; and $k = 1,2,3,...n_z$.

5. Estimate interblock geometric factors in the radial, tangential, and vertical directions using the equations reported in Table 3.3.

3.5.2. Point-distributed grid

The procedure can be simplified using the following algorithm:

1. Define $\alpha_{lg} = \left(\frac{r_e}{r_w}\right)^{1/(n_r - 1)}$. (3.10)

2. Let $r_1 = r_w$. (3.11)

3. Set $r_{i+1} = \alpha_{lg} r_i = \alpha_{lg}^i r_1$, (3.2)

   where $i = 1,2,3,...n_r - 1$.

4. Estimate block bulk volume for $j = 1,2,3,...n_\theta$ and $k = 1,2,3,...n_z$ using

   $V_{b_{i,j,k}} = \{(\alpha_{lg}^2 - 1)^2 / [\alpha_{lg}^2 \log_e(\alpha_{lg}^2)]\} r_i^2 (\frac{1}{2}\Delta\theta_j)\Delta z_k$, (3.24a)

   for $i = 2,3,...n_{r-1}$;

$$V_{b_{1,j,k}} = \{[(\alpha_{lg}^2 - 1)/\log_e(\alpha_{lg}^2)] - 1\} r_w^2 (\tfrac{1}{2}\Delta\theta_j)\Delta z_k, \quad (3.24b)$$

for $i = 1$; and

$$V_{b_{n_r,j,k}} = \{1 - (\alpha_{lg}^2 - 1)/[\alpha_{lg}^2 \log_e(\alpha_{lg}^2)]\} r_e^2 (\tfrac{1}{2}\Delta\theta_j)\Delta z_k, \quad (3.24c)$$

for $i = n_r$.

5. Estimate interblock geometric factors in the radial, tangential, and vertical directions using the equations reported in Table 3.4.

It should be mentioned that equations 3.23 and 3.24, that are proposed in this paper for the calculation of block bulk volumes are simpler than equations 3.9 and 3.12, that have been reported in the literature because equations 3.23 and 3.24 use r_i and α_{lg} only. The proposed equations in Tables 3.3 and 3.4 for the calculation of interblock geometric factors in the radial, tangential, and vertical directions in radial-cylindrical coordinates are simpler and less confusing than those reported in the literature (Tables 3.1 and 3.2) because they use α_{lg} only. In fact, the quotient of the arguments of $\log_e$ terms that appear in Tables 3.1 and 3.2 are functions of the logarithmic spacing constant α_{lg} only as shown in equations A-8, A-10, A-12, A-15, and A-17. Therefore, estimation, in the radial direction, of block boundaries for transmissibility calculations and block boundaries for bulk volume calculations are no longer needed.

3.6. Conclusions

New equations for the calculation of interblock geometric factors and bulk volume of blocks in radial-cylindrical coordinates for both block-centered grid and point-distributed grid are presented. The bulk volume equations are expressed in terms of α_{lg} and r_i only. The interblock geometric factor equations are expressed in terms of α_{lg} only. The new equations are easier to program and eliminate confusion resulting from the estimation, in

the radial direction, of two different sets of block boundaries for transmissibility and bulk volume calculations.

3.7. Nomenclature

B = fluid formation volume factor, RB/STB [m^3/std m^3]

f( ) = function of

f = the pressure and/or saturation dependent term in transmissibility

G = interblock geometric factor

$G_{r_{i\pm1/2,j,k}}$ = interblock geometric factor between Block (i,j,k) and Block $(i\pm1,j,k)$ along the r direction in radial-cylindrical coordinates, defined in Tables 3.1, 3.2, 3.3, and 3.4

$G_{z_{i,j,k\pm1/2}}$ = interblock geometric factor between Block (i,j,k) and Block $(i,j,k\pm1)$ along the z direction in radial-cylindrical coordinates, defined in Tables 3.1, 3.2, 3.3, and 3.4

$G_{\theta_{i,j\pm1/2,k}}$ = interblock geometric factor between Block (i,j,k) and Block $(i,j\pm1,k)$ along the θ direction in radial-cylindrical coordinates, defined in Tables 3.1, 3.2, 3.3, and 3.4

k_r = permeability along the r direction in radial flow, md [μm^2]

k_{rp} = relative permeability to Phase p, dimensionless

k_z = permeability along the z axis, md [μm^2]

k_θ = permeability along the θ direction, md [μm^2]

$\log_e$ = natural logarithm

n_r = number of reservoir gridblocks (or gridpoints) along the r direction

n_z = number of reservoir gridblocks (or gridpoints) along the z axis

n_θ = number of reservoir gridblocks (or gridpoints) in the θ direction

p = pressure, psia [kPa]

r = distance in the r direction in the radial-cylindrical coordinate system, ft [m]

r_e = external radius in Darcy's law for radial flow, ft [m]

$r_{i\pm1}$ = r-direction coordinate of Point $i\pm1$, ft [m]

$r^L_{i\pm1/2}$ = radii for transmissibility calculations, defined by equations 13 and 14, ft [m]

$r^2_{i\pm1/2}$ = radii squared for bulk volume calculations, defined by equations 3.15 and 3.16, ft^2 [m^2]

r_w = well radius, ft [m]

$T_{r_{i\pm1/2,j,k}}$ = transmissibility between Point (i,j,k) and Point $(i\pm1,j,k)$ along the r direction at Time t^m, STB/D-psi or SCF/D-psi [std m^3/(d.kPa)]

$T_{z_{i,j,k\pm1/2}}$ = transmissibility between Point (i,j,k) and Point $(i,j,k\pm1)$ along the z axis, STB/D-psi or SCF/D-psi [std m^3/(d.kPa)]

$T_{\theta_{i,j\pm1/2,k}}$ = transmissibility between Point (i,j,k) and Point $(i,j\pm1,k)$ along the θ direction, STB/D-psi or SCF/D-psi [std m^3/(d.kPa)]

V_b = bulk volume, ft^3 [m^3]

$V_{b_{i,j,k}}$ = bulk volume of Block (i,j,k), ft^3 [m^3]

z = distance in the z direction in the Cartesian coordinate system, ft [m]

Δz = size of block or control volume along the z axis, ft [m]

Δz_k = size of Block k along the z axis, ft [m]

$\Delta z_{i,j,k}$ = size of Block (i,j,k) along the z axis, ft [m]

α_{lg} = logarithmic spacing constant, defined by equation 3.7 or 3.10, dimensionless

β_c = transmissibility conversion factor whose numerical value is 0.001127 for customary units or 0.0864 for SPE preferred metric units

θ = angle in the θ direction, rad

$\Delta\theta_j$ = size of Block (i,j,k) along the θ direction, rad

$\Delta\theta_{j\pm1/2}$ = angle between Point (i,j,k) and Point $(i,j\pm1,k)$ along the θ direction, rad

μ = fluid viscosity, cp [mPa.s]

Subscripts

i	=	index for gridblock, gridpoint, or point along the x or r direction
$i\pm1$	=	index for neighboring gridblock, gridpoint, or point along the x or r direction
$i\pm1/2$	=	between i and $i\pm1$
(i,j,k)	=	index for gridblock, gridpoint, or point in x-y-z (or r-θ-z) space
j	=	index for gridblock, gridpoint, or point along the y or θ direction
$j\pm1$	=	index for neighboring gridblock, gridpoint, or point along the y or θ direction
$j\pm1/2$	=	between j and $j\pm1$
k	=	index for gridblock, gridpoint, or point along the z direction
$k\pm1$	=	index for neighboring gridblock, gridpoint, or point along the z direction
$k\pm1/2$	=	between k and $k\pm1$
lg	=	logarithmic
n_z	=	last gridblock (or gridpoint) in the z direction for a parallelepiped reservoir
p	=	phase
r	=	r-direction, relative
$r_{i\pm1/2}$	=	between i and $i\pm1$ along the r direction
z	=	z-direction
$z_{k\pm1/2}$	=	between k and $k\pm1$ along the z direction
θ	=	θ-direction
$\theta_{j\pm1/2}$	=	between j and $j\pm1$ along the θ direction

3.8. References

Abou-Kassem, J. H., Farouq Ali, S. M., and Islam, M. R., (2006) Petroleum reservoir simulation: A basic approach, Gulf Publishing Company, Houston, 445 p.

Aziz, K. and Settari, A., (1979) Petroleum reservoir simulation, Applied Science Publishers, London, UK

Chappelear, J. E. and Hirasaki, G. J., (1976) A model of oil/water coning for two-dimensional areal reservoir simulation, Society of Petroleum Engineering Journal, vol. 16, no. 2, pp. 65-72

Emmanuel, A. S. and Cook, G. W., (1974) Pseudorelative permeability for well modeling, Society of Petroleum Engineering Journal, vol. 14, no. 1, pp. 7-9

Ertekin, T., Abou-Kassem, J. H., and King, G. R., (2001) Basic applied reservoir simulation, SPE textbook series, vol. 7, 406 p., SPE: Richardson, TX

Farouq Ali, S. M., (1994) Elements of reservoir modeling and selected papers, Course notes: Petroleum engineering, Mineral engineering department, The University of Alberta

MacDonald, R. C. and Coats, K. H., (1970) Methods for numerical simulation of water and gas coning, Society of Petroleum Engineering Journal, vol. 10, no. 4, pp. 425-436

Pedrosa, Jr., Oswaldo, A. and Aziz, K., (1986) Use of hybrid grid in reservoir simulation, SPE 13507, SPE Reservoir Engineering, vol. 1, no. 6, pp. 611-621

3.9 Appendices

3.9.1. Appendix A: Derivation of equations

Derivation of equations 3.13 and 3.14

Using equation 3.2, one obtains-

$$r_{i+1} - r_i = \alpha_{lg} r_i - r_i = (\alpha_{lg} - 1) r_i \tag{A-1}$$

and

$$r_{i+1} / r_i = \alpha_{lg} . \tag{A-2}$$

Substitution of equations A-1 and A-2 into equation 3.3 yields equation 3.13,

$$r^L_{i+1/2} = \frac{r_{i+1} - r_i}{\log_e (r_{i+1} / r_i)} = \frac{(\alpha_{lg} - 1) r_i}{\log_e (\alpha_{lg})_i} = \{(\alpha_{lg} - 1) / \log_e (\alpha_{lg})\} r_i . \tag{A-3}$$

Using equation 3.2 and replacing Subscript $i+1$ with Subscript i,

$$r_i = \alpha_{lg} r_{i-1} \tag{A-4}$$

and

$$r_i / r_{i-1} = \alpha_{lg} . \tag{A-5}$$

Substitution of equations A-4 and A-5 into equation 3.4 yields equation 3.14,

$$r^L_{i-1/2} = \frac{r_i - r_{i-1}}{\log_e (r_i / r_{i-1})} = \frac{r_i - r_i / \alpha_{lg}}{\log_e (\alpha_{lg})} = \{(\alpha_{lg} - 1) / [\alpha_{lg} \log_e (\alpha_{lg})]\} r_i . \tag{A-6}$$

Evaluation of arguments of $\log_e$ ***in Tables 3.1 and 3.2***

Equation A-3 can be rearranged to give-

$$r_{i+1/2}^{L} / r_i = (\alpha_{lg} - 1) / \log_e(\alpha_{lg}), \tag{A-7}$$

from which-

$$\log_e(r_{i+1/2}^{L} / r_i) = \log_e[(\alpha_{lg} - 1) / \log_e(\alpha_{lg})]. \tag{A-8}$$

Equations A-2 and A-3 can be combined by eliminating r_i,

$$r_{i+1/2}^{L} = \frac{1}{\log_e(\alpha_{lg})}(\alpha_{lg} - 1)(r_{i+1} / \alpha_{lg}) = \{(\alpha_{lg} - 1) / [\alpha_{lg} \log_e(\alpha_{lg})]\} r_{i+1}. \tag{A-9}$$

Equation A-9 can be rearranged to give-

$$r_{i+1} / r_{i+1/2}^{L} = [\alpha_{lg} \log_e(\alpha_{lg})] / (\alpha_{lg} - 1), \tag{A-10}$$

from which-

$$\log_e(r_{i+1} / r_{i+1/2}^{L}) = \log_e\{[\alpha_{lg} \log_e(\alpha_{lg})] / (\alpha_{lg} - 1)\}. \tag{A-11}$$

Equation A-6 can be rearranged to give-

$$r_i / r_{i-1/2}^{L} = [\alpha_{lg} \log_e(\alpha_{lg})] / (\alpha_{lg} - 1), \tag{A-12}$$

from which-

$$\log_e(r_i / r_{i-1/2}^{L}) = \log_e\{[\alpha_{lg} \log_e(\alpha_{lg})] / (\alpha_{lg} - 1)\}. \tag{A-13}$$

Equations A-4 and A-6 can be combined by eliminating r_i,

$$r_{i-1/2}^{L} = \frac{1}{\log_e(\alpha_{lg})}[(\alpha_{lg}-1)/\alpha_{lg}](\alpha_{lg} r_{i-1}) = [(\alpha_{lg}-1)/\log_e(\alpha_{lg})]r_{i-1}. \quad \text{(A-14)}$$

Equation A-14 can be rearranged to give-

$$r_{i-1/2}^{L} / r_{i-1} = (\alpha_{lg}-1)/\log_e(\alpha_{lg}), \quad \text{(A-15)}$$

from which-

$$\log_e(r_{i-1/2}^{L} / r_{i-1}) = \log_e[(\alpha_{lg}-1)/\log_e(\alpha_{lg})]. \quad \text{(A-16)}$$

Equations A-3 and A-6 are combined to get-

$$r_{i+1/2}^{L} / r_{i-1/2}^{L} = \frac{\{(\alpha_{lg}-1)/\log_e(\alpha_{lg})\}r_i}{\{(\alpha_{lg}-1)/[\alpha_{lg}\log_e(\alpha_{lg})]\}r_i} = \alpha_{lg}, \quad \text{(A-17)}$$

from which-

$$\log_e(r_{i+1/2}^{L} / r_{i-1/2}^{L}) = \log_e(\alpha_{lg}). \quad \text{(A-18)}$$

Derivation of equations 3.15 and 3.16

Substitution of equations 3.2 and A-2 into equation 3.5 yields equation 3.15,

$$r_{i+1/2}^{2} = \frac{r_{i+1}^{2} - r_i^{2}}{\log_e(r_{i+1}^{2} / r_i^{2})} = \frac{(\alpha_{lg}^{2}-1)r_i^{2}}{\log_e(\alpha_{lg}^{2})} = [(\alpha_{lg}^{2}-1)/\log_e(\alpha_{lg}^{2})]r_i^{2}. \quad \text{(A-19)}$$

Substitution of equations A-4 and A-5 into equation 3.6 yields equation 3.16,

$$r_{i-1/2}^{2} = \frac{r_i^{2} - r_{i-1}^{2}}{\log_e(r_i^{2} / r_{i-1}^{2})} = \frac{(1-1/\alpha_{lg}^{2})r_i^{2}}{\log_e(\alpha_{lg}^{2})} = \{(\alpha_{lg}^{2}-1)/[\alpha_{lg}^{2}\log_e(\alpha_{lg}^{2})]\}r_i^{2}. \quad \text{(A-20)}$$

Derivation of equations 3.23 and 3.24 (block bulk volume equations)

Subtraction of equation A-20 from equation A-19 yields-

$$r_{i+1/2}^2 - r_{i-1/2}^2 = \frac{(\alpha_{lg}^2 - 1)}{\log_e(\alpha_{lg}^2)} r_i^2 - \frac{[(\alpha_{lg}^2 - 1)/\alpha_{lg}^2]}{\log_e(\alpha_{lg}^2)} r_i^2$$
$$= \frac{(\alpha_{lg}^2 - 1)(1 - 1/\alpha_{lg}^2)}{\log_e(\alpha_{lg}^2)} r_i^2 = \{(\alpha_{lg}^2 - 1)^2 / [\alpha_{lg}^2 \log_e(\alpha_{lg}^2)]\} r_i^2. \quad \text{(A-21)}$$

Combining equation 3.9a (or equation 3.12a) and equation A-21 yields-

$$V_{b_{i,j,k}} = \{(\alpha_{lg}^2 - 1)^2 / [\alpha_{lg}^2 \log_e(\alpha_{lg}^2)]\} r_i^2 (\tfrac{1}{2} \Delta\theta_j) \Delta z_{i,j,k}. \quad \text{(A-22)}$$

Equation A-22 can be used to calculate bulk volumes of blocks other than Gridblock n_r for block-centered grid and other than Gridpoints 1 and n_r for point-distributed grid.

For blocks having $i = n_r$ in block-centered grid, equation A-20 becomes-

$$r_{n_r - 1/2}^2 = \{(\alpha_{lg}^2 - 1)/[\alpha_{lg}^2 \log_e(\alpha_{lg}^2)]\} r_{n_r}^2, \quad \text{(A-23)}$$

where r_{n_r} can be expressed in terms of r_e by combining equations 3.2, 3.8, and 3.7 as follows-

$$r_{n_r} = \alpha_{lg}^{n_r - 1} r_1 = \alpha_{lg}^{n_r - 1} [\alpha_{lg} \log_e(\alpha_{lg}) / (\alpha_{lg} - 1)] r_w$$
$$= \alpha_{lg}^{n_r - 1} [\alpha_{lg} \log_e(\alpha_{lg}) / (\alpha_{lg} - 1)][r_e / \alpha_{lg}^{n_r}] = [\log_e(\alpha_{lg}) / (\alpha_{lg} - 1)] r_e. \quad \text{(A.24)}$$

Substitution of equation A-24 into equation A-23 gives-

$$r^2_{n_r-1/2} = \{(\alpha^2_{lg}-1)/[\alpha^2_{lg}\log_e(\alpha^2_{lg})]\}[\log_e(\alpha_{lg})/(\alpha_{lg}-1)]^2 r_e^2 . \quad \text{(A-25)}$$

Substitution of equation A-25 into equation 3.9b results in equation 3.23b,

$$V_{b_{n_r,j,k}} = \{1-[\log_e(\alpha_{lg})/(\alpha_{lg}-1)]^2(\alpha^2_{lg}-1)/[\alpha^2_{lg}\log_e(\alpha^2_{lg})]\} r_e^2(\tfrac{1}{2}\Delta\theta_j)\Delta z_{n_r,j,k} . \quad \text{(A-26)}$$

For blocks having $i = n_r$ in point-distributed grid,

$$\begin{aligned} r_{n_r} &= \alpha_{lg}^{n_r-1} r_1 = \alpha_{lg}^{n_r-1} r_w \\ &= \alpha_{lg}^{n_r-1}[r_e/\alpha_{lg}^{n_r-1}] = r_e. \end{aligned} \quad \text{(A.27)}$$

Substitution of equation A-27 into equation A-23 gives-

$$r^2_{n_r-1/2} = \{(\alpha^2_{lg}-1)/[\alpha^2_{lg}\log_e(\alpha^2_{lg})]\} r_e^2 . \quad \text{(A-28)}$$

Substitution of equation A-28 into equation 3.12c results in equation 3.24c,

$$V_{b_{n_r,j,k}} = \{1-(\alpha^2_{lg}-1)/[\alpha^2_{lg}\log_e(\alpha^2_{lg})]\} r_e^2(\tfrac{1}{2}\Delta\theta_j)\Delta z_k . \quad \text{(A-29)}$$

For blocks having $i = 1$ in point-distributed grid, equation A-19 becomes-

$$r^2_{1+1/2} = [(\alpha^2_{lg}-1)/\log_e(\alpha^2_{lg})] r_1^2 = [(\alpha^2_{lg}-1)/\log_e(\alpha^2_{lg})] r_w^2 . \quad \text{(A-30)}$$

Substitution of equation A-30 into equation 3.12b results in equation 3.24b,

$$V_{b_{1,j,k}} = \{[(\alpha^2_{lg}-1)/\log_e(\alpha^2_{lg})]-1\} r_w^2(\tfrac{1}{2}\Delta\theta_j)\Delta z_k . \quad \text{(A-31)}$$

3.9.2. Appendix B: Tables

Table 3.1. Interblock geometric factors for block-centered grid (Farouq Ali, 1994; Ertekin et al., 2001)

Direction	Geometric Factor
r	$G_{r_{i-1/2,j,k}} = \dfrac{\beta_c \Delta\theta_j}{\log_e(r_i / r^L_{i-1/2})/(\Delta z_{i,j,k} k_{r_{i,j,k}}) + \log_e(r^L_{i-1/2} / r_{i-1})/(\Delta z_{i-1,j,k} k_{r_{i-1,j,k}})}$
	$G_{r_{i+1/2,j,k}} = \dfrac{\beta_c \Delta\theta_j}{\log_e(r^L_{i+1/2} / r_i)/(\Delta z_{i,j,k} k_{r_{i,j,k}}) + \log_e(r_{i+1} / r^L_{i+1/2})/(\Delta z_{i+1,j,k} k_{r_{i+1,j,k}})}$
θ	$G_{\theta_{i,j\pm1/2,k}} = \dfrac{2\beta_c \log_e(r^L_{i+1/2} / r^L_{i-1/2})}{\Delta\theta_j /(\Delta z_{i,j,k} k_{\theta_{i,j,k}}) + \Delta\theta_{j\pm1} /(\Delta z_{i,j\pm1,k} k_{\theta_{i,j\pm1,k}})}$
z	$G_{z_{i,j,k\pm1/2}} = \dfrac{2\beta_c (\frac{1}{2}\Delta\theta_j)(r^2_{i+1/2} - r^2_{i-1/2})}{\Delta z_{i,j,k} / k_{z_{i,j,k}} + \Delta z_{i,j,k\pm1} / k_{z_{i,j,k\pm1}}}$

Table 3.2. Interblock geometric factors for point-distributed grid (Pedrosa and Aziz, 1986)

Direction	Geometric Factor
r	$G_{r_{i-1/2,j,k}} = \dfrac{\beta_c \Delta\theta_j \Delta z_k}{\log_e(r_i / r^L_{i-1/2}) / k_{r_{i,j,k}} + \log_e(r^L_{i-1/2} / r_{i-1}) / k_{r_{i-1,j,k}}}$
	$G_{r_{i+1/2,j,k}} = \dfrac{\beta_c \Delta\theta_j \Delta z_k}{\log_e(r^L_{i+1/2} / r_i) / k_{r_{i,j,k}} + \log_e(r_{i+1} / r^L_{i+1/2}) / k_{r_{i+1,j,k}}}$
θ	$G_{\theta_{i,j\pm1/2,k}} = \dfrac{2\beta_c \log_e(r^L_{i+1/2} / r^L_{i-1/2}) \Delta z_k}{\Delta\theta_{j\pm1/2} / k_{\theta_{i,j,k}} + \Delta\theta_{j\pm1/2} / k_{\theta_{i,j\pm1,k}}}$
z	$G_{z_{i,j,k\pm1/2}} = \dfrac{2\beta_c (\frac{1}{2}\Delta\theta_j)(r^2_{i+1/2} - r^2_{i-1/2})}{\Delta z_{k\pm1/2} / k_{z_{i,j,k}} + \Delta z_{k\pm1/2} / k_{z_{i,j,k\pm1}}}$

Table 3.3. New equations for interblock geometric factors in block-centered grids

Direction	Geometric Factor
r	$G_{r_{i-1/2,j,k}} = \dfrac{\beta_c \Delta\theta_j}{\{\log_e[\alpha_{lg}\log_e(\alpha_{lg})/(\alpha_{lg}-1)]/(\Delta z_{i,j,k}k_{r_{i,j,k}}) + \log_e[(\alpha_{lg}-1)/\log_e(\alpha_{lg})]/(\Delta z_{i-1,j,k}k_{r_{i-1,j,k}})\}}$
	$G_{r_{i+1/2,j,k}} = \dfrac{\beta_c \Delta\theta_j}{\{\log_e[(\alpha_{lg}-1)/\log_e(\alpha_{lg})]/(\Delta z_{i,j,k}k_{r_{i,j,k}}) + \log_e[\alpha_{lg}\log_e(\alpha_{lg})/(\alpha_{lg}-1)]/(\Delta z_{i+1,j,k}k_{r_{i+1,j,k}})\}}$
θ	$G_{\theta_{i,j\pm1/2,k}} = \dfrac{2\beta_c \log_e(\alpha_{lg})}{\Delta\theta_j/(\Delta z_{i,j,k}k_{\theta_{i,j,k}}) + \Delta\theta_{j\pm1}/(\Delta z_{i,j\pm1,k}k_{\theta_{i,j\pm1,k}})}$
z	$G_{z_{i,j,k\pm1/2}} = \dfrac{2\beta_c(V_{b_{i,j,k}}/\Delta z_{i,j,k})}{\Delta z_{i,j,k}/k_{z_{i,j,k}} + \Delta z_{i,j,k\pm1}/k_{z_{i,j,k\pm1}}}$

Table 3.4. New equations for interblock geometric factors in point-distributed grid

Direction	Geometric Factor
r	$G_{r_{i-1/2,j,k}} = \dfrac{\beta_c \Delta\theta_j \Delta z_k}{\log_e[\alpha_{lg}\log_e(\alpha_{lg})/(\alpha_{lg}-1)]/k_{r_{i,j,k}} + \log_e[(\alpha_{lg}-1)/\log_e(\alpha_{lg})]/k_{r_{i-1,j,k}}}$
	$G_{r_{i+1/2,j,k}} = \dfrac{\beta_c \Delta\theta_j \Delta z_k}{\log_e[(\alpha_{lg}-1)/\log_e(\alpha_{lg})]/k_{r_{i,j,k}} + \log_e[\alpha_{lg}\log_e(\alpha_{lg})/(\alpha_{lg}-1)]/k_{r_{i+1,j,k}}}$
θ	$G_{\theta_{i,j\pm1/2,k}} = \dfrac{2\beta_c \log_e(\alpha_{lg})\Delta z_k}{\Delta\theta_{j\pm1/2}/k_{\theta_{i,j,k}} + \Delta\theta_{j\pm1/2}/k_{\theta_{i,j\pm1,k}}}$
z	$G_{z_{i,j,k\pm1/2}} = \dfrac{2\beta_c (V_{b_{i,j,k}}/\Delta z_k)}{\Delta z_{k\pm1/2}/k_{z_{i,j,k}} + \Delta z_{k\pm1/2}/k_{z_{i,j,k\pm1}}}$

Chapter 4

4.1 THE EFFECTS OF LINEARIZATION ON SOLUTIONS OF RESERVOIR ENGINEERING PROBLEMS

4.1.1. Abstract

The natural processes are nonlinear. Each property is affected by the variation of other properties existing in a process. However, it is necessary to impose some simplification and linearization in order to obtain numerical description for majority of the problems in applied sciences. The simplification may take place in mathematical formulation and/or during numerical evaluation of a problem. This paper investigates the effects of nonlinearity in the flow equation of a petroleum reservoir. The petroleum industry is well-known for its intense use of computer models that employ various levels of linearization. Because the computational operation is repeated numerous times for billions of discrete gridblocks, any systematic error induced by linearization can have profound impact on predicted results. In this paper, the dependency of the fluid and formation properties on the variation of the reservoir pressure is evaluated during the solution of the flow equation using the *engineering approach*. The continuous functions and piecewise functions are applied to approximate the variation of viscosity, fluid formation volume factor and permeability. The computational results are compared with the linearized approximation for the variation of these properties. The approximation that imposes linearization on the mathematical formulation is also evaluated. The continuous nonlinear functions are not appropriate to approximate the variation of a process property. The best approximation may be obtained using the piecewise function such as spline function of different orders.

4.1.2. Introduction

In traditional practice, analogical, experimental and mathematical methods are used to predict reservoir performance. The mathematical method, however, is most commonly used by the petroleum community. Methods, such as material balance, decline curve, statistical and analytical techniques are the predominant ones that are used in a mathematical model. However, often it becomes extremely cumbersome to utilize some of these techniques. On the contrary, the advancement in numerical techniques for solving partial differential equations, computing facilities etc. have drawn tremendous attention to the researchers to opt-for computer-aided reservoir simulation. Such trend has resulted in developing reservoir simulators, which are capable of handling increasingly complicated enhanced oil recovery (EOR) techniques. The most common aspect among all the simulators is the development of a set of algebraic equations from a set of partial differential equations (PDEs). By utilizing the appropriate initial and boundary conditions, the reservoir behavior is captured in the simulation approach. Since the equations present the reservoir behavior, they must reflect the physical processes taking place. However, inclusion of all of the physical processes in the simulator is not simple and often requires simplifying assumptions (Ertekin et al., 2001). For example, the classical mathematical representation of the reservoir is described by the material balance equation and its fundamental principle is the conservation of mass. A number of assumptions are imbedded in the material balance equation: (a) rock and fluid properties do not change in space; (b) hydrodynamics of the fluid flow in the porous media is adequately described by Darcy's law; (c) fluid segregation is spontaneous and complete; (d) geometrical configuration of the reservoir is known and exact; (e) PVT data obtained in the laboratory with the same gas-liberation process (flash vs. differential) are valid in the field; (f) sensitive to inaccuracies in measured reservoir pressure. The model breaks down when no appreciable decline occurs in reservoir pressure, as in pressure maintenance operations. The mass-balance equation is also sensitive to inaccuracies in measured reservoir pressure. In addition, the model may breakdown during pressure

maintenance operations when no significant decline occurs in reservoir pressure. During hydrocarbon recovery, the past performance of numerous reservoirs is statistically accounted for to derive empirical correlations (statistical method), which are used for future predictions. Such method is limited to use only when the reservoir properties are within the limit of the regression database. Moreover, the estimation of a portion instead of the whole reservoir may lead to erroneous and unrealistic results as high as 50% (Ertekin et al., 2001).

Newton's calculus and difference-quotient formula are broadly used in any reservoir simulation. The history of differential calculus dates back to the time of Leibnitz and Newton and in this concept, the derivative of a continuous function to the function itself is related. In Newton's calculus, the change in magnitude and direction are independent of one another. There is no problem in having separate derivatives for each component of the vector or in superimposing their effects separately and regardless of order. That is what mathematicians mean when they describe or discuss Newton's derivative being used as a 'linear operator'. When the value of a function is inadequate to solve a problem, the rate at which the function changes, sometimes, becomes useful. Therefore, the derivatives are also important in reservoir simulation. In Newton's difference-quotient formula, the derivative of a continuous function is obtained. However, this method relies implicitly on the notion of approximating instantaneous moments of curvature, or infinitely small segments, by means of straight lines. This alone should have tipped everyone off that this derivative is a linear operator precisely because, and to the extent that, it examines change over time (or distance) within an already established function (Islam, 2006).

One of the most widely accepted mathematical techniques in reservoir simulation is the finite difference calculus, which is used to approximate values of functions and their derivatives at discrete points, where they are not known. This technique is also not free from assumptions and errors. Here the relationship between derivative and the finite

difference operators, e.g., forward difference operator, backward difference operator and the central difference operator is established through the Taylor series expansion. In other word, it assumes that a relationship between the operators for discrete points and the operators of the continuous functions is acceptable. In the Taylor series expansion, most well-behaved functions are converted to simple polynomials and it becomes an approximation of the function when the expansion is carried out for a finite number of terms and the remainder is ignored. The truncation of the Taylor series of the unknown variables after few terms leads to accumulation of error. Mathematically, it can be shown that most of the error occurs in the lowest order terms. There are also the forward difference and the backward difference approximations, which are the first order approximations to the first derivative. The approximation to the second derivative by central difference operator increases accuracy because of a second order approximation but it still suffers from the truncation problem (Mustafiz and Islam, 2006).

Implementation of the finite difference approximations results in finite difference equations. The discretization step involves the conversion of the continuous equations to finite difference equations, which are algebraic in nature. The solutions of the finite difference equations are obtained only at the discrete points. In reservoir simulation, these discrete points are defined either according to block-centered or point distributed grid system. However, the boundary condition, particularly the constant pressure boundary, may appear important in selecting the grid system with inherent restrictions and higher order approximations. Also, the solutions obtained for gridpoints are in contrast to the solutions of the continuous equations. In the finite difference scheme, the local truncation error or the local discretization error is not readily quantifiable because the calculation involves both continuous and discrete forms. Such difficulty can be overcome when the mesh-size or the time step or both are decreased leading to minimization in local truncation error. However, at the same time the computational operation increases, which eventually increases the round-off error.

In reservoir simulation, Darcy's law (1856) is considered to be a cornerstone. It describes the empirical relationship between fluid flow rate through a porous medium and potential gradient. There are also several assumptions in Darcy's law such as (a) the fluid is homogenous, single-phase and Newtonian, (b) no chemical reaction takes place between the fluid and the porous medium, (c) laminar flow conditions prevail, (d) permeability is a property of the porous medium, which is independent of pressure, temperature and the flowing fluid, (e) there is no slippage effect; e.g., Klinkenberg phenomenon, and (f) there is no electro-kinetic effect (Ertekin et al., 2001).

The solution techniques used in reservoir simulation are appropriate only for systems of linear equations. The use of these techniques, therefore, requires linearization of the finite difference equations. Such techniques include the explicit treatment of the transmissibility terms, simple iteration of the transmissibility terms, extrapolation of the transmissibility terms and fully implicit treatment of the transmissibility terms. Transmissibility, T, is a combination of viscosity, μ, formation volume factor, B, and geometric factor, G; where, μ and B are functions of pressure, P and temperature, T. In other words, while modeling single-phase flow, these techniques are used to linearize the pressure-dependent properties. The explicit method does not offer any improvement in the value of the nonlinearities as iterations progress. The simple iteration method presents improvement in the value of nonlinearities in a stepwise manner. In the fully implicit method, the improved value of nonlinearities falls on the tangent of the nonlinearities at the previous iteration as the iteration continues. The same methods are equally applicable to multiphase flow problems. Other linearization methods, such as the linearized-implicit method (MacDonald and Coats, 1970) and the semi-implicit method of Nolen and Berry (1972) are not applicable to single-phase problems. These two methods are used in multiphase problems to deal with nonlinearities due to fluid saturation only (Abou-Kassem et al., 2006).

A number of algorithms can be used to solve a given system of linear equations. The finite difference equations, if written for n simulation grids, produce n x n coefficient matrix. The direct and iterative are the two general methods used in reservoir simulation. Theoretically, the direct methods are capable of obtaining an exact solution after a fixed number of computations are carried out. However, it is assumed that the computer is able to take an infinite number of digits. In reality, no such computer, including the super ones, has limitations leading to round-off errors, no matter how insignificant they are. Numerous articles have been reported to improve the direct methods (i.e., Gaussian elimination, Gauss-Jordan reduction) including the Crout reduction, the Thomas' algorithm etc. Moreover, features such as sparse-matrix technique, pivoting, multiple known vectors and iterative improvements have also appeared to add improvements to the features of direct procedures (Ertekin et al., 2001). The iterative method has emerged as a solution scheme, for which, each iteration experiences gradual reduction of error if the scheme is converging. However, to reduce the slow convergence rate, and in turn, the monotony of the iterative procedure, significant advancements have been made. Factors such as convergence requirements, speed and storage needs have been addressed through earliest attempts of Jacobi iteration, Gauss-Seidel iteration, successive over relaxation (LSOR), block successive over relaxation (BSOR), alternating-direction-implicit-procedure (ADIP) etc. However, the development of more powerful, yet linear solution techniques, such as conjugate-gradient-like (CGL), has replaced the previously popular techniques in the 1960's and 1970's (Ertekin et al., 2001).

This paper investigates the effects of the variation of fluid and formation properties, the value of the time interval Δt and the simplification in formulation, on pressure of a single-phase (compressible fluid) flow problem. In addition, a new approach in search for multiple solutions resulting from nonlinearities is attempted.

4.1.3. Case study

An example (Abou-Kassem et al., 2006) on natural gas reservoir of 20 acre spacing and

30 ft net thickness is taken as the test case in this paper. The reservoir is horizontal and described by four gridblocks in the radial direction. It is also assumed that the reservoir has homogeneous and isotropic rock properties with k=15 md and φ = 0.13. A vertical well (d=0.5 ft) produces from the reservoir at a rate of 1 MMscf/D. The initial reservoir pressure is 4015 psia. The pressure distribution at different time intervals needs to be calculated. The flow is considered to be in radial direction without any variation in z– and θ–directions.

4.1.4. Governing equations

The governing equations of fluid flow through porous media are obtained by combining two basic engineering concepts including the principle of mass conservation and the constitutive equation. In reservoir simulation, the constitutive property, i.e., the rate of fluid movement into (or out of) the reservoir volume element is described by Darcy's law and is related to potential gradient. Therefore, the combination of Darcy's law with the conservation of mass results in the flow equation. The resulting differential form of the flow equation is nonlinear. The discrete form of the flow equation may be obtained directly using the *engineering approach* (Abou-Kassem et al., 2006) without using the partial differential equations. During simulation, the reservoir is divided into gridblocks in different directions and the flow equation is written for each of these gridblocks. Finally, the resulting equations are a system of nonlinear algebraic equations that give the pressure distribution along the reservoir at any time.

The general form of the flow equation for Gridblock n can be written in the *engineering approach* (Abou-Kassem et al., 2006) as

$$\sum_{\ell \in \xi_n} T^m_{\ell,n}\left[(p^m_\ell - p^m_n) - \gamma^m_{\ell,n}(Z^m_\ell - Z^m_n)\right] + \sum_{\ell \in \xi_n} q^m_{sc_{\ell,n}} + q^m_{sc_n} = \frac{V_{b_n}}{\alpha_c \Delta t}\left[\left(\frac{\phi}{B}\right)^{\nu+1}_n - \left(\frac{\phi}{B}\right)^{\nu}_n\right] \qquad (4.1.1)$$

The transmissibility along the *r*-direction in cylindrical coordinates is defined as

$$T_{r_{i\mp\frac{1}{2},j,k}} = G_{r_{i\mp\frac{1}{2},j,k}} \left(\frac{1}{\mu B}\right)_{r_{i\mp\frac{1}{2},j,k}} \tag{4.1.2}$$

Logarithmic spacing constant (α_{lg}), geometric factor (G) in the *r*-direction and bulk volume (V_b) are calculated using the recently reported simple and explicit equations (Abou-Kassem et al., in press)

$$\alpha_{lg} = \left(\frac{r_e}{r_w}\right)^{1/n_r} \tag{4.1.3}$$

$$G_{r_{i-1/2,j,k}} = \frac{\beta_c \Delta\theta_j}{\{\log_e[\alpha_{lg}\log_e(\alpha_{lg})/(\alpha_{lg}-1)]/(\Delta z_{i,j,k} k_{r_{i,j,k}}) + \log_e[(\alpha_{lg}-1)/\log_e(\alpha_{lg})]/(\Delta z_{i-1,j,k} k_{r_{i-1,j,k}})\}} \tag{4.1.4}$$

$$G_{r_{i+1/2,j,k}} = \frac{\beta_c \Delta\theta_j}{\{\log_e[(\alpha_{lg}-1)/\log_e(\alpha_{lg})]/(\Delta z_{i,j,k} k_{r_{i,j,k}}) + \log_e[\alpha_{lg}\log_e(\alpha_{lg})/(\alpha_{lg}-1)]/(\Delta z_{i+1,j,k} k_{r_{i+1,j,k}})\}} \tag{4.1.5}$$

$$V_{b_{i,j,k}} = \{(\alpha_{lg}^2-1)^2/[\alpha_{lg}^2\log_e(\alpha_{lg}^2)]\} r_i^2 (\tfrac{1}{2}\Delta\theta_j)\Delta z_{i,j,k} \tag{4.1.6}$$

for $i = 1,2,3,...n_r - 1$; $j = 1,2,3,...n_\theta$; and $k = 1,2,3,...n_z$;

$$V_{b_{n_r,j,k}} = \{1-[\log_e(\alpha_{lg})/(\alpha_{lg}-1)]^2(\alpha_{lg}^2-1)/[\alpha_{lg}^2\log_e(\alpha_{lg}^2)]\} r_e^2 (\tfrac{1}{2}\Delta\theta_j)\Delta z_{n_r,j,k} \tag{4.1.7}$$

for $i = n_r$;; $j = 1,2,3,...n_\theta$; and $k = 1,2,3,...n_z$.

4.1.5. Results and discussion

The flow equation 4.1.1 can be written as

$$\sum_{\ell\in\psi_n} T_{\ell,n}^m [(p_\ell^m - p_n^m)] + q_{sc_n}^m = \frac{V_{b_n}}{\alpha_c \Delta t}\left[\left(\frac{\phi}{B}\right)_n^{n+1} - \left(\frac{\phi}{B}\right)_n^n\right] \tag{4.1.8}$$

Equation 4.1.8 can be simplified to Eq. 4.1.9 if $\frac{\phi}{B}$ is considered to be a linear function of pressure.

$$\sum_{\ell \in \Omega_n} T^m_{\ell,n}\left[p^m_\ell - p^m_n\right] + q^m_{sc_n} = \frac{V_{b_n}}{\alpha_c \Delta t}\left(\frac{\phi}{B_g}\right)'_n \left[p^{n+1}_n - p^n_n\right] \tag{4.1.9}$$

where, $\left(\frac{\phi}{B}\right)'_n$ is the chord slope of $\left(\frac{\phi}{B}\right)_n$ between $P^{\nu+1}_n$ and P^{ν}_n.

Although, μ and B are function of the fluid temperature and pressure, it is assumed that temperature remains constant throughout the reservoir during the production period. The gas formation volume factor, *GFVF* or B_g, and viscosity, μ as functions of reservoir pressure are shown in Table 4.1.1.

They are expressed in mathematical form using the polynomial of fourth order for μ and the power function for B as shown in Fig. 4.1.1(a). These two fluid properties are also fitted with the spline functions of different degrees as shown in Fig. 4.1.1(b). It is found that the quadratic and cubic splines give a very good approximation to the variation of μ and B with P.

The flow equation for the gridblocks as specified in Eq. 4.1.8 can also be expressed in the following form

$$\begin{cases} G\left(\frac{1}{\mu B}\right)^m_j (P^m_2 - P^m_1) - 10^6 = \beta_1\left[\left(\frac{\phi}{B}\right)^{\nu+1}_1 - \left(\frac{\phi}{B}\right)^{\nu}_1\right] \\ G\left(\frac{1}{\mu B}\right)^m_j (P^m_1 - P^m_2) + G\left(\frac{1}{\mu B}\right)^m_j (P^m_3 - P^m_2) = \beta_2\left[\left(\frac{\phi}{B}\right)^{\nu+1}_2 - \left(\frac{\phi}{B}\right)^{\nu}_2\right] \\ G\left(\frac{1}{\mu B}\right)^m_j (P^m_2 - P^m_3) + G\left(\frac{1}{\mu B}\right)^m_j (P^m_4 - P^m_3) = \beta_3\left[\left(\frac{\phi}{B}\right)^{\nu+1}_3 - \left(\frac{\phi}{B}\right)^{\nu}_3\right] \\ G\left(\frac{1}{\mu B}\right)^m_j (P^m_3 - P^m_4) = \beta_4\left[\left(\frac{\phi}{B}\right)^{\nu+1}_4 - \left(\frac{\phi}{B}\right)^{\nu}_4\right] \end{cases} \tag{4.1.10}$$

and according to Eq. 4.1.9 as

$$\begin{cases} G\left(\frac{1}{\mu B}\right)_j^m (P_2^m - P_1^m) - 10^6 = \beta_1 \left(\frac{\phi}{B}\right)_1^t (P_1^{\nu+1} - P_1^{\nu}) \\ G\left(\frac{1}{\mu B}\right)_1^m (P_1^m - P_2^m) + G\left(\frac{1}{\mu B}\right)_3^m (P_3^m - P_2^m) = \beta_2 \left(\frac{\phi}{B}\right)_2^t (P_2^{\nu+1} - P_2^{\nu}) \\ G\left(\frac{1}{\mu B}\right)_2^m (P_2^m - P_3^m) + G\left(\frac{1}{\mu B}\right)_4^m (P_4^m - P_3^m) = \beta_3 \left(\frac{\phi}{B}\right)_3^t (P_3^{\nu+1} - P_3^{\nu}) \\ G\left(\frac{1}{\mu B}\right)_3^m (P_3^m - P_4^m) = \beta_4 \left(\frac{\phi}{B}\right)_4^t (P_4^{\nu+1} - P_4^{\nu}) \end{cases} \quad (4.1.11)$$

where, $\beta_i = \dfrac{V_{b_i}}{\alpha_c \Delta t}$ is constant for each block. The function $\left(\dfrac{1}{\mu B}\right)_j^m$ depends on pressure distribution in the reservoir. Two cases regarding subscript *j* are considered

I) pressure at the upstream, and

II) pressure at the *i*-th Gridblock.

The superscript *m* is related to the time step, which is taken as *m=v+1*

Case I

For Case (I), Eq. 4.1.10 is written as

$$\begin{cases} G\left(\frac{1}{\mu B}\right)_2^{\nu+1} (P_2^{\nu+1} - P_1^{\nu+1}) - 10^6 = \beta_1 \left[\left(\frac{\phi}{B}\right)_1^{\nu+1} - \left(\frac{\phi}{B}\right)_1^{\nu}\right] \\ G\left(\frac{1}{\mu B}\right)_2^{\nu+1} (P_1^{\nu+1} - P_2^{\nu+1}) + G\left(\frac{1}{\mu B}\right)_3^{\nu+1} (P_3^{\nu+1} - P_2^{\nu+1}) = \beta_2 \left[\left(\frac{\phi}{B}\right)_2^{\nu+1} - \left(\frac{\phi}{B}\right)_2^{\nu}\right] \\ G\left(\frac{1}{\mu B}\right)_3^{\nu+1} (P_2^{\nu+1} - P_3^{\nu+1}) + G\left(\frac{1}{\mu B}\right)_4^{\nu+1} (P_4^{\nu+1} - P_3^{\nu+1}) = \beta_3 \left[\left(\frac{\phi}{B}\right)_3^{\nu+1} - \left(\frac{\phi}{B}\right)_3^{\nu}\right] \\ G\left(\frac{1}{\mu B}\right)_4^{\nu+1} (P_3^{\nu+1} - P_4^{\nu+1}) = \beta_4 \left[\left(\frac{\phi}{B}\right)_4^{\nu+1} - \left(\frac{\phi}{B}\right)_4^{\nu}\right] \end{cases} \quad (4.1.12)$$

and Eq. 4.1.11 is given in the form

$$\begin{cases} G\left(\frac{1}{\mu B}\right)_2^{\nu+1}(P_2^{\nu+1}-P_1^{\nu+1})-10^6=\beta_1\left(\frac{\phi}{B}\right)_1'(P_1^{\nu+1}-P_1^{\nu}) \\ G\left(\frac{1}{\mu B}\right)_2^{\nu+1}(P_1^{\nu+1}-P_2^{\nu+1})+G\left(\frac{1}{\mu B}\right)_3^{\nu+1}(P_3^{\nu+1}-P_2^{\nu+1})=\beta_2\left(\frac{\phi}{B}\right)_2'(P_2^{\nu+1}-P_2^{\nu}) \\ G\left(\frac{1}{\mu B}\right)_3^{\nu+1}(P_2^{\nu+1}-P_3^{\nu+1})+G\left(\frac{1}{\mu B}\right)_4^{\nu+1}(P_4^{\nu+1}-P_3^{\nu+1})=\beta_3\left(\frac{\phi}{B}\right)_3'(P_3^{\nu+1}-P_3^{\nu}) \\ G\left(\frac{1}{\mu B}\right)_4^{\nu+1}(P_3^{\nu+1}-P_4^{\nu+1})=\beta_4\left(\frac{\phi}{B}\right)_4'(P_4^{\nu+1}-P_4^{\nu}). \end{cases}$$

(4.1.13)

The pressure distribution at the center of gridblocks is computed using Eqs. 4.1.12 and 4.1.13. Here μ and B vary with pressure, however, k is assumed constant. The time step is chosen as $\Delta t = 1$ month. Fig. 4.1.2(a) shows pressure at Gridblock 1 as a function of time when the variation of μ and B with pressure is approximated using continuous functions. It is observed that there is no substantial discrepancy between the pressure values obtained through original formulation and approximate formulation at different time steps. However, the computational results suggest that, with increasing time, the difference between the pressures from Eqs. 4.1.12 and 4.1.13 increases. The effect of the simplification of the formulation is more evident when the cubic spline is applied to approximate the variation of μ and B with pressure as shown in Fig. 4.1.2(b).

4.1.5.1. Effect of interpolation functions and formulation

The pressure distribution at the center of Gridblocks is also obtained using different interpolation functions and various formulation. The results for Gridblock 1 is shown in Figures 4.1.3(a) and 4.1.3(b). The non-linear continuous functions as given in Fig. 4.1.1, linear interpolation and cubic spline are applied to approximate μ and B in both figures. The transient pressure results using cubic spline and linear interpolation are very close to each other for both linear formulations [Fig. 4.1.3(a)] and original formulations [Fig. 4.1.3(b)]. It is also noticed that the continuous functional interpolation shows higher values for pressure at different time steps. Such observation is found to be true for other Gridblocks. The solution with the cubic spline is faster and more accurate.

4.1.5.2. Effect of time interval

The effect of the time interval on the accuracy of the computation is obtained by using different time steps (Δt), which was varied from 1 day to 4 months. Results are based on formulation following Eqs. 4.1.12 and 4.1.13 while the interpolation function for μ and B follows the cubic spline. Figure 4.1.4(a), which is the solution with original formulation at different time steps, shows that the accuracy is not affected by the time interval. In most severe case, the mean relative error is

$$\text{relative error} = \sum_{i=1}^{n} \left(\frac{P_{i_{\Delta t=4\ months}} - P_{i_{\Delta t=1\ day}}}{P_{i_{\Delta t=4\ months}}} \right) / n = 0.014\% \tag{4.1.14}$$

Relative errors are also calculated for the case of linear formulation and the results of it at different time steps are shown in Table 4.1.2. The table clearly suggests that the linearized formulation is more sensitive to the value of Δt.

4.1.5.3. Effect of permeability

To investigate the effect of permeability, computation is also carried out with the original formulation. As a case study, a 10% variation in permeability between the boundary blocks is assumed. Such variation can be described by a linear relationship between permeability and pressure through the following equation

$$\boldsymbol{k} = -0.0004286\,\boldsymbol{p} + 15.22 \tag{4.1.15}$$

During this computation, permeability, k, in each time step and iteration is renewed for the gridblocks. The variation of pressure with time for Gridblock 1 with constant and variable permeability is shown in Fig. 4.1.5(a). For the sake of clarity, the results are repeated in a tabular form [4.1.5(b)]. It is noticed that there is a small difference between

the constant permeability result and the variable permeability result. It is also observed that the margin of difference is more evident in initial time than later time.

4.1.5.4. Effect of number of gridblocks

All of the previous computations are carried out with 4 gridblocks are four. In order to investigate the effect of the number of gridblocks, the number of gridblocks is varied from 4 to 64. For this study, the original formulation as given in Eq. 4.1.2 is applied and the systems of algebraic equations are written for each number of gridblocks. The cubic spline is taken as the interpolation function to include the variation of μ and B; and k is considered to vary according to Eq. 4.1.15. The Newton method is followed to solve the systems of algebraic equations. Figures 4.1.6(a) through 4.1.6(d) illustrate the effect of number of gridblocks at various time steps. It is observed that when the number of gridblocks is increased from 4 to 8, there is a difference in the pressure values predicted. However, increasing from 8 to 16 or more than that provides with a smooth curve at all four time steps.

4.1.5.5. Spatial and transient pressure distribution using different interpolation functions

Figures 4.1.7(a) through 4.1.7(d) show pressure distribution based on cubic spline and linear interpolation along the reservoir at different time. These figures show that the linear interpolations of μ and B give higher values of pressure than those predicted by the cubic spline technique for all time period along the reservoir radius. However, the difference is very small and is only about 5 psia in the severe case.

Case II

The original formulation is taken into account and the cubic spline is used to approximate the variation of μ and B. The system of nonlinear algebraic equations is obtained using Eq. 4.1.10 and is given as

$$\begin{cases} G\left(\frac{1}{\mu B}\right)_1^{\nu+1}(P_2^{\nu}-P_1^{\nu+1})-10^6=\beta_1\left[\left(\frac{\phi}{B}\right)_1^{\nu+1}-\left(\frac{\phi}{B}\right)_1^{\nu}\right] \\ G\left(\frac{1}{\mu B}\right)_2^{\nu+1}(P_1^{\nu+1}-P_3^{\nu}-2P_2^{\nu+1})=\beta_2\left[\left(\frac{\phi}{B}\right)_2^{\nu+1}-\left(\frac{\phi}{B}\right)_2^{\nu}\right] \\ G\left(\frac{1}{\mu B}\right)_3^{\nu+1}(P_2^{\nu+1}+P_4^{\nu}-2P_3^{\nu+1})=\beta_3\left[\left(\frac{\phi}{B}\right)_3^{\nu+1}-\left(\frac{\phi}{B}\right)_3^{\nu}\right] \\ G\left(\frac{1}{\mu B}\right)_4^{\nu+1}(P_3^{\nu+1}-P_4^{\nu+1})=\beta_4\left[\left(\frac{\phi}{B}\right)_4^{\nu+1}-\left(\frac{\phi}{B}\right)_4^{\nu}\right]. \end{cases} \quad (4.1.16)$$

A new method is used to formulate the problem. The first equation of the above set (Eq. 4.1.16) is nonlinear, for which the unknown is $P_1^{\nu+1}$. As a nonlinear equation, Equation one of (4.1.16) has the potential to give more than one solution. Using $P_1^{\nu+1}$ from the solution of Equation one in Eq. 4.1.16, Equation two of Eq. 4.1.16 can be solved for $P_2^{\nu+1}$ that may give more than one solution for each of $P_1^{\nu+1}$. The procedure is continued the similar way, i.e., applied to the equations three and four of Eq. 4.1.16. Therefore, theoretically, multiple solutions can be expected for $P_3^{\nu+1}$ and consequently, for $P_4^{\nu+1}$.

To examine the feasibility of the technique mentioned above, we start with Equation one of Eq. 4.1.16. It is found that there are two solutions for P_1 as obtained in the first iteration. The solutions are

P_1 = 4004.566 psia and 9312.639 psia.

The second equation is solved for P_2 using the result of P_1 and similarly the remaining equations of (4.1.16) are solved for P_3 and P_4. Table 4.1.3 shows the results after the first iteration:

The first and second sets give results, which are not only unexpected, but also unrealistic. During the computation, the second iteration resulted in break down of the solutions. However, the last set provides with satisfactory results following several iterations at desired time interval (the table only shows pressure at t=30.42 days).

The pressure values for the gridblocks are also obtained by utilizing Eq. 4.1.16. In this set, the system of algebraic equations is set up with the properties of the gridblock itself. During the computation, μ and B are updated using cubic spline and linear interpolation. Both techniques show almost same results as evident in Fig. 4.1.8(a). The utilization of gridblock and upstream flow properties are also examined in Fig. 4.1.8(b). The system of algebraic equations (Eq. 4.1.12) is based on the upstream flow properties. The figure shows that the results based on these two formulations are also very close to each other. However, the difference increases as time increases (>500 days).

4.1.5.6. CPU time

In continuing discussion of the previous section, it is important to note the CPU time required for computation. In fact, the main constraint during computation with Eq. 4.1.16 is the computing time. The CPU time required to compute pressure for all four gridblocks for a period of 1.5 years with $\Delta t = 1\,\text{month}$ and using the formulation of Eq. 4.1.16, is approximately 510 seconds. On the contrary, the same problem when utilized the formulation of Eq. 4.1.12, takes only 1.156 seconds, which is significantly lower than the previous ones.

It is important when the time step and the number of Gridblocks are increased. The computation of the pressure distribution takes t = 1.672[sec] with formulation 4.1.12 (Eq. 4.1.12) for 64 Gridblocks and $\Delta t = 1\,\text{months}$. The time to compute the pressure with formulation 4.1.12 (Eq. 4.1.12) is t = 31.172[sec] with $\Delta t = 1\,\text{months}$ for a period of 1.5

years. It indicates that the formulation 4.1.12 (Eq. 4.1.12) is more efficient in time than the formulation 4.1.16 (Eq. 4.1.16).

4.1.6. Conclusions

The effects of the nonlinear behavior of some fluid and formation properties and the simplification of the governing equtions and the possibility of having multiple solutions are investigated in this paper. A test example of a reservoir is taken into account and the pressure distribution along the reservoir is computed with different type of the formulations while the viscosity and the fluid formation volume factor is approximated with different types of the interpolating functions.

Linearization of the coefficient of the formulation may lead to less accurate prediction of the pressure distribution along the reservoir. The variation of the fluid and formation properties are obtained more properly if they are approximated with spline functions. The order of the piecewise polynomials has a very minimal effect if the original formulation is applied. However, the computation shows that the pressure dependent properties have a very weak nonlinearity effect and they may be neglected during the computations.

The problem is also formulated in such a way to produce multiple solutions for the pressure distribution in the gridblocks. This formulation is promising and shows the mathematical potential of having multiple solutions. More investigation is required to confirm if multiple-valued solutions of physical significance exist.

4.1.7. Nomenclature

B = fluid formation volume factor, RB/STB [m^3/std m^3]

G = geometric factor

$G_{r_{i\mu 1/2,j,k}}$ = Geometric factor of transmissibility along the *r*-direction between Block (i,j,k) and Block $(i\,\mu\,1,j,k)$ in radial-cylindrical coordinates

$\log_e$ = natural logarithm

n_r = number of reservoir gridblocks along the *r* direction

n_z = number of reservoir gridblocks along the *z* axis

n_θ = number of reservoir gridblocks in the θ direction

k_r = permeability along the *r* direction in radial flow, md [μm^2]

q = well volumetric rate at reservoir conditions, RB/D [m^3/d]

q_{sc} = well volumetric (production) rate at standard conditions, STB/D or scf/D [std m^3/d]

$q_{scl,n}^{m}$ = volumetric rate of fluid at standard conditions crossing reservoir boundary *l* to block *n* at time t^m, STB/D or scf/D [std m^3/d]

q_{scn}^{m} = well volumetric (production) rate at standard conditions from wellblock *n* at time t^m, STB/D or scf/D [std m^3/d]

p = pressure, psia [kPa]

p_l = pressure of neighboring gridblock *l*, psia [kPa]

p_n = pressure of gridblock or wellblock *n*, psia [kPa]

r = distance in the *r* direction in the radial-cylindrical coordinate system, ft [m]

r_e = external radius in Darcy's law for radial flow, ft [m]

r_w = well radius, ft [m]

$T_{l,n}^{m}$ = transmissibility between gridblocks *l* and *n* at time t^m

$T_{r_{i\mu 1/2,j,k}}$ = transmissibility between Point (i,j,k) and Point $(i\,m\,1,j,k)$ along the *r*-direction, STB/D-psi or scf/D-psi [std $m^3/(d.kPa)$]

Δt = time step, day

V_b = bulk volume, ft^3 [m^3]

V_{b_i} = bulk volume of Block i, ft^3 [m^3]

Z = elevation below datum, ft [m]

Z_l = elevation of Gridblock l, ft [m]

Z_n = elevation of Gridblock (Gridpoint) n, ft [m]

Δz = size of block or control volume along the z axis, ft [m]

$\Delta z_{i,j,k}$ = size of Block (i, j, k) along the z axis, ft [m]

α_c = volume conversion factor = 5.614583 for Customary Units

α_{lg} = logarithmic spacing constant, dimensionless

β = ratio of bulk block volume to time step, ft^3/D [m^3/d]

β_c = transmissibility conversion factor whose numerical value is 0.001127 for customary units

θ = angle in the θ direction, rad

$\Delta\theta_j$ = size of Block (i, j, k) along the θ direction, rad

γ = fluid gravity, psi/ft [kPa/m]

ϕ = porosity, fraction

μ = fluid viscosity, cp [mPa.s]

ψ = a set containing gridblock numbers

ψ_n = set of existing gridblocks that are neighbors to Gridblock n

$\sum_{l \in \psi}$ = summation over all members of set ψ

$\sum_{l \in \psi_n}$ = summation over all members of set ψ_n

$\sum_{l \in \xi_n}$ = summation over all members of set ξ_n

Subscripts

b = bulk

g = gas-phase

i = index for gridblock, gridpoint, or point along the x or r direction

$i \mu 1$ = index for neighboring gridblock along the r direction

$i \mu 1/2$ = between i and $i \mu 1$

(i, j, k) = index for gridblock in r-θ-z space

j = index for gridblock along the θ direction

$j \mu 1$ = index for neighboring gridblock along the θ direction

$j \mu 1/2$ = between j and $j \mu 1$

k = index for gridblock along the z direction

$k \mu 1$ = index for neighboring gridblock along the z direction

$k \mu 1/2$ = between k and $k \mu 1$

ℓ = index of neighbouring gridblock

ℓ,n = between gridblocks ℓ and n

n = index for gridblock for which a flow equation is written

Superscripts

m = time level m

n = time level n (old time level)

n+1 = time level n+1 (new time level or current time level)

ν = old iteration ν

$\nu+1$ = current iteration $\nu+1$

‘ = derivative with respect to pressure

4.1.8. References

Abou-Kassem, J. H., Farouq Ali, S. M., and Islam, M. R., (2006) Petroleum reservoir simulation: A basic approach, Gulf Publishing Company, Houston, 445 p.

Abou-Kassem, J. H., Osman, M. E., Mustafiz, S. and Islam, M. R., (in press) New simple equations for interblock geometric factors and bulk volumes in single-well simulation, Petroleum Science and Technology

Darcy, H. P. G., (1856) Les Fontaines Publiques de villle de la Dijon Dalmont, Exposition et Application des Pricipes a Suivre et des Furmules a Emplyer dans les Questions de Distribution d'Eau. Victor Dalmont, Paris

Ertekin, T., Abou-Kassem, J. H., and King, G. R., (2001) Basic applied reservoir simulation, SPE textbook series, vol. 7, 406 p., SPE: Richardson, TX

Islam, M. R., (2006) Computing for the information age, Proc. of the 36th international conference on computers and industrial engineering, Keynote Speech, Taipei, Taiwan, June 20-23

MacDonald, R. C. and Coats, K. H., (1970) Methods for numerical simulation of water and gas coning, Society of Petroleum Engineering Journal, vol. 10, No. 4, pp. 425-436

Mustafiz, S. and Islam, M. R., (2006) The state-of-the-art of reservoir simulation, Petroleum Science and Technology, accepted for publication, August

Nolen, J. S. and Berry, D. W., (1972) Tests of the stability and time step sensitivity of semi-implicit reservoir simulation techniques, Transactions AIME, vol. 253, pp. 253-266

4.1.9. Appendices

4.1.9.1. Appendix A: Tables

Table 4.1.1. The variation of the gas formation volume factor and viscosity with reservoir pressure (Abou-Kassem et al., 2006)

pressure (*psia*)	GFVF (*RB/scf*)	Viscosity (*cp*)	pressure (*psia*)	GFVF (*RB/scf*)	Viscosity (*cp*)
215	0.016654	0.0126	2215	0.001318	0.0167
415	0.008141	0.0129	2415	0.001201	0.0173
615	0.005371	0.0132	2615	0.001109	0.0180
815	0.003956	0.0135	2815	0.001032	0.0186
1015	0.003114	0.0138	3015	0.000972	0.0192
1215	0.002544	0.0143	3215	0.000922	0.0198
1415	0.002149	0.0147	3415	0.000878	0.0204
1615	0.001857	0.0152	3615	0.000840	0.0211
1815	0.001630	0.0156	3815	0.000808	0.0217
2015	0.001459	0.0161	4015	0.000779	0.0223

Table 4.1.2. Relative error at different time steps using linear formulation and cubic spline interpolation

Time step (Δt)	**Relative error (%)**
2 days	0.09
0.5 month	0.68
1 month	1.46
2 months	3.19
4 months	7.82

Table 4.1.3. Pressure solution at t=30.42 days for four gridblocks

time [days]	P_1 [psia]	P_2 [psia]	P_3 [psia]	P_4 [psia]
30.420	9312.639809	-5404.929667	-384.716801	577.929652
30.420	4004.566162	-5147.603731	-310.418879	606.315484
30.420	4004.566162	4009.783158	4012.393337	4012.512134

4.1.9.2. Appendix B: Figures

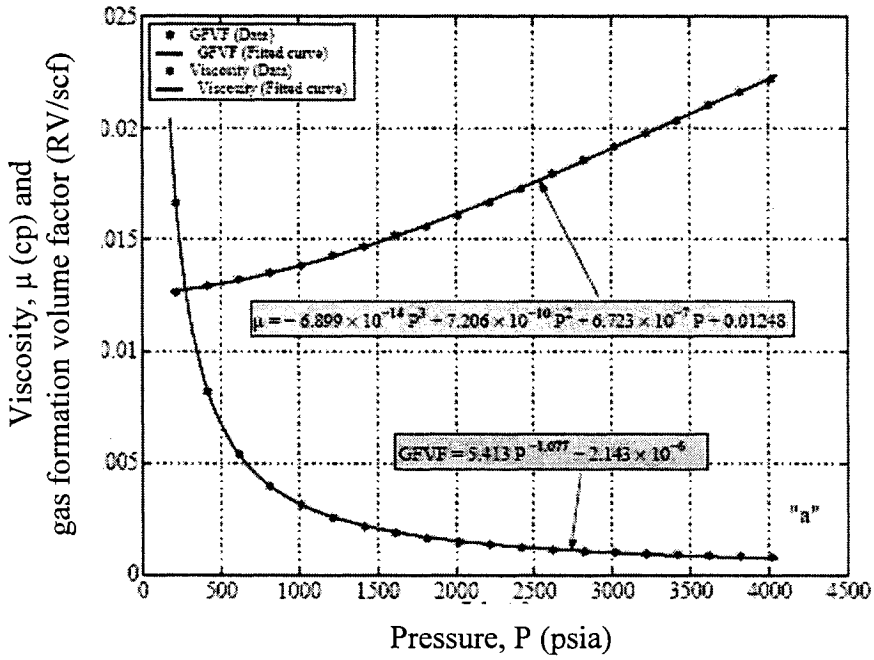

Figure 4.1.1(a). Approximation of variation of μ and *GFVF* with *P* *using continuous functions*

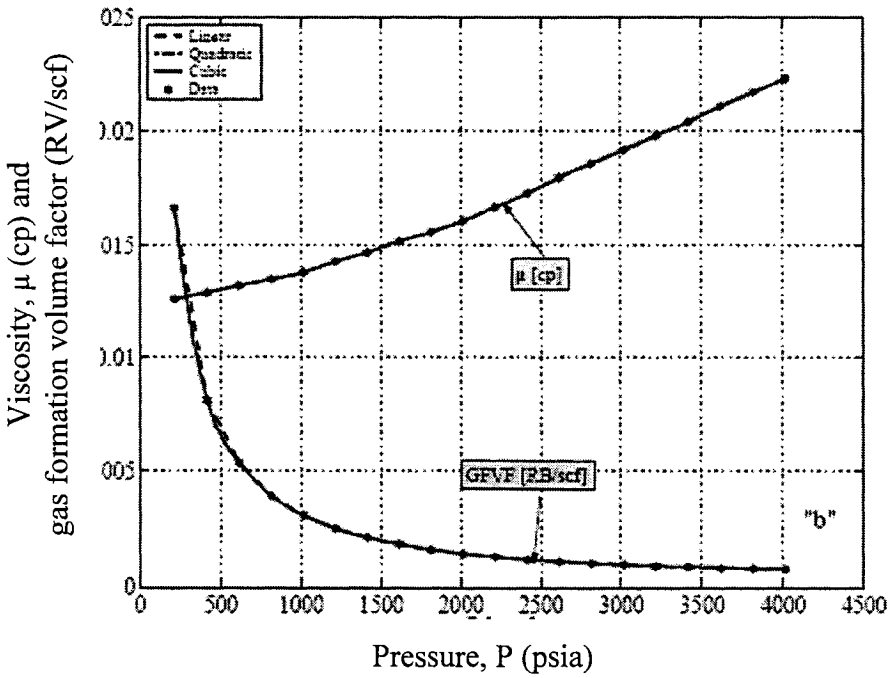

Figure 4.1.1(b). Approximation of variation of μ and *GFVF* with *P* *using spline functions of different order*

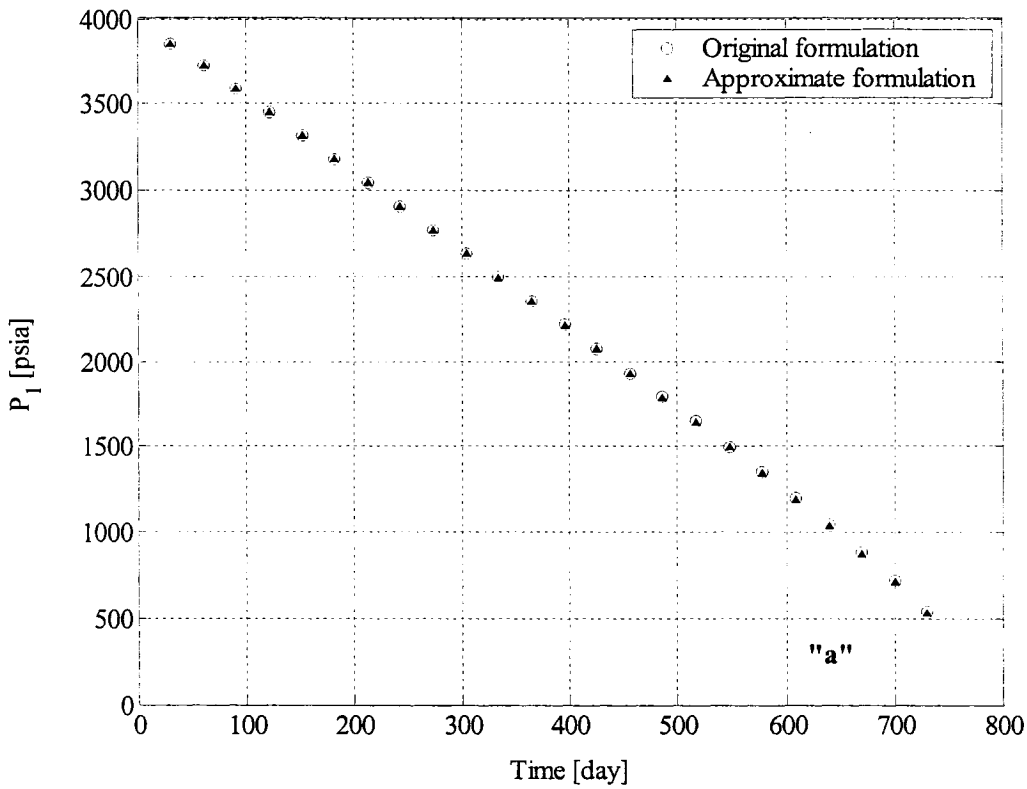

Figure 4.1.2(a). Pressure at Gridblock 1 with the linear and original formulation *using nonlinear continuous functions*

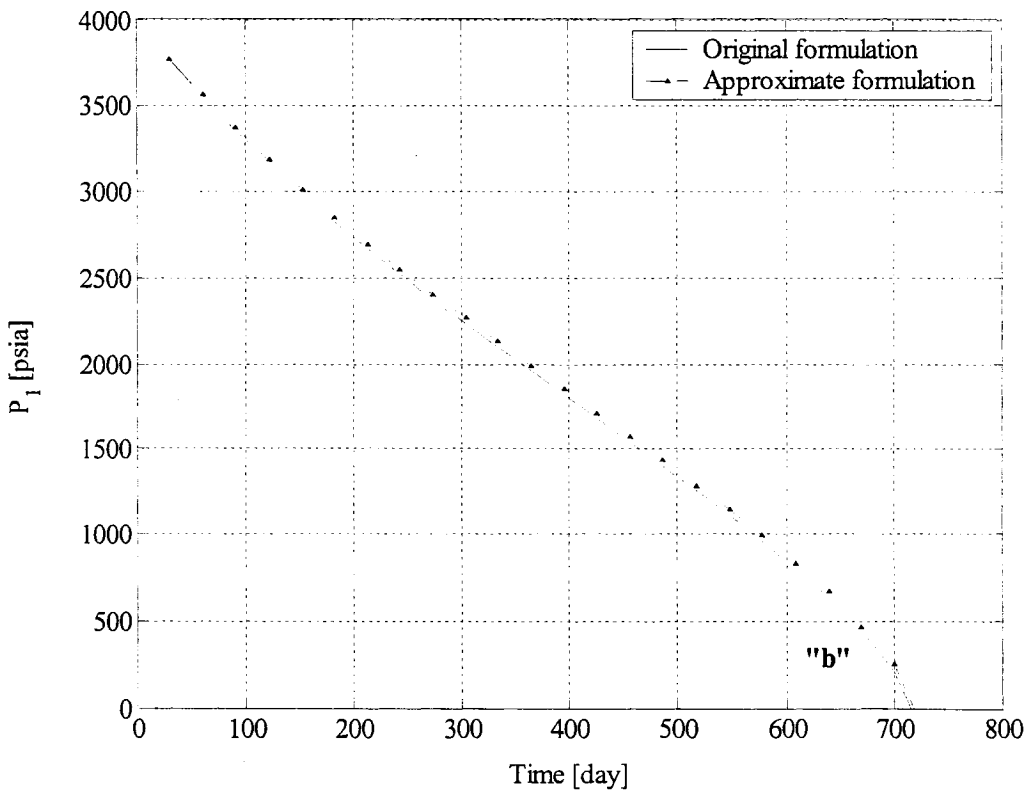

Figure 4.1.2(b). Pressure at Gridblock 1 with the linear and original formulation *using cubic spline*

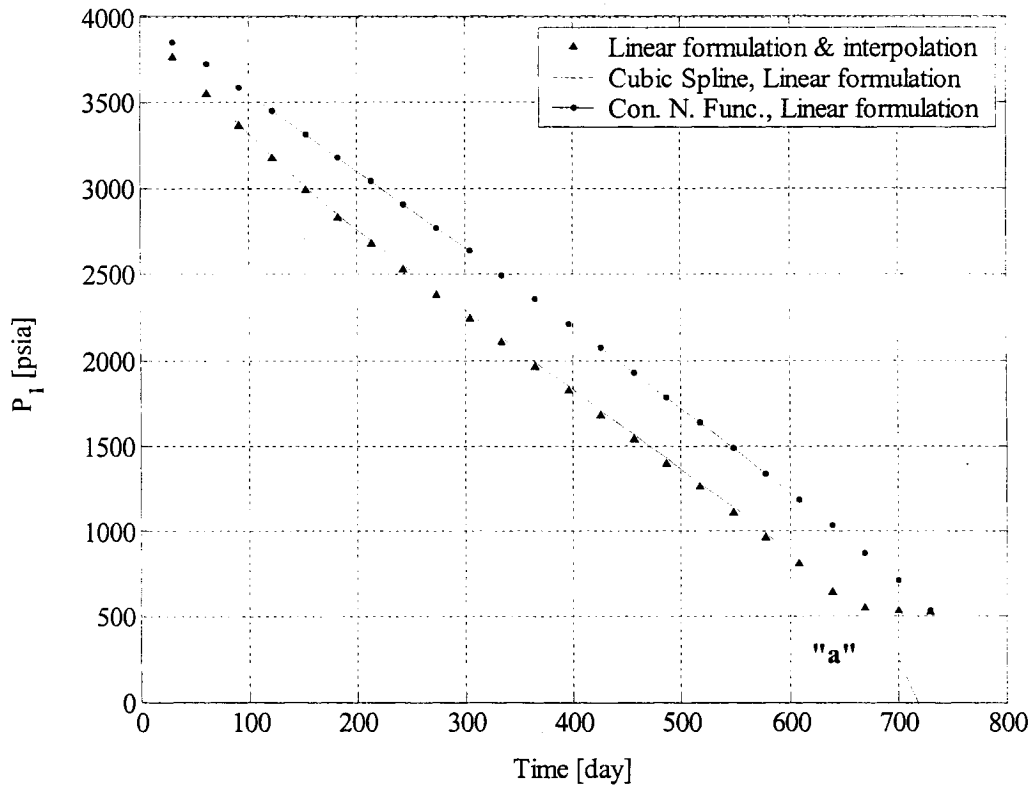

Figure 4.1.3(a). Pressure at Gridblock 1 using the linear interpolation, cubic spline and nonlinear continuous functions *with linear formulation*

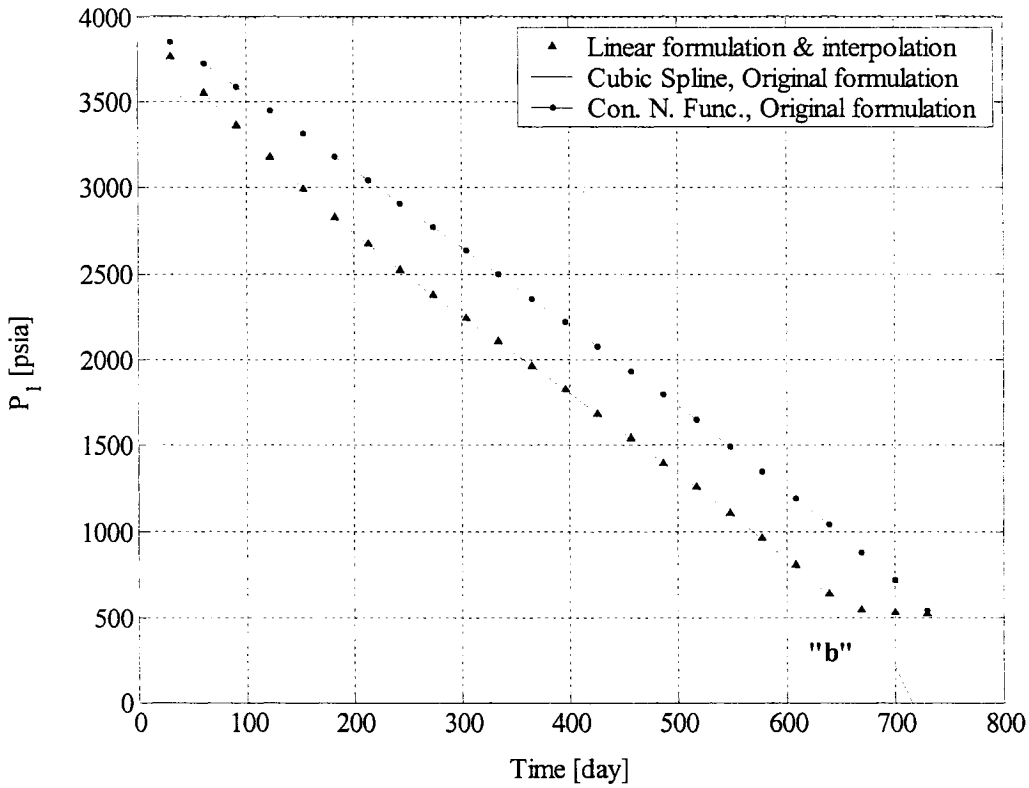

Figure 4.1.3(b). Pressure at Gridblock 1 using the linear interpolation, cubic spline and nonlinear continuous functions *with original formulation*

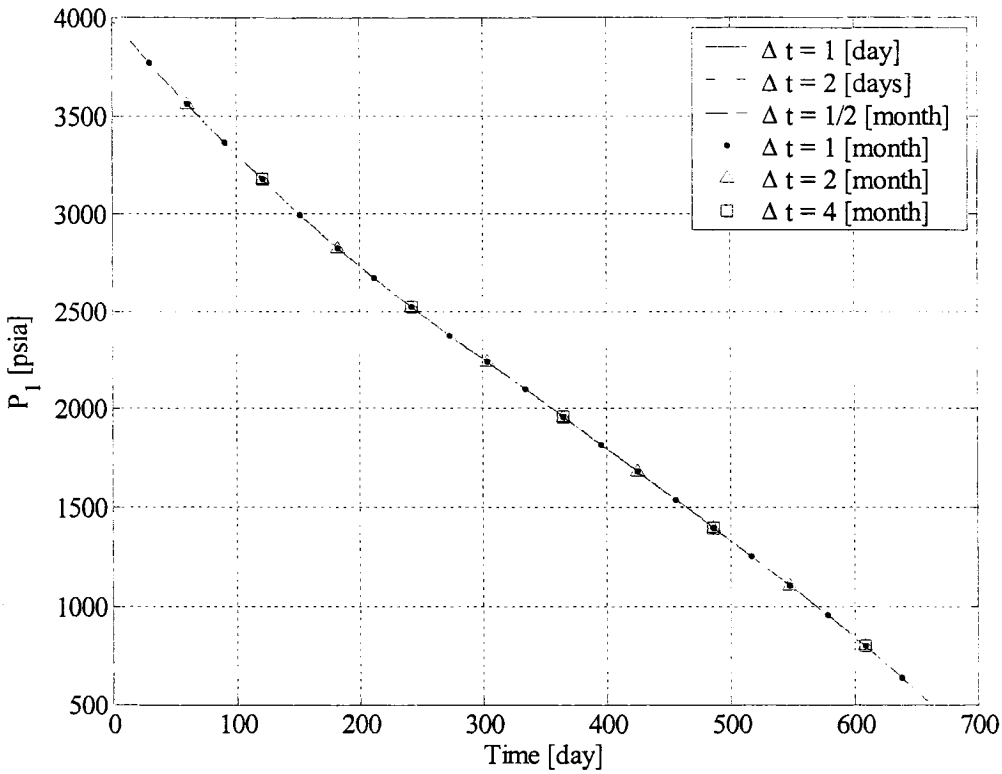

Figure 4.1.4(a). The effect of the time step in computation - cubic spline interpolation *using original formulation*

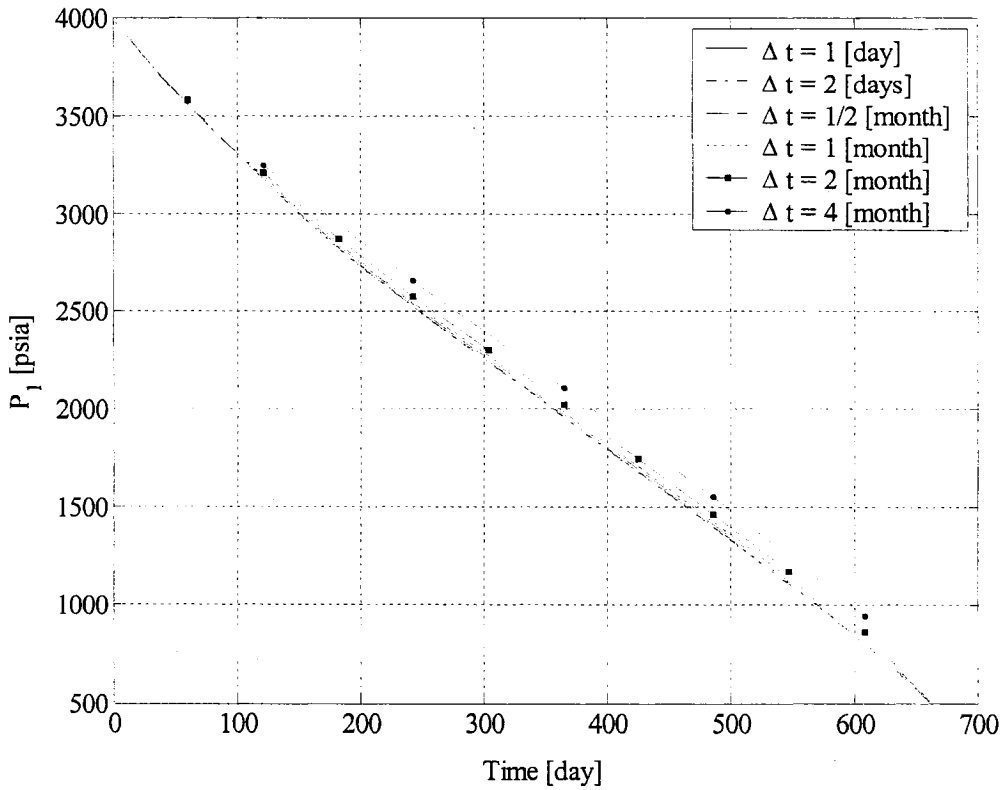

Figure 4.1.4(b). The effect of the time step in computation - cubic spline interpolation *using linear formulation*

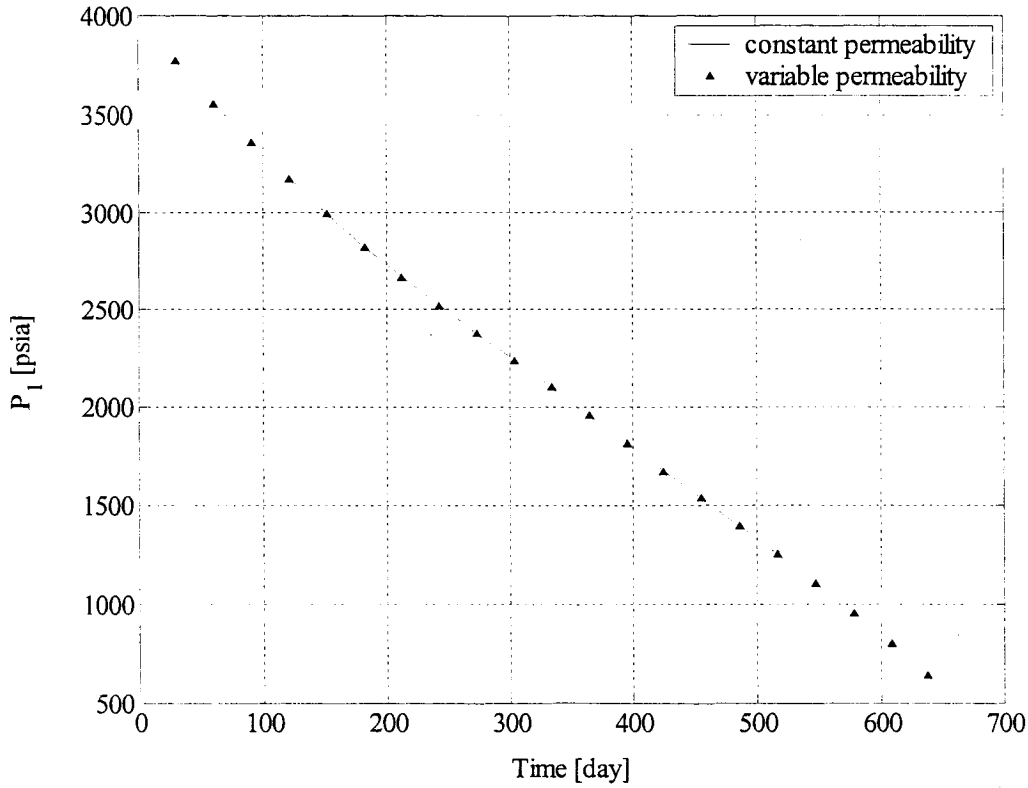

Figure 4.1.5(a). The effect of permeability variation on pressure variation with time

Time [*months*]	P_1 (*k=const.*) [*psia*]	$P_1(k=f(p))$ [*psia*]
1	3765.668915	3762.476196
2	3554.151242	3551.149301
6	2822.768896	2820.363056
12	1959.327022	1957.484815
15	1540.271151	1538.676903
18	1108.891024	1107.635304
20	798.990098	798.110175

Figure 4.1.5(b). The effect of permeability variation on pressure variation with time – *tabular presentation*

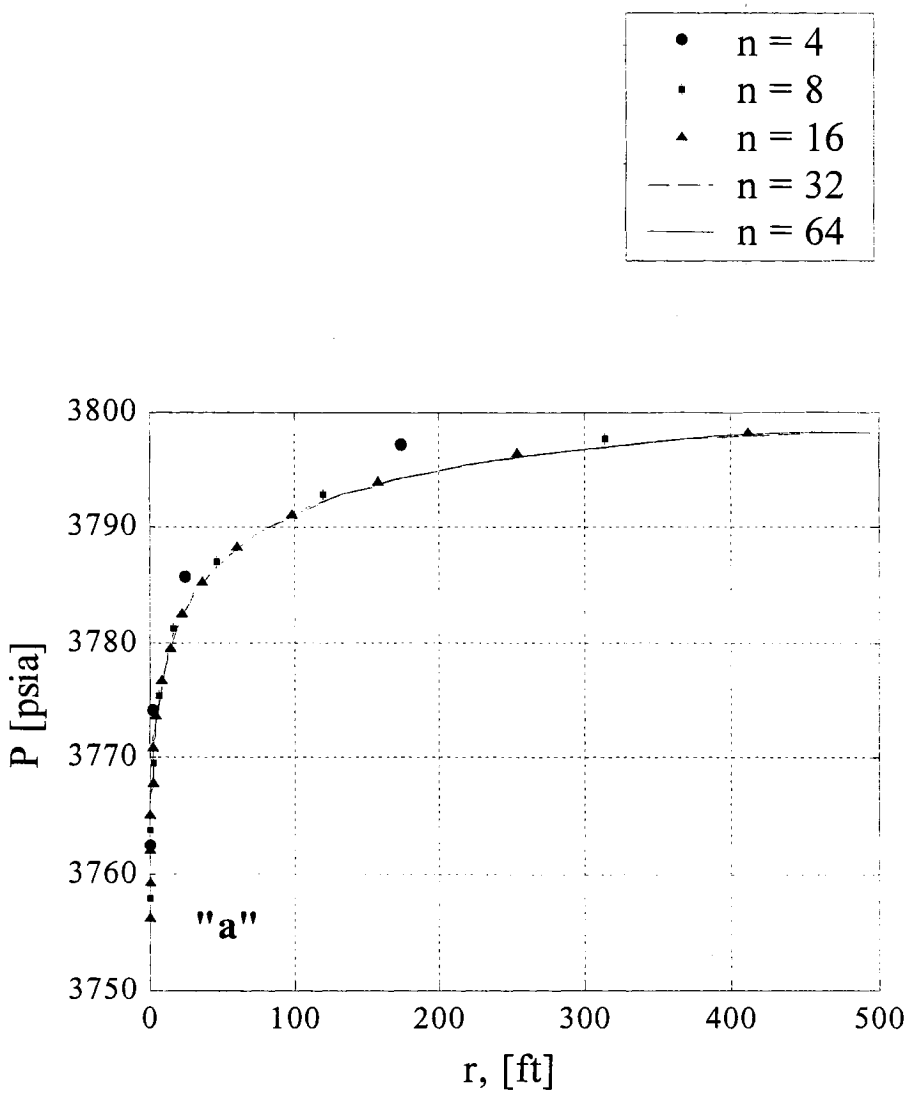

Figure 4.1.6(a). The pressure distribution using different number of gridblocks, $t = 1$ month

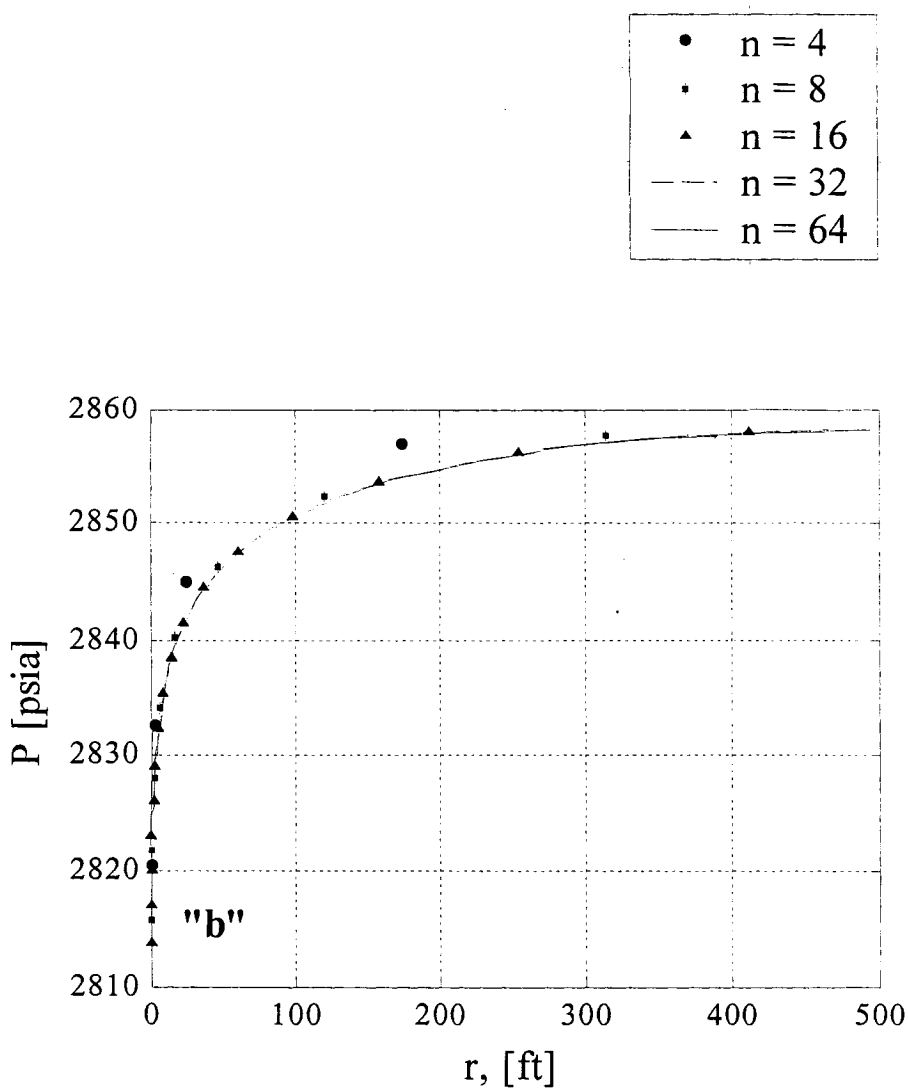

Figure 4.1.6(b). The pressure distribution using different number of gridblocks, $t = 6$ months

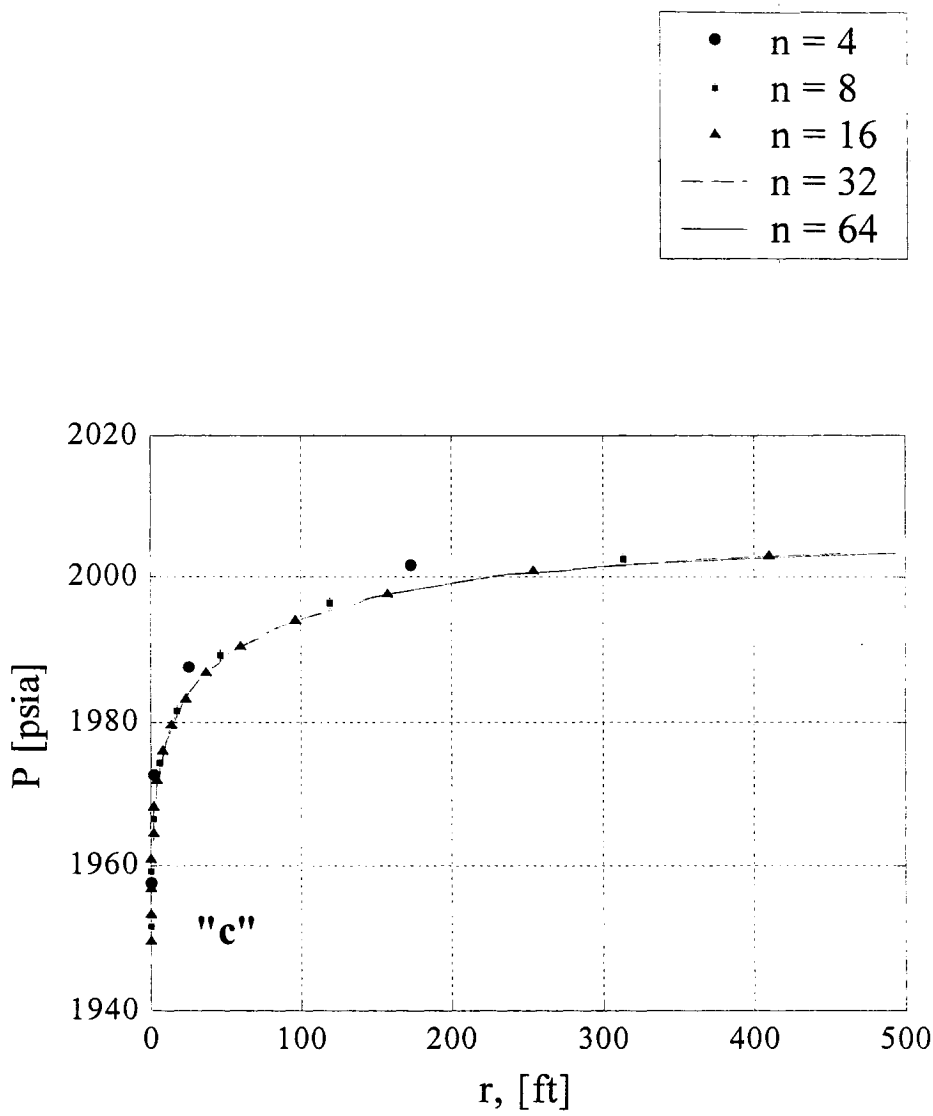

Figure 4.1.6(c). The pressure distribution using different number of gridblocks, t = 12 months

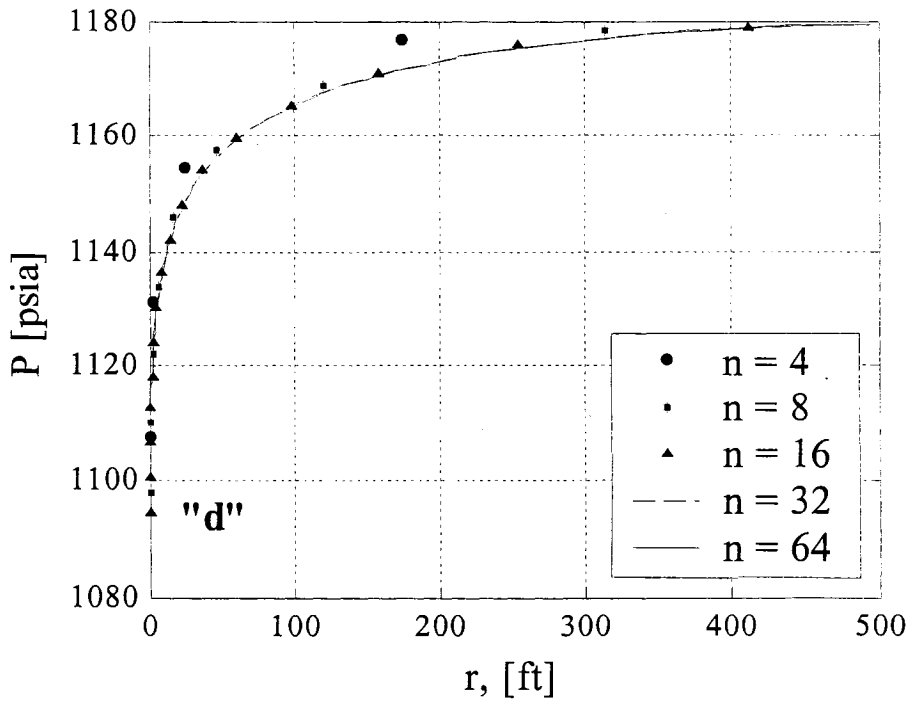

Figure 4.1.6(d). The pressure distribution using different number of gridblocks, $t = 18$ months

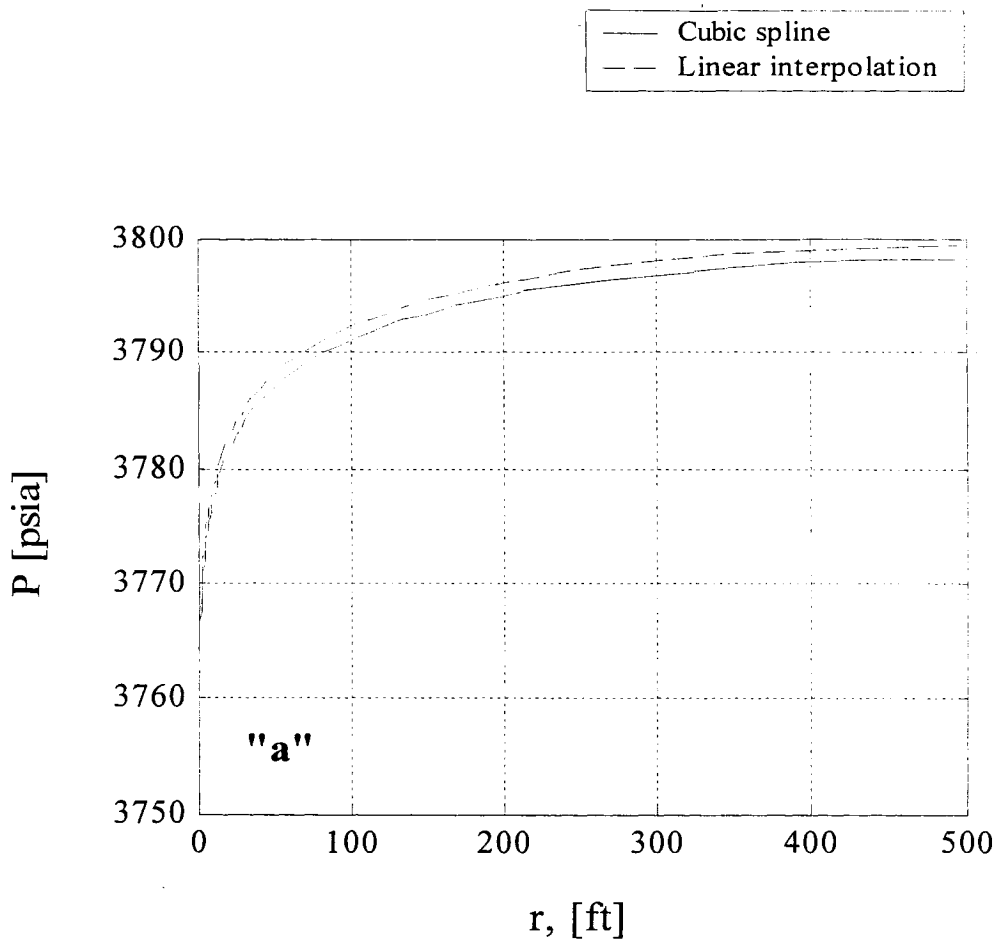

Figure 4.1.7(a). The pressure distribution along the reservoir radius using cubic spline and linear interpolation for variation of μ and B when $n = 64$, $t = 1$ month

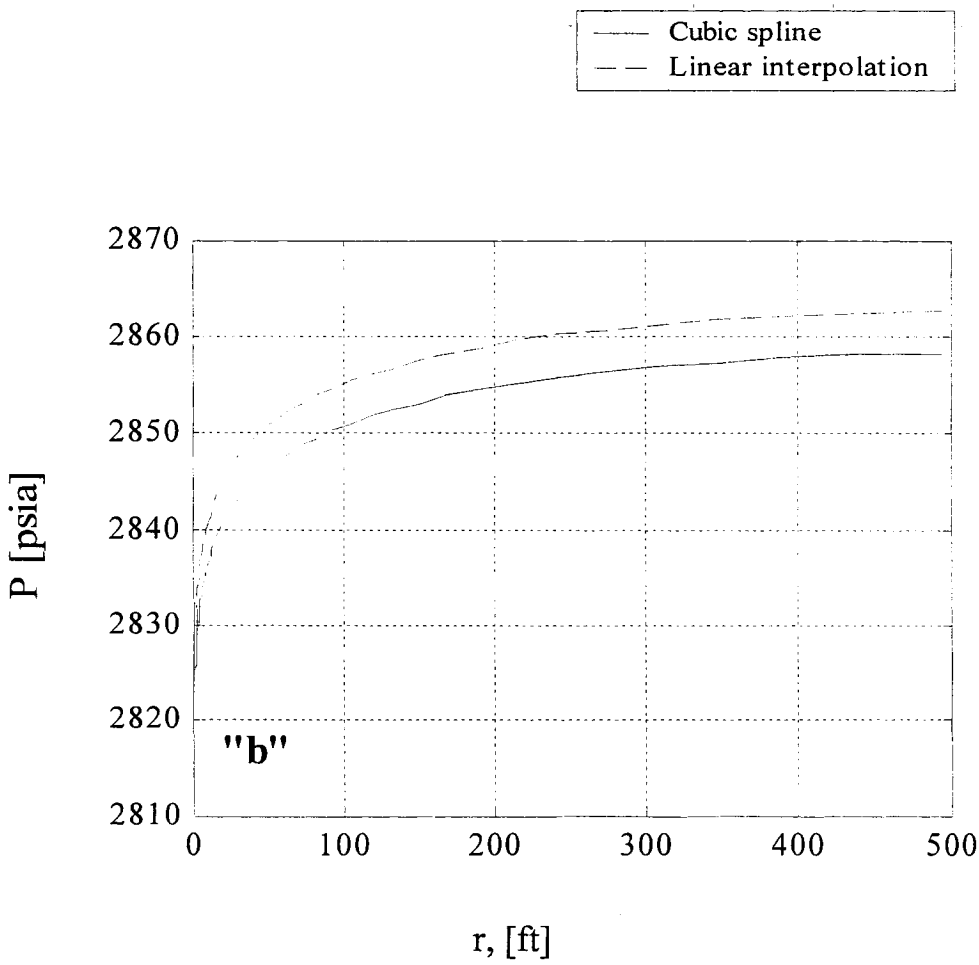

Figure 4.1.7(b). The pressure distribution along the reservoir radius using cubic spline and linear interpolation for variation of μ and B when $n = 64$, $t = 6$ months

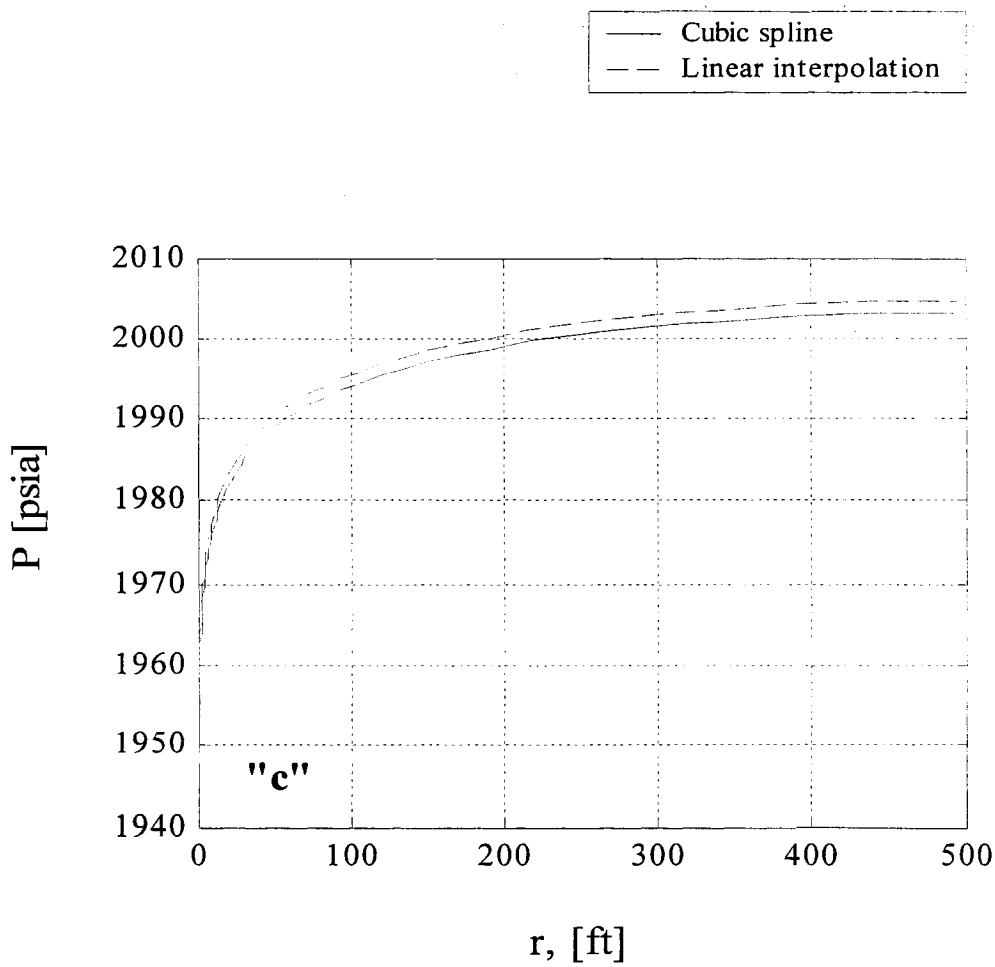

Figure 4.1.7(c). The pressure distribution along the reservoir radius using cubic spline and linear interpolation for variation of μ and B when $n = 64$, $t = 12$ months

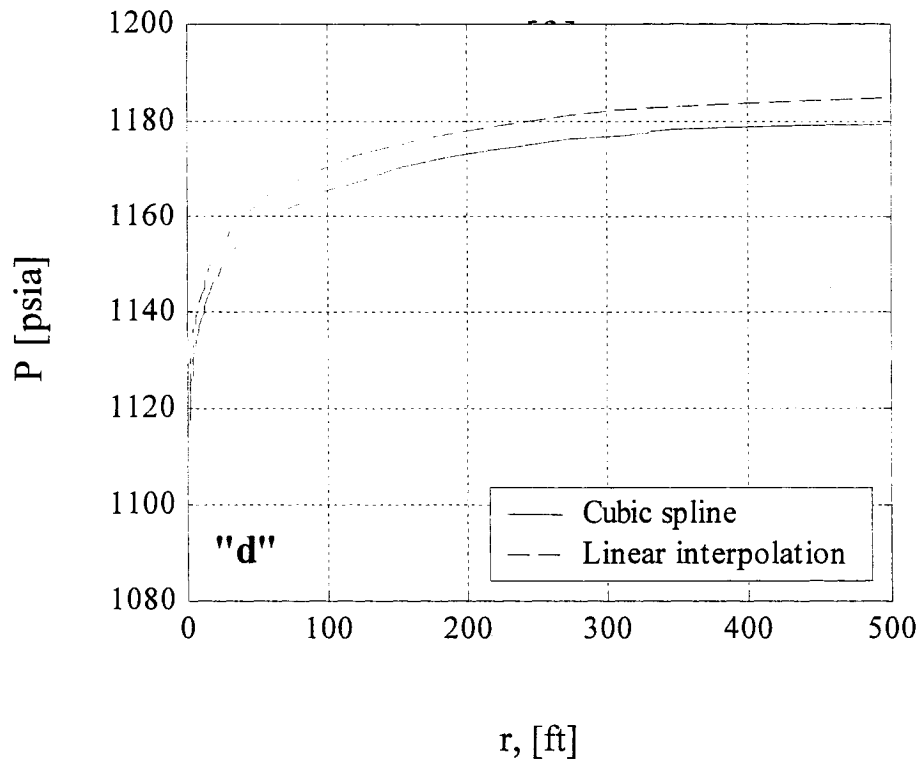

Figure 4.1.7(d). The pressure distribution along the reservoir radius using cubic spline and linear interpolation for variation of μ and B when $n = 64$, $t = 18$ months

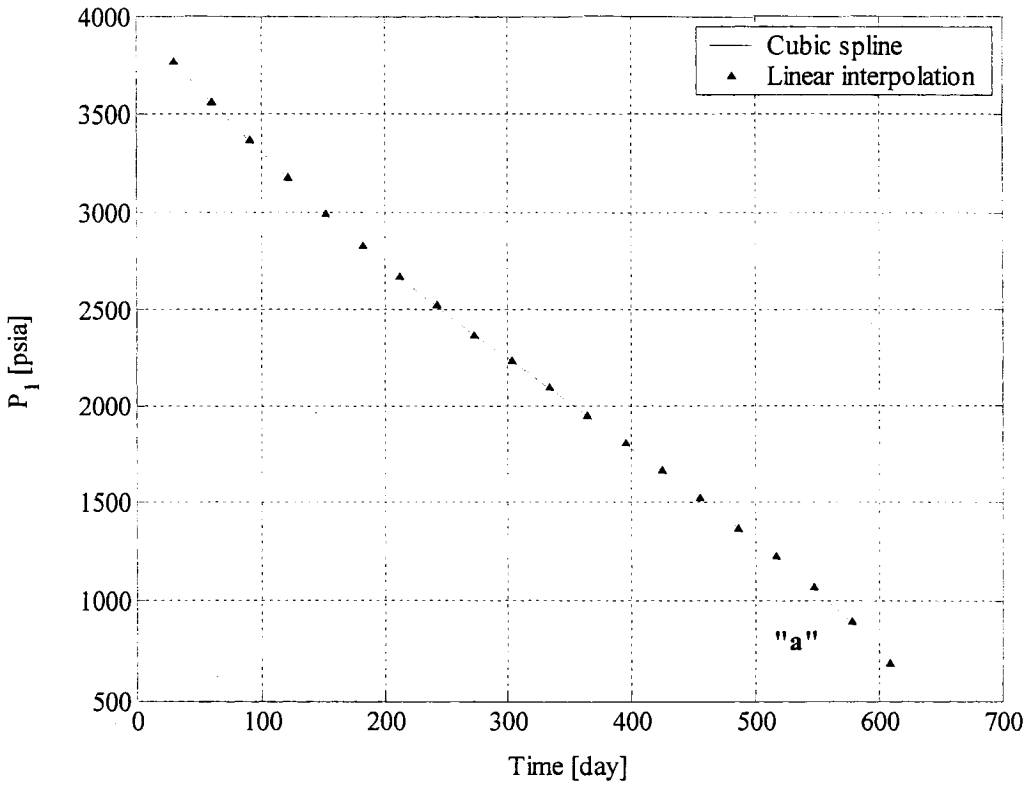

Figure 4.1.8(a). The pressure at Gridblock 1 using different sets of system of algebraic equations and various interpolations, cubic spline and linear interpolation using Eq. 4.1.16

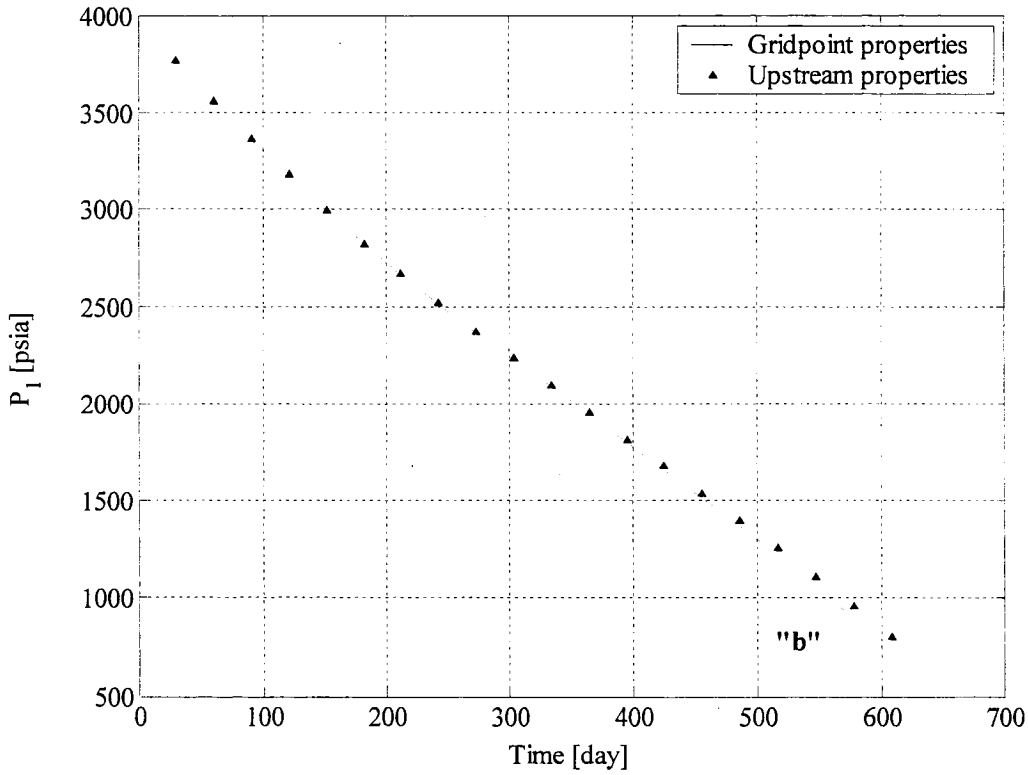

Figure 4.1.8(b). The pressure at Gridblock 1 using different sets of system of algebraic equations and various interpolations, cubic spline using Eqs. 4.1.12 and 4.1.16

Chapter 4

4.2 INVESTIGATION OF DIRICHLET TYPE (CONSTANT PRESSURE) BOUNDARY CONDITION IN *ENGINEERING APPROACH*

4.2.1. Introduction

One of the important tasks in reservoir simulation is reservoir discretization. The discretization involves construction of grid-system in the reservoir, which either follows a block-centred or point-distributed approach. It is also known that any reservoir boundary condition reduces to either Neumann boundary condition or Dirichlet boundary condition. Although, there is no hard and fast rule, yet depending on the reservoir boundary condition, one grid system can be preferable to another grid system. Traditionally, the block-centred grid system is preferable to point-distributed grid system in handling Neumann boundary condition while the point-distributed grid system is chosen over the block-centred grid system in addressing the Dirichlet condition.

Only recently, *engineering approach* is proposed in reservoir simulation and reported not to go through the rigor of partial differential equations (Abou-Kassem et al., 2006). The representation of boundary conditions in this method takes in the form of fictitious wells. In this section, the treatment of Dirichlet condition by 'engineering approach' is examined for compressible and slightly compressible fluids in both point-distributed and block-centred grid systems. Also, the relative merits/demerits of the newly introduced 'engineering approach' in terms of grid-system are discussed.

4.2.2. Case Study

Two problems involving linear flow of single-phase incompressible and slightly compressible fluids respectively are examined here. The reservoir dimensions are 1000 ft x 300 ft x 35 ft. The horizontal reservoir has homogeneous rock properties. The permeability and porosity of the reservoir are 220 md and 0.23 respectively. Initial reservoir pressure is 3600 psia. A Dirichlet type boundary condition (constant pressure of 3600 psia) exists at the left boundary while a Neumann type boundary condition (loss of fluid at a constant rate of 480 STB/D) exists at the right boundary of the reservoir. The reservoir is assumed to have a regular grid size distribution and is described by four equal gridblocks in case of block-centred grid approach and by five equally spaced gridpoints in case of point-distributed grid approach. For both problems, the viscosity of fluid and the fluid formation volume factor are 0.48 cp and 1.0 RB/STB. The compressibility is also known for the slightly compressible fluid, which is 1.1×10^{-5} psi^{-1}.

For both problems, the pressure distribution in the reservoir using block-centred grid and point-distributed grid systems will be compared. For the second problem that involves slightly compressible fluid, the pressure distribution will be calculated after 1 day and 2 days.

4.2.3. Results and discussion

4.2.3.1. Problem 1: Incompressible fluid

Figure 4.2.1 presents the simulation results using the block-centred grid and point distributed grid systems. The block-centred grid results are based on both current (conventional) practice and the engineering approach. The figure shows that the block-centred grid with the engineering approach gives a pressure distribution, which coincides with that produced by the point-distributed grid system. However, the conventional

pressure prediction as of using the block-centred grid (noted by the dotted line) is higher than the predictions produced by the other two systems.

4.2.3.2. Problem 2: Slightly compressible fluid

Figures 4.2.2.1 and 4.2.2.2 give the comparison of the pressure profiles using different grid systems for slightly compressible fluid at 1-day and 2-days respectively. A time step of 1-day was used in the simulation runs. Once again, the block-centred grid with the engineering approach shows an excellent agreement with that produced by the point-distributed grid system. It is also noted that the pressure profiles do not follow straight lines as noted in case of incompressible fluid pressure profiles in Fig. 4.2.1.

4.2.3.3. Theoretical explanations

4.2.3.3.1. General practice

In the point-distributed grid system, the boundary gridpoint falls on the boundary and the specified pressure is assigned at the boundary gridpoint. In the block-centred grid system, the specified pressure is assigned at a point, which is half-block away from the boundary and represents the boundary gridblock. Therefore, there exists a discrepancy between the pressure profile based on the conventional block-centred grid system and the pressure profile based on the point distributed grid system. To predict reservoir pressure more accurately but not at the cost of shifting the grid system from the block-centred to point-distributed, Ertekin et al. (2001) showed an extrapolation of the boundary pressure, p_b from the two closest pressure points to the reservoir boundary

$$(1+\Omega)p_1 - \Omega p_2 = p_b \qquad (4.2.1)$$

where, $\Omega = \Delta x_1 / \Delta x_1 + \Delta x_2)$. For the special case of uniform grid spacing, i.e., $\Delta x_1 = \Delta x_2$, Eq. 1 becomes

$$p_b = \tfrac{1}{2}(3p_1 - p_2) \tag{4.2.2}$$

Equation 4.2.2 is the common form of the extrapolation approach that appears in the petroleum literature (Aziz and Settari, 1979). It has also elevated the improvement from the first-order correct approximation to the second-order correct approximation (Aziz and Settari, 1979; Ertekin et al., 2001) when the block-centred grid system is followed. In spite of being rigorous and to some extent accepted, this method has several shortcomings:

1. Equation 4.2.2 must be solved along with the set of flow equations;
2. Equation 4.2.2 is valid for a reservoir that uses regular grid only;
3. Equation 4.2.2 does not resemble a flow equation. Typically, the flow equations of a multidimensional system are represented by a matrix giving rise of a banded structure inside. However, the non-uniformity of the additional equation may create disturbance to the structural integrity;
4. Equation 4.2.2 neglects the effect of gravity;
5. Equation 4.2.2 is valid for rectangular grid system. However, the use of radial cylindrical grids in single well simulation does not permit of utilizing Eq. 4.2.2.

On the contrary, no extrapolation is required to treat the specified pressure boundary on a point-distributed grid system. Therefore, the common practice is to use the point-distributed grid system for treating a Dirichlet type boundary condition.

4.2.3.3.2. Engineering Approach

In the *engineering approach*, the boundary condition is replaced with a no-flow boundary and a fictitious well. Note that the replacement of a boundary condition by a no-flow boundary and a source term (Aziz and Settari, 1979; Ertekin et al., 2001) is not uncommon in simulation practices. In fact, the presence of a fictitious well in the flow equation of a boundary gridblock give the impression that two wells are present, one real and one fictitious – which is an alternate way of expressing the conventional flow equation without taking into consideration of any other mathematical expression. Recently, Abou-Kassem et al. (2006) presented the expression for the flow equation for Boundary Gridblocks that falls on reservoir boundary (note Fig. 4.2.3), which if written for Gridblock 1 is

$$q_{sc_{b,1}}^{n+1} + T_{x_{1+1/2}}^{n+1}(\Phi_2^{n+1} - \Phi_1^{n+1}) + q_{sc_1}^{n+1} = \frac{V_{b_1}}{\alpha_c \Delta t}[(\frac{\phi}{B})_1^{n+1} - (\frac{\phi}{B})_1^n] \tag{4.2.3}$$

in which, the flow rate of the fictitious well is (Abou-Kassem et al., 2006)

$$q_{sc_{b,1}}^{n+1} = [\beta_c \frac{k_x A_x}{\mu B(\Delta x/2)}]_1^{n+1}[(p_b - p_1^{n+1}) - \gamma_{b,1}^n(Z_b - Z_1)] \tag{4.2.4}$$

Equations 4.2.3 and 4.2.4 were used to plot the pressure profiles based on the block-centred grid system (*engineering approach*) in Figs. 4.2.1, 4.2.2.1 and 4.2.2.2. The pressure profiles based on the block-centred grid system (conventional) were, however, constructed on first-order correct approximations.

4.2.4. Conclusions

The treatment of Dirichlet type (constant pressure) boundary condition is investigated by the *engineering approach*. The fictitious flow rate equation in *engineering approach* alleviates the assumptions involved with the use of equation as a second order correct approximation. This new treatment offers an excellent agreement between the pressure profile based on the block-centred grid system and the pressure profile based on the point-distributed grid system. Therefore, there is no need to give preference to the point-distributed grid sytem over the block-centred grid system for the treatment of constant pressure boundary problems.

4.2.5. Nomenclature

A_x = cross-sectional area normal to x-direction, ft^2

b = reservoir boundary

B = fluid formation volume factor, RB/STB for liquid, RB/scf for gas

B° = fluid formation volume factor at reference pressure p° and reservoir temperature, RB/STB

c = fluid compressibility, psi^{-1}

h = thickness, ft

k_x = permeability along the x axis, md

L_x = reservoir length along the x axis, ft

p = pressure, psia

p_b = pressure at reservoir boundary, psia

p_i = pressure of Gridblock (Gridpoint) i, psia

p_i^{n+1} = pressure of Gridblock (Gridpoint) i at Time t^{n+1}, psia

$p_{i\pm1}^{n+1}$ = pressure of Gridblock (Gridpoint) $i\pm1$ at Time t^{n+1}, psia

q_{sc} = well production rate at standard conditions, STB/D

q_{sc_1} = production rate at standard conditions from Gridblock 1, STB/D

$q_{sc_1}^{n+1}$ = production rate at standard conditions from Gridblock 1 at Time Level $n+1$, STB/D

$q_{sc_{b,1}}$ = volumetric flow rate at standard conditions across reservoir boundary to Boundary Gridblock (Gridpoint) 1, STB/D

t = time, day

Δt = time step, day

t^n = old time level, day

t^{n+1} = new or current time level, day

$T_{x_{1+1/2}}^{n+1}$ = transmissibility between Gridblocks 1 and 2 along the x axis at Time t^{n+1}, STB/D-psi

V_b = bulk volume, ft^3

V_{b_1} = bulk volume of Gridblock 1, ft^3

x = distance in the x direction in the Cartesian coordinate system, ft

Δx = size of block or control volume along the x axis, ft

x_i = x-direction coordinate of Point i, ft

$x_{i\pm1}$ = x-direction coordinate of Point $i\pm1$, ft

$\Delta x_{i\pm1}$ = size of Block $i\pm1$ along the x axis, ft

$x_{i\pm1/2}$ = x-direction coordinate of Block Boundary $x_{i\pm1/2}$, ft

$\Delta x_{i\pm1/2}$ = distance between Point i and Point $i\pm1$ along the x axis, ft

Z_b = elevation of center of reservoir boundary below datum, ft

Z_i = elevation of Gridblock (Gridpoint) i, ft

α_c = volume conversion factor

β_c = transmissibility conversion factor

γ = fluid gravity, psi/ft

Φ = potential, psia

Φ_i^{n+1} = potential of Gridblock (Gridpoint) i at Time t^{n+1}, psia

μ = fluid viscosity, cp

Subscripts

1,2 = between Gridblocks (or Gridpoints) 1 and 2

b = bulk or boundary

i = index for gridblock, gridpoint, or point along the x direction

$i\pm1/2$ = between i and $i\pm1$

sc = standard conditions

x = x-direction

$x_{i\pm1/2}$ = between i and $i\pm1$ along the x direction

Superscripts

n = Time Level n (Old Time Level)

$n+1$ = Time Level $n+1$ (New Time Level, Current Time Level)

$^\circ$ = reference pressure and reservoir temperature

4.2.6. References

Abou-Kassem, J. H., Farouq Ali, S. M., and Islam, M. R., (2006) Petroleum reservoir simulation: A basic approach, Gulf Publishing Company, Houston, 445 p.

Aziz, K. and Settari, A., (1979) Petroleum reservoir simulation, Applied Science Publishers, London, UK

Ertekin, T., Abou-Kassem, J. H., and King, G. R., (2001) Basic applied reservoir simulation, SPE textbook series, vol. 7, 406 p., SPE: Richardson, TX

4.2.7. Appendices

4.2.7.1. Appndix A: Figures

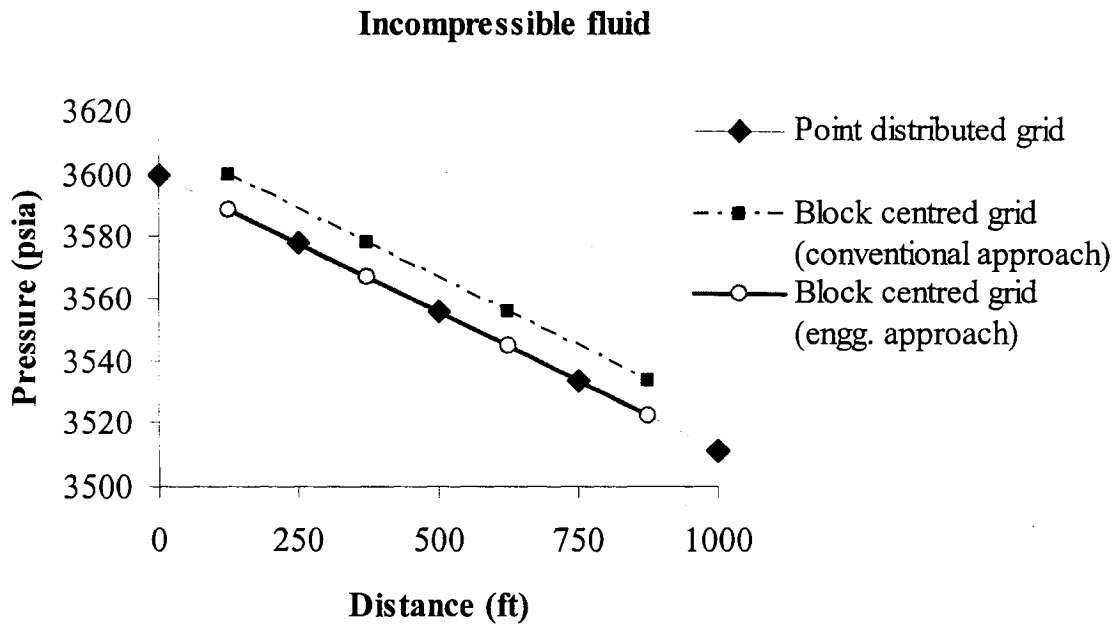

Figure 4.2.1. Pressure distribution in 1-D reservoir for incompressible fluid

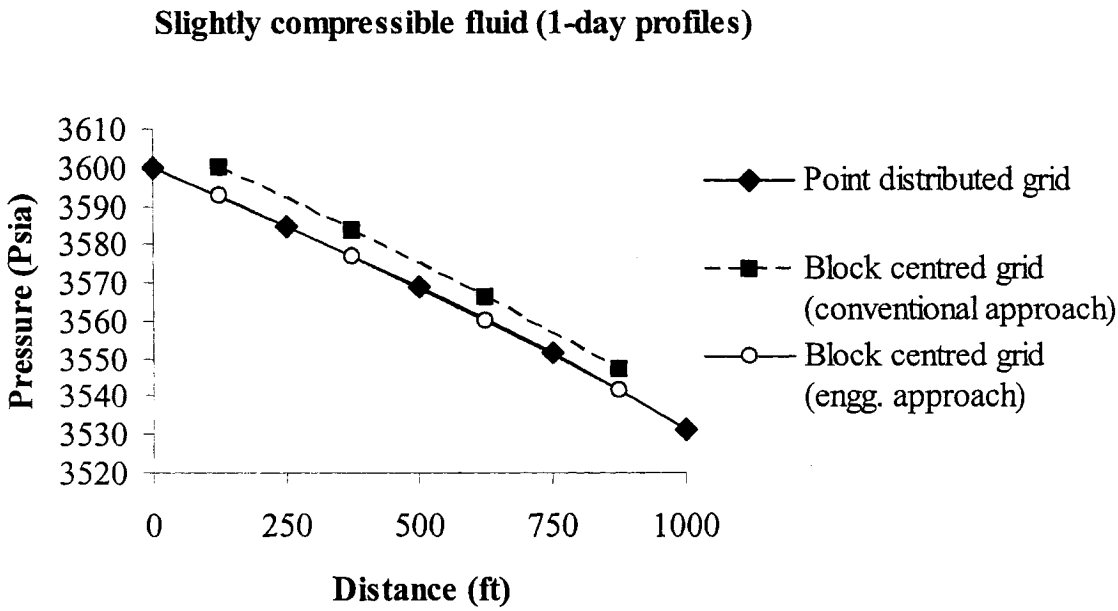

Figure 4.2.2.1. Pressure distribution in 1-D reservoir for slightly compressible fluid (1-day)

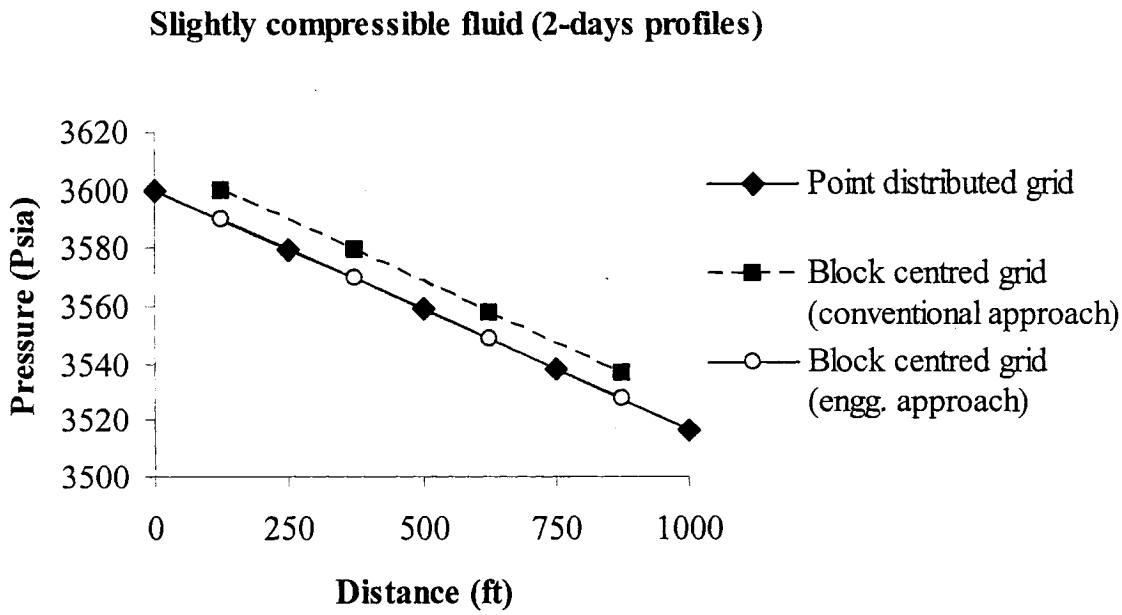

Figure 4.2.2.2. Pressure distribution in 1-D reservoir for slightly compressible fluid (2-days)

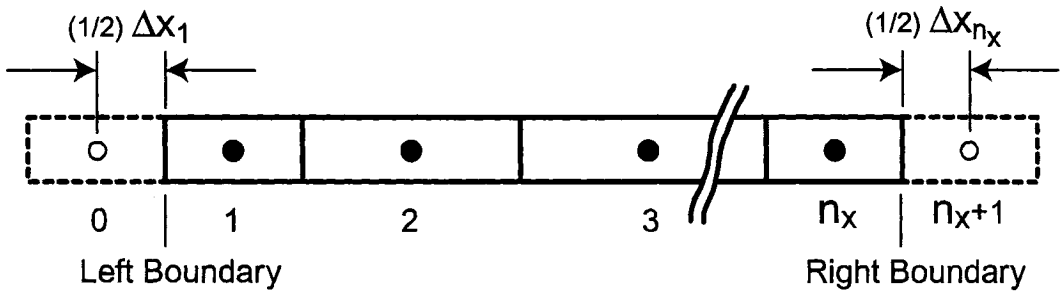

Figure 4.2.3. Boundary gridblocks at left and right boundaries of a 1D reservoir (Abou-Kassem et al., 2006)

Chapter 5

5 MULTIPLE SOLUTIONS IN NATURAL PHENOMENA

5.1. Abstract

Nature is nonlinear and all natural phenomena are multidimensional. The parameters involved in a natural phenomenon are not independent of each other and the variation of each of them causes others to be affected. The natural phenomena are chaotic-not in conventional sense of being arbitrary and/or unpredictable, but in the sense that they always produce multiple solutions and show no reproducibility. We are unaware of the equations that truly govern natural phenomena and also the procedures to obtain multiple solutions. Often several key simplifications are posed to get rid of nonlinearities and find a numerical description of a natural phenomenon. Here, we applied several polynomials and simultaneous equations of two variables as a model for a natural phenomenon in which the other parameters are kept constant. It is shown that they produce multiple solutions regardless of that the solutions are realistic or not and the number of solutions depends on the degree of nonlinearity of the equation. From the study it can be inferred that a phenomenon with only two variables produces more that one solution and, therefore, a multi-variable phenomenon surely has multiple solutions.

5.2. Introduction

Even though claims have been to emulate nature, no modern technology truly emulates the *science* of nature. It has been quite the opposite: observations of nature have rarely been translated into pro-nature technology development. Today, some of the most important technological breakthroughs have been mere manifestations of the *linearization* of nature science: nature linearized by focusing only on its external features.

Modeling is no exception. For instance, the knowledge that nature is strictly non-linear has been there for centuries, yet currently used mathematical or numerical tools can only handle nonlinearity of only trivial problems (Islam, 2006).

All mathematical models of the real physical problems are nonlinear. The nonlinearity is related to the interaction and inclusion of different parameters involved in a physical problem. Several key assumptions are posed to get rid of nonlinearities and find out a numerical description of the problem. Some simplifications may also be imposed during the numerical evaluation of a problem. In this way, a problem is forced to have a single solution ignoring the possibility of having multiple solutions. In addition, not all of the available methods are capable of predicting multiple solutions. In fact, until now, a systematic method for determining multiple solutions is limited to three variables.

The general development of the set of governing equations always proceeds the same way for any material. A set of conservation laws is usually applied in integral form to a finite mass of material. Typical 'laws' express the conservation of mass, momentum, and energy. It is asserted that the 'laws' are true and the problems become that of solving the constitutive relationship of the 'law'. These equations are then converted to a local form and are cast in the form of partial differential equations. These differential equations cannot be solved in a general way for the details of the material motion. In order to close the system, the next step, always, is to specify the material response. The mathematical conditions are usually referred to as the constitutive relations. The last step is to combine these constitutive relations with the local form of the balance equations. The combination of these two sets of relations is called the field equations which are the differential equations governing the material of interest.

We are unaware of the mathematical model that truly simulates a natural phenomenon. The available models are based on several assumptions. For examples, there are many models that describe different fluid flows. The most general equations in fluid mechanics

are the Navier-Stokes equations. The assumptions in derivation the Navier-Stokes equation are:

- The fluid is a continuum media; it indicates that we deal with a continuous matter.
- The fields of interest such as pressure, velocity, density, temperature etc., are piecewise continuous functions of space and time.
- The fluid is Newtonian; a further, and very strong, restriction used is a linear stress-rate of strain relationship.

In the above, the term 'Continuous' means, there should be no boundary. Even quarks are not continuous. In fact, unless the size of the constitutive particles is zero, there cannot be any continuity. For any variable to be continuous in space, the above requirement of zero size must apply. For a variable to be continuous in time, the notion of 'piecewise' is absurd. Both space and time domains are continuous and must extend to infinity for 'conservation of mass' to hold true. There is not a single linear object in nature, let alone a linear relationship. In reality, there is not a single Newtonian fluid. The assumption of linear stress-rate of strain relationship is as *aphenomenal* (Zatzman and Islam, 2006; Khan and Islam, 2006) as the steady state assumption, in which the time dimension is eliminated.

A general model that explains completely the fluid motion and describes the nonlinearity due to the turbulence and chaotic motion of a fluid flow has not been developed so far. The solution for a turbulent flow is usually obtained based on the Navier-Stokes equations that are not developed for such a flow. Note that none of the above assumptions can be remediated by invoking non-linear form of an equation. For instance, non-linear power law equations cannot be invoked after the formulation, based on Newtonian fluid rheology, is completed.

The numerical description is also found based on some simplification and linearization during the solution process. After the first linearization of the process itself by imposing 'laws' to forcibly describe natural phenomena, further linearization is involved during solution schemes (Mustafiz et al., 2006). All analytical methods impose linearization by dropping nonlinear terms, which is most often accomplished by neglecting terms or by imposing a fictitious boundary condition. Numerical techniques, on the other hand, impose linearization through discretization (Taylor series expansion), followed by solutions of a linear matrix.

The existence of multiple solutions can be found in numerous problems. The occurrence of multiple solutions in solving the TSD-Euler equation was examined by Nixon (1989) and it was found that such solutions exist for a small range of Mach numbers and airfoil thicknesses. Nixon (1989) also found that a vorticity flux on the airfoil surface can enhance the appearance of multiple solutions.

We also observe the presence of multiple solutions, which depend on the pathway, in material processing operations. The existence of multiple roots in isothermal ternary alloys was discovered by Coates and Kirkaldy (1971) and was further explored by (Maugis et Al. (1996). Coriell et Al. (1998) continued investigation of one-dimensional similarity solutions during solidification/melting of a binary alloy. Their study, to some extent, was analogous to the isothermal ternary system, except that the phases were then solid and liquid and temperature played the role of one of the components of the ternary. The diffusivity equation was used to express the variation of temperature and concentration of fluid and solid in time and space. The equation was transferred to an ordinary differential equation using the similarity technique and the existence of multiple similarity solutions for the solidification/melting problem was noticed. These results corresponded to significantly different temperature and composition profiles. Recently, a computational procedure to find the multiple solutions of convective heat transfer was proposed by Mishra and DebRoy (2005). In this approach, the conventional method of

numerical solution was combined with a real number genetic algorithm (GA). These led the researchers to find a population of solutions and search for and obtain multiple set of input variable, all of which gave the desired specific output.

The existence of multiple solutions was investigated in separation technology using membrane separators by Tiscareno-Lechuga (1999). The author discussed conditions of the occurrence of multiple solutions when the mole fraction of a component with intermediate permeability was specified as a design variable. When the pressure in the permeate chamber was significantly lower than that of the rententate, the conditions turned to be simpler and were expressed through equations, which involved only the composition of the feed and the permeability of the membrane.

The existence of multiple solutions in porous media mixed convection problems was identified by Islam and Nandakumar (1986). They justified the existence of multiple solutions due to the nonlinearity in the energy balance equation. When non-Darcy flow equations were used, the range of multiple solutions became more discernible (Islam and Nandakumar, 1988). They extended this work to unsteady state systems (Nandakumar and Islam, 1990). In 1990, Islam et al. introduced solutions to the water heating/cooling problem, near 4°C, for which an additional nonlinearity due to peculiar water density behavior arises. Islam (1993) included the effect of chemical convection and showed detailed maps of multiples solutions. Sattar and Islam (1993) showed that the number of multiples solutions increases for large aspect ratios. Basu and Islam (1993) investigated multiple solutions invoked by by large aspect ratios in the presence of thermo-chemical convection.

We take into account some bivariate polynomials of different degree as a token-model for a natural phenomenon. It is assumed that the other contributing parameters of the model of the bivariate polynomial are constant. The number of solutions depends on the degree

of the nonlinearity of the polynomial. The solutions are obtained using the Newton's method and presented in graphical form for a limited region.

Some nonlinear simultaneous equations are also taken into account and the solutions of them are obtained with the Newton and Adomian decomposition methods (ADM). Our objective is to show that conventional techniques do not generate multiple solutions, for instance, the ADM, which is a very powerful method for solving nonlinear equations can not produce multiple solutions. We also proposed a new scheme to show the feasibility of generating multiple solutions.

5.3. Knowledge dimension

Dimensions provide the existence and imagination of the universe. It may be defined as the elements or factors making up a complete personality or entity. The dimensions are unique (each dimension has unique properties that makes it different from others), codependent (the dimensions are equally dependent to each other for their existence) and transcendent (dimensions have the ability of extending or lying beyond what would otherwise be possible). Higher dimensions include all lower dimensions but opposite is not true: lower dimensions do not include information in higher dimensions; e.g., length do not include area or volume.

Knowledge is synonymous to truth and reflects information about the properties, which exist in objects, events or facts. Knowledge explains the physical properties (which are observable and measurable), date, history, theories, opinions, etc. It includes but goes beyond, finite or particular space, mass and energy. Knowledge is a dimension for phenomena and may be possible to measure it by bits of information. Information can lead to an increase in knowledge only if proper science (science of nature) is used.

Some knowledge can be obtained through the physical and/or mathematical simulation of

a phenomenon. The physical simulation is carried out by geometrical, kinematical and dynamical scaling up or down of a problem. In many cases, it is not possible to obtain a complete physical simulation and, therefore, the experimental results are based on several assumptions. The mathematical simulation is obtained by finding the governing equation and the internal relationships between the parameters involved. Since any phenomenon is affected by a number of factors, any attempt to find the truth greatly relies on how closely these factors are addressed. It is observed that when governing equations are used to describe physical phenomena, several assumptions are needed. It is understandable that as we reduce the number of assumptions, we reach closer to the truth.

The multiplicity of possible solutions is another aspect of the knowledge dimension. As time is passes, knowledge is increased if the path of nature science is followed. This process is just like time, irreversible. Knowledge cannot regress. Whenever, it is necessary to retract or "lose" information, it becomes a matter of disinformation, which is the pre-cursor to anti-Knowledge. Consciousness, which is knowledge of the knowledge, is another distinct stage within the dimension. It may be considered as the second stage of the knowledge dimension as compared to information alone. Each stage is naturally independent and, therefore, it may allow independent knowledge to enter. There is no limitation or beginning and end, of the knowledge dimension. This multiplicity of possible solutions in the knowledge dimension is indicated as a range of solutions for a specific phenomenon, arising from the presence of all those different factors that contribute to the phenomenon.

If we consider a pure material and plot the curve for melting or freezing of it at a certain pressure, there is a constant temperature during the freezing or melting process. However, there is no pure substance. In fact, when we refer to 100% pure, it pertains to detection limit. It is impossible to create a 100% pure substance, at least under terrestrial conditions. This is the nature of science of intangibles, which does not allow any exactness (Islam and Zatzman, 2006). If an isomorphous alloy, which consists of an

arbitrary composition of components A and B, is taken into account, the freezing or melting process is taken place in a range of temperature depends on the composition of the alloy and the pressure, as shown in Fig. 5.1(a). Therefore, we are dealing with a range of temperature instead of a constant temperature. Another interesting point is that during the freezing and melting process the concentrations of the equilibrium liquid or solid phases are changing and varying in a certain range dependent on the final concentration of liquid or solid state. This is more pronounced for an alloy of more components. Figure 5.1(b) shows how multiple solutions can be extremely valuable while making decisions. With conventional analysis, most likely solutions that would be considered is the one marked by dark bold line. With conventional mathematics, the focus is on tangible and exactness, leading one to accept the first number that appears to be 'real'. Because no more solutions are sought, one is limited to a large domain of choice and options. Note that, every natural process is high on intangibles (as manifested by the time space) and therefore has many more solutions than than the one provided by the mathematics of tangible.

There should be a population of solutions for a problem related to a natural phenomenon, dependent on the number and the behavior of involved parameters. There are many situations that the variation of parameters involving in a natural phenomenon is approximated with a polynomial function (Bjorndalen, 2002; Bjorndalen et al., 2005; Mustafiz et al., 2006). This is because we do not know the governing equation for that phenomenon. The number of solution for such a function depends on the nonlinearity of that function. There are also roots that are not real. All of the roots of such a polynomial indicate that we should expect different solutions regardless of the physical significance of them. It also indicates that if we can represent the natural data as a polynomial function at any given time, we can determine the roots, all of which should be considered for reporting some natural phenomena. Thus, roots including the imaginary ones are considered as the multiple solutions.

We take into account three bivariate polynomials and solve them for all possible roots. These polynomials are a third-, two forth- and a fifth-degree polynomials with two variables x and y.

5.3.1. Example 1.

The first polynomial is a third degree bivariate polynomial.

$$4y^3 - 3y^2 - 2y + 2 = -5x^3 + 4x^2 + 3x + 1 \tag{5.1}$$

The solution of this third degree polynomial is shown in Figs. 5.2 to 5.4. The real roots of the bivariate polynomial are depicted in Fig. 5.2. This polynomial gives three real roots in a limited range of x and y. In general, the polynomial has three complex roots at each constant real value of x and y. These roots can not be shown in a single graph. These are depicted in Figs. 5.3 when the variable y is a fixed real number and in Figs. 5.4 for a fixed real value of x.

This figure indicates that with such a simple nonlinear problem we are dealing with a population of solutions, some of which them may not be tangible. However, It does not mean that the intangible solutions are not natural. A complex number consists of a real part and an imaginary part. In many cases, it was understood that the only real part describing the real world. The later applications of the complex number in different branch of sciences such as quantum mechanics, control theory, fluid dynamics and signal analysis reveal that nature has no preference for the real number and the imaginary part being just as physical as the real part. The reason that focus has been on tangible forms, exactness, and uniqueness of solutions has its root in Eurocentric mathematics (Joseph, 2000). Recently, Islam and Zatzman (2006) pointed out that reality has little to do with exactness and everything tangible that form the core of European mathematics.

5.3.2. Example 2.

The second example is a fourth degree polynomial.

$$5y^4 + 4y^3 - 3y^2 - 2y + 2 = 6x^4 - 5x^3 - 4x^2 + 3x - 2 \tag{5.2}$$

The roots of the fourth degree polynomial are given in Figs. 5.5 to 5.7. In general, this polynomial should have four roots for each constant value of the variables. Four real roots for x can be found four real roots in a limited range of the variable y. It does not have four real roots for the variable y for a fixed real value of x. At most two real roots for the variable y can be obtained if x has a real value. All of the imaginary roots for y = 0,±1,±2,±3,±4,±5 is given in Figs. 5.6. The same graphs are shown for the roots of the forth degree polynomial in Figs. 5.7 when x = 0,±1,±2,±3,±4,±5.

5.3.3. Example 3.

The next example is a fifth degree polynomial.

$$6y^6 + 5y^4 + 4y^3 + 3y^2 + 2y + 1 = 7x^5 + 6x^4 + 5x^3 + 4x^2 + 3x + 2 \tag{5.3}$$

The real roots of this polynomial are depicted in Figs. 5.8 to 5.10. This fifth degree polynomial has a real root for every real value of x and y. All roots of the polynomial are shown in the complex planes in Figs. 5.9-a and 5.10-a for y, x = 0,±1,±2,±3,±4,±5, respectively. The figures show that each two of the four complex roots are complex conjugate.

The variation of a parameter causes other parameters to be affected and prescribes some changes during the process. This indicates that all of the contributing parameters in a natural phenomenon are dependent on each other. The dependence may be described with

some nonlinear simultaneous equations. The solution for these systems of nonlinear function is obtained mostly by the numerical methods. However, in many cases, the restriction of the applied method may limit in obtaining all of the solutions possible.

The well known method in solution of nonlinear algebraic and simultaneous equations is the Newton method. The main restriction of this method is that the initial value for starting the iteration should be near the exact solution. If the initial guess is far from the exact solution it may result in a divergent iterations. We also applied the ADM. This is a powerful method that can be used to obtain the solutions of systems of nonlinear simultaneous equations. This technique was first proposed by a physicist, G. Adomian (1923-1996). The method is well addressed in Mousavizadegan et al. (2006) to discuss the limitations of ADM for partial differential equations and Mustafiz et al. (2006) to solve the Buckley-Leverett equation with the effect of the capillary pressure.

The ADM solution is obtained in a series form while the nonlinear term is decomposed into a series in which the terms are calculated recursively using Adomian polynomials. A simultaneous algebraic equation with n independent variables is taken into account. It may be written that

$$f_i(x_1, x_2, ..., x_n) = 0 \qquad \text{and} \qquad i = 1,2,...,n \tag{5.4}$$

Each equation can be solved for an independent variable as

$$x_i = a_i + g_i(x_1, x_2, ..., x_n) \qquad \text{and} \qquad i = 1,2,...,n \tag{5.5}$$

The solution may be expressed in a series solution as

$$x_i = \sum_{i=0}^{\infty} x_{i,j} \qquad \text{and} \qquad i = 1,2,...,n \tag{5.6}$$

The components of the series solution are obtained using the Adomian decomposition method in the form

$$\sum_{i=0}^{\infty} x_{i,j} = \mathrm{a_i} + \sum_{k=0}^{\infty} A_{i,k} \tag{5.7}$$

where

$$x_{i,0} = \mathrm{a_i},\quad x_{i,1} = A_{i,0},\quad x_{i,2} = A_{i,1},\ \ldots,\quad x_{i,m} = A_{i,m-1},\quad x_{i,m+1} = A_{i,m},\ \ldots \tag{5.8}$$

The term $A_{i,m}$ is obtained by using the Adomian polynomial that is given in the following form

$$A_{i,m} = \frac{1}{m!}\left[\frac{d^m}{d\lambda^m} g_i\left(\sum_{k=0}^{\infty}\lambda^k x_{1,k},\ \sum_{k=0}^{\infty}\lambda^k x_{2,k},\ldots,\ \sum_{k=0}^{\infty}\lambda^k x_{n,k}\right)\right]_{\lambda=0} \tag{5.9}$$

$$\text{and} \qquad m = 1,2,\ldots,\infty \qquad \text{for} \qquad i = 1,2,\ldots,n$$

These are the first three elements of the Adomian polynomials.

$$\begin{aligned}
A_{i,0} &= g_i(x_{1,0}, x_{2,0}, \ldots, x_{n,0}) \\
A_{i,1} &= x_{1,1}\frac{\partial}{\partial x_1} g_i(x_{1,0}, x_{2,0}, \ldots, x_{n,0}) + \ldots + x_{n,1}\frac{\partial}{\partial x_n} g_i(x_{1,0}, x_{2,0}, \ldots, x_{n,0}) \\
A_{i,2} &= x_{1,2}\frac{\partial}{\partial x_1} g_i(x_{1,0}, x_{2,0}, \ldots, x_{n,0}) + \ldots + x_{n,2}\frac{\partial}{\partial x_n} g_i(x_{1,0}, x_{2,0}, \ldots, x_{n,0}) + \\
&\quad \frac{1}{2}x_{1,1}^2\frac{\partial^2}{\partial x_1^2} g_i(x_{1,0}, x_{2,0}, \ldots, x_{n,0}) + \ldots + \frac{1}{2}x_{n,1}^2\frac{\partial^2}{\partial x_n^2} g_i(x_{1,0}, x_{2,0}, \ldots, x_{n,0}) + \\
&\quad x_{1,1}x_{2,1}\frac{\partial^2}{\partial x_1 x_2} g_i(x_{1,0}, x_{2,0}, \ldots, x_{n,0}) + \ldots + x_{1,1}x_{n,1}\frac{\partial^2}{\partial x_1 x_n} g_i(x_{1,0}, x_{2,0}, \ldots, x_{n,0}) + \\
&\quad x_{2,1}x_{3,1}\frac{\partial^2}{\partial x_2 x_3} g_i(x_{1,0}, x_{2,0}, \ldots, x_{n,0}) + \ldots + x_{2,1}x_{n,1}\frac{\partial^2}{\partial x_2 x_n} g_i(x_{1,0}, x_{2,0}, \ldots, x_{n,0}) + \\
&\quad \ldots \qquad + \ldots \qquad + x_{n-1,1}x_{n,1}\frac{\partial^2}{\partial x_2 x_3} g_i(x_{1,0}, x_{2,0}, \ldots, x_{n,0})
\end{aligned} \tag{5.10}$$

The rest is lengthy and more complicated. MATLAB is used to compute the elements of $A_{i,j}$. The elements of the series solution x_i are obtained according to Eq. (5.6).

5.3.4. Example 4.

The first nonlinear system of equation is

$$\begin{cases} x^2 - 10x + 4y^2 + 9 = 0 \\ xy^2 + x - 10y + 5 = 0 \end{cases}, \tag{5.11}$$

The real solutions can be obtained by plotting the equations as given in Fig. 5.11. The plot indicates that there are two common real roots for this nonlinear SAE.

We use the ADM to find the solution for Eq. (5.11). The series solutions are obtained using the equations (5.4) to (5.10) with different numbers of the elements. The computations are carried on using MATLAB. The solutions and the errors with different umber of elements are

$x = 1.21244$ & $y = 0.669277$ if $i = 4$ $E_1 = 0.1373$ & $E_2 = 0.0627$
$x = 1.23491$ & $y = 0.679418$ if $i = 8$ $E_1 = 0.0223$ & $E_2 = 0.0108$
$x = 1.23802$ & $y = 0.680857$ if $i = 12$ $E_1 = 0.0046$ & $E_2 = 0.0023$
$x = 1.23916$ & $y = 0.681396$ if $i = 16$ $E_1 = 0.0011$ & $E_2 = 0.0006$
$x = 1.23933$ & $y = 0.681474$ if $i = 20$ $E_1 = 0.0003$ & $E_2 = 0.0001$

where E_1 and E_2 are the deviation of the first and second equation from zero. However, it gives a good approximation for the solution of this system of simultaneous equations. The deficiency of the ADM is that it is not able to give the second solution as seen in Fig. 5.11. The other restriction is that the Adomian polynomial does not always give a convergent series solution. It depends on the type of the equations and the first term of

the series solution. Sometimes it is necessary to change the form of the equations to a get a convergent series solution for the problem.

5.3.5. Example 5.

The second nonlinear SAE is

$$\begin{cases} x^2 + 4y^2 - 16 = 0 \\ -2x^2 + xy - 3y + 10 = 0 \end{cases} \tag{5.12}$$

This system of simultaneous equations has four real common roots as shown in Fig. 5.12. These roots are computed with ADM. The system of equations is written in the form

$$\begin{cases} x = \pm\sqrt{0.5(xy - 3y + 10)} \\ y = \pm 0.5\sqrt{16 - x^2} \end{cases} \tag{5.13}$$

for each of the variables. It is assumed that $x = \sum_{i=0}^{\infty} x_i$ and $y = \sum_{i=0}^{\infty} y_i$. Using ADM, it is set that $x_0 = 0$ and $y_0 = 0$. The elements of the series solutions are obtained using the Adomian polynomial as given in Eq. (5.9).

$$x_m = \frac{1}{m!}\left\{\frac{\partial^{m-1}}{\partial\lambda^{m-1}}\left[\pm\sqrt{0.5\left(\sum_{k=0}^{\infty}\lambda^k x_m \sum_{k=0}^{\infty}\lambda^k y_k - 3\sum_{k=0}^{\infty}\lambda^k y_k + 10\right)}\right]\right\}_{\lambda=0} \quad \text{for } m = 1,2,....$$

$$y_m = \frac{1}{m!}\left\{\frac{\partial^{m-1}}{\partial\lambda^{m-1}}\left[\pm 0.5\sqrt{16 - \sum_{k=0}^{\infty}\left(\lambda^k x_k\right)^2}\right]\right\}_{\lambda=0} \quad \text{for } m = 1,2,....$$

The computation are carried out and the solution are obtained when the series solution are truncated to $i = 10$. The solutions are

$x = 2.0426 \;\; \& \;\; y = 1.7144$; $\quad x = -1.0435 \;\; \& \;\; y = 1.9316$;

$x = -2.9794 \;\& \; y = -1.3193$; and $\quad x = 2.3554 \;\& \; y = -1.6235$.

which are very accurate. The more accurate result can be found with increasing the number of the series solution elements. The multiple solutions can be found if the solution is arranged in proper form. It can be considered as one of the most challenging tasks in application of ADM. A proper arrangement should be selected to obtain a convergent result as well as the multiple solutions if there are.

5.3.6. Example 6.

The third example is a third degree system of two simultaneous equations of the variables x and y.

$$\begin{cases} x^3 + y^3 - 10x - 5 = 0 \\ x^3 - y^3 - 15y^2 + 2 = 0 \end{cases} \tag{5.14}$$

The equations are plotted in Fig. 5.13. It is realized that there are four real solution for this system of nonlinear equations. The solution for the variables may be arranged in the form

$$\begin{cases} x = -0.2 + 0.1(x^3 + y^3) \\ y = \pm\sqrt{\dfrac{1}{15}(2 + x^3 - y^3)} \end{cases} \tag{5.15}$$

Using ADM, the solutions are expressed in the series form as Eq. (5.6). The elements of the series solution for x and y are computed by taking into account that $x_0 = -0.5$ and $y_0 = 0$ the rest are computed using Adomian polynomial in Eq. (5.9). The arrangement of the SAE in the form of Eq. (5.15) gives two of the common real roots that are ($x = -0.5089$ & $y = 0.3489$) and ($x = -0.5185$ & $y = -0.3565$). This arrangement in the form of Eq. (5.15) does not give all the common real roots of the SAE of Eq. (5.14). The other solutions may be obtained with another arrangement for x and y. Different arrangement for the variables are attempted but almost all of them result in divergent series.

5.3.7. Example 7.

The next example is a fourth degree system of simultaneous equations.

$$\begin{cases} x^4 + x^3 y + \frac{1}{5} y^4 - 15x - 3 = 0 \\ 2x^4 - y^4 - 10y + 3 = 0 \end{cases} \tag{5.16}$$

There are four common real roots for this system of equations as shown in Fig. 5.14. This system of equations are rearranged in the form

$$\begin{cases} x = -\frac{1}{5} + \frac{1}{15}(x^4 + x^3 y + \frac{1}{5} y^4) \\ y = \frac{3}{10} + \frac{1}{10}(2x^4 - y^4) \end{cases} \tag{5.17}$$

for x and y variables. The only solution that can be obtained with the ADM and the arrangement of Eq. (5.17) is $x = -0.19995$ & $y = 0.29952$ where the series solution is truncated to $i = 5$.

5.4. Conclusions

Our objective in this paper is to discuss the possibility of the multiple solution for natural phenomena. In many cases, it is possible to express or approximate a natural phenomenon by a nonlinear polynomial. This nonlinear polynomial has multiple solutions which depends on nonlinearity and number of variables. A number of bivariate polynomials of different degrees were used in this paper and it was shown that a population of solutions in the complex plane exists.

The other objective is to show the limitation of the methods in finding the complete solutions of a given nonlinear problem. The mathematical model for many real problems are given in the form of partial differential equations. In most of the cases, the solution of these PDEs are obtained by the numerical methods. The normal procedure is to recast the PDE in the form of nonlinear simultaneous algebraic equations (SAE). The solutions of this nonlinear SAE are obtained by some linearization during the process of computations. This may affect the quality as well as the quantity of the solutions.

We introduce several bivariate nonlinear SAEs with different degrees of nonlinearity. The real roots of these bivariate SAEs can be obtained graphically as shown in the previous sections. All of the SAEs are solved with Adomain decomposition method (ADM) and show the limitation of the ADM method, which is used as a sample method. However, other methods such as Newton's method can provide one with all probable solutions but it is necessary to know the region of each solution to start a convergent iteration and find the roots. If the number of variables are increased, it will be a challenging task to find the region of all roots. Such investigation will enable one to get the complete picture of the knowledge dimension, which will be useful in decision making.

5.5. References

Basu, A. and Islam, M.R., (1996) Instability in a combined heat and mass transfer problem in porous media, Chaos, Solitons & Fractals, vol. 7, no. 1, pp. 109-123

Bjorndalen, N., (2002) Irradiation techniques for improved performance of horizontal wells, MASc Thesis, Dalhousie University, Halifax, Canada

Bjorndalen, N., Mustafiz, S. and Islam, M.R., (2005) The effect of irradiation on immiscible fluids for increased oil production with horizontal wells, ASME International Mechanical Engineering Conference and Exposition, Orlando, Florida, USA, November 6-11

Coates, D. E, and Kirkaldy, J. S., (1971) Morphological stability of alpha-beta phase interfaces in the Cu- Zn- Ni system at 775 C , Metallurgy Transactions, vol. 2, no. 12, pp. 3467-3477, December

Coriell, S.R., McFadden, G.B., Sekerka, R.F.and Boettinger W.J., (1998) Multiple similarity solutions for solidification and melting, Journal of Crystal Growth, vol. 191, pp. 573-585

Islam, M.R., (1993) Route to chaos in chemically enhanced thermal convection in porous media, Chemical Engineering Communications, vol. 124, pp. 77-95

Islam, M.R., (2006) Computing for the information age, Proc. of the 36th International Conference on Computers and Industrial Engineering, Keynote Speech, Taipei, Taiwan, June 20-23

Islam, M.R., Chakma, A. and Nandakumar, K., (1990) Flow transition in mixed convection in a porous medium saturated with water near 4C, Canadian Journal of Chemical Engineering, vol. 68, pp. 777-785

Islam, M.R. and Nandakumar, K., (1986) Multiple solution for buoyancy-induced flow in saturated porous media for large Peclet numbers, Transactions ASME Journal of Heat Transfer, vol.108, no. 4, pp. 866-871

Islam, M.R. and Nandakumar, K., (1988) Mixed convection heat transfer in porous media in the non-Darcy regime, Canadian Journal of Chemical Engineering, vol. 66, no. 1, pp. 68-74

Islam, M.R. and Nandakumar, K., (1990) Transient convection in saturated porous layers with internal heat sources, International Journal of Heat and Mass Transfer, vol. 33, no. 1, pp. 151-161

Joseph, G.G., (2000) The crest of the peacock: Non-European roots of mathematics, Ed. 2, Penguin Books, London

Khan, M.I. and Islam, M.R., (2006) True sustainability in technological development and natural resources management, Nova Science Publishers, NY, USA

Islam, M.R. and Zatzman, G.M., (2006) Emulating nature in the information age, Chemcon-06, 59th Annual Conference of the Indian Chemical Engineering Congress, Gujarat, December 27-30

Maugis, P.; Hopfe, W.D.; Morral, J.E.; Kirkaldy, J.S., (1996) Degeneracy of diffusion paths in ternary, two-phase diffusion couples, Journal of Applied Physics, vol. 79, no. 10, pp. 7592-7596

Mishra, S., and DebRoy, T., (2005) A computational procedure for finding multiple solutions of convective heat transfer equations, Journal of Physics D: Applied Physics, vol. 38, pp. 2977–2985

Mustafiz, S., Moussavizadegan, H., and Islam, M.R., (2006) The effects of linearization on solutions of reservoir engineering problems, Journal of Petroleum Science and Technology, accepted for publication, July, 17 pg.

Nixon, D., (1989) Occurence of multiple solutions for the TSD-Euler equation Source: Acta Mechanica, vol. 80, no. 3-4, pp. 191-199

Sattar, M.A. and Islam, M.R., (1993) Flow instability in a large aspect ratio porous medium with an internal heat source, Chaos, Solitons & Fractals, vol. 3, no. 2, pp. 149-169

Tiscareno-Lechuga, F., (1999) A sufficient condition for multiple solutions in gas membrane separators with perfect mixing, Computers and Chemical Engineering, vol. 23, no. 3, pp. 391-394

Zatzman, G.M. and Islam, M.R., (in press) Economics of intangibles: Nova Science Publisher, NY, USA

5.6. Appendices

5.6.1. Appendix A: Figures

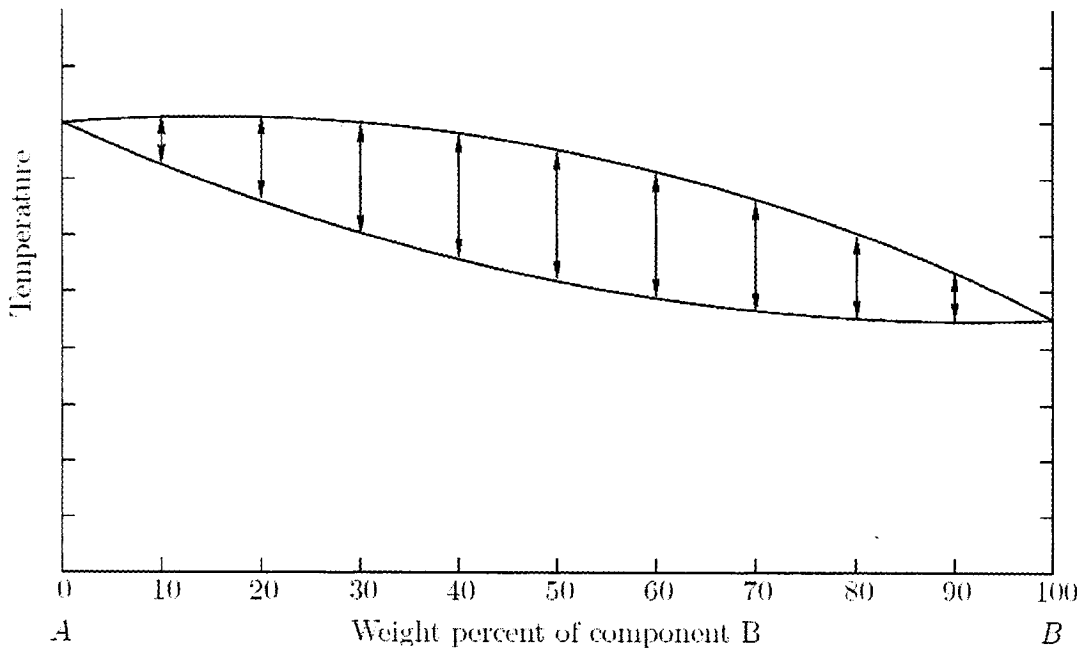

Figure 5.1(a). The phase diagram for an isomorphous alloy

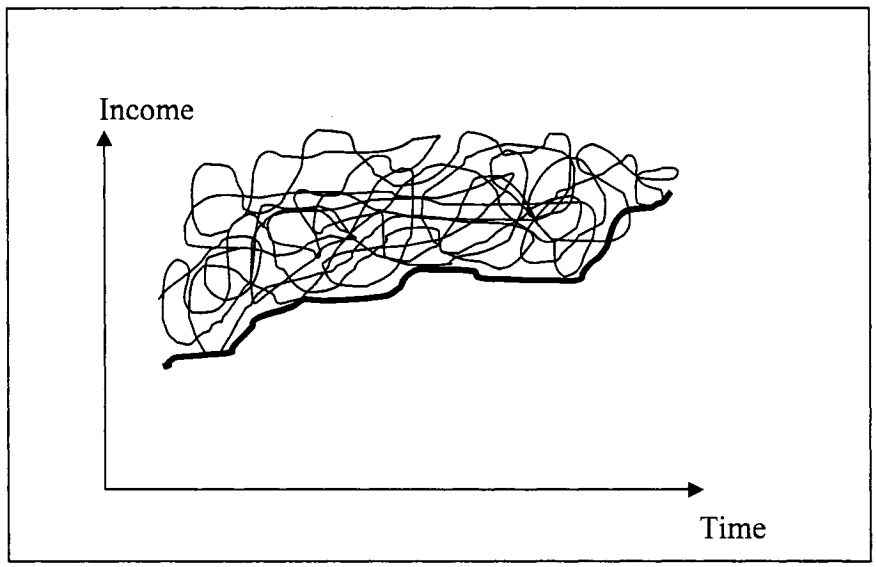

Figure 5.1(b). The value of the knowledge dimension (after Zatzman and Islam, 2006)

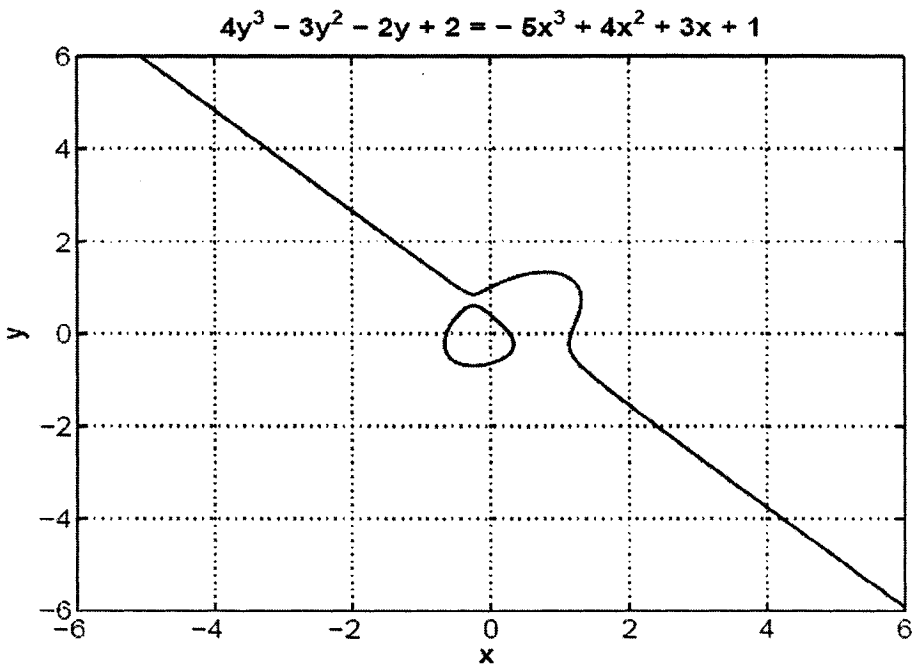

Figure 5.2. The graph of a third degree polynomial

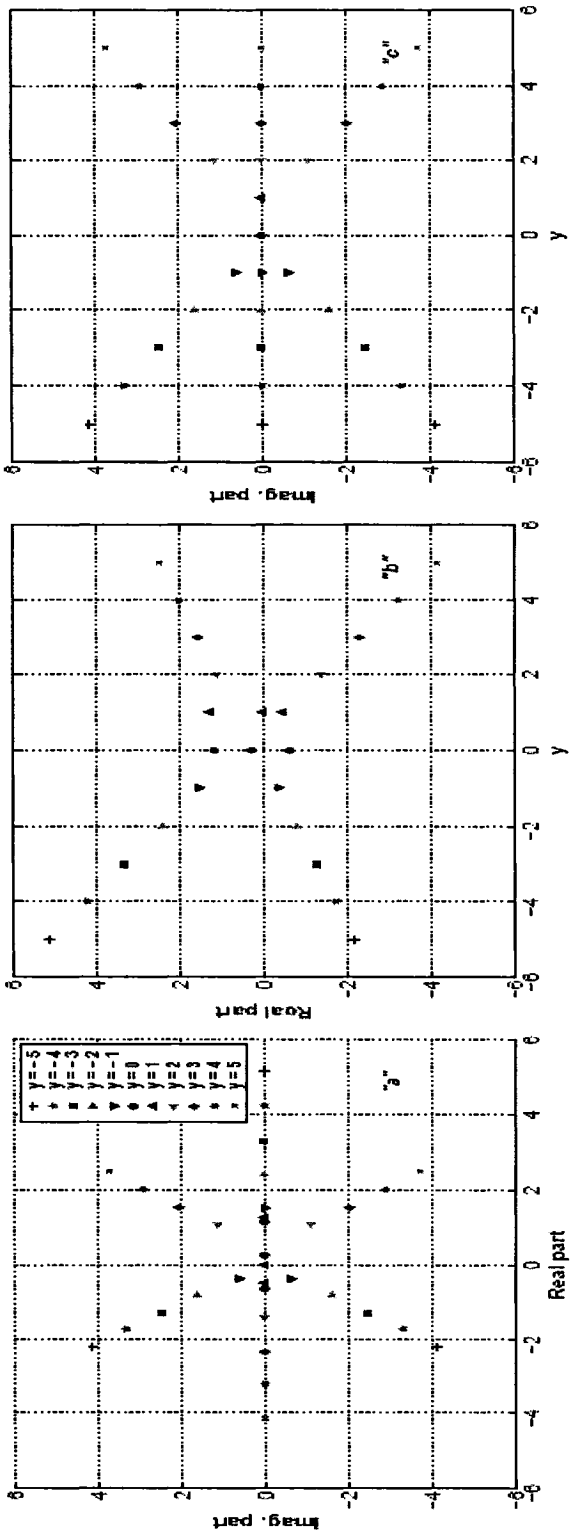

Figure 5.3. The roots of the third degree polynomial for a fixed value of y

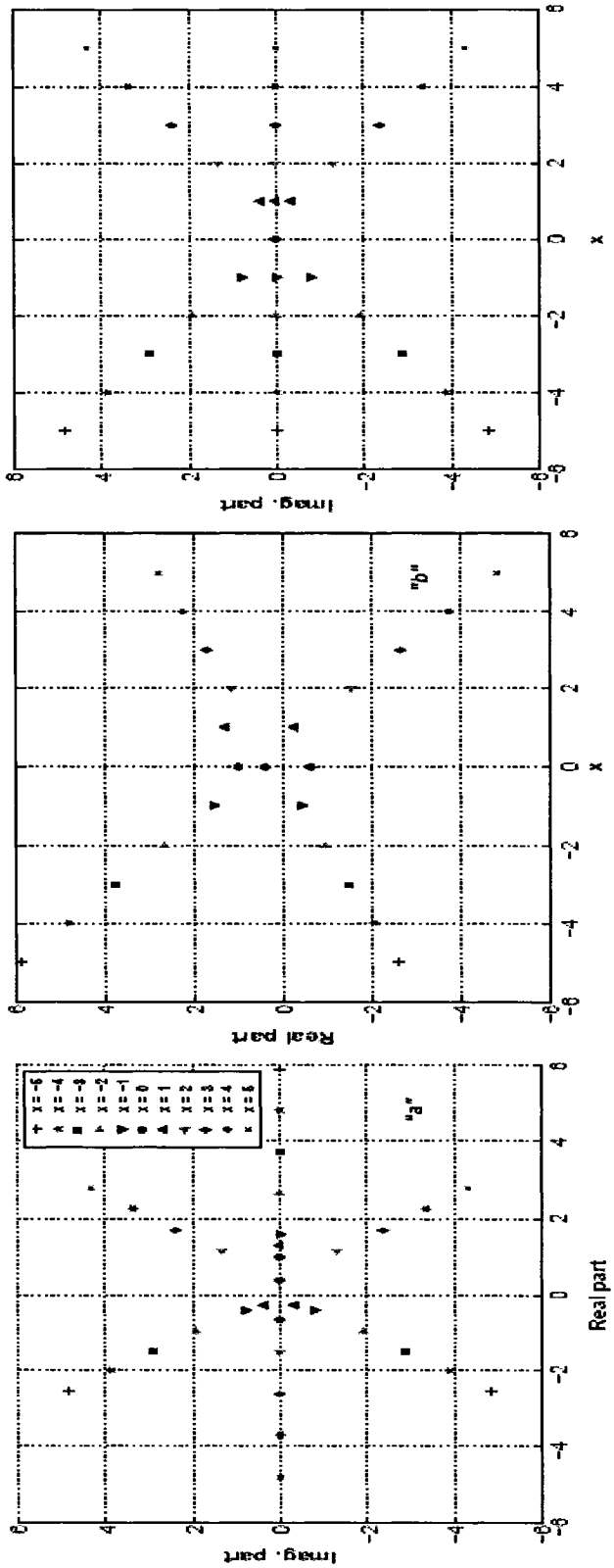

Figure 5.4. The roots of the third degree polynomial for a fixed value of x

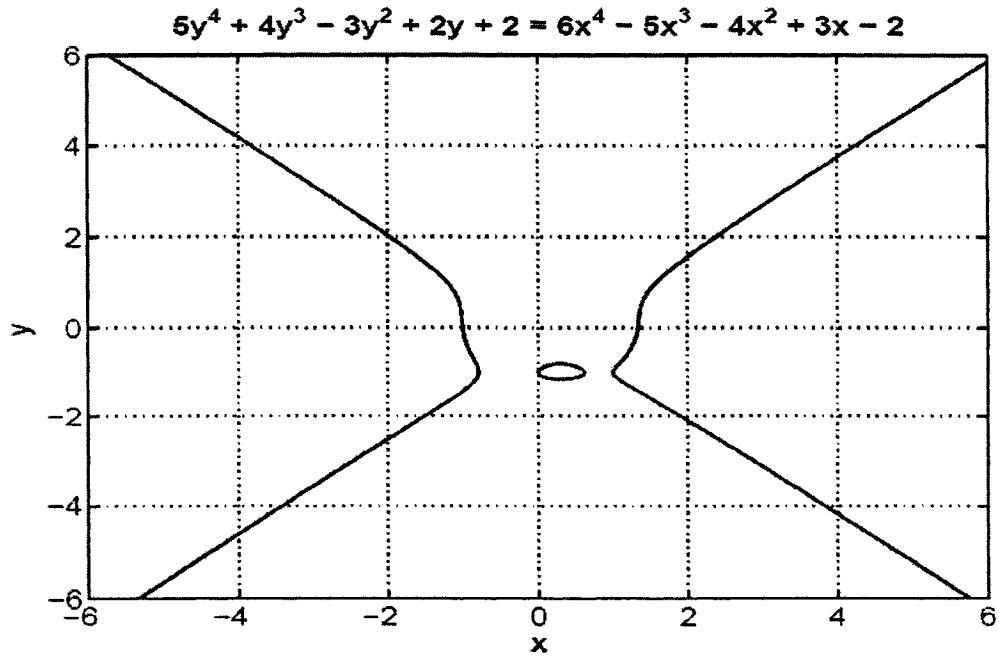

Figure 5.5. The graph of the real value of the first fourth degree of polynomial

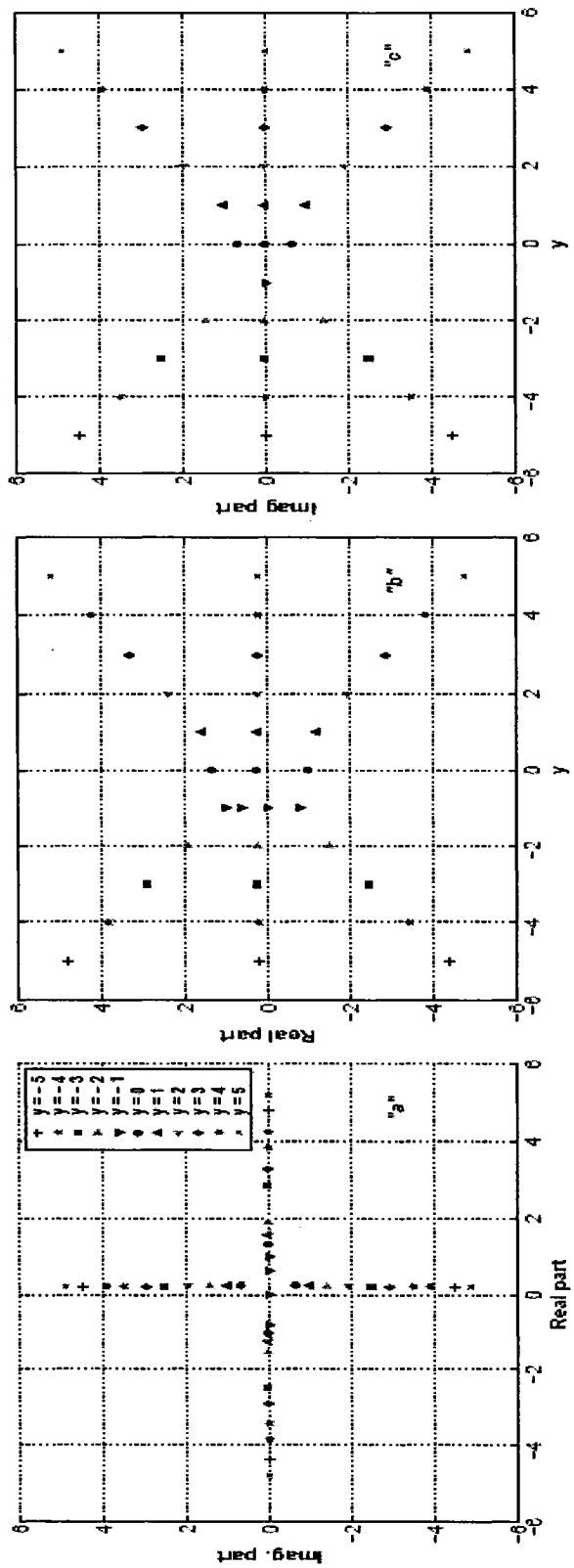

Figure 5.6. The roots of the first fourth degree polynomial for a fixed real value of y

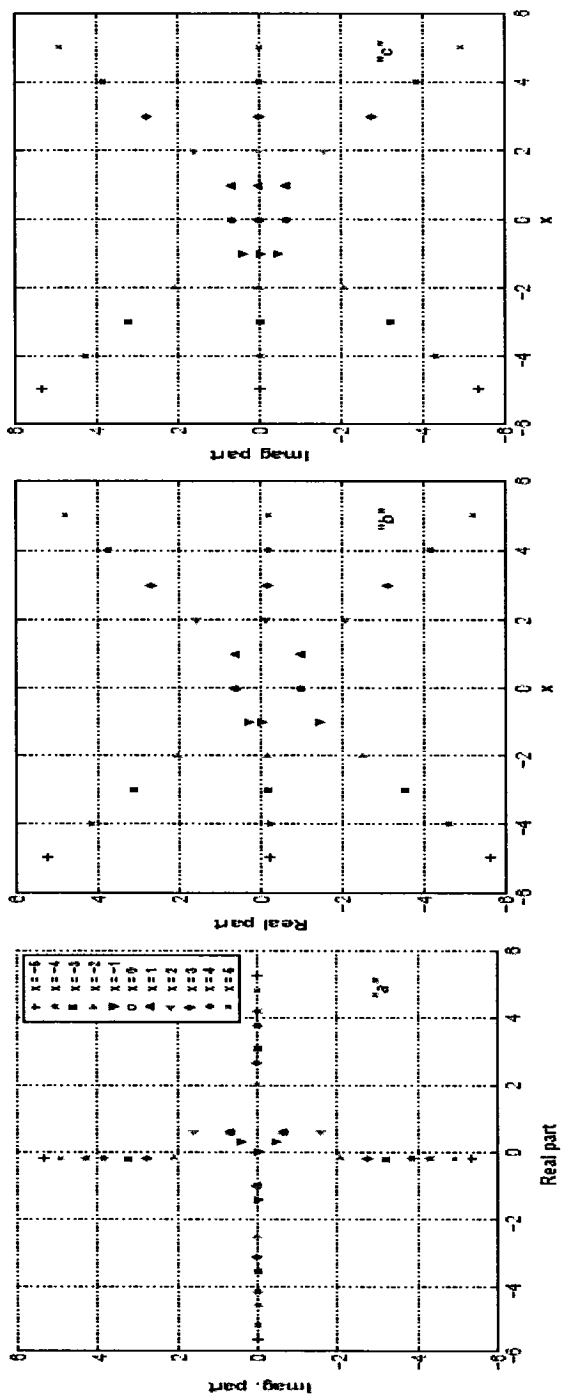

Figure 5.7. The roots of the first fourth degree polynomial for a fixed real value of x

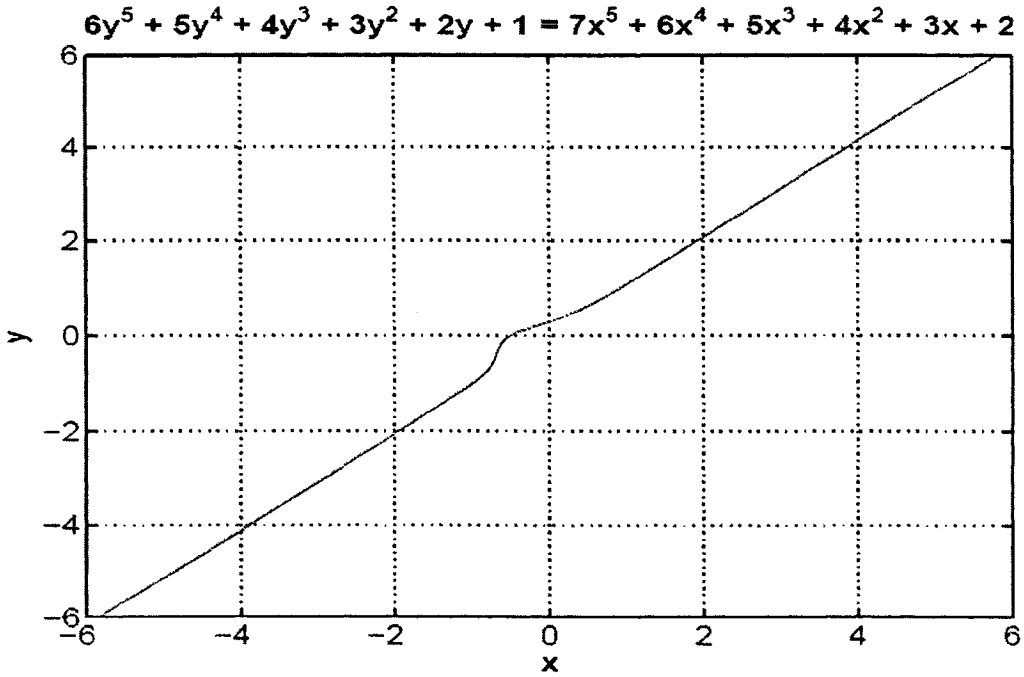

Figure 5.8. The graph of the real roots of the fifth degree polynomial

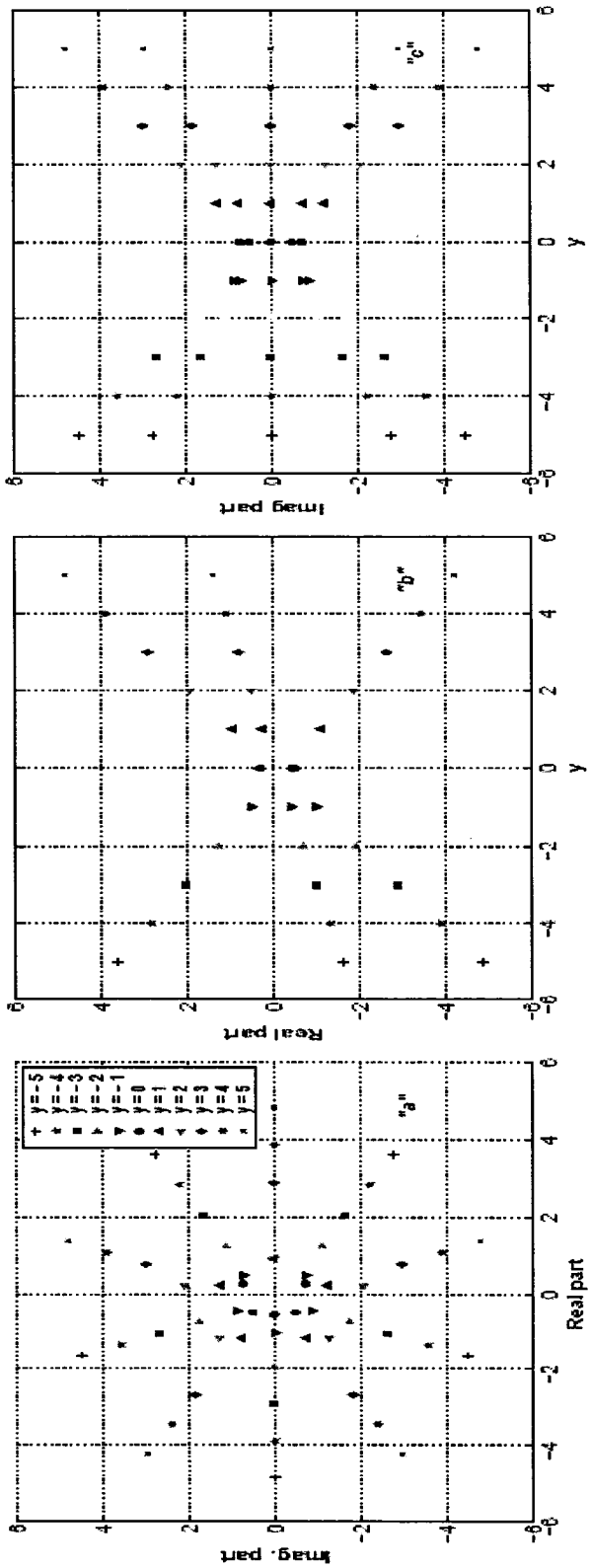

Figure 5.9. The roots of the fifth degree polynomial for a fixed real value of y

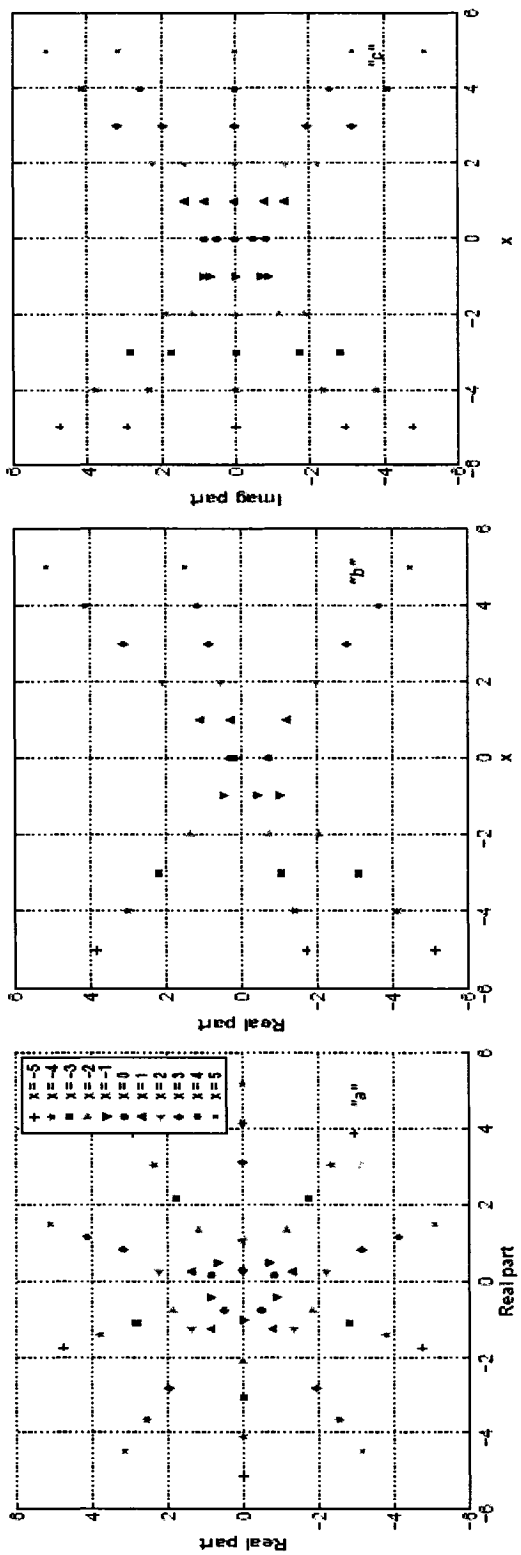

Figure 5.10. The roots of the fifth degree polynomial for a fixed real value of x

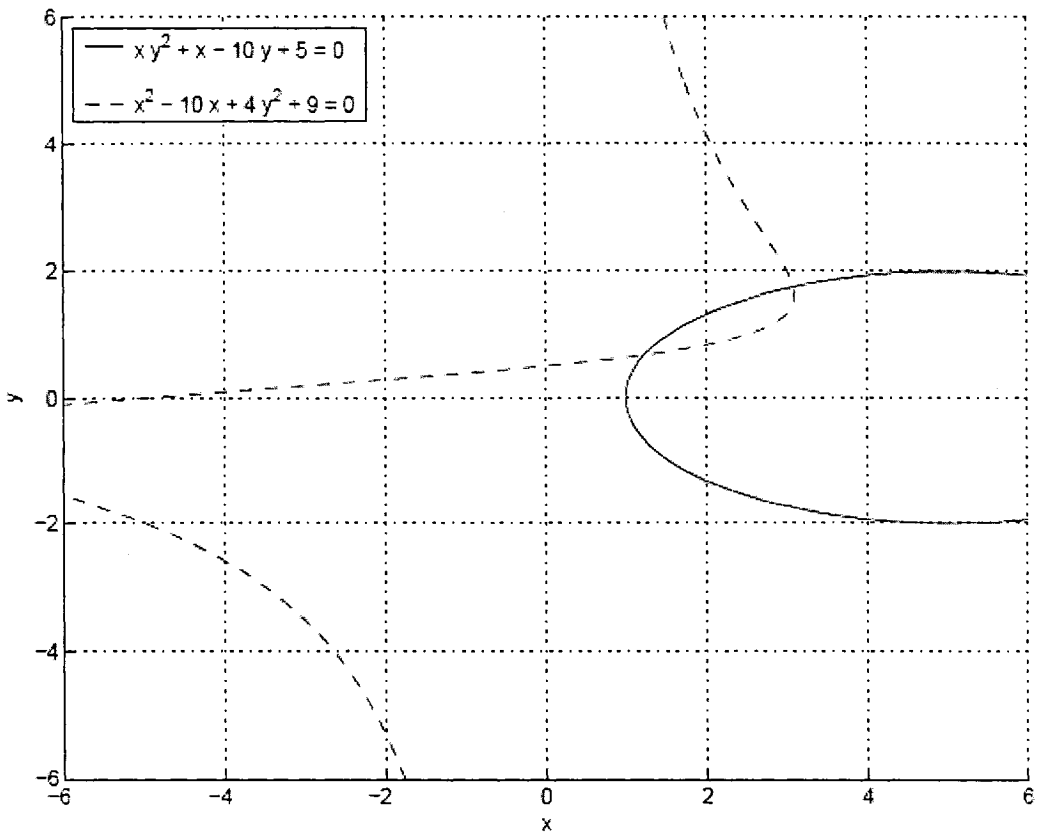

Figure 5.11. The graphs of the simultaneous equations of (5.11)

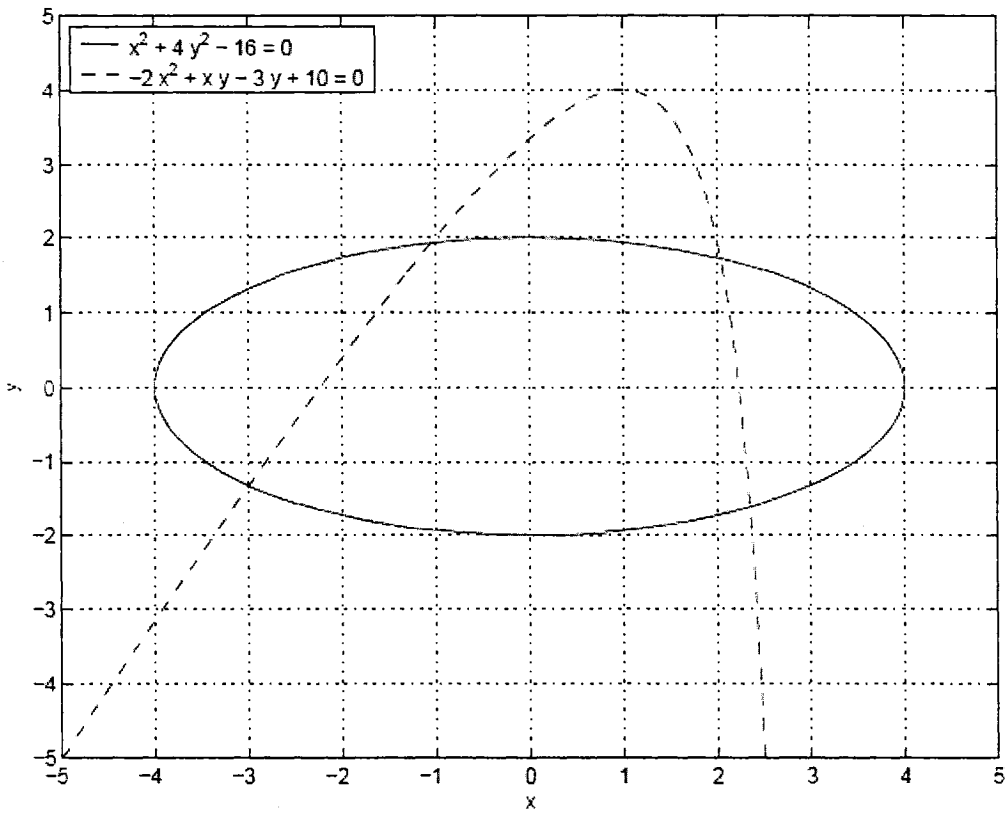

Figure 5.12. The graphs of the simultaneous equations of (5.12)

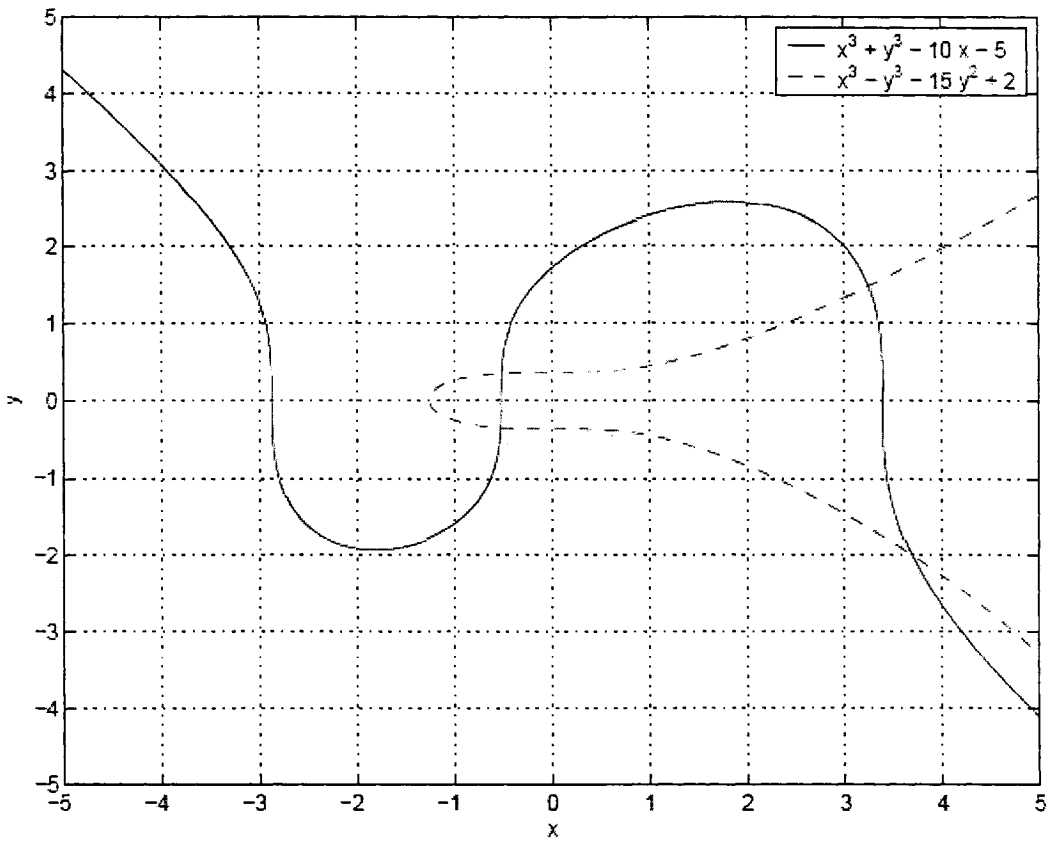

Figure 5.13. The graphs of the simultaneous equations of (5.14)

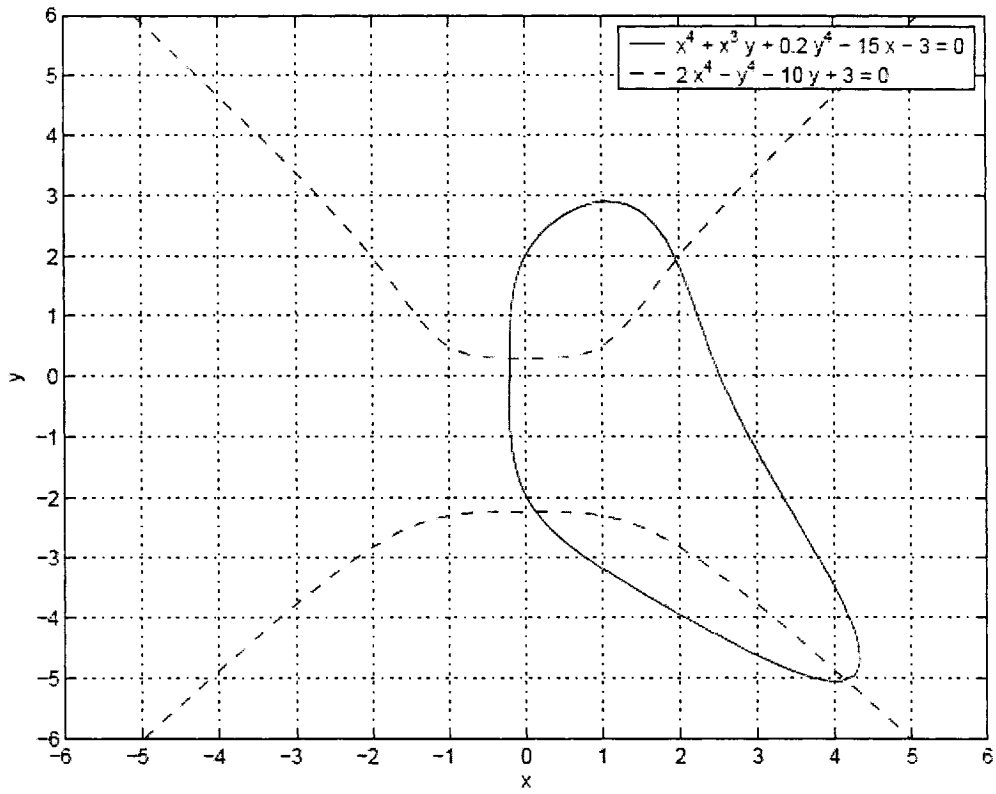

Figure 5.14. The graphs of the simultaneous equations of (5.16)

Chapter 6

6 THE ADOMIAN DECOMPOSITION METHOD ON SOLUTIONS OF NON-LINEAR PARTIAL DIFFERENTIAL EQUATIONS

6.1. Abstract

The Adomian decomposition method (ADM) is applied to solve nonlinear differential equations of various types. The ADM solution is an infinite series that is constructed using the initial and boundary conditions and the forcing function. The numerical result is approximated by truncation of the series solution to a finite number. The effect of this truncation on the final result is investigated in this paper. The accuracy of the ADM depends on the number of series solution terms. The solution is good for a very small value of the independent variables. The ADM solution is susceptible to instability with increasing the spatial or time variables.

6.2. Introduction

The methods of the solution of the nonlinear partial differential equations (PDE) and integral equations (IE) may be categorized as exact, approximate and numerical methods. In the approximate methods, the solutions are obtained in the form of functions which are close to the exact solution. The exact solutions are constructed by using analytical procedures. The Adomian decomposition method is an approximate scheme and the solution is obtained recursively using the forcing function and the initial and boundary conditions. This method was first proposed by a North American physicist, G. Adomian (1923-1996) and well addressed in (Adomian and Adomian, 1984; Adomian, 1989 and

Adomian, 1994). The ADM solution is obtained in a series form while the nonlinear term is decomposed into a series in which the terms are calculated recursively using Adomian polynomials.

There are several published papers on the solution of the linear and nonlinear partial differential equation using the Adomian decomposition method. Recently, Biazar and Islam (2004) have used ADM to solve the linear wave equation in 3-dimensional space. They indicate that ADM is very sensitive to initial and boundary conditions and do not function if the initial and boundary conditions are constant. The nonlinear dispersive KdV equation with initial profile is solved by Wazwaz (2001) using ADM. The approximate solutions are arranged in power polynomials that are applied to find out the closed form solutions for different test examples. The truncated ADM solution for the two solitons solution are reported for a very small time interval and does not match with the closed form solution of the problem. Deeba and Khuri (1996) have applied ADM for solving the nonlinear Klein-Gordon (KG) Equation. The tabulated errors for a nonlinear test example show that the accuracy of the ADM solution is impaired with increasing time intervals.

We investigate the influence of the truncation of the ADM series solution on the accuracy and the stability of the results in this article. The ADM is applied to solve the nonlinear Burger's equation with various initial and boundary conditions, the nonlinear KdV equation with one and two solitons solution and the KG-equation of different types. The formulation of the Adomian decomposition method is presented for the general case of functional equations and then extended to each of these PDEs. Several examples for each type of these PDEs are taken into account and the ADM solutions are obtained for different number of series solution terms. The approximate solutions are compared with the closed form solutions that are obtained from the published literatures. All numerical results are obtained using MATLAB.

6.3. Adomian Decomposition Method

Let us consider the non-linear functional equation in the form

$$u(\mathrm{x},t) = f(\mathrm{x},t) + L[u(\mathrm{x},t)] + N[u(\mathrm{x},t)], \tag{6.1}$$

where, L and N represent known linear and nonlinear operators respectively and $f(x,t)$ is a given function. The problem is to determine the solution $u(x,t)$ of (6.1). This solution may be expressed in a series form as $u(x,t) = \sum_{n=0}^{\infty} u_n$. The functional equation (6.1) may be written in the following form using the ADM.

$$\sum_{n=0}^{\infty} u_n = f(\mathrm{x},t) + \sum_{n=0}^{\infty} B_n + \sum_{n=0}^{\infty} A_n \tag{6.2}$$

The term denoted by B_n is associated with the linear operator L and A_n is the Adomian polynomial element that is given by

$$A_n = \frac{1}{n!}\frac{d^n}{d\lambda^n}\left[N\left(\sum_{i=0}^{\infty}\lambda^i u(\mathrm{x},t)_i\right)\right]_{\lambda=0}. \tag{6.3}$$

where, λ is a parameter introduced for convenience sake. The elements of the series solution for $u(x,t)$ are obtained recursively by

$$u_0(\mathrm{x},t) = f(\mathrm{x},t), \quad u_1(\mathrm{x},t) = B_0 + A_0, \quad \cdots \quad u_k(\mathrm{x},t) = B_{k-1} + A_{k-1} \quad \cdots. \tag{6.4}$$

By this arrangement, the linear and nonlinear part of the functional equation (6.1) is replaced by a known function in each step using the recursive equations (6.4).

6.4. Application of the Adomian decomposition method

The method is applied to three partial differential equations with various initial and boundary conditions. The PDEs that are taken into account are:

- The Burgers equation that is the simplest model for the one-dimensional turbulence in fluid flow. This equation can be also applied to describe many physical events such as sound-wave in a viscous medium, waves in fluid-filled viscous elastic tubes, etc. (Debnath, 2005).

$$\begin{aligned} &u_t + uu_x = \nu u_{xx} \quad \text{and} \\ &u(x,0) = u_0(x), \quad \text{where} \quad a < x < b \\ &u(a,t) = C_1(t), \quad u(b,t) = C_2(t), \quad \text{where} \quad t > 0 \end{aligned} \tag{6.5}$$

where, ν is the kinematic viscosity

- The Korteweg-de Vries (KdV) equation that describes the motion of nonlinear long wave in shallow water under gravity

$$\begin{aligned} &u_t - 6uu_x + \nu u_{xxx} = 0 \quad \text{and} \\ &u(x,0) = u_0(x), \quad \text{where} \quad |x| < \infty \end{aligned} \tag{6.6}$$

- The Klein-Gordon (KG) equation in the from

$$\begin{aligned} &u_{tt} - \sum_{j=1}^{m} \left\{ \partial_{x_j} \left[f_j(\mathbf{x}) u_{x_j} \right] \right\} + g\big(u(\mathbf{x},t)\big) = h(\mathbf{x},t) \\ &u(\mathbf{x},0) = C_1(\mathbf{x}), \; u_t(\mathbf{x},0) = C_2(\mathbf{x}), \quad \text{where} \quad |\mathbf{x}| < \infty \end{aligned} \tag{6.7}$$

where, $h(x,t)$ is the forcing function.

6.4.1. The Burgers Equation

The Burgers equation (6.5) may be integrated with respect to time variable and written as

$$u(x,t) = u(x,0) + \int_0^t \nu u_{xx} dt - \int_0^t u u_x dt. \tag{6.8}$$

Using the ADM, (6.8) can be written as (6.2), where

$$
\begin{aligned}
&f(x,t) = u(x,0)\\
&B_n = \int_0^t \nu(u_n)_{xx}dt\\
&A_n = \int_0^t \left\{ \frac{1}{n!}\frac{d^n}{d\lambda^n}\left\{ \left[\sum_{i=0}^{\infty}(\lambda^i u_i)\right]\left[\sum_{i=0}^{\infty}\left(\lambda^i (u_i)_x\right)\right]\right\}\right\}_{\lambda=0} dt,
\end{aligned}
\tag{6.9}
$$

and the elements of the series solution are obtained according to (6.4).

$$
\begin{aligned}
&u_0 = u(x,0)\\
&u_1 = \int_0^t \Big[\nu(u_0)_{xx} - u_0(u_0)_x\Big]dt\\
&u_2 = \int_0^t \Big[\nu(u_1)_{xx} - \Big[u_0(u_1)_x + u_1(u_0)_x\Big]\Big]dt\\
&\cdots \quad \cdots \quad \cdots \quad \cdots\\
&u_n = \int_0^t \Big[\nu(u_{n-1})_{xx} - \Big[u_0(u_{n-1})_x + u_1(u_{n-2})_x + \cdots + u_{n-1}(u_0)_x\Big]\Big]dt\\
&\cdots \quad \cdots \quad \cdots \quad \cdots
\end{aligned}
\tag{6.10}
$$

It can be observed from (6.10) that if the initial condition is constant the ADM is not any more applicable for this type of PDE and the solution will be the same as initial value.

6.4.2. The Korteweg-de Vries (KdV) Equation

The KdV equation (6.6) is integrated with respect to time variable and written as

$$
u = u(x,0) + 6\int_0^t uu_x dt - \int_0^t u_{xxx}dt. \tag{6.11}
$$

The solution can be constructed using ADM in series form as (6.2).

$$
u_0 = u(x,0),\ \ u_1 = 6A_0 - B_0,\ \ \cdots, u_n = 6A_{n-1} - B_{n-1}, \tag{6.12}
$$

The components of B_n series are computed by $B_n = \int_0 (u_n - 1)_{xxx} dt$ and the A_n series terms are found the same as given in (6.9) for the Burgers equation. The series solution terms are computed recursively by

$$
\begin{aligned}
&u_0 = u(x,0)\\
&u_1 = \int_0^t \left[6\, u_0(u_0)_x - (u_0)_{xxx}\right] dt\\
&u_2 = \int_0^t \left[6\left[u_0(u_1)_x + u_1(u_0)_x\right] - (u_1)_{xxx}\right] dt\\
&\cdots \quad \cdots \quad \cdots \quad \cdots\\
&u_n = \int_0^t \left[6\left[u_0(u_{n-1})_x + u_1(u_{n-2})_x + \cdots + u_{n-1}(u_0)_x\right] - (u_{n-1})_{xxx}\right] dt\\
&\cdots \quad \cdots \quad \cdots \quad \cdots .
\end{aligned}
\tag{6.13}
$$

If the initial condition is constant, the ADM is not any more functional for this type of PDE.

6.4.3. The Klein-Gordon (KG) Equation

The Klein-Gordon (KG) equation (6.7) may be written in the following form by integrating in respect to time variable.

$$
u = u(\mathrm{x},0) + u_t(\mathrm{x},0)t + \int_0\int_0^t h(\mathrm{x},t)\,(dt)^2 + \int_0\int_0^t \sum_{j=1}^{m} \left\{\partial_{x_j}\left[f_j(\mathrm{x})u_{x_j}\right]\right\}(dt)^2 - \int_0\int_0^t g(u)\,(dt)^2 \tag{6.14}
$$

The function $g(u)$ may be written as $g(u) = Lg(u) + Ng(u)$, where $Lg(u)$ is the linear part and $Ng(u)$ is the nonlinear part. Using ADM, the solution is approximated by a series solution as $u(x,t) = \sum_{n=0}^{\infty} u_n$ and (6.14) is expressed in the form of (6.2) where

$$f(\mathrm{x},t) = u(\mathrm{x},0) + u_t(\mathrm{x},0)t + \int_0^t\int_0^t h(\mathrm{x},t)\ (dt)^2$$

$$B_n = \int_0^t\int_0^t \sum_{j=1}^{m} \left\{ \partial_{x_j} \left[f_j(\mathrm{x})(u_{n-1})_{x_j} \right] \right\} (dt)^2 - \int_0^t\int_0^t Lg(u_{n-1})\ (dt)^2$$

$$A_n = -\int_0^t\int_0^t \frac{1}{n!}\frac{d^n}{d\lambda^n}\left[Ng\left(\sum_{i=0}^{\infty} \lambda^i u(\mathrm{x},t)_i \right) \right]_{\lambda=0} (dt)^2. \tag{6.15}$$

The series solution may be constructed according to (6.4). The function $f(x,t)$ may be composed of several parts as given in (6.15). For convenience of computation, some part of the whole of $f(x,t)$ may be added to the other series solution terms instead of u_0.

6.5. Implementation of Adomian decomposition method

The Adomian decomposition method (ADM) is applied to several test examples of the nonlinear PDEs that are explained in previous section. The objective is to study the effect of truncation of the series solution on the accuracy and the stability of results.

6.5.1. The Burgers Equation

The ADM is implemented to the Burgers equation with three different conditions.

6.5.1.1. Example 1.

In the first example, the initial condition is

$$u(x,0) = \frac{x}{\nu} + 1, \quad \text{and} \quad |x| < \infty. \tag{6.16}$$

Using ADM, a series solution can be constructed according to (6.10) as

$$
\begin{aligned}
u_0 &= \frac{x}{\nu} + 1 \\
u_1 &= -\frac{t}{\nu}(\frac{x}{\nu} + 1) \\
u_2 &= \frac{t^2}{\nu^2}(\frac{x}{\nu} + 1) \\
u_3 &= -\frac{t^3}{\nu^3}(\frac{x}{\nu} + 1) \\
u_4 &= \frac{t^4}{\nu^4}(\frac{x}{\nu} + 1) \\
&\cdots \quad \cdots \quad \cdots \quad \cdots \\
u_n &= (-1)^n \frac{t^n}{\nu^n}(\frac{x}{\nu} + 1).
\end{aligned}
\tag{6.17}
$$

The final solution may be written in the form of

$$
u = (\frac{x}{\nu} + 1)(1 - \frac{t}{\nu} + \frac{t^2}{\nu^2} - \frac{t^3}{\nu^3} + \cdots + (-1)^n \frac{t^n}{\nu^n} + \cdots) = (\frac{x}{\nu} + 1) \sum_{n=0}^{\infty} (-1)^n \frac{t^n}{\nu^n}. \tag{6.18}
$$

The closed form solution is in the form $u = (x/\nu + 1)(1 + t/\nu)^{-1}$ for this initial value problem.

The solution are illustrated in Fig. 6.1 as a function of time at x = 1 for ν = 1. The ADM solution is shown for different truncation number M. The closed form solution is also shown to provide a comparison among them. The ADM solutions even with small value of truncation number are in excellent agreement with the exact solution for small values of t. However, the accuracy of the approximate solution decreases with increasing the time interval. The inception point that the approximate solution deviates from the exact solution depends on the truncation number M. The diagrams in Fig. 6.1 show that the ADM solution is applicable for a limited time interval.

6.5.1.2. Example 2.

It is an initial value problem with the initial condition as

$$u(x,0) = 2(1+e^{\frac{x}{\nu}})^{-1}, \quad \text{and} \quad |x| < \infty. \tag{6.19}$$

Some of the first elements of the series solution according to ADM are

$$\begin{aligned}
u_0 &= 2(1+e^{x/\nu})^{-1} \\
u_1 &= 2(t/\nu)\, e^{x/\nu}(1+e^{x/\nu})^{-2} \\
u_2 &= (t/\nu)^2\, e^{x/\nu}(e^{x/\nu}-1)(1+e^{x/\nu})^{-3} \\
u_3 &= \frac{1}{3}(t/\nu)^3\, e^{x/\nu}(1-4e^{x/\nu}+e^{2(x/\nu)})(1+e^{x/\nu})^{-4} \\
u_4 &= \frac{1}{12}(t/\nu)^4\, e^{x/\nu}(e^{x/\nu}-1)(e^{2(x/\nu)}-10e^{x/\nu}+1)(1+e^{x/\nu})^{-5} \\
&\cdots \quad \cdots \quad \cdots \quad \cdots \\
u_n &= \frac{2}{n!}(t)^n \frac{d^n}{dt^n}\left(\frac{2}{1+e^{(x-t)/\nu}}\right)_{t=0}.
\end{aligned} \tag{6.20}$$

The closed form solution can be written as $u = \dfrac{2}{1+e^{(x-t)/\nu}}$ according to the Taylor series expansion as $n \to \infty$.

The effects of the truncation of the series solution to a finite number M are illustrated in Fig. 6.2 for this test example. The computations are carried out at $x = 1$ for $\nu = 1$ at different time intervals. The same trend as the first example is observed. The accuracy of the ADM solution significantly depends on the truncation number M. The other difficulty is the instability of the approximate solution with increasing M. The ADM solutions deviate from the exact solution at a small value of t when $M = 99, 100$ and are unstable after that time. This is due to the inherent properties of the power polynomials that are susceptible to the severe instability with increasing order.

6.5.1.3. Example 3.

The Adomian decomposition method is also implemented to an example that shows the decay of an arbitrary periodic initial disturbance. This can be taken into account as a theoretical model for free turbulence in a box. It is assumed that

$$\begin{aligned} &u(x,0) = \sin \pi x \qquad \text{and} \quad 0 \le x \le 1 \\ &u(0,t) = u(1,t) = 0. \end{aligned} \tag{6.21}$$

The analytical solution for this problem is given by Cole (1951) as

$$u(x,t) = \frac{4\pi\nu \sum_{n=1}^{\infty} n I_n(\frac{1}{2\pi\nu}) \sin n\pi x e^{-n^2\pi^2\nu t}}{I_0(\frac{1}{2\pi\nu}) + 2\sum_{n=1}^{\infty} n I_n(\frac{1}{2\pi\nu}) \cos n\pi x e^{-n^2\pi^2\nu t}} \tag{6.22}$$

where, I_n In is the modified Bessel function of first kind and order n.

Substituting (6.18) into (6.13), the elements of the series solution are found for this example as

$$\begin{aligned} u_0 &= \sin \pi x \\ u_1 &= -\pi t\left(\nu\pi \sin \pi x + \frac{1}{2}\sin 2\pi x\right) \\ u_2 &= \frac{\pi^2 t^2}{2}\left[\left(\nu^2\pi^2 - \frac{1}{4}\right)\sin \pi x + 3\nu\pi \sin 2\pi x + \frac{3}{4}\sin 3\pi x\right] \\ u_3 &= -\frac{\pi^3 t^3}{6}\left[\nu\pi\left(\nu^2\pi^2 - \frac{9}{4}\right)\sin \pi x + (14\nu^2\pi^2 - 1)\sin 2\pi x + \right. \\ &\qquad \left. \frac{51}{4}\nu\pi \sin 3\pi x + 2\sin 4\pi x\right] \\ u_4 &= \frac{\pi^4 t^4}{24}\left[\left(\nu^4\pi^4 - \frac{245}{2}\nu^2\pi^2 - 7\right)\sin \pi x + (60\nu^3\pi^3 - 22)\sin 2\pi x + \right. \\ &\qquad \left. \left(\frac{29}{2}\nu^2\pi^2 + \frac{147}{16}\right)\sin 3\pi x + (60\nu\pi + 11)\sin 4\pi x + \frac{11}{16}\sin 5\pi x\right] \\ &\ldots \quad \ldots \quad \ldots \quad \ldots \end{aligned} \tag{6.23}$$

The ADM solution may be constructed as $u(x,t)=\sum_{n=0}^{\infty}u_n$ where M is the truncation number.

The computations are carried out at different time intervals as a function of x when $M=20$ for $\nu=0.01$. The approximate solutions are depicted in Fig. 6.3 along with the analytical solution. The ADM solutions comply with the analytical solution for a limited time. The ADM solutions for $t>0.25$ starts to oscillate and for $t>0.4$, they become completely unstable.

If the nonlinear part of the Burgers equation is omitted, the equation reduces to a one dimensional heat equation, $u_t=\nu u_{xx}$. If the same initial and boundary conditions as (6.18) are used, the ADM solution can be constructed as

$$\begin{aligned} u &= \sin\pi x\left[1-\nu\pi^2 t+\frac{1}{2!}(\nu\pi^2 t)^2-\frac{1}{3!}(\nu\pi^2 t)^3+\frac{1}{4!}(\nu\pi^2 t)^4-\cdots+(-1)^n\frac{1}{n!}(\nu\pi^2 t)^n\right] \\ &= \sin\pi x\sum_{n=0}^{\infty}(-1)^n\frac{1}{n!}(\nu\pi^2 t)^2. \end{aligned} \qquad (6.24)$$

If $n\to\infty$, the solution corresponds to the closed form of $u=\sin\pi x\exp(-\nu\pi^2 t)$.

In order to see the effect of truncation of the series, The solution is examined for different number of the series elements in Fig. 6.4. The solutions are the same as the closed form solution up to a certain time and after that the solution will diverges. If M is reduced the deviation of the ADM solution from the closed form starts earlier.

6.5.2. The KdV Equation

6.5.2.1. Example 1.

The first example is a single-soliton solution for a sech^2 potential. If the KdV equation is subjected to the initial condition of $u(x,0) = -2\sec h^2 x,\ |x| < \infty$, the ADM series solution can be constructed according to (6.13) as following forms.

$$
\begin{aligned}
u_0 &= -2\,\text{sech}^2 x \\
u_1 &= -16\,t\,\sinh x\,\text{sech}^3 x \\
u_2 &= -32\,t^2\,(2\cosh^2 x - 3)\,\text{sech}^4 x \\
u_3 &= -\frac{512}{3}\,t^3\,\sinh x(\cosh^2 x - 3)\,\text{sech}^5 x \\
u_4 &= -\frac{512}{3}\,t^4\,(2\cosh^4 x - 15\cosh^2 x + 15)\,\text{sech}^6 x \\
&\ldots \quad \ldots \quad \ldots \quad \ldots
\end{aligned}
\tag{6.25}
$$

The closed form solution of this problem is $u(x,t) = -2\sec h^2(x - 4t)$.

The computational results of u using the ADM are shown in Fig. 6.5 as a function of spatial variable at different elapsing time. The analytical solution is also presented. The ADM solution is obtained with $M = 20$. The ADM results are in excellent agreement with the analytical solution for a very small elapsing time ($t = 0.3$). The ADM solution becomes unstable for a elapsing time of $t > 0.3$.

6.5.2.2. Example 2.

It is a two-soliton solution for a sech^2 potential. The KdV equation is subjected to the initial condition of $u(x,0) = -6\sec h^2 x,\ |x| < \infty$. The ADM series solution is constructed according to (6.13) for the first four terms

$$
\begin{aligned}
u_0 &= -\,6\,\operatorname{sech}^2 x \\
u_1 &= -\,48\,t\,\sinh x(\cosh^2 x + 6)\,\operatorname{sech}^5 x \\
u_2 &= -\,96\,t^2\,(2\cosh^6 x + 117\cosh^4 x - 96\cosh^2 x - 63)\,\operatorname{sech}^8 x \\
u_3 &= -\,256\,t^3\,\sinh x(2\cosh^8 x + 1002\cosh^6 x - 594\cosh^4 x \\
&\qquad -1728\cosh^2 x - 405)\,\operatorname{sech}^{11} x.
\end{aligned} \tag{6.26}
$$

The two-soliton solution of the KdV equation using ADM is shown in Fig. 6.6 along with the closed form solution at different time interval. Moreover, the closed form solution of this problem is given in Rahman (1995)

$$
u(x,t) = -12\frac{3 + 4\cosh(8t - 2x) + \cosh(64t - 4x)}{\left(\cosh(36t - 3x) + 3\cosh(28t - x)\right)^2}. \tag{6.27}
$$

In this case, the ADM solution are obtained with $M = 18$. Once again, the ADM results are found to be in excellent agreement with the analytical solution for a very small elapsing time. The solution with ADM becomes unstable for $t > 0.05$.

6.5.3. The KG Equation

6.5.3.1. Example 1.

The first test example is a linear nonhomogeneous KG-equation in the form

$$
\begin{aligned}
&u_{tt} - u_{xx} + 2u = -\sin x \sin t \\
&u(x,0) = 0 \quad , \quad u_t(x,0) = \sin x, \quad \text{and} \quad u(0,t) = u(\pi,t) = 0.
\end{aligned} \tag{6.28}
$$

The ADM series solution according to (6.15) may be constructed as

$$
\begin{aligned}
u_0 &= \sin x(2\sin t - t) \\
u_1 &= \sin x(-2\sin t + 2\,t - 1/3!\,t^3) \\
u_2 &= \sin x(2\sin t - 2\,t + 2/3!\,t^3 - 1/5!\,t^5) \\
u_3 &= \sin x(-2\sin t + 2\,t - 2/3!\,t^3 + 2/5!\,t^5 + 1/7!\,t^7) \\
u_4 &= \sin x(2\sin t - 2\,t + 2/3!\,t^3 - 2/5!\,t^5 - 2/7!\,t^7 + 1/9!\,t^9) \\
&\cdots \quad \cdots \quad \cdots \quad \cdots .
\end{aligned} \tag{6.29}
$$

The solution of the problem can be written in a series form, which is as follows

$$u(x,t) = \sin x\left[2\sin t - \left(t - \frac{1}{3!}t^3 + \frac{1}{5!}t^5 - \frac{1}{7!}t^7 + \frac{1}{9!}t^9 - \frac{1}{11!}t^{11} + \frac{1}{13!}t^{13} - \ \ldots\ \right)\right]$$
$$= \sin x\left[2\sin t - \sum_{k=0}^{2M}\frac{(-1)^{k/2}}{(k+1)!}t^{k+1}\right] \quad \text{and} \quad M = 1,2,3,\cdots. \tag{6.30}$$

The closed form solution of Example 1 is $u(x,t) = \sin x \sin t$ as $M \to \infty$.

The effect of the truncation of the series solution on the accuracy of the result is shown in Fig. 6.7. The solutions are obtained as a function of time for $x = \pi/2$ using different truncation number M. When $M = 20$, the ADM results are in excellent agreement with the closed form solution in the time range as shown in the Fig. 6.7. The ADM solution shows a very good agreement with the closed form solution even for $M = 4$. However, the accuracy of the results are impaired with increasing time.

6.5.3.2. Example 2.

This example is a Sine-Gordon equation in the form

$$u_{tt} - u_{xx} + \sin u = 0$$
$$u(x,0) = 4\tan^{-1}(e^{2x}), \quad u_t(x,0) = \frac{-4\sqrt{3}\ e^{2x}}{1+e^{4x}}, \quad \text{and} \quad |x| < \infty. \tag{6.31}$$

The computation of B_n terms, which are associated to the linear operators, is straight forward. The A_n terms due to the nonlinear sine-operator are obtained recursively by

$$A_0 = -\int_0^t\int_0^t \sin u_0 (dt)^2$$

$$A_1 = -\int_0^t\int_0^t u_1 \cos u_0 (dt)^2$$

$$A_2 = -\int_0^t\int_0^t (u_2 \cos u_0 - \frac{u_1^2}{2!}\sin u_0)(dt)^2$$

$$A_3 = -\int_0^t\int_0^t (u_3 \cos u_0 - u_2 u_1 \sin u_0 - \frac{u_1^3}{3!}\cos u_0)(dt)^2$$

$$A_4 = -\int_0^t\int_0^t \left(u_4 \cos u_0 - u_3 u_1 \sin u_0 - \frac{1}{2}u_2^2 \sin u_0 - \frac{1}{2}u_2 u_1^3 \cos u_0 + \frac{u_1^4}{4!}\sin u_0\right) (dt)^2$$

$$\ldots \quad \ldots \quad \ldots \quad \ldots . \tag{6.32}$$

If the regular form of the ADM is applied the computation will be very complicated. Therefore, the modified form of ADM is used according to Wazwaz (1999). It simplifies the computation and makes the ADM feasible for this type of nonlinear PDEs. It is assumed that $u_0 = 0$ and the other terms of the ADM series solution are constructed in the form

$$u_1 = 4\tan^{-1}(e^{2x}) - \frac{4\sqrt{3}\ e^{2x}}{1+e^{4x}}t$$

$$u_2 = -\frac{8\,e^{2x}\,t^2}{3(1+e^{4x})^3}\left(\sqrt{3}\,t\,e^{8x} + 3\,e^{8x} - 6\sqrt{3}\,t\,e^{4x} - 3 + \sqrt{3}\,t\right) - 2\,t^2\tan^{-1}(e^{2x}) + \frac{2\sqrt{3}\,t^3 e^{2x}}{3(1+e^{4x})}$$

$$u_3 = \frac{2e^{2x}t^4}{5(1+e^{4x})^5}\Big(-\sqrt{3}\,t\,e^{16x} - 5\,e^{16x} + 100\sqrt{3}\,t\,e^{12x} + 150\,e^{12x} - 310\sqrt{3}\,t\,e^{8x} + 100\sqrt{3}\,t\,e^{4x}$$
$$- 150\,e^{4x} + 5 - \sqrt{3}\,t\Big) - \frac{8\,e^{2x}}{3(1+e^{4x})^3}\left[\frac{t^5}{20}\Big(-\sqrt{3}e^{8x} + 6\sqrt{3}e^{4x} - \sqrt{3}\Big) + \frac{t^4}{12}\Big(-3\,e^{8x} + 3\Big)\right]$$
$$+\frac{t^4}{6}\tan^{-1}(e^{2x}) - \frac{t^5\sqrt{3}\,e^{2x}}{30(1+e^{4x})}$$

$$u_4 = -\frac{e^{2x}\,t^6}{105(1+e^{4x})^7}\Big(21\,e^{24x} + 3\sqrt{3}\,t\,e^{24x} - 8428\,e^{20x} - 3654\sqrt{3}\,t\,e^{20x} + 56013\sqrt{3}\,t\,e^{16x}$$
$$+54761\,e^{16x} - 126420\sqrt{3}\,t\,e^{12x} + 56013\sqrt{3}\,t\,e^{8x} - 54761\,e^{8x} + 8428\,e^{4x} - 3654\sqrt{3}\,t\,e^{4x}$$
$$-21 + 3\sqrt{3}\,t\Big) - \frac{2\,e^{2x}}{5(1+e^{4x})^5}\left[\frac{t^7}{42}\Big(100\sqrt{3}\,e^{12x} - \sqrt{3}\,e^{16x} - 310\sqrt{3}\,e^{8x} + 100\sqrt{3}\,e^{4x} - \sqrt{3}\Big)\right.$$
$$\left.+\frac{t^6}{30}\Big(-5e^{16x} - 150e^{4x} + 150e^{12x} + 5\Big)\right] - \frac{8e^{2x}}{3(1+e^{4x})^3}\left[\frac{t^7}{840}\Big(\sqrt{3}\,e^{8x} - 6\sqrt{3}\,e^{4x} + \sqrt{3}\Big)\right.$$

$$+\frac{t^6}{120}\left(e^{8x}-1\right)\Bigg] + \frac{\sqrt{3}\,t^7\,e^{2x}}{1260(1+e^{4x})} + \frac{(1+e^{4x})^2}{5760\,e^{4x}}\left[4\,\tan^{-1}(e^{2x}) - \frac{4\sqrt{3}te^{2x}}{1+e^{4x}}\right]^5$$
$$-\frac{8\,(1+e^{4x})^2}{45\,e^{4x}}\left[\tan^{-1}(e^{2x})\right]^5 + \frac{8\sqrt{3}\,t\,(1+e^{4x})}{9\,e^{2x}}\left[\tan^{-1}(e^{2x})\right]^4 - \frac{t^6\,\tan^{-1}(e^{2x})}{180}$$

... ... (6.33)

The approximate solution should be obtained by taking into account a finite number of series solution terms. The results are computed as a function of spatial variable at different time steps. The ADM solutions are obtained with $M = 4$ and 7 where M is the number of the series solution terms. The closed form solution of this problem is $u(x,t) = 4\tan^{-1}\left(e^{2x-\sqrt{3}t}\right)$, which is a solitary wave equation with the speed of $v = \sqrt{3}$ in the positive x-direction. This analytical solution is also illustrated in Fig. 6.8. The accuracy of the approximate solution is reasonable for small values of the time and spatial variables. The solution is susceptible to the severe instability as time and spatial coordinate increase. The solution can be improved with increasing the number of series solutions terms.

6.6. Conclusions

The Adomian decomposition method is applied to solve several partial differential equations of different types. A general formulation of the method is explained for nonlinear functional equations and then a detailed mathematical description of the method is presented for the nonlinear Burgers equation, the Korteweg-de Vries equation and the multi-dimensional Klein-Gordon equation. The method is implemented to several test examples of each type of these PDEs. The approximate solutions are found using the ADM with different number of series solution terms and compared with the closed form solution obtained from the published literatures. All the computations are carried out using the MATLAB software.

The Adomian decomposition method gives a stable solution with high degree of accuracy for a very small range of the independent variables in almost all test examples of these nonlinear PDEs. The accuracy of the approximate solution is impaired significantly and severe instability occurs with increasing the values of the independent variables from certain points. The point, at which the deviation of the approximate solution from the analytical results starts, depends on the truncation number of the ADM series solution. The point is also sensitive to the initial conditions. The accuracy of the ADM solution is improved and the deviation point is delayed with increasing the truncation number of the series solution. However, an increased in number of the series solution terms may result in an earlier occurrence of instability. The linear test examples show that the method may be more suitable for linear PDEs than the nonlinear PDEs.

6.7. References

Adomian, G. and Adomian, G.E., (1984) A Global method for solution of complex systems, Journal of Mathematical Modelling, vol. 5, pp. 521-568

Adomian, G., (1989) Nonlinear stochastic systems theory and applications to physics, Kluwer Academic Publishers, MA

Adomian, G., (1994) Solving frontier problems of physics: The decomposition method, Kluwer Academic Publishers, Dordrecht

Biazar, J. and Islam, R., (2004) Solution of wave equation by Adomian decomposition method and the restrictions of the method, Applied Mathematics and Computation, vol. 149, pp. 807-814

Cole, J.D., (1951) On a quasi-linear parabolic equations occurring in aerodynamics, Quarterly of Applied Mathematics, vol. 9, pp. 225-236

Debnath, L., (2005) Nonlinear partial differential equations for scientists and engineers, 2nd edition, Boston: Birkhäuser

Deeba, E. Y. and Khuri, S. A., (1996) A decomposition method for solving the nonlinear Klein-Gordon equation, Journal of computational physics, vol. 124, pp. 442-448

Rahman, M., (1995) Water Waves: Relating Modern Theory to Advanced Engineering Practice, Oxford University Press Inc., New York

Wazwaz, A.M., (1999) A reliable modification of Adomian decomposition method, Applied Mathematics and Computation, vol. 102, pp. 77-86

Wazwaz, A.M., (2001) Construction of solitary wave solutions and rational solutions for the KdV equation by Adomian decomposition method, Chaos, Solitons and Fractals, vol. 12, no. 12, pp. 2283-2293

6.8. Appendices

6.8.1. Appendix A: Figures

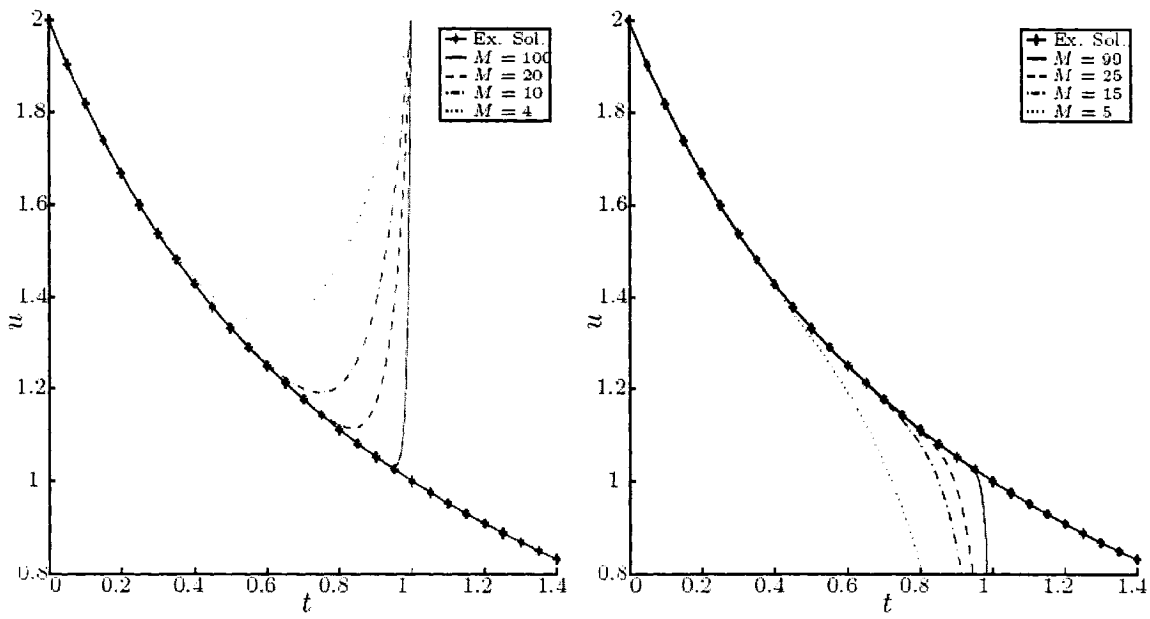

Figure 6.1. The effect of truncation of the ADM series solution for the first example of the Burgers equation, $\nu = 1$, x = 1, Left: M is even number Right: M is odd number

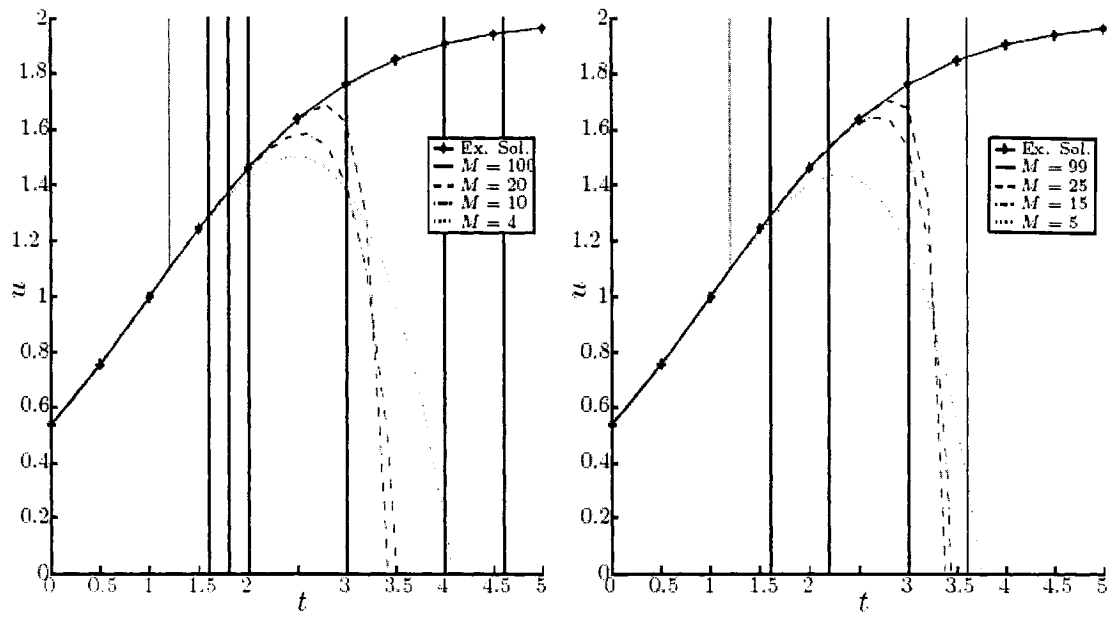

Figure 6.2. The effect of truncation of the ADM series solution for the second example of the Burgers equation, $\nu = 1$, x = 1, Left: M is even number Right: M is odd number

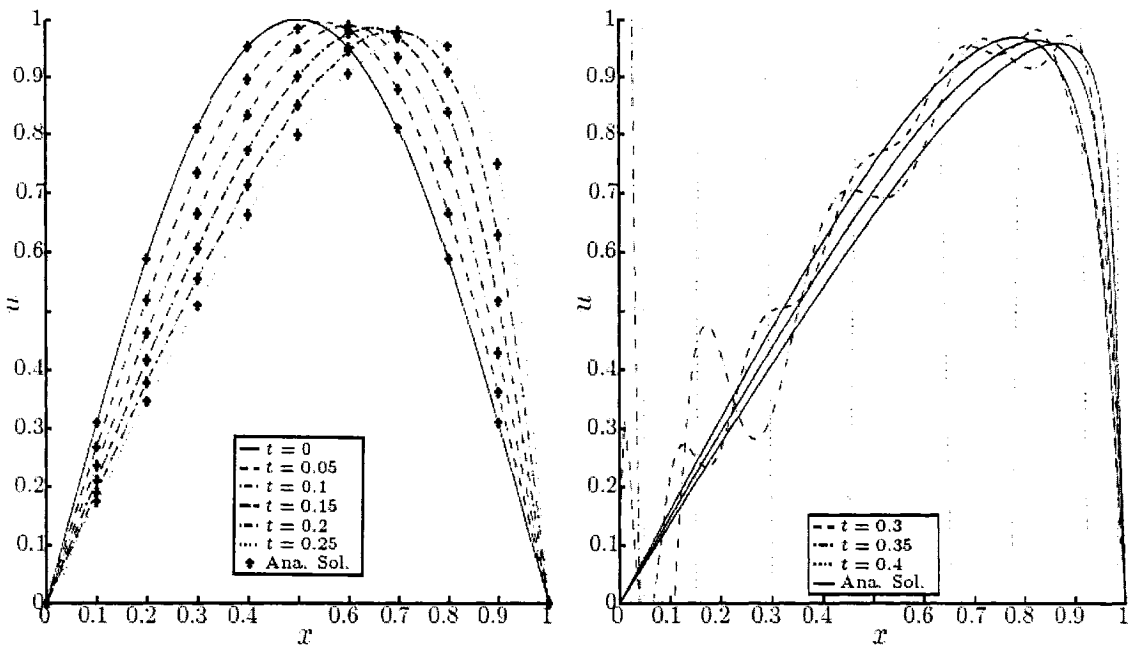

Figure 6.3. The comparison of the ADM and closed form solution of the third example of the Burgers equation, $\nu = 0.01$.

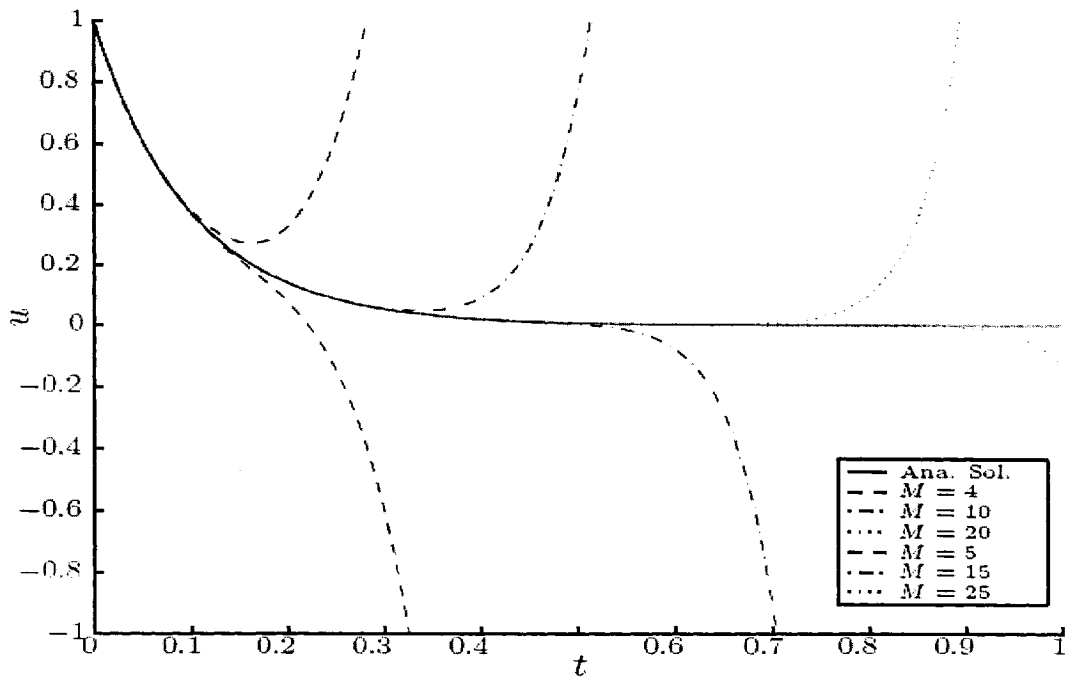

Figure 6.4. Deviation of the ADM solution from the close form solution due to the truncation of the series solution at different number for the linear heat equation at $x = 0.5$ and $\nu = 1$

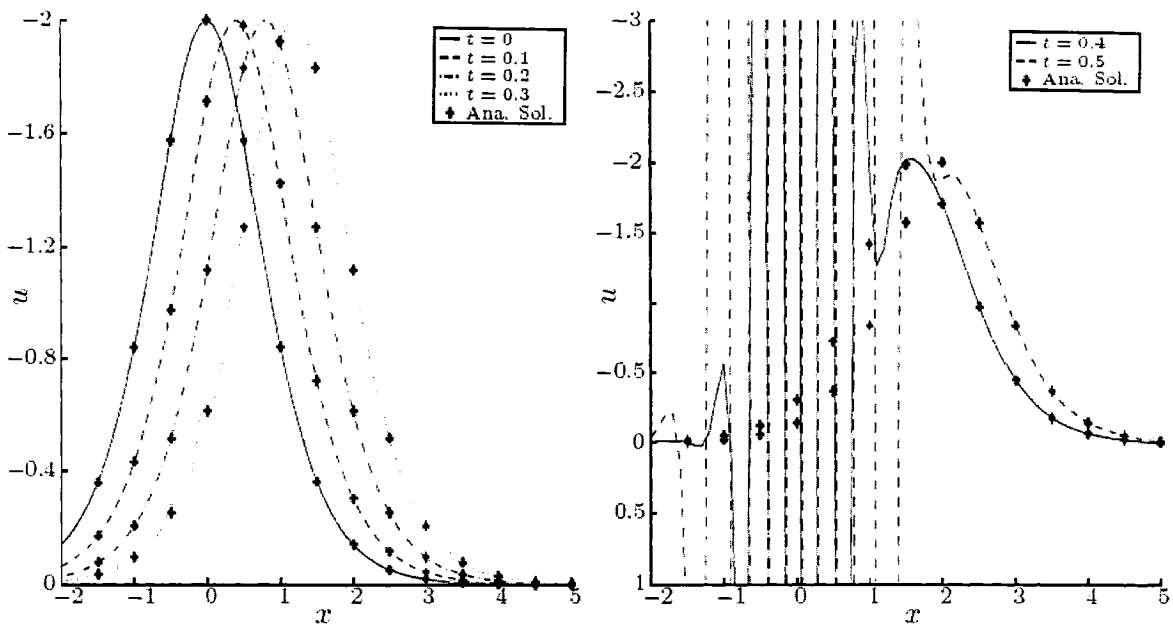

Figure 6.5. The single-soliton solution of the KdV equation at different elapsing time, $M = 20$.

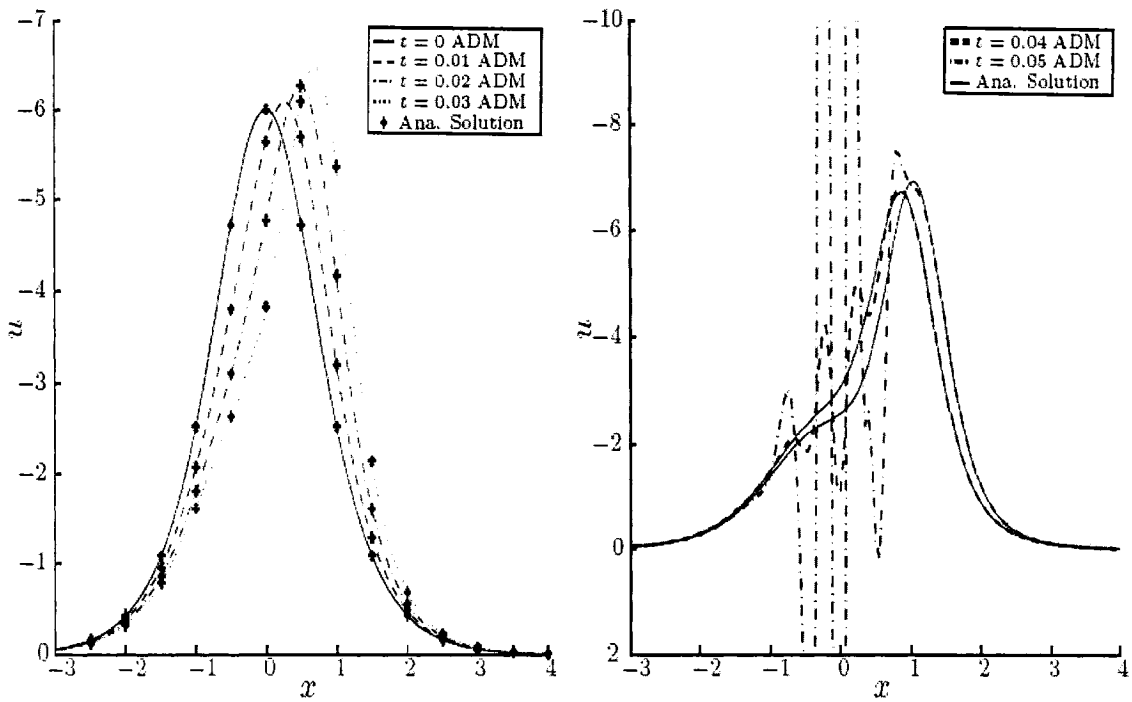

Figure 6.6. The two-soliton solution of the KdV equation at different elapsing time, $M = 18$

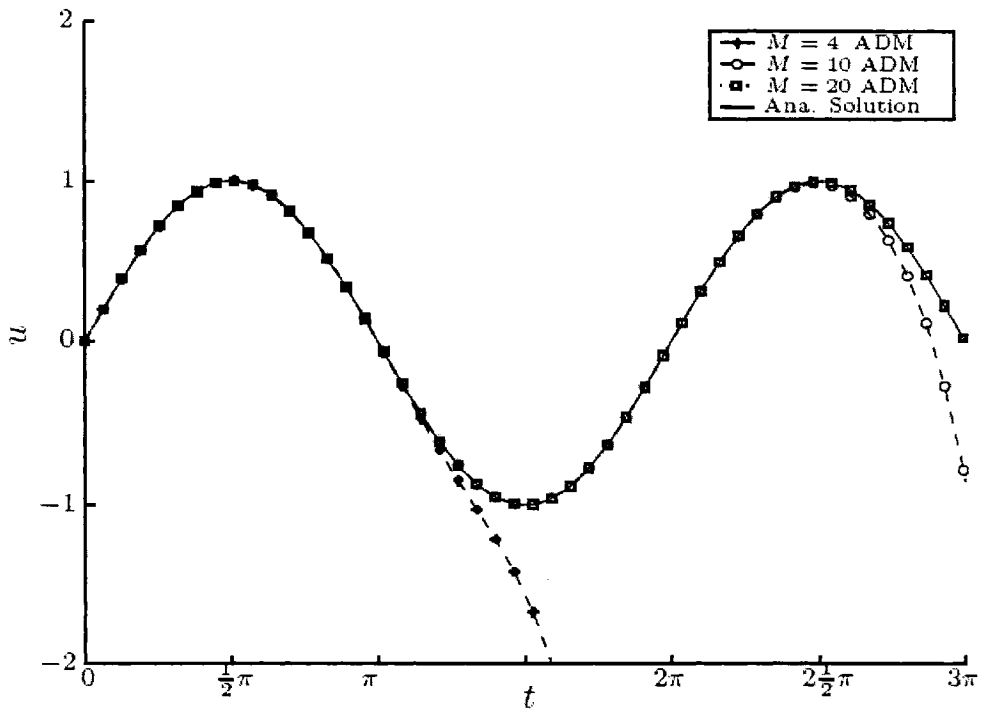

Figure 6.7. The effect of the truncation of the ADM series solution on a linear non-homogeneous KG-equation

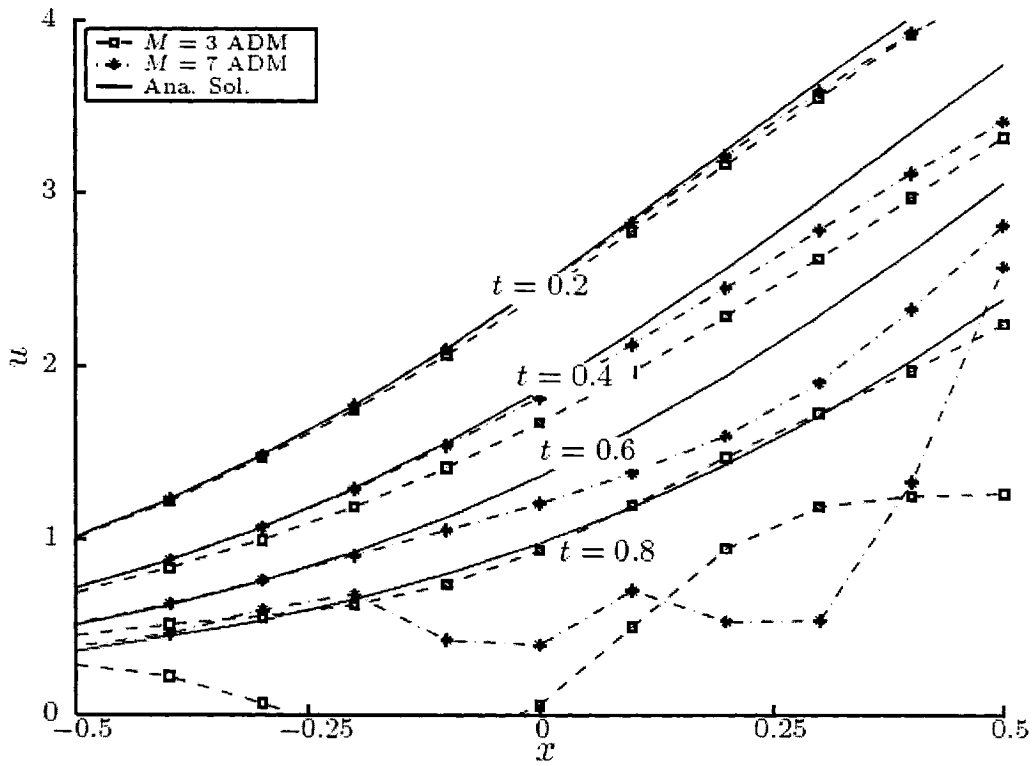

Figure 6.8. The effect of the truncation of the ADM series solution on the accuracy and stability of the results for a sine-Gordon equation

Chapter 7

7 ADOMIAN DECOMPOSITION OF BUCKLEY-LEVERETT EQUATION WITH CAPILLARY EFFECTS

7.1. Abstract

Petroleum reservoir engineering problems are known to be inherently nonlinear. Consequently, solutions to the complete multiphase flow equations have been principally attempted with numerical methods. However, simplified forms of the problem have been solved some 60 years ago, when the Buckley-Leverett formulation was introduced. Ever since that pioneer work that neglected the capillary term, this formulation has been widely accepted in the petroleum industry. By using the method of characteristic, the multiphase one-dimensional fluid flow was solved. However, the resulting solution was a triple-valued one for a significant region. For decades, the existence of multiple solutions was considered to be the result of nonlinearity. Buckley and Leverett introduced shock utilizing the concept of material balance and two decades later, when numerical solutions were possible, it was discovered that the triple-value problem disappeared if the complete flow equation, including the capillary pressure form, is solved. Numerical methods, however, are not free from linearization. In fact, every numerical solution imposes linearization at some point of the solution scheme. Therefore, a numerical technique cannot be used to definitively state the origin of multiple solutions. In this paper, a semi-analytical technique, the Adomian decomposition method (ADM), capable of solving nonlinear partial differential equations without any linearizing assumptions, is used to unravel the true nature of the one-dimensional, two-phase flow. Results show that the Buckley-Leverett shock is neither necessary nor accurate portrayal of the displacement process. By using the ADM, the

solution profile observed through, numerous experimental studies was rediscovered. This paper opens up an opportunity to seek approximate but close to exact solutions to the multiphase flow problems in porous media.

7.2. Introduction

Since Adomian (1984) proposed his decomposition technique, the Adomian decomposition method (ADM) has gained significant interests among researchers, particularly in the fields of physics and mathematics. They applied this method to many deterministic and stochastic problems (Adomian, 1986; Eugene, 1993; Adomian, 1994). In this method, the governing equation is transformed into a recursive relationship and the solution appears in the form of a power series. The ADM has emerged as an alternative method to solve various mathematical models including algebraic, differential, integral, integro-differential, partial differential equations (PDEs) and systems, higher-order ordinary differential equations, and others.

Guellal and Cherruault (1995) utilized the method to solve an elliptical boundary value problem with an auxiliary condition. Laffez and Abbaoui (1996) used it in modeling thermal exchanges associated to drilling wells. The application of this method is also noticeable in medical research; in which the decomposition technique is used to solve differential system of equations in modeling of HIV immune dynamics (Adjedj, 1999). Wazwaz (2001) and Wazwaz and El-Sayed (2001) reported that the ADM could be useful in solving problems without considering linearization, perturbation, or unjustified assumptions that may alter the nature of the problem under investigated. Also there have been suggestions that this method can be more advantageous over numerical methods by providing analytic, verifiable, rapidly convergent approximations, which add insight into the character and the behavior of the solution as obtainable in the closed form solution (El-Sayed and Abdel-Aziz, 2003). In particular, they noticed the strength of the ADM in handling nonlinear problems in terms of rapid convergence. Biazar and Ebrahimi (2005)

also expressed similar notion about rapid convergence and further added the advantage of the technique in terms of considerable savings in computation time when they attempted to solve hyperbolic equations.

Even though, petroleum problems are some of the most intrigue candidates for the ADM, there have been sparse attempts to utilize the method in the petroleum problems. Only recently, Mustafiz et al. (2005) reported the decomposition of the non-Darcy flow equations in porous media. In a different paper, Mustafiz and Islam (2005) transformed the diffusivity equations in well-test applications into canonical forms. There is some success with Adomian method in modeling drilling activities, such as perforation by drilling (Rahman et al., in press) specified drilling operations (Biazar and Islam, in press).

The Buckley-Leverett (1942) analysis is considered to be the first pioneer work in the study of linear displacement of a fluid by another fluid. The solution of their displacement study on two-phase fluid excluded the effect of capillary and gave multiple results for saturation at a given position. Realizing the fact that such co-existence of multiple saturation values is physically unrealistic, Buckley and Leverett (1942) used the fundamental concept of material-balance to explain the shock. However, the lack of theoretical justification of shock was a major constraint in understanding the displacement phenomenon more vividly than before, and would not be re-evaluated until the next significant work published by Holmgren and Morse (1951). They utilized the Buckley-Leverett theory to calculate the average water saturation at breakthrough and explained dispersion as a consequence of capillary effects. Welge (1952) continued the effort in finding the average saturation at water breakthrough in an oil reservoir. He also found that the method of *tangent construction* by Terwilliger et al. (1951) was equivalent to the shock proposed by Buckley and Leverett.

To solve the displacement equation including capillary as well as gravity, Fayers and Sheldon (1959) attempted a Lagrangian approach. They, however, did not succeed to

determine the time required to obtain a particular saturation, which later was explained by Bentsen (1978) revealing the fact that the distance traveled by zero saturation is governed by a separate equation. Bentsen also noted that at slower injection rates, the input boundary condition of constant normalized saturation that Fayers and Sheldon used was incorrect in formulation. Also, there have been numerical investigations in the past to solve the displacement equation. Hovanessian and Fayers (1961) were able to avoid profiles of multiple valued saturations by considering the capillary pressure.

The Adomian decomposition method is applied to solve the nonlinear Buckley-Leverett equation. The solution for the water saturation is expressed in a series form. The base element of the series solution is obtained using the solution of the linear part of the Buckley-Leverett equation without the effect of the capillary pressure using the characteristic method. The other elements of the series solution are obtained recursively using the Adomian polynomial. The modification of the ADM in selection of the base element of the series solution makes the ADM feasible in solution of the nonlinear Buckley-Leverett equation. The computation is carried out for a reservoir of certain properties and initial conditions.

7.3. Governing equations

The Buckley-Leverett equation is given by

$$\frac{\partial S_w}{\partial t} + \frac{q}{A\phi}\frac{\partial f_w}{\partial S_w}\frac{\partial S_w}{\partial x} = 0 \tag{7.1}$$

where f_w is expressed in the form

$$f_w = \left(\frac{1}{1 + \frac{k_{ro}\mu_w}{k_{rw}\mu_o}} \right) \left\{ 1 + \frac{Akk_{ro}}{q\mu_o} \left[\frac{\partial P_c}{\partial x} - (\rho_w - \rho_o) g \sin \alpha \right] \right\}. \tag{7.2}$$

This equation indicates that the fractional flow rate of water depends on reservoir characteristics, water injection rate, viscosity and direction of flow. The effect of capillary pressure, P_c, which appears in the fractional flow equation, on saturation profiles is important, since these profiles affect the ultimate economic oil recovery (Bentsen, 1978). The ratio of effective permeability to viscosity is defined as the mobility which is shown for water and oil, respectively

$$\lambda_w = \frac{kk_{rw}}{\mu_w} \text{ and } \lambda_o = \frac{kk_{ro}}{\mu_o}. \tag{7.3}$$

The mobility ratio of oil to water is defined by

$$M = \frac{\lambda_o}{\lambda_w} = \frac{k_{ro}\mu_w}{k_{rw}\mu_o}. \tag{7.4}$$

The assumptions associated with the Buckley-Leverett equation, according to Ertekin et al. (2001) are:

- oil and water phases are assumed incompressible;
- the porous medium is assumed incompressible, which implies that porosity is constant;
- injection and production are taken care of by means of boundary conditions, which indicate that there are no external sink or source in the porous medium;
- the cross-sectional area that is open to flow is constant;

- the saturation-constraint equation for two-phase flow is valid; and
- the fractional flow of water is dependent on water saturation only.

The expression of the fractional flow rate of water in Eq. 7.2 suggests that Eq. 7.1 is a nonlinear differential equation and it is due to the effect of capillary pressure. In the simplest case of horizontal flow and neglecting the effects of capillary pressure variation along the reservoir, the expression for f_w in Eq. 7.2 is simplified to a linear differential equation, which is given by

$$f_w = \frac{1}{1+M}. \tag{7.5}$$

The water saturation distribution along the reservoir can be found at different time steps by knowing the injection flow rate, the initial water saturation distribution, and the variation of fractional water flow rate. The water is normally the wetting fluid in the water-oil two phase flow systems. The relative permeability of the water and oil for a specific reservoir are obtained with the drainage and imbibitions process on the core in the laboratory. However, in this paper, the variation of relative permeability to water and oil as a function of water saturation are obtained using from following empirical relationships respectively

$$k_{rw} = \alpha_1 S_{wn}{}^{n1} \tag{7.6.1}$$

$$k_{ro} = \alpha_2 (1 - S_{wn})^{n2} \tag{7.6.2}$$

where the normalized water saturation, S_{wn}, is defined as

$$S_{wn} = \frac{S_w - S_{wi}}{1 - S_{wi} - S_{or}} \tag{7.7}$$

If the effects of capillary pressure are included in a horizontal reservoir, Eq. 7.2 takes the form

$$f_w = \frac{1}{1+\frac{k_{ro}\mu_w}{k_{rw}\mu_o}}\left[1+\frac{Akk_{ro}}{q\mu_o}\frac{\partial P_c}{\partial x}\right]. \tag{7.8}$$

Capillary pressure at any point is directly related to the mean curvature of the interface, which, in turn, is a function of saturation (Leverett, 1941). Therefore, it can be safely assumed that capillary pressure is only a function of water saturation. By applying the chain rule,

$$P_c = f(S_w) \qquad \rightarrow \qquad \frac{\partial P_c}{\partial x} = \frac{\partial P_c}{\partial S_w}\frac{\partial S_w}{\partial x} \tag{7.9}$$

and by incorporating Eqs. 7.8 and 7.9 in Eq. 7.1, the following partial differential equation is obtained

$$\frac{\partial S_w}{\partial t} + \frac{q}{A\phi}\frac{\partial}{\partial S_w}\left(\frac{1}{1+\frac{k_{ro}\mu_w}{k_{rw}\mu_o}}\right)\frac{\partial S_w}{\partial x} + \frac{kk_{ro}}{\mu_o\phi}\frac{\partial}{\partial S_w}\left(\frac{1}{1+\frac{k_{ro}\mu_w}{k_{rw}\mu_o}}\right)\frac{\partial P_c}{\partial S_w}\left(\frac{\partial S_w}{\partial x}\right)^2$$
$$+\frac{k}{\mu_o\phi}\left(\frac{1}{1+\frac{k_{ro}\mu_w}{k_{rw}\mu_o}}\right)\frac{\partial k_{ro}}{\partial S_w}\frac{\partial P_c}{\partial S_w}\left(\frac{\partial S_w}{\partial x}\right)^2 + \frac{kk_{ro}}{\mu_o\phi}\left(\frac{1}{1+\frac{k_{ro}\mu_w}{k_{rw}\mu_o}}\right)\frac{\partial^2 P_c}{\partial S_w^2}\left(\frac{\partial S_w}{\partial x}\right)^2 = 0 \tag{7.10}$$

Equation 7.10 is a nonlinear partial differential equation and the nonlinearity arises because of the inclusion of capillary pressure in it.

7.4. Adomian decomposition of Buckley-Leverett equation

In the Adomian decomposition method, the solution of a given problem is considered as a series solution. Therefore, the water saturation is expressed as

$$S_w(x,t) = \sum_{n=0}^{\infty} S_{wn} \ . \tag{7.11}$$

If a functional equation is taken into account for water saturation, it can be written in the form

$$\sum_{n=0}^{\infty} S_{wn} = f(x,t) + \sum_{n=0}^{\infty} A_n \ . \tag{7.12}$$

where $f(x,t)$ is a given function and A_n (S_{wo}, S_{w1}, S_{w2},...., S_{wn}) or, simply, A_n's are called Adomian polynomials. The Adomian polynomials are expressed as

$$A_n = \frac{1}{n!}\frac{d^n}{d\lambda^n}\left[N\left(\sum_{i=0}^{\infty}\lambda^i S_{wn}(x,t)_i\right)\right]_{\lambda=0} \tag{7.13}$$

where N is an operator and λ is a parameter. The elements of the series solution for $S_{wn}(x, t)$ are obtained recursively by

$$S_{w0}(x,t) = f(x,t), \quad S_{w1}(x,t) = A_0, \quad \cdots \quad S_{wk}(x,t) = A_{k-1} \quad \cdots . \tag{7.14}$$

By this arrangement, the linear and nonlinear part of the functional Eq. 7.12 is replaced by a known function using the recursive Eq. 7.14. By integrating Eq. 7.10 with respect to t

$$
\begin{aligned}
S_w = S_w(x,0) - \int_0^t & \left[\frac{q}{A\phi}\frac{\partial}{\partial S_w}\left(\frac{1}{1+\frac{k_{ro}\mu_w}{k_{rw}\mu_o}}\right)\frac{\partial S_w}{\partial x}\right]dt \\
- \int_0^t & \left[\frac{kk_{ro}}{\mu_o\phi}\frac{\partial}{\partial S_w}\left(\frac{1}{1+\frac{k_{ro}\mu_w}{k_{rw}\mu_o}}\right)\frac{\partial P_c}{\partial S_w}\left(\frac{\partial S_w}{\partial x}\right)^2\right. \\
& + \frac{k}{\mu_o\phi}\left(\frac{1}{1+\frac{k_{ro}\mu_w}{k_{rw}\mu_o}}\right)\frac{\partial k_{ro}}{\partial S_w}\frac{\partial P_c}{\partial S_w}\left(\frac{\partial S_w}{\partial x}\right)^2 \\
& \left. + \frac{kk_{ro}}{\mu_o\phi}\left(\frac{1}{1+\frac{k_{ro}\mu_w}{k_{rw}\mu_o}}\right)\frac{\partial^2 P_c}{\partial S_w^2}\left(\frac{\partial S_w}{\partial x}\right)^2\right]dt.
\end{aligned}
\tag{7.15}
$$

Comparing Eq. 7.15 with Eq. 7.12 and taking into account of Eq. 7.14, the elements of the water saturation series are obtained

$$
S_{w0}(x,t) = S_w(0,x) - \int_0^t \left[\frac{q}{A\phi}\frac{\partial}{\partial S_{w0}}\left(\frac{1}{1+\frac{k_{ro}\mu_w}{k_{rw}\mu_o}}\right)\frac{\partial S_{w0}}{\partial x}\right]dt
$$

$$
\begin{aligned}
S_{w1}(x,t) = - \int_0^t & \left[\frac{kk_{ro}}{\mu_o\phi}\frac{\partial}{\partial S_{w0}}\left(\frac{1}{1+\frac{k_{ro}\mu_w}{k_{rw}\mu_o}}\right)\frac{\partial P_c}{\partial S_{w0}} + \frac{k}{\mu_o\phi}\left(\frac{1}{1+\frac{k_{ro}\mu_w}{k_{rw}\mu_o}}\right)\frac{\partial k_{ro}}{\partial S_{w0}}\frac{\partial P_c}{\partial S_{w0}}\right. \\
& \left. + \frac{kk_{ro}}{\mu_o\phi}\left(\frac{1}{1+\frac{k_{ro}\mu_w}{k_{rw}\mu_o}}\right)\frac{\partial^2 P_c}{\partial S_{w0}^2}\right]\left(\frac{\partial S_{w0}}{\partial x}\right)^2 dt
\end{aligned}
$$

$$
\begin{aligned}
S_{w2}(x,t) = -\frac{d}{d\lambda}\int_0^t & \left[\frac{kk_{ro}}{\mu_o\phi}\frac{\partial}{\partial(S_{w0}+S_{w1})}\left(\frac{1}{1+\frac{k_{ro}\mu_w}{k_{rw}\mu_o}}\right)\frac{\partial P_c}{\partial(S_{w0}+S_{w1})}\right. \\
& + \frac{k}{\mu_o\phi}\left(\frac{1}{1+\frac{k_{ro}\mu_w}{k_{rw}\mu_o}}\right)\frac{\partial k_{ro}}{\partial(S_{w0}+S_{w1})}\frac{\partial P_c}{\partial(S_{w0}+S_{w1})} \\
& \left. + \frac{kk_{ro}}{\mu_o\phi}\left(\frac{1}{1+\frac{k_{ro}\mu_w}{k_{rw}\mu_o}}\right)\frac{\partial^2 P_c}{\partial(S_{w0}+S_{w1})^2}\right]\left(\frac{\partial(S_{w0}+\lambda S_{w1})}{\partial x}\right)^2 dt
\end{aligned}
$$

$$
\begin{aligned}
S_{w3}(x,t) = -\frac{1}{2!}\frac{d^2}{d\lambda^2}\int_0^t & \left[\frac{kk_{ro}}{\mu_o\phi}\frac{\partial}{\partial(S_{w0}+S_{w1}+S_{w2})}\left(\frac{1}{1+\frac{k_{ro}\mu_w}{k_{rw}\mu_o}}\right)\frac{\partial P_c}{\partial(S_{w0}+S_{w1}+S_{w2})}\right. \\
& + \frac{k}{\mu_o\phi}\left(\frac{1}{1+\frac{k_{ro}\mu_w}{k_{rw}\mu_o}}\right)\frac{\partial k_{ro}}{\partial(S_{w0}+S_{w1}+S_{w2})}\frac{\partial P_c}{\partial(S_{w0}+S_{w1}+S_{w2})} \\
& \left. + \frac{kk_{ro}}{\mu_o\phi}\left(\frac{1}{1+\frac{k_{ro}\mu_w}{k_{rw}\mu_o}}\right)\frac{\partial^2 P_c}{\partial(S_{w0}+S_{w1}+S_{w2})^2}\right]\left(\frac{\partial(S_{w0}+\lambda S_{w1}+\lambda^2 S_{w2})}{\partial x}\right)^2 dt
\end{aligned}
$$

$$
\cdots \quad \cdots \quad \cdots \quad \cdots \quad \cdots \quad \cdots \quad \cdots \quad \cdots
\tag{7.16}
$$

7.5. Results and discussion

The method is applied to a given reservoir with the initial water saturation of 0.18. This value is corresponding to the irreducible water saturation of the reservoir. Water is injected into the reservoir with a linear flow rate of 1 ft/day. The oil and water viscosities are 1.73 cp and 0.52 cp, respectively. The flow of the displaced phase (oil) ceases at S_{oc} = 0.1. The porosity of the medium is 0.25 with an absolute permeability of k = 10 md.

The normalized water saturation and the water and oil relative permeability are obtained using

$$S_{wn} = \frac{S_w - 0.18}{1 - 0.1 - 0.18}, \qquad k_{rw} = 0.59439\, S_{wn}{}^4, \qquad k_{ro} = (1 - S_{wn})^2 \tag{7.17}$$

A typical plot of variation of relative permeability to water, k_{rw}, relative permeability to oil, k_{ro}, fractional flow curve, f_w and its derivative, df_w/dS_w are shown in Fig. 7.1. The capillary pressure data are also known as shown in Table 7.1.

The solution for the first base element of the series solution of the water saturation, S_{w0}, is obtained through the solution of the first equation in Eq. 7.16. It can be written by integrating from the both sides of the first equation in Eq. 7.16 and using Eq. 7.4 that

$$\frac{\partial S_{w0}}{\partial t} + \frac{q}{A\phi}\frac{\partial}{\partial S_{w0}}\left(\frac{1}{1+M}\right)\frac{\partial S_{w0}}{\partial x} = 0. \tag{7.18}$$

This equation suggests that S_{w0} is constant along a direction that is called characteristic direction. The characteristic direction can be obtained by

$$\left(\frac{dx}{dt}\right)_{S_{w0}} = \frac{q}{A\phi}\frac{\partial}{\partial S_{w0}}\left(\frac{1}{1+M}\right)_t \tag{7.19}$$

that is the Buckley-Leverett frontal advance equation. Integrating respect to time, the distribution of S_{w0} is found in the form of

$$x(t, S_{w0}) = \frac{qt}{A\phi}\frac{\partial}{\partial S_{w0}}\left(\frac{1}{1+M}\right)_t . \tag{7.20}$$

The solution of Eq. 7.20 gives the variation of the S_{w0} along the reservoir at certain time. The distribution of S_{w0} along the reservoir is obtained based on the definition of the mobility ratio Eq. 7.4 and the relations for the relative permeability of water and oil in Eq. 7.17. It corresponds to the variation of the water saturation when the effect of the capillary pressure is ignored. The computations are carried out at different time of $t = 0.5,1,2,5$ and 10 [days]. The solution for the water saturation without the capillary pressure effect shows the unrealistic physical situation that Buckley-Leverett mentioned in their pioneer paper with multiple-saturations at each distance (x-position) as given partly in Fig. 7.3. In order to avoid multiple saturation values at a particular distance, a saturation discontinuity at a distance, x_f is generally created in such a way that the areas ahead of the front and below the curve are equal to each other.

The other elements of the series solution for the water are obtained recursively using Eq. 7.16 and the solution for S_{w0}. The solution for S_{w1} is obtained using the solution of S_{w0} at a certain point for a given time. To induce the nonlinear dependence of capillary on saturation, during decomposition, the capillary pressure and its derivatives are approximated by using the cubic spline, as shown in Fig. 7.2. The interpolating splines are preferred over interpolating polynomials as they do not suffer from oscillations between the knots and are smoother and more realistic than linear splines (Ertekin et al.,

2001). Such technique is also used to observe the effects of linearization in pressure in reservoir flow equations (Mustafiz et al., 2006). The solutions for S_{w2} and S_{w3} are obtained recursively using Eqs. 7.16. The computations shows that the series solution converges very fast and it is not necessary to go further than S_{w3}.

The distribution of the water saturation along the reservoir is given in Fig. 7.3. The results of the water saturation without the effect of the capillary pressure are also depicted in Fig. 7.3 for the sake of comparison. This figure shows that by considering the effects of capillary pressure, it is possible to avoid unrealistic multiple saturation values. Moreover, the decomposition approach shows notable prediction of saturation profiles along the length. The gradual and mild changes observed in the saturation profile here, are perhaps less severe than the conventional prediction of shock-fronts.

7.6. Conclusions

To unravel the lure of finding a justifiable answer to the shock-front which is often less severe in the experiments than in the theoretical postulations, the Adomian decomposition method is investigated to solving the Buckley-Leverett equation. The solution by the ADM also assures that the nonlinear dependence of capillary pressure on saturation is maintained. The term, $S_{w0}(x, t)$, is prepared through the method of characteristics, which subsequently becomes useful for the purpose of evaluation of the other elements in water saturation series. The saturation at a point and at a given time is evaluated through recursion. The term $S_{w1}(x, t)$ is calculated using the solution of $S_{w0}(x, t)$ at any distance and time. The solutions for $S_{w2}(x, t)$ and $S_{w3}(x, t)$ are obtained using the results of $S_{w1}(x, t)$ and $S_{w2}(x, t)$, respectively. The computation is done up to the term $S_{w3}(x, t)$, as it is found that the series solution converges very quickly.

The most significant observation is that by considering the effects of capillary pressure, it is possible to avoid unrealistic multiple saturation values. Moreover, the saturation

profiles along the length are noted with gradual and mild changes as predicted by the decomposition approach. Perhaps the slope is less severe than predicted by the conventional finite difference approach, a study remains for future.

7.7. Nomenclature

A cross-sectional area in the x-direction

A_n Adomian polynomial

f_w fractional flow of water

g acceleration of gravity

k absolute permeability

k_{ro} relative permeability to oil

k_{rw} relative permeability to water

M mobility ratio of oil to water

N operator in the expression (Eq. 7.14) for Adomian polynomial

n_1 empirical constant in the relationship between relative permeability to water and normalized water saturation

n_2 empirical constant in the relationship between relative permeability to oil and normalized water saturation

P_c capillary pressure

q total fluid flow rate

S_{or} residual oil saturation

S_w water saturation

S_{wi} irreducible water saturation

S_{wn} normalized water saturation

t time

x distance

x_f location of the front of saturation discontinuity in the x-direction

α angle of inclination of reservoir (positive for the x axis rotated in the counter clockwise direction from the horizon)

α_1 constant coefficient in the relationship between relative permeability to water and normalized water saturation

α_2 constant coefficient in the relationship between relative permeability to oil and normalized water saturation

λ parameter in the expression (Eq. 7.14) of Adomian polynomial

λ_o mobility of oil

λ_w mobility of water

μ_o viscosity of oil

μ_w viscosity of water

ρ_o density of oil

ρ_w density of water

φ porosity

7.8. References

Adjedj, B., (1999) Application of the decomposition method to the understanding of HIV immune dynamics, Kybernetes, vol. 28, no. 3, pp. 271-283

Adomian, G., (1984) A New approach to nonlinear partial differential equations, Journal of Mathematical Analysis and Applications, vol. 102, pp. 420-434

Adomian, G., (1986) Nonlinear stochastic operator equations, Academic Press, San Diego

Adomian, G., (1994) Solving frontier problems of physics: The decomposition method, Kluwer Academic Publishers, Dordrecht

Adomian, G., Cherruault, Y. and Abbaoui, K., (1996) A nonperturbative analytical solution of immune response with time-delays and possible generalization, Mathematical and Computer Modelling, vol. 20, no. 10, pp. 89-96

Bentsen, R. G., (1978) Conditions under which the capillary term may be neglected, Journal of Canadian Petroleum technology, vol. 17, no. 4, pp. 25-30

Biazar, J. and Ebrahimi, H., (2005) An approximation to the solution of hyperbolic equations by Adomian decomposition method and comparison with characteristics method, Applied Mathematics and Computation, vol. 163, pp. 633–638

Biazar, J. and Islam, M. R., (in press) The Adomian decomposition method for the solution of transient energy equation in rocks subjected to laser irradiation, International Journal of Science and Technology

Buckley, S. E. and Leverett, M. C., (1942) Mechanism of fluid displacement in sands, Trans. AIME, vol. 146, pp. 187–196

El-Sayed, S. M. and Abdel-Aziz, M. R., (2003) A comparison of Adomian's decomposition method and wavelet-Galerkin method for solving integro-differential equations, Applied Mathematics and Computation, vol. 136, pp. 151-159

Ertekin, T., Abou-Kassem, J. H., and King, G. R., (2001) Basic applied reservoir simulation, SPE textbook series, vol. 7, 406 p., SPE: Richardson, TX

Eugene, Y., (1993) Application of the decomposition method to the solution of the reaction-convection-diffusion equation, Applied Mathematics and Computation, vol. 56, pp. 1–27

Fayers, F. J., and Sheldon, J. W., (1959) The effect of capillary pressure and gravity on two-phase fluid flow in a porous medium, Transactions AIME, vol. 216, pp. 147-155

Guellal, S. and Cherruault, Y., (1995) Application of the decomposition method to identify the distributed parameters of an elliptical equation, Mathematical and Computer Modelling, vol. 21, no. 4, pp. 51-55

Holmgren, C. R. and Morse, R. A., (1951) Effect of Free gas saturation on oil recovery by waterflooding, Trans., AIME, vol. 192, pp. 135-140

Hovanessian, S. A., and Fayers, F. J., (1961) Linear water flood with gravity and capillary effects, Society of Petroleum Engineering Journal, March, pp. 32-36

Laffez, P. and Abbaoui, K., (1996) Modelling of the thermic exchanges during a drilling: resolution with Adomian's decomposition method, Mathematical and Computer Modelling, vol. 23, no. 10, pp. 11-14

Mustafiz, S., Biazar, J. and Islam, M. R., (2005) An Adomian decomposition solution to the modified Brinkman model (MBM) for a 2-dimensional, 1-phase flow of petroleum fluids, Proc. CSCE 33rd Annual Conference, Toronto, Canada, June 2-4

Mustafiz, S. and Islam, M. R., (2005) Adomian decomposition of two-phase, two-dimensional non-linear PDEs as applied in well testing, Proc. 4th International Conference on Computational Heat and Mass Transfer, Paris-Cachan, May 17-20

Mustafiz, S., Moussavizadegan, H., and Islam, M. R., (2006) The effects of linearization on solutions of reservoir engineering problems, Journal of Petroleum Science and Technology, accepted for publication, July, 17 pg.

Rahman, M. A., Mustafiz, S., Biazar, J., Koksal, M. and Islam, M. R., (in press) Investigation of a novel perforation technique in petroleum wells - perforation by drilling, Journal of the Franklin Institute

Terwilliger, P. L., Wilsey, L. E., Hall, H. N., Bridges, P. M. and Morse, R. A., (1951) An experimental and theoretical investigation of gravity drainage performance, Trans. AIME, vol. 192, pp. 285-296

Wazwaz, A. M. (2001) A new algorithm for calculating Adomian polynomials for nonlinear operators, Applied Mathematics and Computation, vol. 111, no. 1, pp. 33–51

Wazwaz, A. M. and El-Sayed, S. M., (2001) A new modification of Adomian decomposition method for linear and nonlinear operators, Applied Mathematics and Computation, vol. 122, no. 3, pp. 393-405

7.9. Appendices

7.9.1. Appendix A: Table

Table 7.1. Capillary pressure data

S_{wn}	$P_c, [atm]$	S_{wn}	$P_c, [atm]$	S_{wn}	$P_c, [atm]$	S_{wn}	$P_c, [atm]$
0.00	3.9921	0.11	1.2036	0.30	0.3600	0.65	0.0550
0.01	3.5853	0.15	0.8745	0.36	0.2699	0.72	0.0350
0.02	3.1987	0.18	0.7010	0.42	0.1980	0.87	0.0100
0.05	2.2577	0.21	0.5709	0.48	0.1450	0.95	0.0027
0.08	1.6209	0.25	0.4592	0.56	0.0920	1.00	0.0000

7.9.2. Appendix B: Figures

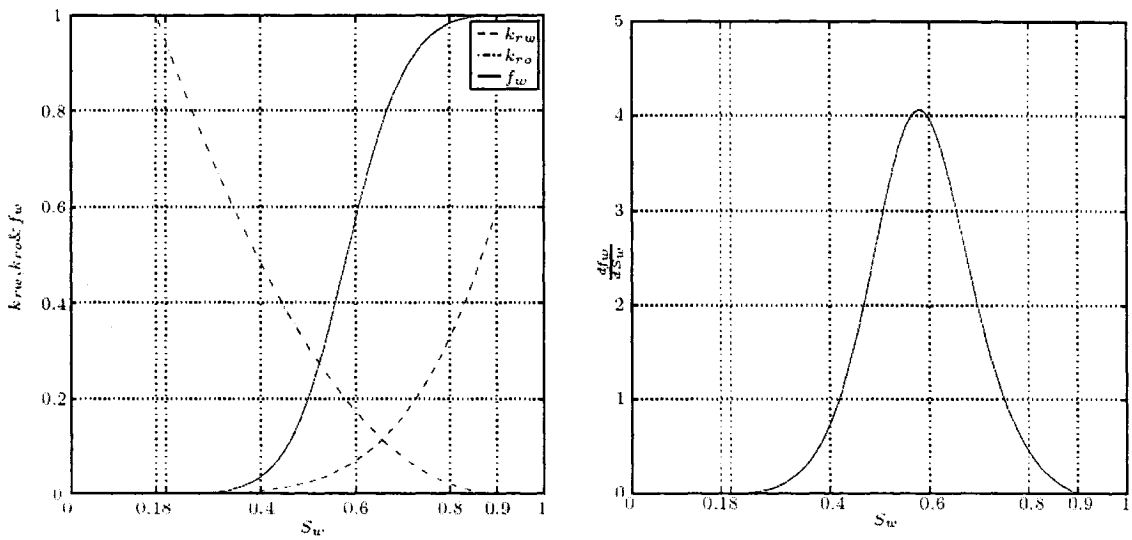

Figure 7.1. The variation of the water and oil relative permeability, the fractional water flow rate and the differentiation of fractional water flow rate with the water saturation

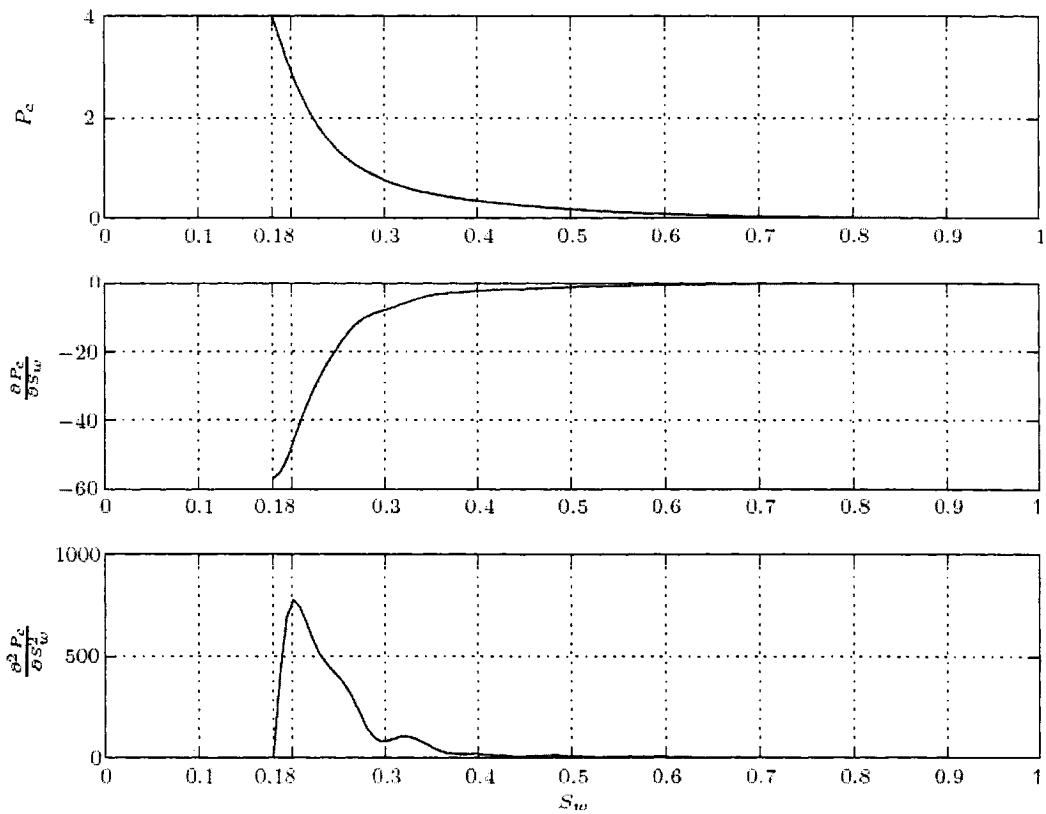

Figure 7.2. The capillary pressure variation and its first and second derivatives as a function of the water saturation

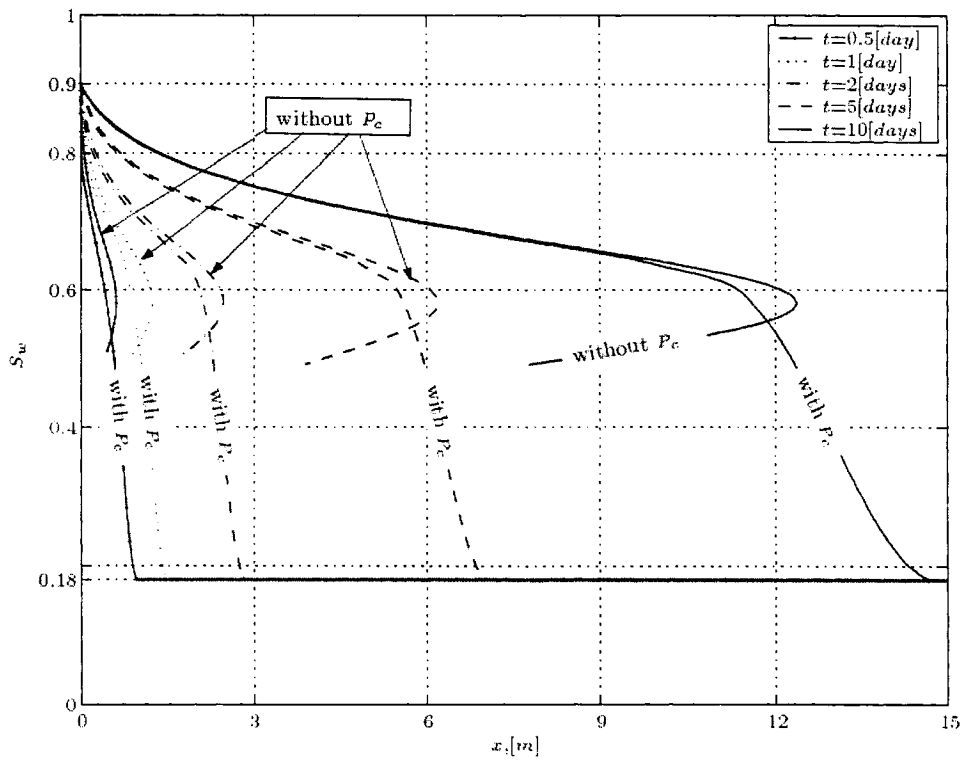

Figure 7.3. The water saturation distribution with and without the effect of capillary pressure using ADM

Chapter 8

8 ADOMIAN DECOMPOSITION OF TWO-PHASE, TWO-DIMENSIONAL NON-LINEAR PDEs AS APPLIED IN WELL TESTING

8.1. Abstract

The Diffusivity equation is one of the most widely used equations when describing the fluid flow in the porous media. It is also very popular in the well-testing world. Previously, numerical attempts have been made to solve the non-linear partial differential equations for multi-dimensional, multi-phase conditions with relevant initial and boundary conditions. However, problems such as multi-dimensional, multi-phase have never been solved for well-testing. Therefore, when the typical non-dimensionless groups of well-testing problems are imported into the basic Diffusivity equations, a set of non-dimensional, non-linear, partial differential equations resulted. This paper finds possible application of Adomian Decomposition Method (ADM) into a recently formulated multiphase reservoir/well-testing problem, which is novel and unique up-to-date from theoretical reservoir engineering to well-testing research.

8.2. Introduction

Quite frequently, researchers have used three-dimensional, three-phase equations for reservoir simulation. In reservoir simulation, Darcy's Law (Darcy, 1856) makes a major contribution. It is often combined with the equation of continuity to develop a partial differential equation, which describes flow through porous media (Ertekin et al., 2001). This partial differential equation is often regarded as the diffusivity equation.

Now, if intended for well-testing, the diffusivity equation is a radial flow equation and can be nonlinear in nature, which is difficult to solve. However, over the years, numerous methods including analytical techniques and empirical equations are used in solving problems in well testing.

8.3. Formulation

The diffusivity equations for a two-phase (oil-water) system in their 3-D forms are expressed by the following equations (Mustafiz et al., 2005):

Oil phase

$$\frac{\partial p_0}{\partial t} = \frac{k_0}{\phi \mu_0 S_0 c_0}\left[\frac{\partial^2 p_0}{\partial r^2} + \frac{1}{r}\frac{\partial p_0}{\partial r} + \frac{1}{r^2}\frac{\partial^2 p_0}{\partial \theta^2} + \frac{\partial^2 p_0}{\partial z^2}\right] - \frac{1}{S_0 c_0}\frac{\partial S_0}{\partial t} \tag{8.1}$$

Water phase

$$\frac{\partial p_W}{\partial t} = \frac{k_W}{\phi \mu_W S_W c_W}\left[\frac{\partial^2 p_W}{\partial r^2} + \frac{1}{r}\frac{\partial p_W}{\partial r} + \frac{1}{r^2}\frac{\partial^2 p_W}{\partial \theta^2} + \frac{\partial^2 p_W}{\partial z^2}\right] - \frac{1}{S_W c_W}\frac{\partial S_W}{\partial t} \tag{8.2}$$

Equations 8.1 and 8.2 assume that permeability and viscosity are constants and the medium is isotropic. Furthermore, in non-dimensional expressions (Craft and Hawkins, 1991; Mustafiz et al., 2005) when pressure profile is homogeneous and independent of angle (θ) (Panawalage, 2002), Equations 8.1 and 8.2 turn to Equations 8.3 and 8.4 respectively:

Oil phase

$$\frac{\partial p_{oD}}{\partial t_D} = \frac{k_{ro} c_t}{[1 - S_{wi} - S_{WD}(1 - S_{wi} - S_{or})]c_0}\left[\frac{\partial^2 p_{oD}}{\partial r_D^2} + \frac{1}{r_D}\frac{\partial p_{oD}}{\partial r_D} + \left(\frac{r_w}{h}\right)^2 \frac{\partial^2 p_{oD}}{\partial z_D^2}\right]$$
$$- \frac{2\pi kh}{q\mu_o c_o}\frac{(1 - S_{wi} - S_{or})}{[1 - S_{wi} - S_{WD}(1 - S_{wi} - S_{or})]}\frac{\partial S_{wD}}{\partial t_D} \tag{8.3}$$

Water phase

$$\frac{\partial p_{wD}}{\partial t_D} = \frac{\mu_o k_{rw} c_t}{\mu_W S_W c_W}\left[\frac{\partial^2 p_{wD}}{\partial r_D^2} + \frac{1}{r_D}\frac{\partial p_{wD}}{\partial r_D} + \left(\frac{r_w}{h}\right)^2 \frac{\partial^2 p_{wD}}{\partial z_D^2}\right] + \frac{2\pi kh}{q\mu_w c_W}\frac{(1 - S_{wi} - S_{or})}{[S_{wi} + S_{WD}(1 - S_{wi} - S_{or})]}\frac{\partial S_{wD}}{\partial t_D} \tag{8.4}$$

8.4. Adomian Decomposition

In recent years, *Adomian Decomposition Method* (ADM) has been successfully applied to solve wave equations (Biazar and Islam, 2004), system of ordinary differential equations (Biazar et al., 2004), etc. Equations 8.3 and 8.4 can be approached in the same technique where any governing equation is converted into recursive relations.

In this section, Equation 8.5, which is similar to Equations 8.3 and 8.4, is approached to explain how decomposition method works:

$$\frac{\partial p}{\partial t} = E\left[\frac{\partial^2 p}{\partial r^2} + \frac{1}{r}\frac{\partial p}{\partial r} + F\frac{\partial^2 p}{\partial z^2}\right] + G\frac{\partial S}{\partial t} \tag{8.5}$$

In Canonical form Equation 8.5 is written as

$$Lp = E\left[\frac{\partial^2 p}{\partial r^2} + \frac{1}{r}\frac{\partial p}{\partial r} + F\frac{\partial^2 p}{\partial z^2}\right] + G\frac{\partial S}{\partial t} \tag{8.6}$$

where, $L = \frac{\partial}{\partial t}$ with the inverse $L^{-1} = \int_0^t (.)dt$, which means $L^{-1}L = I$.

Applying the inverse operator to Equation 8.6 we derive canonical form of the equation

$$P(r,z,t) = P(r,z,0) + E\int_0^t \left(\frac{\partial^2 p}{\partial r^2} + \frac{1}{r}\frac{\partial p}{\partial r} + F\frac{\partial^2 p}{\partial z^2}\right)dt + G(S_t - S_0) \tag{8.7}$$

Similarly, Equation 8.5 can be re-arranged to apply the inverse operators $L^{-1} = \int_{R_2}^{r}\int_{R_2}^{r}(.)drdr$ where $L = \frac{\partial^2}{\partial r}$ and $L^{-1} = \int_{Z_2}^{z}\int_{Z_2}^{z}(.)dzdz$, $L = \frac{\partial^2}{\partial z}$, which result in two more pressure expressions

$$P(r,z,t) = P(R_2,z,0) + \frac{1}{E}\int_{R_2}^{r}\int_{R_2}^{r}(\frac{\partial p}{\partial t} - C\frac{\partial S}{\partial t})dr - \frac{1}{r}\int_{R_2}^{r}\int_{R_2}^{r}\frac{\partial p}{\partial r}dr - F\int_{R_2}^{r}\int_{R_2}^{r}\frac{\partial^2 p}{\partial z^2}dz \quad (8.8)$$

$$P(r,z,t) = P(r,z_2,t) + \frac{1}{EF}\int_{Z_2}^{z}\int_{Z_2}^{z}(\frac{\partial p}{\partial t} - C\frac{\partial S}{\partial t})dz - \frac{1}{Fr}\int_{Z_2}^{z}\int_{Z_2}^{z}\frac{\partial p}{\partial r}dz - \frac{1}{F}\int_{Z_2}^{z}\int_{Z_2}^{z}\frac{\partial^2 p}{\partial r^2}dz \quad (8.9)$$

Now, Equations 8.7-8.9 can be averaged to obtain the expression for pressure. Adomian decomposition method considers the solution as the sum of the following series:

$$p(r,z,t) = \sum_{n=0}^{\infty} p_n \quad (8.10)$$

where p_0 is defined to be the summation of the terms on the right hand side of Equation 8.8; derived from initial conditions and those terms that do not depend on the unknown function p.

$$p_0 = \frac{1}{3}[P(r,z,0) + P(R_2,z,0) + P(r,z_2,t) + G(S_t - S_0)] \quad (8.11)$$

The other terms of the series are defined as:

$$p_{n+1} = A_n(p_0, p_1, ..., p_n) \quad n = 0,1,2,.. \quad (8.12)$$

Where $A_n(p_0, p_1,..., p_n)$ or the Adomian polynomials are computed using an alternate algorithm:

$$A_n(p_0, p_1,..., p_n) =$$

$$\frac{1}{3}[E\int_0^t(\frac{\partial^2 p_n}{\partial r^2}+\frac{1}{r}\frac{\partial p_n}{\partial r}+F\frac{\partial^2 p_n}{\partial z^2})dt+\frac{1}{E}\int_{R_2}^{r}\int_{R_2}^{r}(\frac{\partial p_n}{\partial t}-C\frac{\partial S}{\partial t})drdr$$

$$-\frac{1}{r}\int_{R_2}^{r}\int_{R_2}^{r}\frac{\partial p_n}{\partial r}drdr-F\int_{R_2}^{r}\int_{R_2}^{r}\frac{\partial^2 p_n}{\partial z^2}dzdz+\frac{1}{EF}\int_{Z_2}^{z}\int_{Z_2}^{z}(\frac{\partial p_n}{\partial t}-C\frac{\partial S}{\partial t})dzdz \qquad (8.13)$$

$$-\frac{1}{Fr}\int_{Z_2}^{z}\int_{Z_2}^{z}\frac{\partial p_n}{\partial r}dzdz-\frac{1}{F}\int_{Z_2}^{z}\int_{Z_2}^{z}\frac{\partial^2 p_n}{\partial r^2}dzdz]$$

To derive the solution we have to evaluate the parameters E, F and G. This requires information on fluid and matrix properties, which can also be available. Relationships about phase-saturation constraint and capillary pressures as functions of phase saturations for an oil-water system will be necessary to solve Equations 8.3 and 8.4.

$$S_o + S_w = 1 \qquad (8.14)$$

$$P_{cow} = P_o - P_w = f(S_w) \qquad (8.15)$$

8.5. Example

In this section, a solution to the simplest form of diffusivity equation is given. The solution of this classic equation is important as Equations 8.1 and 8.2 are similar to it. In radial form, the diffusivity equation is as follows:

$$\frac{\partial p}{\partial t} = \frac{\partial^2 p}{\partial r^2} + \frac{1}{r}\frac{\partial p}{\partial r} \qquad (8.16)$$

With the initial condition described as:

$$P(r,0)=A.r \tag{8.17}$$

Let, $L = \frac{\partial}{\partial t}$ with the inverse $L^{-1} = \int_0^t (.)dt$. So, we have:

$$P(r,t) = P(r,0) + \int_0^t (\frac{\partial^2 p}{\partial r^2} + \frac{1}{r}\frac{\partial p}{\partial r})dt \tag{8.18}$$

Using the procedure described previously, we have:

$$A_n(p_0, p_1, ..., p_n) = \frac{\partial^2 p_n}{\partial r^2} + \frac{1}{r}\frac{\partial p_n}{\partial r} \tag{8.19}$$

The solution by Adomian Decomposition method consists of the following scheme:

$$P_0 = Ar \tag{8.20}$$

$$P_{n+1} = \int_0^t (\frac{\partial^2 p_n}{\partial r^2} + \frac{1}{r}\frac{\partial p_n}{\partial r})dt \tag{8.21}$$

where, n=0,1,2,.....

$$A_0(P_0) = \frac{\partial^2 p_0}{\partial r^2} + \frac{1}{r}\frac{\partial p_0}{\partial r} = \frac{A}{r} \tag{8.22}$$

$$P_1 = \frac{At}{r} \tag{8.23}$$

$$A_1(P_0, P_1) = \frac{At}{r^3} \tag{8.24}$$

$$P_2 = \frac{At^2}{2r^3} \tag{8.25}$$

$$A_2(P_0, P_1, P_2) = \frac{9At^2}{2r^5} \tag{8.26}$$

$$P_3 = \frac{3At^3}{2r^5} \tag{8.27}$$

In general, the expression can be written as:

$$A_{n-1}(P_0, P_1, p_2, .. p_{n-1}) = \frac{1^2 * 3^2 * .... * (2n-3)^2}{(n-1)! r^{2n-1}} A t^{n-1} \tag{8.28}$$

$$p_n = \frac{1^2 * 3^2 * .... * (2n-3)^2}{n! * r^{2n-1}} A t^n \tag{8.29}$$

Therefore,

$$p(r,t) = A[r + \sum_{n=1}^{\infty} \frac{1^2 * 3^2 * .... * (2n-3)^2}{n! * r^{2n-1}} t^n] \tag{8.30}$$

8.6. Conclusions

Adomian decomposition technique has the potential to apply to the newly developed equations. This paper outlines how a multiphase, multidimensional well-testing system is structured in the decomposition technique. The paper also provides a solution to the classic diffusivity problem. Such solution is important as problems of higher dimensions (multiphase, multidimensional with initial and boundary equations) can also be solved by similar approaches.

8.7. References

Darcy, H.P.G., (1856) Les Fontaines Publiques de villle de la Dijon Dalmont, Exposition et Application des Pricipes a Suivre et des Furmules a Emplyer dans les Questions de Distribution d'Eau. Victor Dalmont, Paris

Ertekin, T., Abou-Kassem, J. H., and King, G. R., (2001) Basic applied reservoir simulation, SPE textbook series, vol. 7, 406 p., SPE: Richardson, TX

Mustafiz, S., Biazar, J. and Islam, M.R., (2005) Formulation of two-phase, two-dimensional non-linear PDE's as applied in well testing, proceeding of the 1st International Conference on Modeling, Simulation and Applied Optimization, Sharjah, UAE, February 1-3

Craft, B.C. and Hawkins, M.F., (1991) Applied petroleum reservoir engineering, 2nd edition, Prentice Hall PTR, Englewood Cliffs, NJ

Panawalage, S.P., (2002) The solution of an inverse problem in reservoir permeability, Masters Thesis, Dalhousie University, Halifax, Canada

Biazar, J. and Islam, R., (2004) Solution of wave equation by Adomian decomposition method and the restrictions of the method, Applied Mathematics and Computation, vol. 149, pp. 807-814

Biazar, J., Babolian, E. and Islam, R., (2004) Solution of the system of ordinary differential equations by Adomian decomposition method, Applied Mathematics and Computation, vol. 147, pp. 713-719

Chapter 9

9 WELL TEST ANALYSES FOR DARCY AND NON-DARCY FLOW USING AN ADVANCED NUMERICAL SCHEME

9.1. Abstract

An accurate prediction of reservoir performance has tremendous benefits to the petroleum industry. The state of the art in predicting production has been advanced considerably in last few decades. However, geological features such as natural fracture or damaged matrix continue to perplex engineers and scientists and an accurate prediction tool is much to be desired. One of the shortcomings of the present methods is the use of numerical schemes that are not adequate for describing fluid flow under complex production scenarios. Darcy's law may not be suitable for complex reservoirs, particularly for near-wellbore applications. Another source of error is in the use of conventional Darcy's law for describing fluid flow in the petroleum reservoir. Because most petroleum reservoirs are complex, such numerical schemes and fluid flow models can lead to distorted representation of the oil production capabilities of a reservoir. This, in turn, can affect energy pricing. This paper uses an advanced numerical scheme to study fluid flow governed by both Darcy and non-Darcy conditions. The numerical scheme offers comparable precision with recent scheme reported to be Δx^4 and Δt^4 accurate. This scheme is applied to a one-dimensional radial system with no-flow at the outer boundary and fluid is being produced at a constant rate from a single well placed at the centre. The model utilizes upwind technique for the convective term of the convection-diffusion equation. Numerical results include transient pressure and velocity profiles for the entire reservoir, using both Darcy and non-Darcy options. The change in

pressure with time at the wellbore is compared with the results obtained using the exact solution and the theory presented. The applied scheme is found to be significantly accurate for results of pressure drop as function of time and production velocity, when compared with the results predicted by a recently developed scheme. In addition, the conditions for which Darcy and non-Darcy flow models give different predictions, are discussed.

9.2. Introduction

Fluid flow in porous media is described by the diffusivity equation, which is most widely used in well testing analysis. There are generally four solutions to the diffusivity equation: the solution for a bounded cylindrical reservoir, the solution for an infinite reservoir while the well acts as the line source, the pseudosteady-state solution and the solution that includes wellbore storage for a well in an infinite reservoir (Lee, 2002). For example, the approach suggested by Matthews and Russell (1967) can be used in the solution of a bounded radial, homogeneous and isotropic reservoir of uniform thickness. In the approach, for which slightly compressible Darcy flow governs, the flowing pressure at the sandface is a function of time, and fluid and reservoir rock properties. The solution requires the knowledge of one initial and two boundary conditions. Although the Laplace transformation is proven useful in handling the problem (Everdingen and Hurst, 1949); the functional dependence of dimensionless pressure on dimensionless variables, which are time and radius, introduces infinite series of exponentials and Bessel functions. It adds complexity to the solution and additional uncertainties due to the assumptions that are intrinsic to infinite series. Therefore, the limiting forms of the solution are found to be more useful when the infinite series is evaluated for various dimensionless radii over a broad range of dimensionless time. Such evaluation leads to Chatas' (1953) tabulation, which presents dimensionless pressure based on dimensionless time. A number of relationships appear to determine dimensionless pressure and selection of each of them is governed by dimensionless time and radii values. These

solutions often referred as the van Everdingen-Hurst constant rate terminal solution and serve as the standard in well problems (Lee, 2002). Besides Stehfest (1970) presented an algorithm of inverse Laplace transformation that gained significant attention to the researchers.

In the past, researchers have utilized approximate methods such as exponential integral or Ei function to solve well testing problems. Although, it is not exact, the method has found applications in recent time because of its simplicity. Rahman et al. (in press) used it to compare with their experimental investigation of perforation by drilling with reasonable agreement. However, the very assumption of zero radius of a well remains questionable.

It is imperative to note that all of the above approaches provide one with satisfactory results for creeping flow. Darcy's law (Darcy, 1856) is the widely accepted relationship that characterizes single-phase fluid flow in homogeneous porous media (Adler, 1992; Dullien, 1992; and Sahimi, 1994 and 1995). The law is also used with necessary adjustments for non-homogenous and multiphase problems. When the flow rate is low, there exists a linear relationship between the differential pressure and the flow rate. Although fluid flow in petroleum reservoirs is seldom Darcian, non-Darcy flow can occur in many instances (Choi et al., 1997; Belhaj et al., 2003a, 2003b and 2003c). Particularly near the wellbore or in fractures, fluid flow is considered to be non-Darcian (Cheema and Islam, 1995). In rapid flow condition, the inertia force (convection) to the flow in the pore space affects significantly. The high velocity around the wellbore in gas wells and the propped hydraulic fracture are few examples that require consideration of non-Darcy effects. Ucan and Civan (1996) report that the consideration of non-Darcy effect eliminates the need to use skin factor to treat the wellbore region since flow functions are well- estimated. Typically, in high flow condition, the fluid flow deviates from the linear relationship between the differential pressure and the flow rate (Li, 2002).

Forchheimer (1901) proposed a non-Darcy coefficient of the porous medium because of inertial losses to account for the pressure drop. Such characterization is supported in several publications (Dullien, 1992; Sahimi, 1994 and Sahimi, 1995). Andrade et al. (1999) also report the Forchheimer equation to be a valid and classic one when pressure deviation from Darcy's law occurs.

This paper investigates both Darcy and Forchheimer models for a bounded reservoir in a radial system. The paper also features new theoretical analyses for both models. The extensive use of numerical techniques in petroleum problems have resulted in significant improvements on schemes. Features such as stability, ease and accuracy of the Barakat-Clark (1966) scheme have attracted many researchers (Basu et al., 2006; Bjorndalen et al., 2005; Rahman et al., 2003; Bjorndalen et al., 2003; Bjorndalen, 2002; Mustafiz, 2002 and Ali and Islam, 1998) to apply the scheme. Extensive interest in last five years resulted in an increased efficiency when Bokhari and Islam (2005) makes some improvement to the Barakat-Clark (1966) scheme. The modified scheme is later applied to petroleum problems such as in modeling of viscous fingering (Bokhari and Islam, 2005a). The numerical scheme followed in this paper is compared with the Bokhari-and Islam scheme (2005) in several instances and applied to model both Darcy and non-Darcy problems. To validate the model, the results are also compared with the exact (analytical) solution. On the other hand, the independently obtained numerical solution is used to justify the starting assumption for the analytical approach and furthermore to confirm the analytical procedure and its results.

9.3. Governing equations and theoretical analysis

9.3.1. Darcy flow condition

A theoretical case is considered where an isothermal fluid with small and constant compressibility is flowing toward a well in a circular, homogeneous reservoir of uniform

thickness in a radial manner. For developing analysis and computational solution techniques, the following governing equations are taken into consideration:

(1) Conservation of mass:

$$-\phi\frac{\partial\rho}{\partial t}=v\frac{\partial\rho}{\partial r}+\rho\frac{\partial v}{\partial r}+\rho\frac{v}{r} \tag{9.1}$$

(2) Darcy law:

$$\frac{\partial p}{\partial r}=-\frac{\mu}{k}v \tag{9.2}$$

(3) Equation of state:

$$c=\frac{1}{\rho}\frac{\partial\rho}{\partial p} \tag{9.3}$$

where, ρ is density and p is pressure; v is velocity; r is distance. It is assumed that compressibility (c) is small, both compressibility and viscosity, (μ) are independent of pressure; the medium is isotropic and permeability, (k) and porosity, ϕ are constants.

Substituting v from Eq. (9.2) into Eq. (9.1), and applying the chain rule $\frac{\partial\rho}{\partial r}=\frac{\partial\rho}{\partial p}\frac{\partial p}{\partial r}$ and $\frac{\partial\rho}{\partial t}=\frac{\partial\rho}{\partial p}\frac{\partial p}{\partial t}$ and replacing ρ with p by means of Eq. (9.3), the following governing is obtained

$$\frac{\partial p}{\partial t}=\frac{k}{c\phi\mu}\left(\frac{\partial^2 p}{\partial r^2}+\frac{1}{r}\frac{\partial p}{\partial r}\right) \tag{9.4}$$

However, the equation assumes the square of differential pressure $\left(\frac{\partial p}{\partial r}\right)^2$ negligible.

Solution to Eq. (9.4) requires two boundary conditions and an initial condition. A realistic and useful situation is when (1) a single well centered in the reservoir with a wellbore radius r_i in a cylindrical reservoir of radius r_o as illustrated in Fig. 9.1, produces at a constant rate with a production velocity V_p, (2) no flow occurs across the outer boundary ($r = r_o$) and (3) prior to production, the reservoir remains at uniform pressure (p_{ini}).

9.3.1.1. Initial and boundary conditions

Using Darcy's law, the two boundary conditions and the initial condition can be mathematically translated as

$$\begin{cases} \dfrac{\partial p(r_i,t)}{\partial r} = \dfrac{\mu}{k} V_p \\ \dfrac{\partial p(r_o,t)}{\partial r} = 0 \\ p(r,0) = p_{ini} \end{cases} \tag{9.5}$$

Governing equation (9.4) and its solution conditions (9.5) are the working source in both analytical and numerical approaches, which are complementary to each other in the present work.

The diffusivity equation (Eq. 9.4) describes pressure (p) as a function of both space (r) and time (t). The fluid production process can be rationally divided into two periods: it begins with an unsteady-state when the velocity distribution in the reservoir progressively adjusts itself. Because the production rate at the inner boundary of the wellbore is constant, velocity in the reservoir tends to approach constant. Then a quasi-steady state follows when the velocity distribution in the reservoir is almost unchanged.

$$\frac{\partial v_{q-s}}{\partial t} = 0 \tag{9.6}$$

That is,

$$v_{q-s} = v(r) \tag{9.7}$$

The quasi-steady-state velocity v_{q-s} is only a function of r. According to Eq. (9.2), the quasi-steady-state pressure gradient $\frac{\partial p_{q-s}}{\partial r}$ is also only a function of r. During the quasi-steady-state, the governing equation (9.4) has the form

$$\frac{\partial p_{q-s}}{\partial t} = \frac{k}{c\phi\mu}\left(\frac{\partial^2 p_{q-s}}{\partial r^2} + \frac{1}{r}\frac{\partial p_{q-s}}{\partial r}\right) = \frac{k}{c\phi\mu}\left[\frac{\partial\left(\frac{\partial p_{q-s}}{\partial r}\right)}{\partial r} + \frac{1}{r}\frac{\partial p_{q-s}}{\partial r}\right] \tag{9.8}$$

Since the right hand side of Eq. (9.8), $\frac{\partial p_{q-s}}{\partial r}$ is only a function of r, the left hand side, $\frac{\partial p_{q-s}}{\partial t}$ must also be only a function of r

$$\frac{\partial p_{q-s}}{\partial t} = f(r) \tag{9.9}$$

$$p_{q-s}(r,t) = \int f(r)dt = f(r)t + p_1(r) \tag{9.10}$$

In which $f(r)$ and $p_1(r)$ are functions of r and need to be determined by solution conditions. Now, substituting Eq. (9.10) into Eq. (9.2), the following expression is obtained

$$v_{q-s} = -\frac{k}{\mu}\frac{\partial p_{q-s}}{\partial r} = -\frac{k}{\mu}\left[f'(r)t + p_1'(r)\right] \tag{9.11}$$

Substituting Eq. (9.11) into Eq. (9.6), it is obvious that

$$f'(r) = 0 \tag{9.12}$$

Therefore, $f(r)$ must be a constant, which is simply denoted by c_0. Then, Eq. (9.10) becomes

$$p_{q-s}(r,t) = c_0 t + p_1(r) \tag{9.13}$$

Substituting Eq. (9.13) into the governing equation (9.4)

$$\frac{d^2 p_1}{dr^2} + \frac{1}{r}\frac{dp_1}{dr} = \frac{c\phi\mu}{k}c_0 \tag{9.14}$$

Considering $\frac{dp_1}{dr}$ as the unknown, Eq. (9.14) is an ordinary first-order differential equation, and it is linear. The solution to this equation is

$$\frac{dp_1}{dr} = \frac{c\phi\mu}{2k}c_0 r + \frac{c_1}{r} \tag{9.15}$$

where, c_1 is another constant and need to be determined as c_0 is. Now, the two boundary conditions are applied for quasi-steady state when Eqs. (9.15) and (9.13) are incorporated into Eq. (9.5). It leads to the set of Eq. (9.16)

$$\begin{cases} \dfrac{c\phi\mu}{2k} c_0 r_i + \dfrac{c_1}{r_i} = \dfrac{\mu}{k} V_p \\ \dfrac{c\phi\mu}{2k} c_0 r_o + \dfrac{c_1}{r_o} = 0 \end{cases} \tag{9.16}$$

The solution to the algebra equation of set (9.16) is

$$\begin{cases} c_0 = \dfrac{2V_p}{c\phi} \dfrac{r_i}{\left(r_i^2 - r_o^2\right)} \\ c_1 = -\dfrac{\mu V_p}{k} \dfrac{r_i r_o^2}{\left(r_i^2 - r_o^2\right)} \end{cases} \tag{9.17}$$

Eq. (9.15) becomes

$$\frac{dp_1}{dr} = \frac{\mu}{k} V_p \frac{r_i}{\left(r_i^2 - r_o^2\right)} \left(r - \frac{r_o^2}{r} \right) \tag{9.18}$$

The partial derivative of Eq. (9.13) with respect to r and introducing Eq. (9.18) into it gives

$$\frac{\partial p_{q-s}}{\partial r} = \frac{\mu}{k} V_p \frac{r_i}{\left(r_i^2 - r_o^2\right)} \left(r - \frac{r_o^2}{r} \right) \tag{9.19}$$

By comparing the first parts of Eq. (9.11) and Eq. (9.19)

$$v_{q-s} = V_p \frac{r_i}{\left(r_i^2 - r_o^2\right)} \left(r - \frac{r_o^2}{r} \right) \tag{9.20}$$

By Eq. (9.18)

$$p_1 = \frac{\mu}{k} V_p \frac{r_i}{\left(r_i^2 - r_o^2\right)}\left(\frac{1}{2} r^2 - r_o^2 \ln(r)\right) + c_2 \tag{9.21}$$

where, the parameter c_2 can be determined from the initial unsteady state. Then, the final solution for the quasi-steady state is derived by substituting Eqs. (9.21) and (9.16) into Eq. (9.13)

$$p_{q-s}(r,t) = \frac{2V_p}{c\phi} \frac{r_i}{\left(r_i^2 - r_o^2\right)} t + \frac{\mu}{k} V_p \frac{r_i}{\left(r_i^2 - r_o^2\right)}\left(\frac{1}{2} r^2 - r_o^2 \ln(r)\right) + c_2 \tag{9.22}$$

From Eq. (9.22), it is evident that in the quasi-steady state, the pressure in the reservoir consists of two distinct parts. The first part is insensitive to the position in the reservoir and is a function of time only. A linear relationship exists between pressure and time with a negative proportionality of $\frac{2V_p}{c\phi} \frac{r_i}{\left(r_i^2 - r_o^2\right)}$. In other word, it signifies the declination of pressure in the reservoir with time at a constant rate. An observation to Eq. (9.2) also infers that this part has no effect on the velocity and does not contribute to production. Rather it is the second part of Eq. (9.22), which determines the velocity distribution of the whole reservoir and eventually the production. This part is only a function of the space (r) in the reservoir.

A practical practice in well study is to know the relationship between the pressure drop across the reservoir and the production rate. If the production velocity (V_p) in Eq. (9.22) is considered a variable, the pressure drop across the reservoir $[(\Delta p)_{q-s} = (p_o - p_i)_{q-s}]$ becomes a function of V_p

$$(\Delta p)_{q-s} = \frac{\mu}{k} \frac{r_i}{\left(r_i^2 - r_o^2\right)}\left[\frac{r_o^2 - r_i^2}{2} - r_o^2 \ln\left(\frac{r_o}{r_i}\right)\right] V_p \tag{9.23}$$

Eq. 23 reveals that the pressure drop across the reservoir is proportional to production velocity V_p and the proportionality is $\frac{\mu}{k}\frac{r_i}{\left(r_i^2-r_o^2\right)}\left[\frac{r_o^2-r_i^2}{2}-r_o^2\ln\left(\frac{r_o}{r_i}\right)\right]$. The proportionality does not depend on fluid compressibility, although oil production from a bounded reservoir relies on fluid compressibility.

9.3.2. Non-Darcy flow condition

The non-Darcy flow condition is presented by the Forchheimer equation as described by Eq. (9.24) in this paper

$$\frac{\partial p}{\partial r}=-\left(\frac{\mu}{k}v+\beta\rho|v|\right)v \tag{9.24}$$

where, β is the Forchheimer non-Darcy coefficient of the porous medium. In this paper, the flow is in the direction of the wellbore, which is negative with respect to the radial coordinate r. Therefore, Eq. (9.24) has the following form

$$\frac{\partial p}{\partial r}=-\left(\frac{\mu}{k}v-\beta\rho v^2\right) \tag{9.25}$$

An explicit solution of velocity v in Eq. (9.25) gives

$$v=\frac{\frac{\mu}{k}-\sqrt{\left(\frac{\mu}{k}\right)^2+4\beta\rho\frac{\partial p}{\partial r}}}{2\beta\rho} \tag{9.26}$$

Since the other solution, which is $v = \frac{\frac{\mu}{k} + \sqrt{\left(\frac{\mu}{k}\right)^2 + 4\beta\rho\frac{\partial p}{\partial r}}}{2\beta\rho}$ is always positive and contradicts the direction of flow towards the wellbore, is not considered the paper. Similar techniques such as use of chain rule, replacing ρ with p by means of Eq. (9.3), dropping the negligible pressure gradient squared $\left(\frac{\partial p}{\partial r}\right)^2$ etc. the governing equation for Forchheimer model is obtained

$$\frac{\partial p}{\partial t} = \frac{1}{c\phi\sqrt{\left(\frac{\mu}{k}\right)^2 + 4\beta\rho\frac{\partial p}{\partial r}}}\left(\frac{\partial^2 p}{\partial r^2} + \frac{1}{r}\frac{\partial p}{\partial r}\right) \tag{9.27}$$

9.3.2.1. Initial and boundary conditions

The initial condition and the two boundary conditions in non-Darcy condition have the following form

$$\begin{cases} \frac{\partial p(r_i,t)}{\partial r} = \frac{\mu}{k}V_p + \beta\rho V_p^{\,2} \\ \frac{\partial p(r_o,t)}{\partial r} = 0 \\ p(r,0) = p_{ini} \end{cases} \tag{9.28}$$

Equation (9.27) under the solution condition of Eq. (9.28) is a non-linear differential equation. Theoretically, the same approach of two-period theory developed for Darcy flow can be used for the solution of non-Darcy flow. Therefore, Eq. 14, in a non-Darcy condition takes the following form

$$\frac{d^2 p_1}{dr^2} + \frac{1}{r}\frac{dp_1}{dr} = c\phi\sqrt{\left(\frac{\mu}{k}\right)^2 + 4\beta\rho\frac{dp_1}{dr}}c_0 \tag{9.29}$$

Equation (9.29) is also an ordinary first-order differential equation similar to Eq. (9.14) where $\frac{dp_1}{dr}$ is the unknown. The non-linearity involved in the equation limits to perform the theoretical analysis through an analytical means, although, not impossible. Rather, a numerical solution, which is easy to perform, is implemented.

9.4. Numerical schemes

9.4.1. Barakat-Clark scheme

The Barakat-Clark scheme (Barakat and Clark, 1966) is an explicit-finite difference approximation. It has a simple form and it is unconditionally stable. Similar to fully implicit methods, there is no severe restriction on the time step size in this method. For the second-order space derivatives, it uses a partially implicit central difference, while for the time derivative the simple forward scheme is followed. In this scheme, a general one dimensional unsteady diffusion equation is considered

$$\frac{\partial p}{\partial t} = D\frac{\partial^2 p}{\partial r^2} \tag{9.30}$$

An ordinary explicit time forward and space central difference approximation for Eq. (9.30) is

$$\frac{p_i^{n+1} - p_i^n}{\Delta t} = D\frac{p_{i+1}^n - 2p_i^n + p_{i-1}^n}{(\Delta r)^2} \tag{9.31}$$

However, the ordinary scheme is is stable only under the condition $\frac{D\Delta t}{(\Delta r)^2} \leq \frac{1}{2}$ (Power, 1979), which is a severe restriction on time step. Barakat and Clark (1966) used a multilevel finite-difference representation of Eq. (9.30)

$$\frac{p_i^{n+1} - p_i^n}{\Delta t} = D\frac{p_{i+1}^n - p_i^n - p_i^{n+1} + p_{i-1}^{n+1}}{(\Delta r)^2} \tag{9.32}$$

or,

$$p_i^{n+1} = \frac{1-\lambda}{1+\lambda} p_i^n + \frac{\lambda}{1+\lambda} p_{i-1}^n + \frac{\lambda}{1+\lambda} p_{i+1}^n \tag{9.33}$$

In which λ is $\frac{D\Delta t}{(\Delta r)^2}$. Equation (9.32) is proven unconditionally stable, which is an important feature in the implicit scheme. In addition, the scheme gives the ease of explicit scheme in time.

9.4.2. Bokahri-Islam scheme

Bokahri and Islam (2005) applied the extended Barakat-Clark scheme into a convective-dispersion equation

$$\frac{\partial p}{\partial t} = D\frac{\partial^2 p}{\partial r^2} + U\frac{\partial p}{\partial r} \tag{9.34}$$

They used similar technique as Barakat and Clark (1966) did for both first-order and second order space derivatives. However, instead of using the forward time difference (FTD) term, they proposed the central time difference (CTD) term

$$\frac{p_i^{n+1}-p_i^{n-1}}{2\Delta t}=D\frac{p_{i+1}^n-p_i^n-p_i^{n+1}+p_{i-1}^{n+1}}{(\Delta r)^2}+U\frac{p_{i+1}^n-p_{i-1}^n}{2\Delta r} \tag{9.35}$$

The utilization of the central difference scheme is reported to improve the accuracy in time in the order of Δt^4. The numerical algorithm of the paper, however, uses the simple time forward scheme.

9.4.3. Applied numerical scheme

To have the benefit of small grid size, a numerical scheme that utilizes the upwind technique in the first-order space derivative, is employed. The accuracy of the upwind technique ensures that $\begin{cases} U\dfrac{p_{i+1}^n-p_i^n}{\Delta r} & if \quad U\geq 0 \\ U\dfrac{p_i^n-p_{i-1}^n}{\Delta r} & if \quad U<0 \end{cases}$ is higher than the central difference scheme $\dfrac{p_{i+1}^n-p_{i-1}^n}{2\Delta r}$.

Overall, the convection-diffusion equation based on the proposed scheme becomes

$$\frac{p1_i^{n+1}-p1_i^n}{\Delta t}=D\frac{p1_{i+1}^n-p1_i^n-p1_i^{n+1}+p1_{i-1}^{n+1}}{(\Delta r)^2}+\begin{cases} U\dfrac{p1_{i+1}^n-p1_i^n}{\Delta r} & if \quad U\geq 0 \\ U\dfrac{p1_i^n-p1_{i-1}^n}{\Delta r} & if \quad U<0 \end{cases}$$

$$\frac{p2_i^{n+1}-p2_i^n}{\Delta t}=D\frac{p2_{i+1}^{n+1}-p2_i^{n+1}-p2_i^n+p2_{i-1}^n}{(\Delta r)^2}+\begin{cases} U\dfrac{p2_{i+1}^n-p2_i^n}{\Delta r} & if \quad U\geq 0 \\ U\dfrac{p2_i^n-p2_{i-1}^n}{\Delta r} & if \quad U<0 \end{cases} \tag{9.36}$$

The scheme also gives the same level of advantage in time step as obtained in the explicit method. The stable condition (Courant et al., 1952) is controlled by the convection term

$$\left|\frac{U\Delta t}{\Delta r}\right| \leq 1 \tag{9.37}$$

The stable condition is much less severe than that by the diffusion term as in the case of Eq. (9.31).

9.5. Results and validation of numerical scheme

9.5.1. Darcy flow condition

The proposed numerical scheme is used to solve the governing equation (9.4) based on its solution conditions as specified in the set of Eq. (9.5). The parameters in Eq. (9.36) are $D = \frac{k}{c\phi\mu}$ and $U = \frac{k}{c\phi\mu r}$. Other parameters used in this work are ρ = 1000 m^3/s; $\mu = 10^{-3}$ $\frac{kg}{ms}$; r_i = 1 m; r_o = 10 m; $c = 10^{-5}$ $\frac{m^2}{N}$; $k = 10^{-9}$ m^2; ϕ = 0.1. The initial pressure is chosen as the reference pressure (p_{ini} = 0) and is followed throughout the paper. The space increment is maintained uniform, which is $\Delta r = \frac{r_o - r_i}{100}$.

Results are based on the scheme followed in this paper as well as the Bokahri-Islam (2005) scheme and they are compared with the exact solutions. It is to be noted that because the flow is in the direction toward the wellbore, the velocity v is always negative with respect to r. The velocity curves are plotted for u = -v. For the case study, the production velocity is assumed to be $\left(\frac{\mu}{k}V_p\right) = 1$ N/m^3.

Figure 9.2 shows the pressure profile at the wellbore. In the early stage of production, the wellbore pressure decreases. This unsteady state is marked by the change in slope in the figure. As time passes, the quasi-steady state is reached and the slope becomes a constant. The applied numerical scheme calculates the rate, $\left|\frac{\partial p_{q-s}}{\partial t}\right|$ to be $0.021\frac{V_p}{c\phi}$, which is very close to the theoretical prediction, $\frac{2}{99}\frac{V_p}{c\phi}$, as determined by Eq. (9.22). The figure also shows the results using the Bokhari-Islam (2005) scheme and Matthews and Russell (1967) approach. The presented scheme gives very close results as obtained using the Bokahri-Islam (2005) scheme and both are very close to exact solution.

The differential pressure between the outer boundary and the inner boundary of the reservoir is plotted against time in Figure 9.3. Based on numerical analysis, the time free, quasi-steady pressure difference is found to be 1.86 N/m^2. The exact solution, which uses Eq. (9.23), finds the value 1.83 N/m^2. A small difference of only 2% illustrates a very good agreement between the numerical and analytical results. The steepness in slope can be explained by the immediate pressure loss the wellbore experiences in the early stages of production. In response to pressure drop at the wellbore, the reservoir including its outer boundary start readjusting until the quasi-steady state is reached. Thereafter the differential pressure becomes insensitive to time as suggested by Eq. (9.22). The presented scheme once again finds very close approximation to the Bokahri-Islam (2005) scheme as well as to the exact solution, which involved only an error of 3% in time free, quasi-steady state differential pressure estimation.

Figure 9.4 illustrates the velocity distribution in the reservoir during quasi-steady state where, $\nu = \frac{\mu}{\rho}$. It shows that the reservoir experiences a maximum velocity, which is also the production velocity (V_p) at the wellbore and a minimum velocity of zero at the outer boundary because of the boundary conditions as specified in Eq. (9.5). An increasing

trend in velocity is noticeable starting from the outer boundary to the wellbore. It is because a smaller volume of the drainage area has to contribute to the same level of production any larger area does and unless the fluid of a closer block to the wellbore gains velocity, the constant production will cease. In addition, the property of slight compressibility of the fluid adds more volume to the flowing body closer to wellbore, which later gains velocity. The graph also shows that the presented model gives almost identical results to the Bokahri-Islam (2005) model and an excellent agreement between the numerical model and analytical solution of Eq. (9.20) is observed. It can be added that the curve does not follow a pure hyperbolic pattern rather follows a function of $\left(r-\frac{r_o^2}{r}\right)$ as indicated by the exact solution of Eq. (9.20). The solution for an incompressible fluid follows the hyperbola function $(\frac{1}{r})$.

The relationship between pressure drop and production rate is also of practical interest, which is shown in Fig. 9.5. By giving a series of different values for production velocity (V_p) in the simulation, the objective is achieved. It is confirmed during simulation that the flow process reaches the quasi-steady state. As pointed out in Eq. (9.23), this relationship gives a straight line with a theoretical proportionality of $\left(\frac{100}{99}\ln 10-\frac{1}{2}\right)\frac{\mu}{k}$. The numerical proportionality using the presented scheme and the Bokahri-Islam scheme (2005) is found to be $1.86\frac{\mu}{k}$ with a 2% deviation from the exact solution and $1.89\frac{\mu}{k}$ with a 3% deviation from the same respectively.

In addition, the numerical model is extended to obtain pressure and velocity details of the through Figs. 9.6-9.10. Figure 9.6 shows pressure profile at different locations in the reservoir. The fact that the curves are parallel to each other following the unsteady state demonstrates that the pressure is decreasing at the same rate during this phase of production. Similar discussion is reported above about Fig. 9.2. It might be reiterated

that at the initial period, the reservoir experiences the adjustment in pressure from the wellbore, which gradually progresses towards the outer boundary.

Figure 9.7 is an alternate presentation of pressure distribution of Fig. 9.6. Initially, pressure near the wellbore decreases very sharply, while pressure close to the outer boundary decreases in a much slower manner. As time approaches to the quasi-steady state, the decrease in pressure becomes uniform in the entire reservoir.

Figure 9.8 is an excellent way to understand the phenomenon of pressure adjustment from the unsteady state to the quasi-steady state. At an early stage, the differential pressure, $(p\text{-}p_i)$ only increases near the wellbore, while the area far from the wellbore experiences zero pressure gradient. Such phenomenon can also be related to zero velocity in Eq. (9.2), when the corresponding velocity line falls on the abscissa of Fig. 9.9. The horizontal segment in each line in Fig. 9.8 indicates the no-velocity area. It indicates that the area close to the wellbore is only affected in the early stage of production. As time increases, the point of inception of each horizontal line moves further away from the wellbore, an indication that larger area is affected and contributing in production. Finally, the horizontal line vanishes at the outer boundary ($r = r_o$) when each point of the entire reservoir experiences velocity vector. The same phenomenon is observed in Fig. 9.9 as no portion of the line falls on the r-axis any more except at the end point.

The velocity profile undergoes similar experience as evident in Figs. 9.9 and 9.10. Fluid flow starts from the vicinity of the wellbore where the magnitude of velocity follows the boundary condition. At the same time, the velocity far away the wellbore is zero as demonstrated firstly, by the curve aligned to the horizontal axis of Fig. 9.9 and secondly, by the velocity vector of Fig. 9.10 (a). The adjustment in velocity occurs with time between 0 and 100 seconds (Fig. 9.9). Fig. 9.10 (b) shows the growth in area of the velocity vector towards the outer boundary. In Fig. 9.10 (c), the velocity vector fills all

over the flow domain after 100 seconds or in other word, the profile is completely adjusted. The topmost curves of Fig. 9.8 and Fig. 9.9 also represent similar situation.

9.5.2. Non-Darcy flow condition

Equation 27 under its solution conditions of Eq. (9.28) is solved by the numerical scheme of Eq. (9.36). The parameters in Eq. (9.36) are $D = \dfrac{1}{c\phi\sqrt{\left(\dfrac{\mu}{k}\right)^2 + 4\beta\rho\dfrac{\partial p}{\partial r}}}$ and $U = \dfrac{1}{c\phi r\sqrt{\left(\dfrac{\mu}{k}\right)^2 + 4\beta\rho\dfrac{\partial p}{\partial r}}}$. The grid-size and all of the parameters are assumed to have same values as used in the Darcy model except the non-Darcy coefficient (β) term, which exists in the Forchheimer model. A value of $\beta = 10^7 \dfrac{1}{m}$ is arbitrarily assigned in the model.

The numerical results of the non-Darcy results are shown in Figs. 9.11, 9.12, and 9.13. Figure 9.11 shows that the Forchheimer result takes the shape of a concave curve in contrast to the shape of a straight line as predicted by Darcy's model. The pressure by the Forchheimer model is almost the same as that by the Darcy model when production velocity V_p is low. However, it is much higher than the Darcy result when V_p increases. It is because the porous medium results in substantial hindrance on the fast moving fluid body due to its inertia for which the non-Darcy coefficient is used. Consequently, a much higher pressure is required to force the fluid to flow through the medium than that without the additional blockage in a Darcy flow.

Figures 9.12 and 9.13 illustrate the velocity field by two different models during the quasi-steady state. The pseudo-steady velocity profiles suggest that the non-Darcy (Forchheimer) velocity is higher than that predicted by Darcy for the entire reservoir. It

also shows that the points near the wellbore have higher velocity vector than the points far away from the wellbore in both models. Since velocity is high near the wellbore, the non-Darcy contribution becomes higher because of the velocity square term (v^2) in the second term of Forchheimer's equation. Interestingly, the deviation in velocity in both models ceases at the wellbore and at the outer boundary because of the boundary conditions. Perhaps the boundary conditions has significant influence on non-Darcy coefficient (β), adding more hindrance to the movement of the fluid body through the medium. An alternate way to address the issue is the velocity vector has variable power, which is assumed constant in this study. Literature suggest that the power can be in between 1.6 and 1.8 (Li and Engler, 2002) which is also in consistent with Forchheimer's (Forchheimer, 1930) later work. Although, it is to be remembered that Li and Engler (2002) dealt a different issue, a problem of wafer-non-Darcy flow. Bear (1972) proposed the power to be in between 1.6 and 2. A pictorial presentation of the velocity vector in Fig. 9.12 is given in Fig. 9.13. Figures 9.13 (a) and 9.13 (b) show the full reservoir while the inner dark dotted circles of Figs. 9.13 (a) and 9.13 (b) are magnified to Figs. 9.13 (c) and 9.13 (d) respectively. A scale of 1 mm/sec is used to describe the magnitude of the velocity vector in the four figures. A comparison between 9.13 (a) and 9.13 (b) or 9.13 (c) and 9.13 (d) clearly reinstates the same fact that the velocity by the Forchheimer model is higher than that by the Darcy model and the vector is high in magnitude in both models near the wellbore.

9.6. Conclusions

The use of upwind technique instead of central difference approximation in the convective term of the convection-diffusion equation and the choice of time forward scheme provided competitive results in compare to the results using recently published advanced scheme. The differences in results were not significant. For Darcy flow, the theoretical quasi-steady pressure difference is found to be within 2% of the numerical prediction. The theoretical and numerical quasi-steady state velocities along reservoir

radius also match excellent. Due to its excellent accuracy, the presented scheme is also used in solving non-Darcy flow equations. It becomes particularly important when an analytical solution of the non-linear Forchheimer model is not available or is too cumbersome to obtain. The numerical model also shows with increasing velocity, the quasi-steady state pressure drop becomes appreciably higher than that predicted by Darcy model and the linear relationship between the quasi-steady state pressure drop and production velocity ceases. Furthermore, the quasi-steady state velocity predicted by Forchheimer model is found to be higher than that predicted by Darcy model. There is also an indication that a critical distance from the well may exist at which the difference between the Darcy and Forchheimer quasi-steady state velocity is most significant.

9.7. Nomenclature

c	compressibility
c_1, c_2, c_3	constants
D	diffusivity
i	space position index
k	permeability
n	time level index
p	pressure
p_i	pressure at the inner boundary
p_{ini}	initial pressure
p_o	pressure at the outer boundary
q-s	quasi-steady-state
r	radial coordinate
r_i	inner radius of the wellbore
r_o	outer radius of the wellbore
t	calculation time
u	velocity = $-v$

U	negative convection velocity
v	velocity
V_p	production velocity
β	Forchheimer non-Darcy coefficient
ϕ	porosity
Δr	space increment
Δt	time increment
ν	fluid kinematics viscosity
μ	viscosity
ρ	density

9.8. References

Aboudheir, A., Kocabas, I. and Islam, M. R., (1999) Improvement of numerical methods in petroleum engineering problems, Proc. of the IASTED International Conference, Applied Modeling and Simulation, Cairns, Australia, September 1-3

Adler, P. M., (1992) Porous media: geometry and transport, Butterworth-Heinemann, Stoneham, MA, USA

Ali, M. A. and Islam, M. R., (1998) The effect of asphaltene precipitation on carbonate-rock permeability: an experimental and numerical approach, SPE Production and Facilities. SPE 50963, vol. 13, no. 3, pp. 178-183

Andrade, J. S., Jr., Costa, U. M. S., Almeida, M. P., Makse, H. A. and Stanley, H. E., (1999) Inertial effects on fluid flow through disordered porous media, Physical Review Letters, vol. 82, no. 26, pp. 5249-5252

Barakat, H. Z. and Clark, J. A., (1966) On the solution of the diffusion equations by numerical methods, Transactions ASME, Journal of Heat Transfer, vol. 88, pp. 421-427

Basu, A., Mustafiz, S., Bjorndalen, N., Rahaman, S. and Islam, M. R., (2006) A comprehensive approach for modeling sorption of lead and cobalt ions through fish-scales as an adsorbent, Chemical Engineering Communications, vol. 193, pp. 580-605

Bear, J., (1972) Dynamics of Fluids in Porous Media. Dover, New York: American Elsevier

Belhaj, H. A., Agha, K. R, Butt, S. D. and Islam, M. R., (2003a) Simulation of non-Darcy flow in porous media including viscous, inertial and frictional effects, SPE 84879, Proc. 2003 SPE International Improved Oil Recovery Conference, Asia Pacific, Kuala Lumpur, Malaysia, October 20-21

Belhaj, H. A., Agha, K. R, Nouri, A. M., Butt, S. D. and Islam, M. R., (2003b) Numerical and experimental modeling of non-Darcy flow in porous media, SPE 81037, Proc. SPE Latin American and Caribbean Petroleum Engineering Conference, Port-of-Spain, Trinidad, West Indies, April 27-30

Belhaj, H. A., Agha, K. R, Butt, S. D. and Islam, M. R., (2003c) A comprehensive numerical simulation model for non-Darcy flow including viscous, inertial and convective contributions, SPE 85678, Proc. 27th Annual SPE International Technical Conference and Exhibition, Abuja, Nigeria, August 4-6

Bjorndalen, N., Mustafiz, S. and Islam, M. R., (2005) The effect of irradiation on immiscible fluids for increased oil production with horizontal wells, ASME International Mechanical Engineering Conference and Exposition, Orlando, Florida, USA, Nov. 6-11

Bjorndalen, N., Mustafiz, S. and Islam, M. R., (2003) Numerical modeling of petroleum fluids under microwave irradiation for improved horizontal well performance, International Communications in Heat and Mass Transfer, vol. 30, no. 6, pp. 765-774

Bjorndalen, N., (2002) Irradiation techniques for improved performance of horizontal wells, MASc Thesis, Dalhousie University, Halifax, Canada

Bokhari, K. and Islam, M.R., (2005) Improvement in the time accuracy of numerical methods in petroleum engineering problems – A new combination, Energy Sources, vol. 27, no. 1-2, 45-60

Bokhari, K., Mustafiz, S. and Islam, M. R., (2006) Numerical modeling of viscous fingering under combined effects of thermal, solutal and mixed convection in liquid-liquid miscible displacements, Journal of Petroleum Science and Technology, accepted for publication, May

Cheema, T. J. and Islam, M. R., (1995) A new modeling approach for predicting flow in fractured formations, In: El-Kady (Editor), Groundwater Models for Resources Analysis and Management, Lewis Publishers, Boca Raton, FL, pp. 327-338

Choi, I., Cheema, T. and Islam, M. R., (1997) A new dual-porosity/dual permeability model with non-Darcian flow through fractures, Journal of Petroleum Science and Engineering, vol. 17, pp. 331-344

Courant, R., Isaacson, E. and Rees, M., (1952) On the solution of nonlinear hyperbolic differential equations by finite differences, Communications on Pure and Applied Mathematics, vol. 5, pp. 243-249

Darcy, H. P. G., (1856) Les Fontaines Publiques de villle de la Dijon Dalmont, Exposition et Application des Pricipes a Suivre et des Furmules a Emplyer dans les Questions de Distribution d'Eau., Victor Dalmont, Paris

Dullien, F. A. L., (1992) Porous Media: Fluid transport and pore structure, 2nd edition, Academic Press, San Diego, USA

Lee, J., (2002) Well Testing, SPE textbook series, vol. 1, SPE, Richardson, TX

Li, D. and Engler, T. W., (2002) Modeling and simulation of non-Darcy flow in porous media, SPE 75216, SPE/DOE Improved Oil Recovery Symposium, Tulsa, OK, April 13-17

Matthews, C. S. and Russell, D. G., (1967) Pressure buildup and flow tests in wells, Monograph Series: SPE, Dallas, USA

Mustafiz, S., (2002) A novel method for heavy metal removal from aqueous streams, MASc Thesis, Dalhousie University, Canada

Powers, D. L., (1979) Boundary value problems, 2nd edition, Academic Press, New York

Rahman, M. A., Mustafiz, S., Biazar, J., Koksal, M. and Islam, M. R., (in press) Investigation of a novel perforation technique in petroleum wells - perforation by drilling, Journal of the Franklin Institute

Rahman, H., Wasiuddin, N. M., Islam, M. R., (2003) Experimental and numerical modeling studies of arsenic removal with wood ash from aqueous streams, The Canadian Journal of Chemical Engineering, vol. 82, no. 5, pp. 968-977

Sahimi, M., (1994) Applications of percolation theory, Taylor &Francis, London, UK

Sahimi, M., (1995) Flow and transport in porous media and fractured rock, VCH, Weinheim, Germany

Ucan, S. and Civan, F., (1996) Simultaneous estimation of relative permeability and capillary pressure for non-Darcy flow-steady state, SPE 35271, Mid-Continent Gas Symposium, Amarillo, TX, April 26-30

Van Everdingen, A. F. and Hurst, W., (1949) The application of the Laplace transformation to flow problems in reservoirs, Transactions AIME, vol. 186, pp. 305-324

9.9. Appendices

9.9.1. Appendix A: Figures

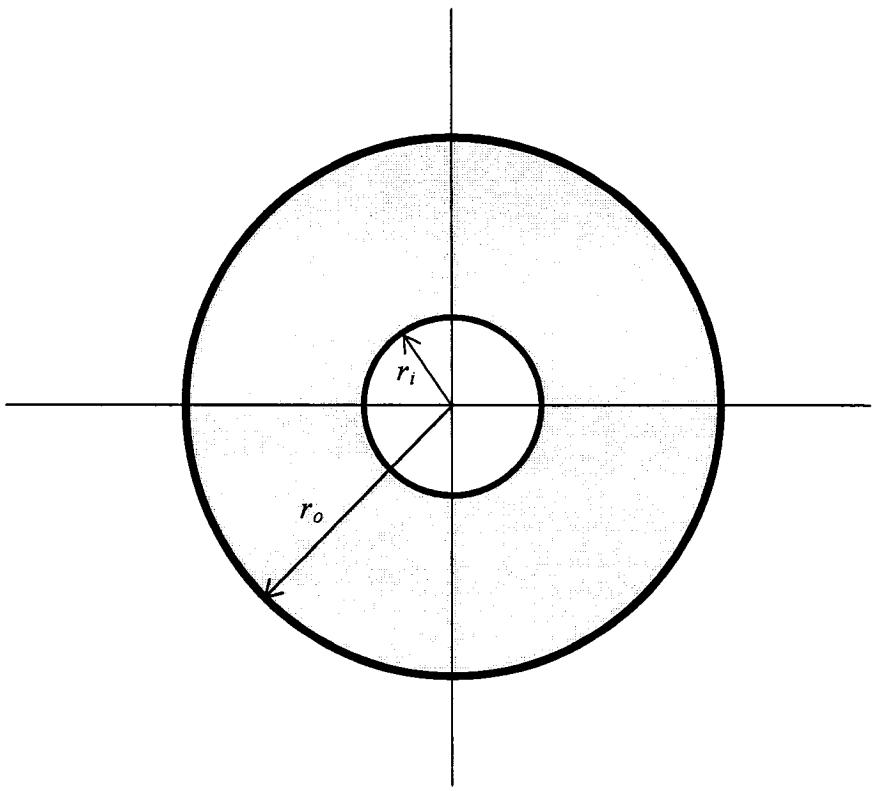

Figure 9.1. Illustration of the wellbore

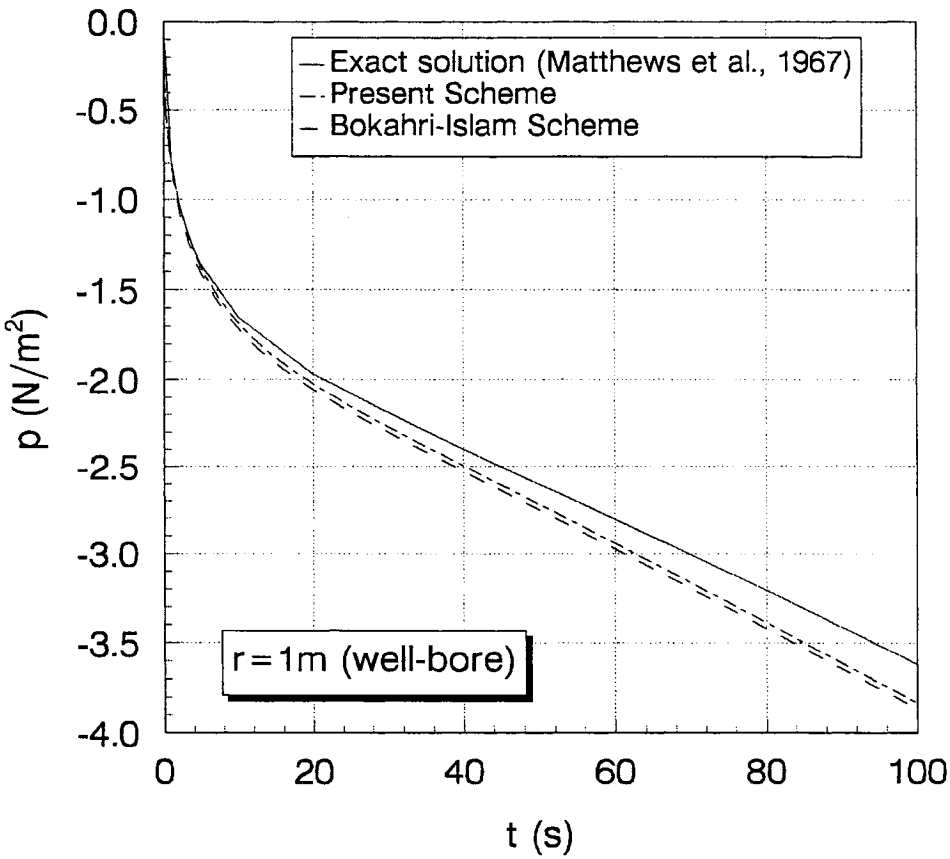

Figure 9.2. Pressure development at the wellbore

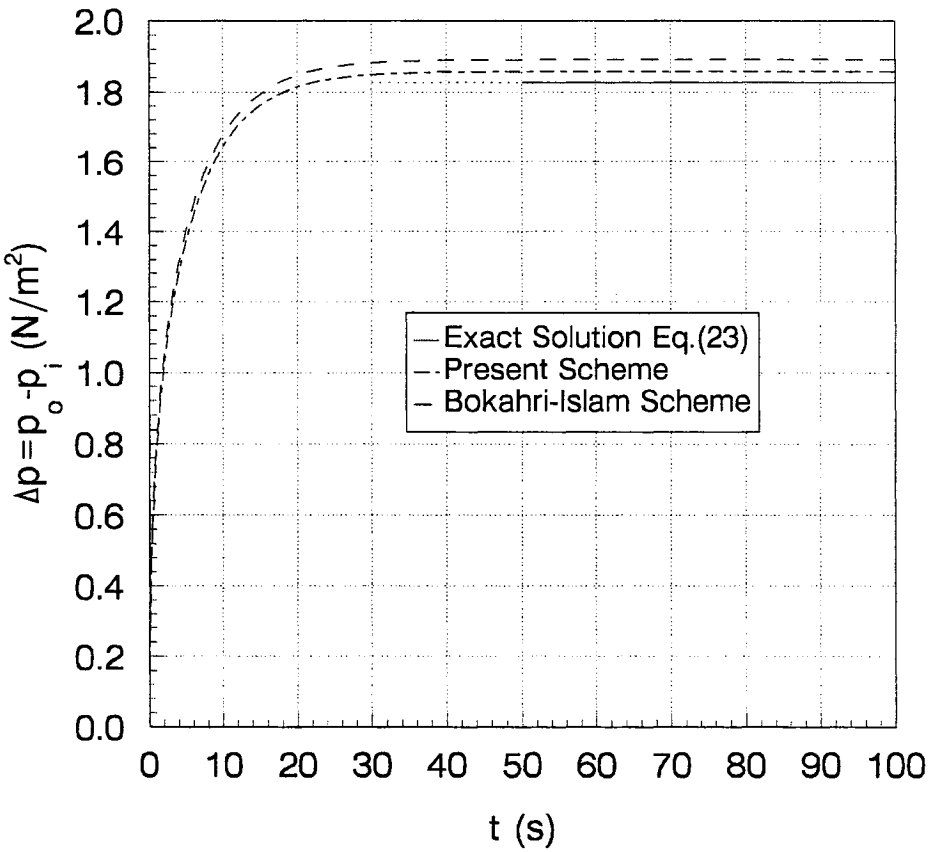

Figure 9.3. Pressure drop across the reservoir

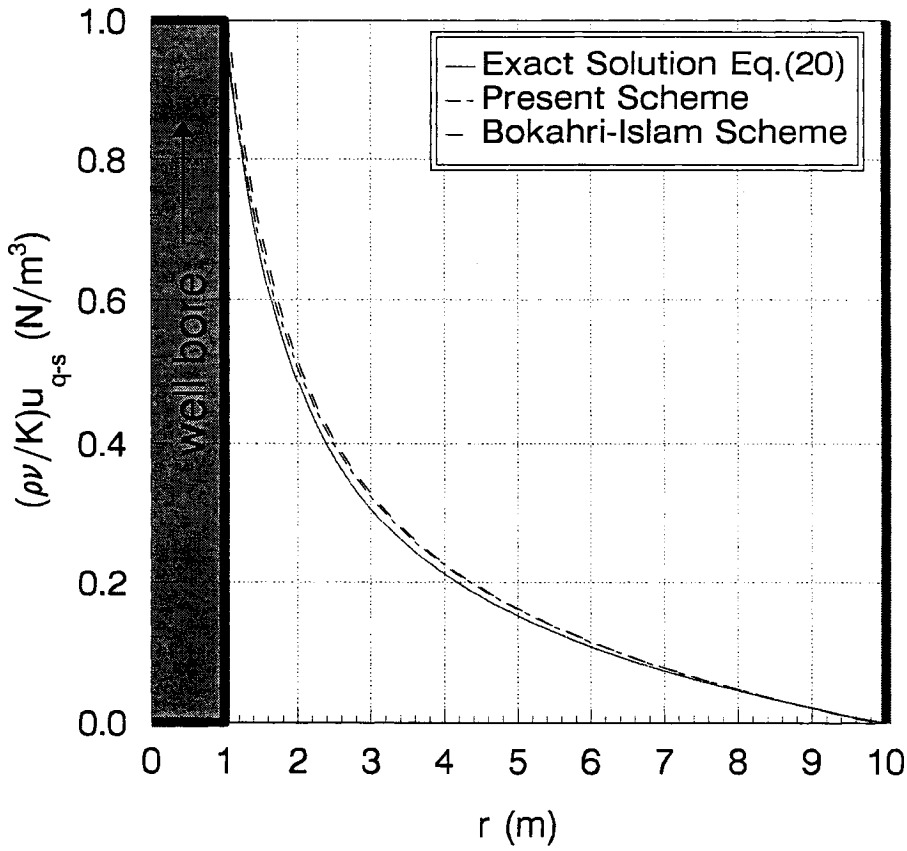

Figure 9.4. Quasi-steady-state velocity distribution across the reservoir

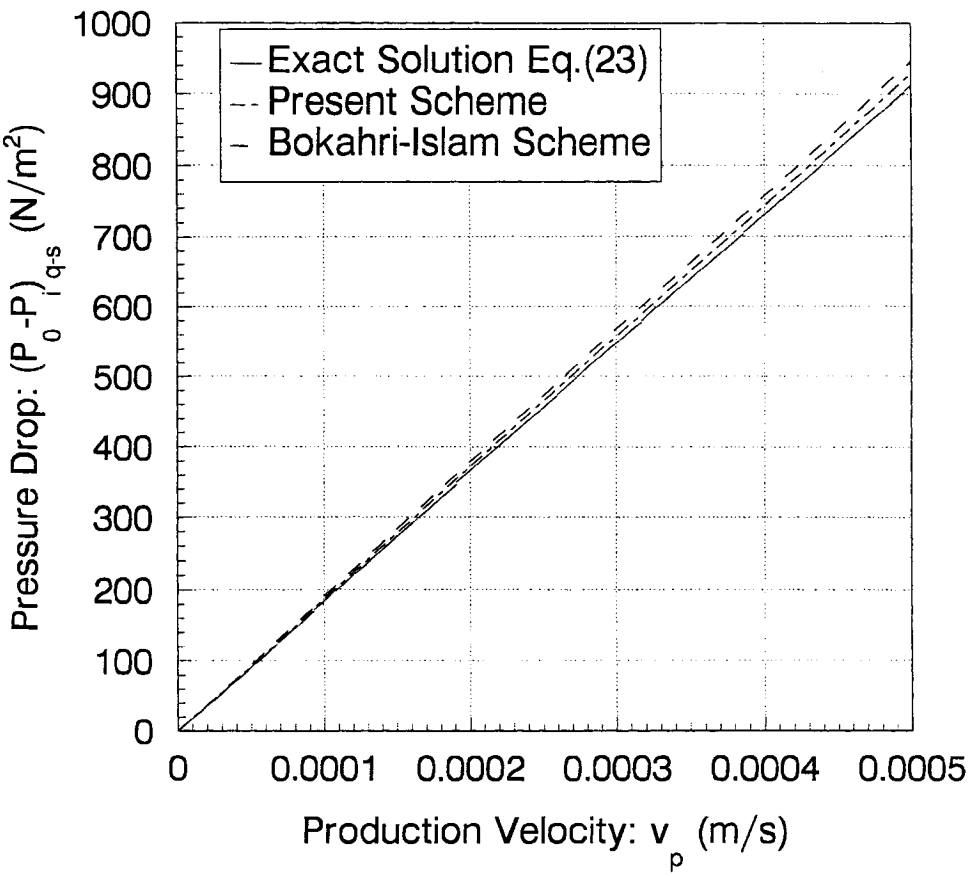

Figure 9.5. Pressure-drop versus production velocity

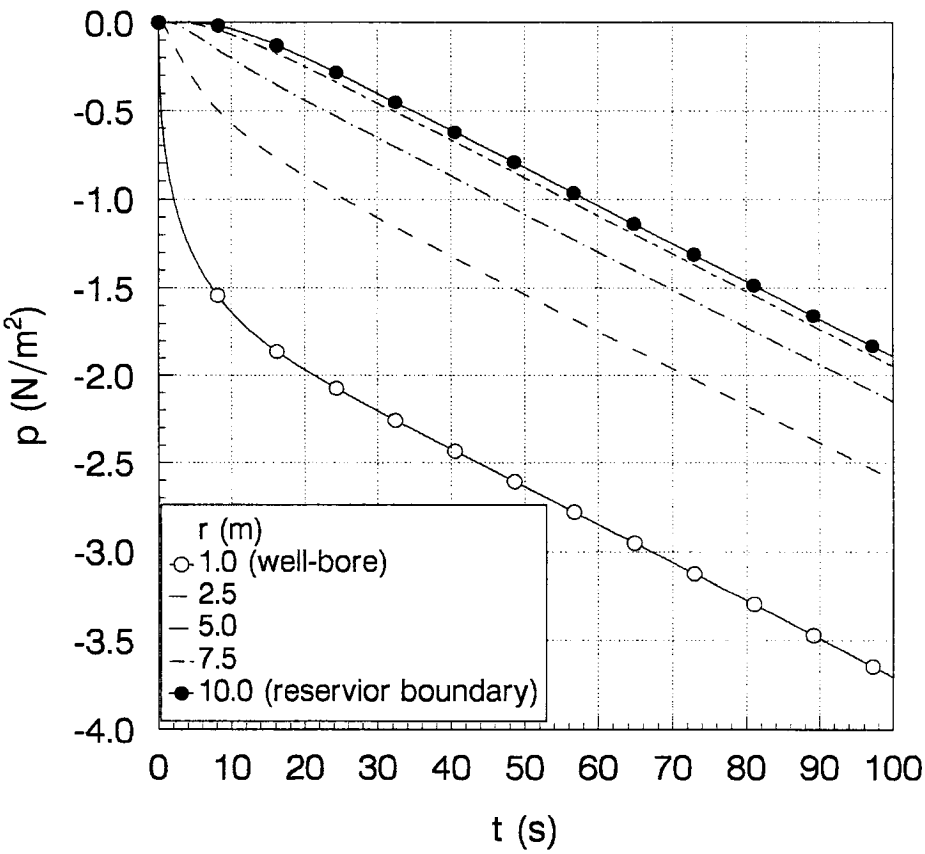

Figure 9.6. Transient pressure profile in the reservoir

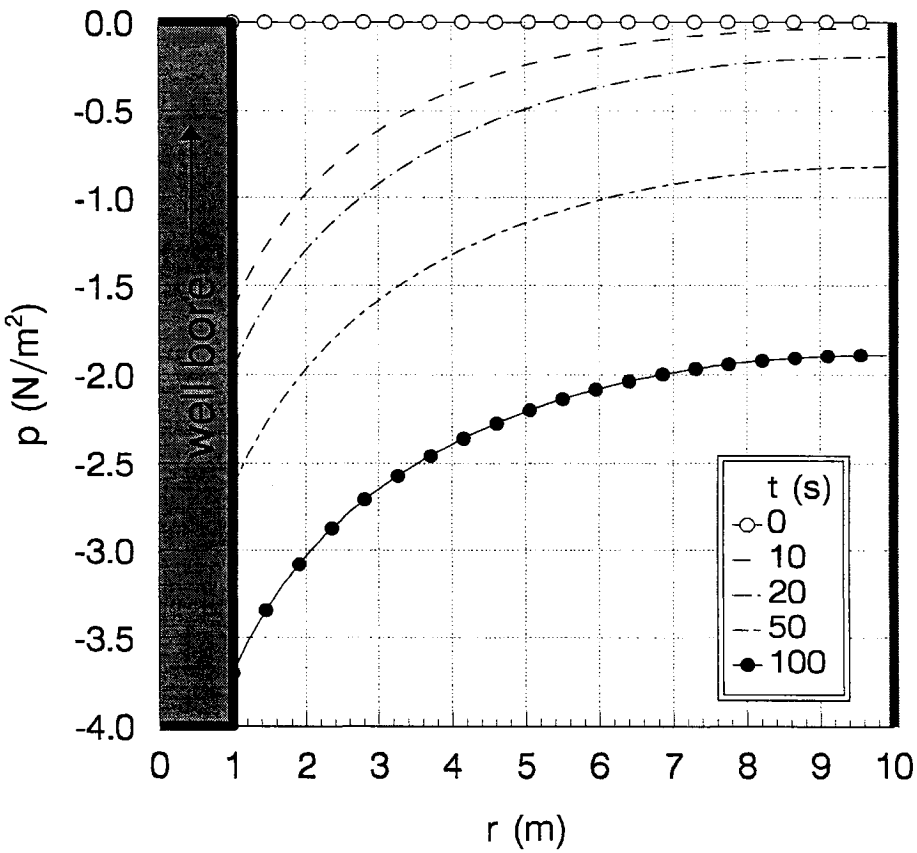

Figure 9.7. Pressure profile along (*r*-direction) the reservoir

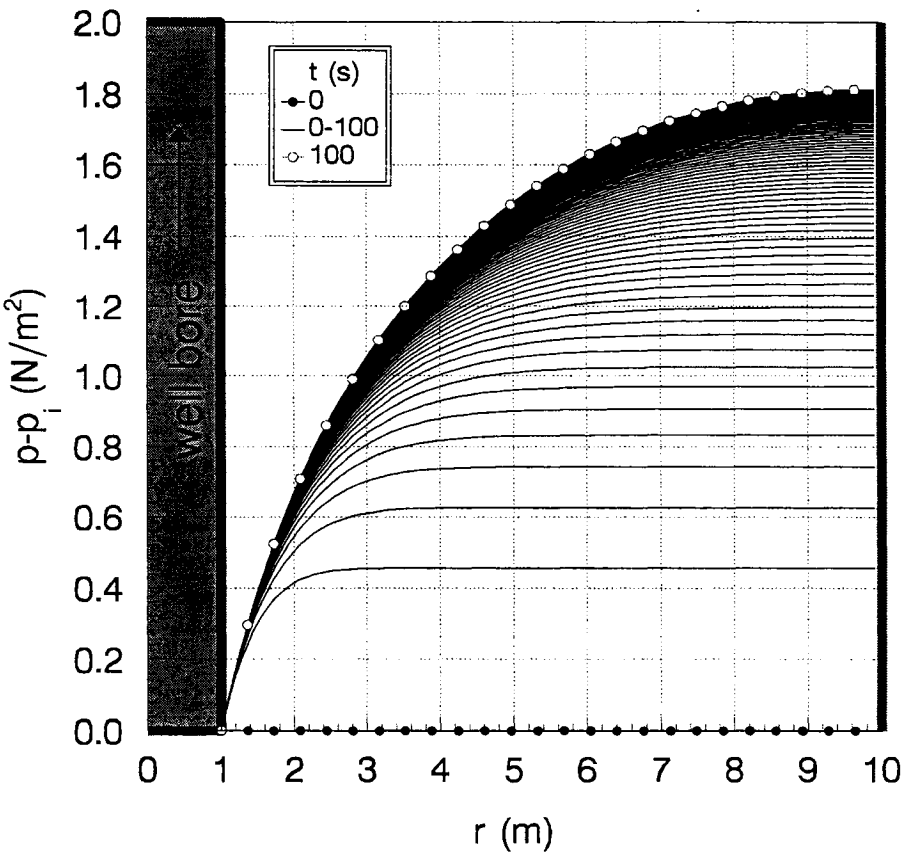

Figure 9.8. Pressure drop along (r-direction) the reservoir

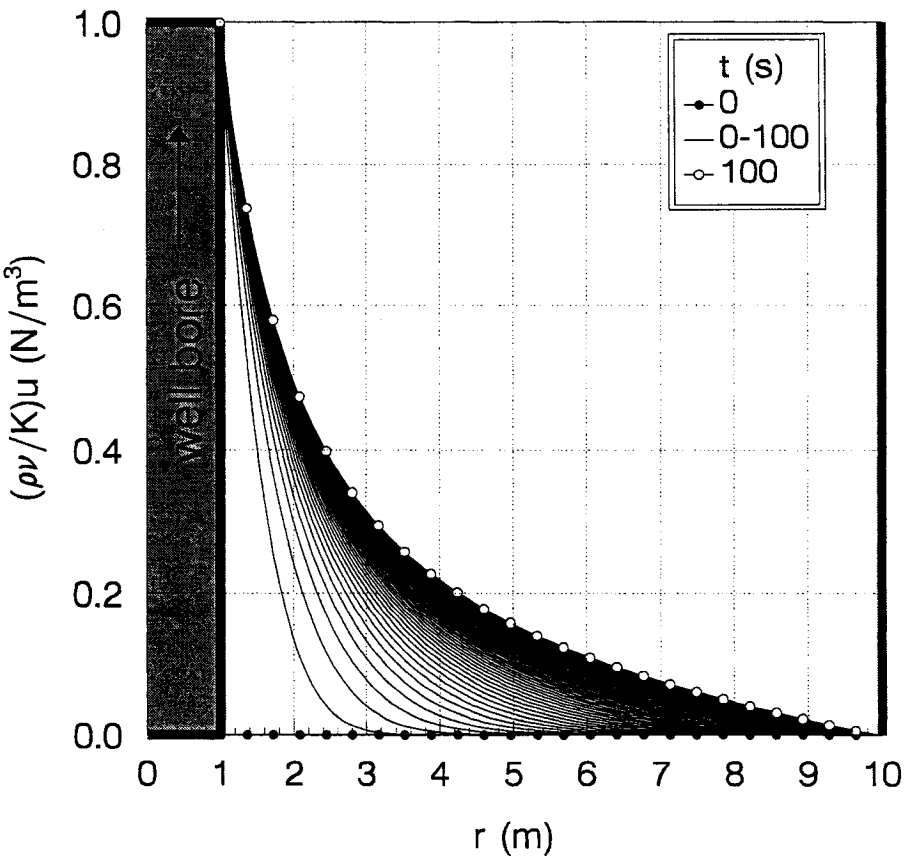

Figure 9.9. Development of velocity-distribution in the reservoir

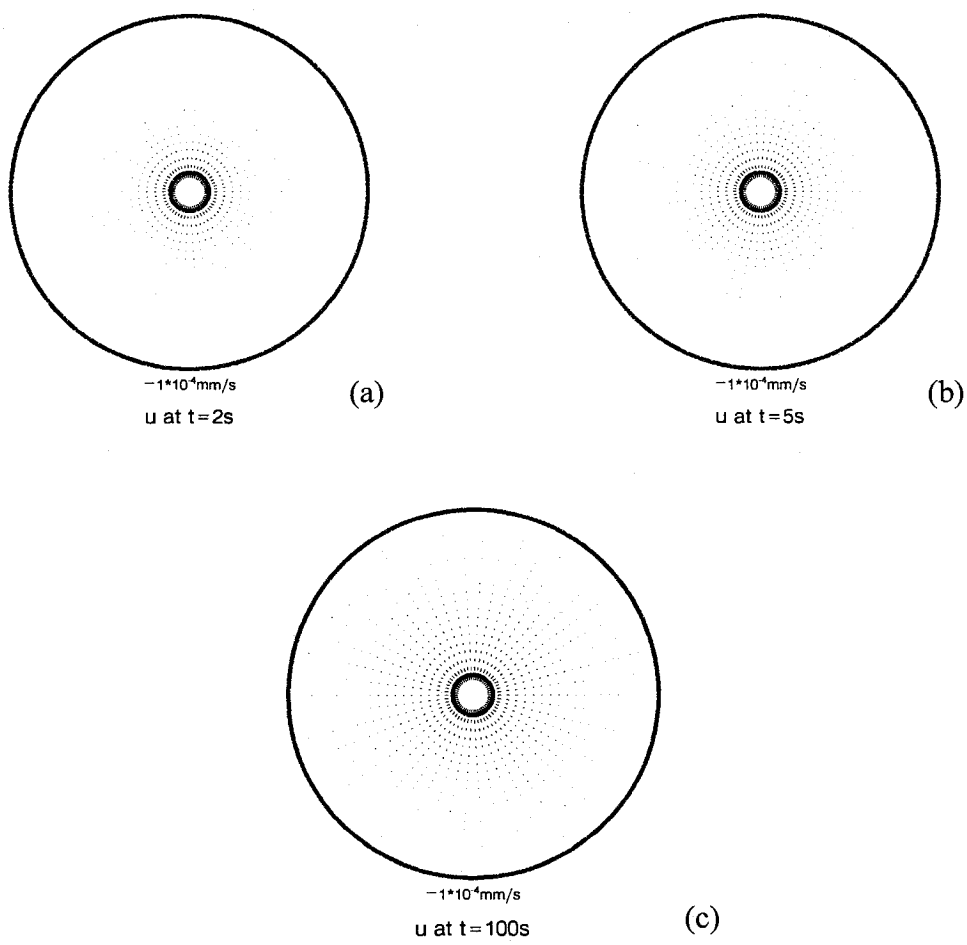

Figure 9.10. Development of velocity vector field in the reservoir

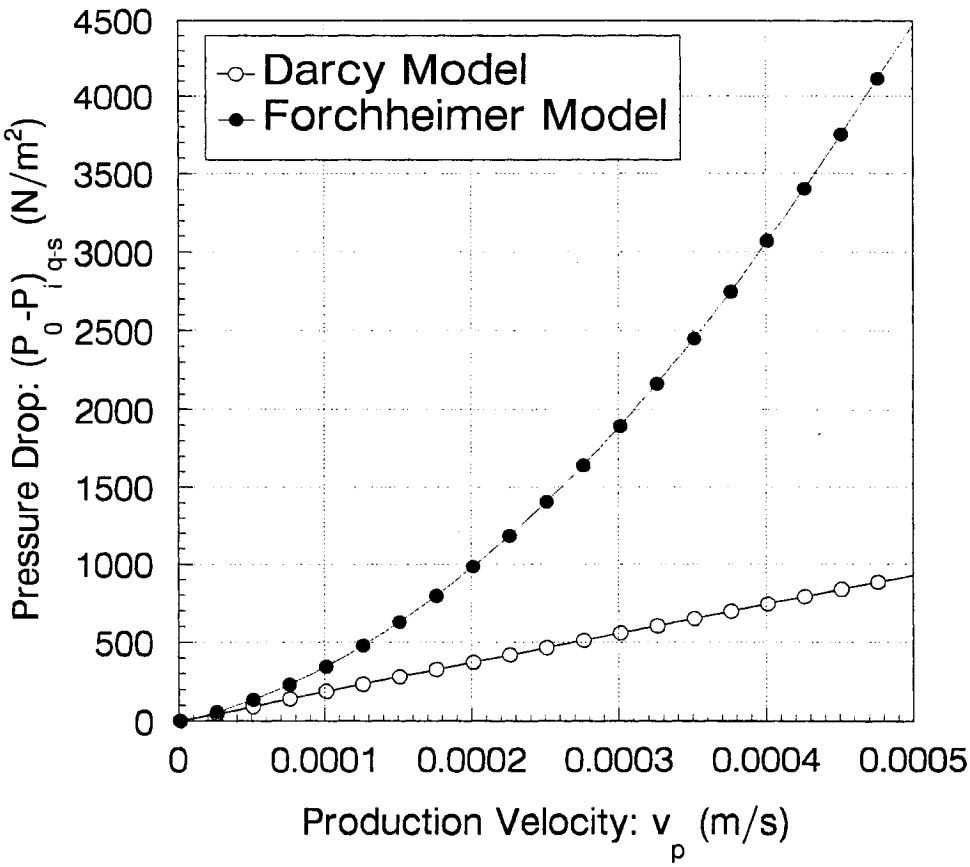

Figure 9.11. Pressure-drop versus production velocity by two models

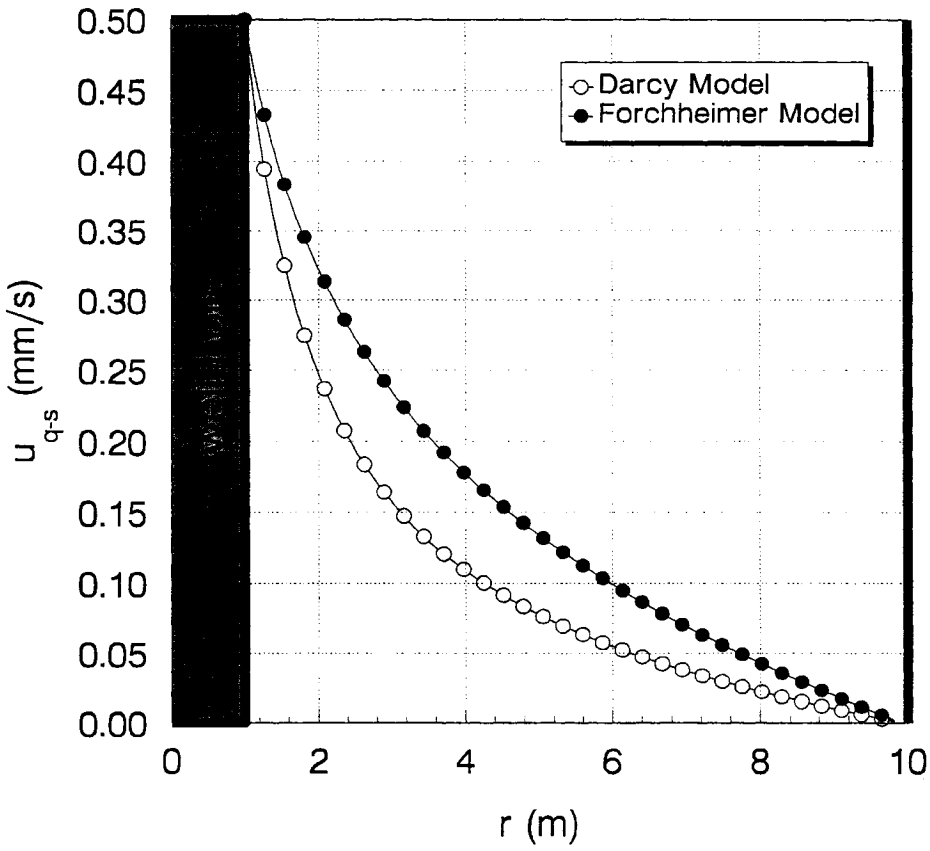

Figure 9.12. Quasi-steady-state velocity distribution in the reservoir by two models

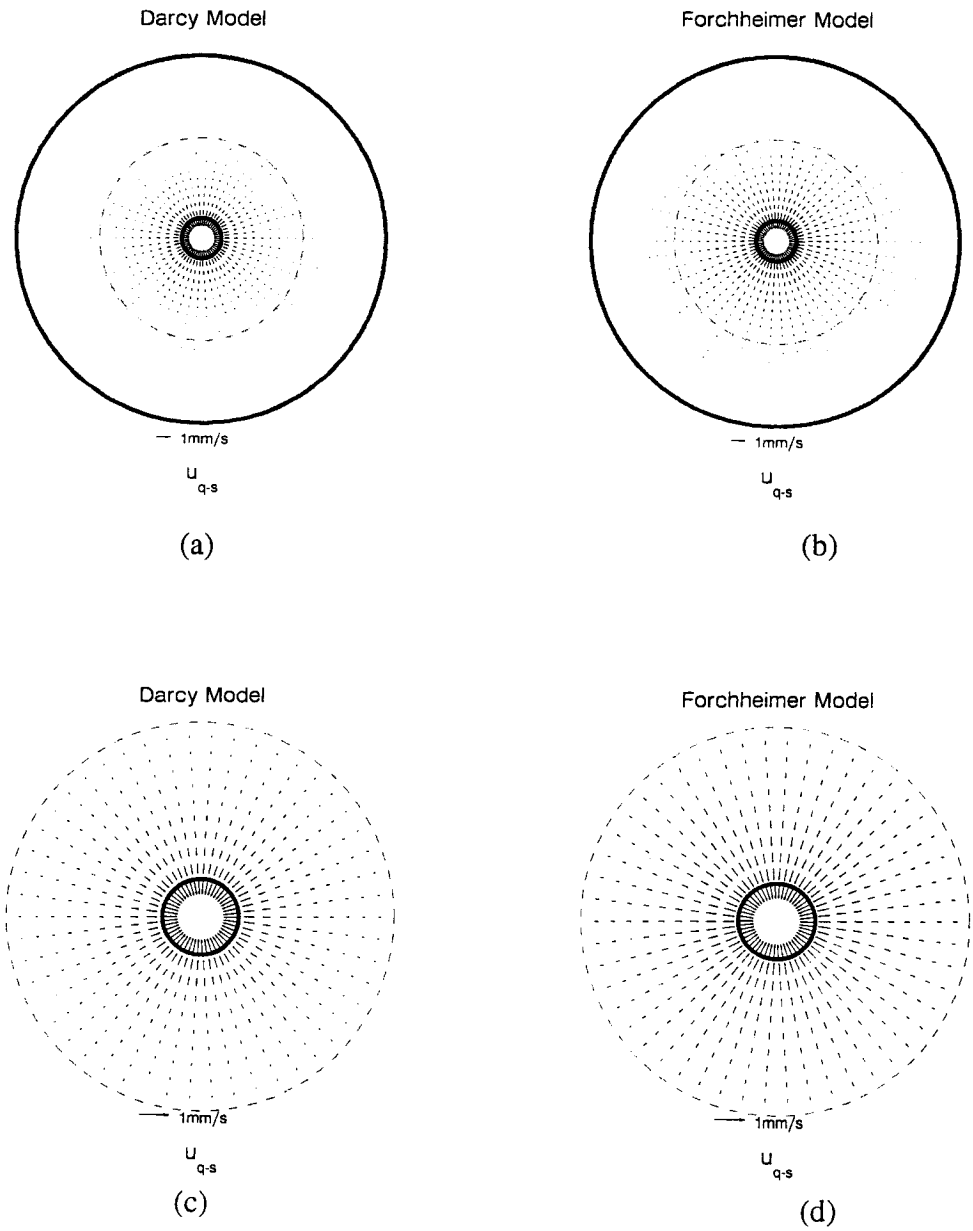

Figure 9.13. Quasi-steady-state velocity vector field in the reservoir by two models

Chapter 10

10 THE EFFECTS OF DARCY AND FORCHHEIMER FLOW PHENOMENA ON MISCIBLE DISPLACEMENTS

10.1. Abstract

The recovery of petroleum fluids using miscible liquid-liquid displacement offers an excellent benefit to the petroleum industry. Typically, the displacement studies are conducted assuming a uniform velocity reservoir and the corresponding pressure analysis is rarely performed. If there is any pressure analysis, it is based on Darcian flow and, often, such analyses can be flawed because of the presence of certain geological challenges. This paper provides numerical results of frontal displacement features, such as, concentration profile, displacement front mixing length, displacement efficiency of varying (accumulating and depleting) reservoir types. The results are also compared with those of a uniform, steady reservoir. In addition, the transient pressure and velocity profiles of accumulating and depleting reservoirs undergoing non-uniform flow are modeled, analytically and numerically. Such analyses are conducted using both Darcian and non-Darcian (Forchheimer) flow equations. The proposed analytical and numerical solutions will provide a better understanding of the various effects of Darcy and Forchheimer flow models during a miscible liquid-liquid displacement and be useful in miscible secondary recovery schemes.

10.2. Introduction

Most enhanced recovery schemes involve the displacement of one fluid by another. In a miscible displacement process, the displacement front depends on the intensity of the

local movement. The mixing length and displacement efficiency are also dependent on the flow characteristics of the fluid. Literature is available (Adewale et al., 2004) on analytical techniques for the solution of miscible flow when the flow is uniform throughout the reservoir. Analytical error function solution is one of the techniques derived by Laplace transforms (Marle, 1981). The analytical models are instructive for understanding the basic mechanisms of displacement and serve as benchmarks for numerical models. However, the uniform flow assumption in an unsteady state regime is not acceptable. In these papers, pertinent features of tracer flow, such as mixing coefficient, Peclet number, displacement efficiency etc. are discussed. For example, Adewale et al. (2004) investigated the effects of Peclet number on miscible displacement process and an integral transformation technique was used to solve the 1-D linear convection-dispersion equation. The analytical solutions are also available for pressure for slightly compressible Darcy flow in a bounded radial reservoir (Matthews *et al.*, 1967; Everdingen and Hurst, 1949).

A comprehensive prediction of miscible displacement is best achieved by numerical models. In the past, a number of numerical studies on miscible flow have been conducted (Peaceman and Rachford, 1962; Stone and Brian, 1964; Larson, 1987). Issues such as grid size, numerical dispersion, orientation effects and unphysical oscillations have been the challenging features of the numerical modeling of chemical transport (Kokabas, 2003). In cases of mixing, for which Fickian dispersion is prevalent, the early models supplemented microscopic inhomogeneity factor to simulate pore-level heterogeneity. Typically, mixing coefficients are of the order of 0.1-2.0 ft in the field and 0.005-0.02 ft in the laboratory scale (Stalkup, 1983). Since the scale of heterogeneity in the field is more severe than that in the laboratory, scale-dependent dispersion coefficient is also recommended (Numbere and Erkal, 1998). As for pressure analyses of slightly compressible Darcy flow in a bounded radial reservoir, the numerical solution is notably comparable to its analytical solution (Mustafiz et al., 2006). In addition to compositional

analyses, thermal aspects for heterogeneous porous media are also studied in both linear and radial system by Kocabas *et al.* (2000a and 2000b).

Coskuner and Hyde (1998) studied the displacement of one fluid by another miscible fluid in fractured porous media. They investigated the existence of an equivalent porous medium for various fracture networks of finite dimensions. Such equivalency, e.g., the normality of the outlet concentration profile was tested by employing a number of statistical measures. They used a particle walk model to represent the miscible displacement of an equal viscosity, equal density liquid and concluded that if a given volume of rock contains more than certain number of fractures, it can replaced by a homogeneous porous medium of equivalent porosity and dispersion coefficient. However, the study is based on the assumption that particles do not interact with each other and the flow has reached the steady state. The study was further complemented by using the 1-D convective dispersion equation, in which the equivalent porosity and dispersion coefficient for the combined fracture and matrix system were used.

The solutions presented in earlier works on miscible displacement assume Darcy's flow is applicable. The frontal displacement assuming non-uniform velocity or the pressure analysis based on non-Darcy flow phenomenon are never addressed in the study of miscible liquid-liquid displacement, as these were beyond the scopes of the objectives.

As early as 1901, Forchheimer pointed at that Darcian flow model may not be applicable for certain cases. Early descriptions used to point at turbulence being the reason for the onset of nonlinearity. Later experimental results have found that an increase in macroscopic velocity results in divergence from linear Darcian flow, prior to real onset of turbulence in porous media. Diverse opinions persist in explaining the non-Darcy phenomenon in porous media. Hassanizadeh and Gray (1987) described microscopic viscous force is the reason of non-linearity while Barak (1987) commented microscopic inertial force to be the reason of non-linearity. His discussion includes the formation of

local vortices and development of streamlines inside pores with an increase in pore Reynolds number. This explanation was accepted by several other researchers (Cvetkovic, 1987; Couland et al., 1988; Blick and Civan, 1988). Later the non-linear effects were taken into account by using the Forchheimer equation (Choi et al., 1997). Ma and Ruth (1997) also attempted to explain the flow characteristics through the concept of dimensionless Forchheimer number ($F_0=\beta k\rho U/\mu$), which is an indication when microscopic effects could lead to macroscopic non-linear effects (Ruth and Ma, 1992). The importance of investigating the non-Darcy flow for pressure analyses is also evident in recent studies (Mustafiz et al. (2006). The theoretical as well as the numerical results in a radial system are reported in that paper.

In a miscible liquid-liquid displacement, transient pressure profile can be important in addition to its concentration profile. In the current work, both analytical and numerical approaches followed by Ma *et al.* (2006) for flow in radial system are extended to 1-D linear systems for the solution of quasi-steady state flow. The velocity thus obtained is employed for the purpose of displacement. The flow characteristics and corresponding displacements are investigated for Darcy and non-Darcy conditions using numerical techniques. The investigation, however, does not include the microscopic flow and the macroscopic response. The results include movement of the displacement front, front mixing length and overall displacement efficiency.

10.3. Governing equations

In this paper, the isothermal miscible liquid-liquid displacement in porous media is considered. The porous medium is considered to be one-dimensional, homogeneous and isotropic. The convection-diffusion equation describes the conservation of the displacing component with a dimensionless mass concentration C

$$\phi\frac{\partial C}{\partial t}+u\frac{\partial C}{\partial x}=D\frac{\partial^2 C}{\partial x^2} \tag{10.1}$$

where, ϕ is porosity, t is time, x is distance, and D is dispersivity. Since this paper is designed for the laboratory scale, the assumption that the dispersion coefficient is constant is not unreasonable. The flowing velocity u can be determined by Darcy's law (Darcy, 1856; Dullien, 1992; Adler, 1992; and Sahimi, 1994 and 1995)

$$\frac{\partial p}{\partial x} = -\frac{\mu}{k} u \tag{10.2}$$

in which μ is viscosity and k *is* permeability of the porous medium. Or, in the case of non-Darcy flow, it can be derived from the Forchheimer model (Dullien, 1992; Sahimi, 1994 and 1995; Andrade *et al.*, 1999; and Belhaj *et al.*, 2003)

$$\frac{\partial p}{\partial x} = -\left(\frac{\mu}{k} + \beta\rho|u|\right)u \tag{10.3}$$

where, β is the non-Darcy coefficient of the porous medium.

When the fluid is slightly compressible, the following continuity equation needs to be satisfied

$$\phi\frac{\partial \rho}{\partial t} + \frac{d(u\rho)}{dx} = 0 \tag{10.4}$$

Pressure p and density ρ are related by the concept of compressibility c through the equation of state

$$c = \frac{1}{\rho}\frac{\partial \rho}{\partial p} \tag{10.5}$$

Now, u from Eq. (10.2) is substituted into Eq. (10.4) and the chain rules $\frac{\partial \rho}{\partial x} = \frac{\partial \rho}{\partial p}\frac{\partial p}{\partial x}$ and

$\frac{\partial \rho}{\partial t} = \frac{\partial \rho}{\partial p}\frac{\partial p}{\partial t}$ are applied. In addition, when ρ is replaced by p by making use of Eq. (10.5), the Darcy diffusivity equation becomes

$$\frac{\partial p}{\partial t} = \frac{k}{c\phi\mu}\frac{\partial^2 p}{\partial x^2} \tag{10.6}$$

Equation (10.6) also assumes that and the pressure gradient squared term is negligible. For Forchheimer model Eq. (10.3), the flow is in x direction; velocity u is always positive. Therefore, Eq. (10.3) has the following alternative form

$$\frac{\partial p}{\partial x} = -\left(\frac{\mu}{k}u + \beta\rho u^2\right) \tag{10.7}$$

By this equation, velocity u can be explicitly expressed as

$$u = \frac{\sqrt{\left(\frac{\mu}{k}\right)^2 - 4\beta\rho\frac{\partial p}{\partial x}} - \frac{\mu}{k}}{2\beta\rho} \tag{10.8}$$

The other solution to Eq. (10.7), $u = \frac{-\frac{\mu}{k} - \sqrt{\left(\frac{\mu}{k}\right)^2 - 4\beta\rho\frac{\partial p}{\partial x}}}{2\beta\rho}$, is always negative and cannot be a solution for the flow in the x-direction. Substituting u from Eq. (10.8) into Eq. (10.4) and incorporating Eq. (10.5), the governing equation for the Forchheimer model takes the following form

$$\frac{\partial p}{\partial t} = \frac{1}{c\phi\sqrt{\left(\frac{\mu}{k}\right)^2 - 4\beta\rho\frac{\partial p}{\partial x}}}\frac{\partial^2 p}{\partial x^2} \tag{10.9}$$

Equations (10.1), (10.6) and (10.9) set the platform for the study of one-dimensional Darcy and non-Darcy miscible displacements.

10.4. Analytical and numerical development

Different boundary conditions determine the behavior of the flow and the mixing zones in the reservoir. In this section, flow through a 1-D laboratory scale reservoir is discussed in three categories according to the inlet and outlet boundary conditions:

1. Steady state uniform flow
2. Accumulating flow, and
3. Depleting flow

10.4.1. Steady state, uniform flow

10.4.1.1. Analytical solution

a) Displacement velocity and pressure

By Eqs. (10.6) and (10.9), it can be noted that as

$$\frac{\partial^2 p}{\partial x^2} = 0 \tag{10.10}$$

$$\frac{\partial p}{\partial t} = 0 \tag{10.11}$$

This equation means that regardless whether the flow is governed by Darcy's law or by Forchheimer's law, the pressure throughout the reservoir does not vary with time, or, the reservoir is in steady state. Further, by Eq. (10.2) or Eq. (10.8), velocity u is also independent on time because of the independence of pressure on time. Therefore, Eq.

(10.10) becomes an ordinary differential equation ($\frac{d^2p}{dx^2}=0$) and has the following solution

$$p = c_1 x + c_2 \tag{10.12}$$

where, c_1 and c_2 are integral constants. Equation (10.12) reveals that the pressure distribution in a one-dimensional flow along the reservoir follows a straight line during the steady state. By taking the first derivative of Eq. (10.12) with respect to x,

$$\frac{dp}{dx} = c_1 \tag{10.13}$$

By substituting Eq. (10.13) into Eqs. (10.2) and (10.8), it can be shown that velocity is constant throughout the reservoir. In other word, when the pressure in the reservoir is independent of time, the velocity will be both steady and constant; i.e., it does not vary with space and time. In a reverse way, when the velocity is uniform and steady in the reservoir, i.e.,

$$u = c_3 \tag{10.14}$$

it can be found from Eqs. (10.2) and (10.7) that the pressure derivative is steady and constant too. Therefore, Eq. (10.13) in addition to Eq. (10.10) are satisfied. Also, by using Eqs. (10.6) and (10.9), Eq. (10.11) can be satisfied, which means that the pressure field is time-independent.

In summary, it can be stated that if and only if the velocity is steady and constant throughout the reservoir, the pressure in the reservoir will be steady, and the flow will be characterized as having complete steady flow. In other word, a steady and constant velocity throughout the reservoir is the only condition for the steady flow in the reservoir.

b) Tracer concentration, front mixing and displacement efficiency

For the displacement in the reservoir under the condition of steady and uniform flow, Marle (1981) reported Laplace transform error function solution to Eq. (10.1) for the half infinitive space domain $[0,\infty]$ with the following solution conditions

$$\begin{cases} C(0,t)=1 \\ C(+\infty,t)=0 \\ C(x,0)=0 \end{cases} \tag{10.15}$$

The results are plotted in Figs. 10.1-10.4, including concentration, displacement front mixing length, and displacement efficiency (Lake, 1989).

10.4.1.2. Numerical solution

Numerical modeling is also carried out in the study for the convection-dispersion equation (Eq. 10.1). The authors have used the modified Barakat Clarke scheme, which is an advanced numerical scheme. According to the scheme, the discretization of the displacement Eq. (10.1) is as follows

$$\begin{cases} \phi\dfrac{C1_i^{n+1}-C1_i^n}{\Delta t}=D\dfrac{C1_{i+1}^n-C1_i^n-C1_i^{n+1}+C1_{i-1}^{n+1}}{(\Delta x)^2}-\begin{cases} u\dfrac{C1_{i+1}^n-C1_i^n}{\Delta x} & if\ \ u\geq 0 \\ u\dfrac{C1_i^n-C1_{i-1}^n}{\Delta x} & if\ \ u<0 \end{cases} \\ \phi\dfrac{C2_i^{n+1}-C2_i^n}{\Delta t}=D\dfrac{C2_{i+1}^{n+1}-C2_i^{n+1}-C2_i^n+C2_{i+1}^n}{(\Delta x)^2}-\begin{cases} u\dfrac{C2_{i+1}^n-C2_i^n}{\Delta x} & if\ \ u\geq 0 \\ u\dfrac{C2_i^n-C2_{i-1}^n}{\Delta x} & if\ \ u<0 \end{cases} \end{cases} \tag{10.16}$$

Note that this paper involves conditions for which u>0. In Eq. (10.16), $C1$ and $C2$ satisfy the following boundary and initial conditions

$$\begin{cases} C(0,t) = 1 \\ C(L,t) = 0 \\ C(x,0) = 0 \end{cases} \tag{10.17}$$

The solution for Eq. (10.1) is the average of $C1$ and $C2$

$$C = \frac{C1 + C2}{2} \tag{10.18}$$

The parameters used for both numerical computation and theoretical analyses are: $\phi = 0.1$, $u = 0.1$ *m/s*. The dispersivity is calculated based on the empirical formula: $D = 0.01Lu$, which is suggested by Lake (1989). The reservoir length is $L = 2$ *m* and the numerical space and time increments are $\Delta x = \frac{L}{N}$ and $\Delta t = 0.001$ s respectively, where N denotes number of grids. A value of $N = 1000$ is used in the paper. For comparison purpose, the numerical results are presented alongside the theoretical results in Figs. 10.1-10.4. These results include concentration, displacement front mixing length, and displacement efficiency.

The following dimensionless terms are used as in the figures:

Dimensionless distance: $x^* = \frac{x}{L}$

Dimensionless time: $t^* = \frac{tu}{\phi L}$

Dimensionless mixing length: $L^*_{mix} = \frac{L_{mix}}{L}$

The mixing length (L_{mix}) is determined as (Lake, 1989):

$$L_{mix} = x\big|_{C=0.1} - x\big|_{C=0.9} \tag{10.19}$$

The displacement efficiency is defined to be the amount of fluid displaced in proportion to the amount of fluid contacted by displacing agent. In a 1-D miscible displacement, the efficiency can be expressed as (Lake, 1989):

$$E = \overline{C} = \frac{1}{L}\int_0^L C(x,t)dx \tag{10.20}$$

10.4.2. Quasi-steady state, non-uniform flow

When the inlet flow rate is different from the outlet flow rate, the flow in the reservoir cannot reach steady state. However, if the inlet and outlet flow rates are fixed in time, the velocity in the reservoir undergoes a time-adjustment process and finally reaches the steady sate. In this section, both analytical and numerical techniques are followed to find results for the quasi-steady state under Darcy and non-Darcy flow in a linear system. Later the results are used for the purpose of tracking tracer displacement profiles.

10.4.2.1. Analytical solution

The solution for pressure (p) of the diffusivity Equations (10.6) and (10.9), in general, is a function of space (x) and time (t). In case of constant inflow and outflow rates of a 1-D reservoir system, the process begins with an unsteady-state period while the velocity-distribution in the reservoir is adjusted gradually. Eventually, a quasi-steady state follows, for which the velocity-distribution u_{q-s} in the reservoir does not change.

$$\frac{\partial u_{q-s}}{\partial t} = 0 \tag{10.21}$$

This equation indicates that u_{q-s} is only a function of space x,

$$u_{q-s} = u(x) \tag{10.22}$$

By Eqs. (10.2) and (10.7), the quasi-steady state pressure gradient $\frac{\partial p_{q-s}}{\partial x}$ is also only a function of x. In the quasi-steady state period, the governing Eqs. (10.6) and (10.9) have the following forms for Darcy and Forchheimer flow, respectively

$$\frac{\partial p_{q-s}}{\partial t} = \frac{k}{c\phi\mu}\frac{\partial^2 p_{q-s}}{\partial x^2} = \frac{k}{c\phi\mu}\frac{\partial\left(\frac{\partial p_{q-s}}{\partial x}\right)}{\partial x} \tag{10.23}$$

and

$$\frac{\partial p_{q-s}}{\partial t} = \frac{1}{c\phi\sqrt{\left(\frac{\mu}{k}\right)^2 - 4\beta\rho\frac{\partial p_{q-s}}{\partial x}}}\frac{\partial^2 p_{q-s}}{\partial x^2} = \frac{1}{c\phi\sqrt{\left(\frac{\mu}{k}\right)^2 - 4\beta\rho\frac{\partial p_{q-s}}{\partial x}}}\frac{\partial\left(\frac{\partial p_{q-s}}{\partial x}\right)}{\partial x} \tag{10.24}$$

Since the term $\frac{\partial p_{q-s}}{\partial x}$ on the right hand side of Eqs. (10.23) and (10.24) is only a function of x, the term $\frac{\partial p_{q-s}}{\partial t}$ appearing on the left hand side must also be a function of x. Therefore,

$$\frac{\partial p_{q-s}}{\partial t} = f(x) \tag{10.25}$$

$$p_{q-s}(x,t) = \int f(x)dt = f(x)t + P(x) \tag{10.26}$$

where, $f(x)$ and $P(x)$ are functions of x and are determined using the solution conditions. By substituting Eq. (10.26) into Eqs. (10.2) and (10.8), Darcy and Forchheimer quasi-

steady state velocities are obtained

$$u_{q-s} = -\frac{k}{\mu}\frac{\partial p_{q-s}}{\partial x} = -\frac{k}{\mu}[f'(x)t + P'(x)] \quad \text{(Darcy flow)} \tag{10.27}$$

$$u_{q-s} = \frac{\sqrt{\left(\frac{\mu}{k}\right)^2 - 4\beta\rho\frac{\partial p_{q-s}}{\partial x}} - \frac{\mu}{k}}{2\beta\rho} = \frac{\sqrt{\left(\frac{\mu}{k}\right)^2 - 4\beta\rho[f'(x)t + P'(x)]} - \frac{\mu}{k}}{2\beta\rho} \quad \text{(Forchheimer flow)} \tag{10.28}$$

Substitution of Eqs. (10.27) and (10.28) into Eq. (10.21) leads to

$$f'(x) = 0 \tag{10.29}$$

Therefore, $f(x)$ must be a constant, and if denoted by c_4, Eq. (10.26) becomes

$$p_{q-s}(x,t) = c_4 t + P(x) \tag{10.30}$$

From this equation, it is evident that during the quasi-steady state of Darcy or non-Darcy flow, the pressure in the reservoir can be described by two terms. The first term is a linear function of time with a proportionality c_4. Since $\frac{\partial p_{q-s}}{\partial t} = c_4$, this proportionality is the constant rate at which the pressure varies with time. According to Equations (10.2) and (10.8), it is further known that this part does not contribute to the velocity in the reservoir rather it changes the pressure distribution throughout the reservoir as a whole at different time. The second term describes pressure as a function of space only. It is the part that affects the velocity distribution in the reservoir, which in turn, determines the displacement mixing zone.

a) Darcy flow

For Darcy flow, by substituting Eq. (10.30) into Eq. (10.6)

$$\frac{d^2P}{dx^2} = \frac{c\phi\mu}{k}c_4 \tag{10.31}$$

The solution Eq. (10.31) is

$$P(x) = \frac{c\phi\mu}{2k}c_4x^2 + c_5x + c_6 \tag{10.32}$$

where, c_5 and c_6 are two integral constants. Therefore, Eq. (10.30) can be written as

$$p_{q-s}(x,t) = c_4t + \frac{c\phi\mu}{2k}c_4x^2 + c_5x + c_6 \tag{10.33}$$

The two boundary conditions can be described using Eq. (10.2)

$$\begin{cases} \dfrac{\partial p(0,t)}{\partial x} = -\dfrac{\mu}{k}u_{in} \\ \dfrac{\partial p(L,t)}{\partial x} = -\dfrac{\mu}{k}u_{out} \end{cases} \tag{10.34}$$

The application of these two boundary conditions to Eq. (10.33) leads to

$$\begin{cases} c_4 = \dfrac{\left(u_{in} - u_{out}\right)}{c\phi L} \\ c_5 = -\dfrac{\mu}{k}u_{in} \end{cases} \tag{10.35}$$

Then, Eq. (10.33) changes to

$$p_{q-s}(x,t) = \frac{(u_{in} - u_{out})}{c\phi L} t + \frac{\mu}{2k} \frac{(u_{in} - u_{out})}{L} x^2 - \frac{\mu}{k} u_{in} x + c_6 \tag{10.36}$$

For engineering practices, the pressure-drop ($\Delta p = p_{in} - p_{out}$) across the reservoir, may be of significant importance

$$(\Delta p)_{q-s} = p_{q-s}(0,t) - p_{q-s}(L,t) = \frac{\mu}{k} \frac{(u_{in} + u_{out})}{2} L \tag{10.37}$$

Equation (10.37) shows that the pressure-drop remains constant in the quasi-steady state. It does not vary with time, although pressure itself changes linearly as time progresses for the entire reservoir as evident in Eq. (10.36).

Generally, if pressure at the outlet boundary is considered as the reference pressure, the relative-pressure ($p - p_{out}$) in the quasi-steady state is derived from Eq. (10.36) and is given by

$$(p - p_{out})_{q-s} = \frac{\mu}{2k} \frac{(u_{in} - u_{out})}{L} x^2 - \frac{\mu}{k} u_{in} x + \frac{\mu}{2k} (u_{in} + u_{out}) L \tag{10.38}$$

Further, substitution of Eq. (10.37) into Eq. (10.2) leads to an expression for the velocity distribution in the quasi-steady state, as follows

$$u_{q-s} = -\frac{k}{\mu} \frac{\partial p_{q-s}}{\partial x} = u_{in} - \frac{(u_{in} - u_{out})}{L} x \tag{10.39}$$

b) Forchheimer flow

For Forchheimer flow, by substituting Eq. (10.30) into Eq. (10.9),

$$\frac{d^2P}{dx^2} - \frac{\mu}{2k\beta\rho\phi} c\phi \sqrt{\left(\frac{\mu}{k}\right)^2 + 4\beta\rho\frac{dP}{dx}} \frac{dP}{dx} - c_4 c\phi \sqrt{\left(\frac{\mu}{k}\right)^2 + 4\beta\rho\frac{dP}{dx}} = 0 \tag{10.40}$$

Unlike the Darcy case, it is a non-linear, second order differential equation. Considering $\frac{dP}{dx}$ as the unknown, generally

$$\frac{dP}{dx} = \int_0^x \frac{d^2P}{dx^2} dx + \left.\frac{dP}{dx}\right|_{x=0} \tag{10.41}$$

By substituting Eq. (10.40) into Eq. (10.41),

$$\frac{dP}{dx} = \int_0^x \left[\frac{\mu}{2k\beta\rho\phi} c\phi \sqrt{\left(\frac{\mu}{k}\right)^2 + 4\beta\rho\frac{dP}{dx}} \frac{dP}{dx} + c_4 c\phi \sqrt{\left(\frac{\mu}{k}\right)^2 + 4\beta\rho\frac{dP}{dx}} \right] dx + \left.\frac{dP}{dx}\right|_{x=0} \tag{10.42}$$

Where, c_4 *is* an unknown in Eq. (10.42). At this point, the finite difference approach is followed to solve the equation, making the technique semi-analytical. However, it is only followed for the Forchheimer flow with the following steps:

1.

$$\left.\frac{dP}{dx}\right|_i = \left.\frac{dP}{dx}\right|_{i-1} + \left[\frac{\mu}{2k\beta\rho\phi} c\phi \sqrt{\left(\frac{\mu}{k}\right)^2 + 4\beta\rho\left.\frac{dP}{dx}\right|_{i-1}} \left.\frac{dP}{dx}\right|_{i-1} + c_4 c\phi \sqrt{\left(\frac{\mu}{k}\right)^2 + 4\beta\rho\left.\frac{dP}{dx}\right|_{i-1}} \right] \Delta x \qquad i = 1,\ldots,N \tag{10.43}$$

in which, when i = 1, by Eq. (10.7), the inlet boundary condition applies

$$\left.\frac{dP}{dx}\right|_0 = -\left(\frac{\mu}{k}u_{in} + \beta\rho u_{in}^{\,2}\right) \tag{10.44}$$

2. An iteration method is implemented to obtain the value of c_4.

3. By assuming an initial value for c_4 and starting from $i = 1$ till $i = N$ in Eq. (10.43), $\left.\frac{dP}{dx}\right|_N$ is obtained.

4. If it satisfies the outlet boundary condition

$$\left.\frac{dP}{dx}\right|_N = -\left(\frac{\mu}{k}u_{out} + \beta\rho u_{out}^{\,2}\right) \tag{10.45}$$

the assumed value for c_4 is satisfactory.

5. Else, adjustment is made and the procedure is continued until a satisfactory value is reached.

In the numerical algorithm, $N = 1000$, the same as the grid number employed for the numerical partition of the reservoir domain, is employed. An error criterion of 10^{-6} is applied on the basis of u_{out}. This grid number is found to be adequate.

6. With the pressure gradient $\left.\frac{dP}{dx}\right|_i$ $i = 1,\ldots,N$ being known, the pressure-drop across the reservoir ($\Delta p = p_{in} - p_{out}$) and the relative-pressure ($p - p_{out}$) in the reservoir in the quasi-steady state are obtained

$$(\Delta p)_{q-s} = \sum_{N}^{0} \left.\frac{dP}{dx}\right|_i \Delta x \tag{10.46}$$

$$\left(p - p_{out}\right)_{q-s} = \sum_{N}^{i} \left.\frac{dP}{dx}\right|_i \Delta x \tag{10.47}$$

where, the summation index i corresponds to the space position x (i.e., at the inlet boundary $i = 0$, $x = 0$ and at the outlet boundary $i = N$, $x = L$).

7. The velocity distribution for the quasi-steady state can be obtained using Eq. (10.8)

$$u_{q-s} = \frac{\sqrt{\left(\frac{\mu}{k}\right)^2 - 4\beta\rho\left.\frac{dP}{dx}\right|_i} - \frac{\mu}{k}}{2\beta\rho} \tag{10.48}$$

The above semi-analytical approach, however, does not explain the manner how flow is evolved from unsteady state into the quasi-steady state. The same numerical scheme, which is used to solve Eq. (10.1) and presented through Eq. (10.16), can be applied with no convection term to solve the unsteady state governing Eqs. (10.6) and (10.9). For the brevity of the paper, they are not included in the paper. The same boundary conditions are applied in both the analytical approach and the numerical method. As for the initial condition, the reservoir is assumed to experience steady uniform flow, a velocity of either u_{out} or u_{in} throughout the reservoir. Therefore, by recalling Equations (10.2) and (10.7), the following conditions are stated

Initial Condition I

$$\begin{cases} \dfrac{\partial p(x,0)}{\partial x} = -\dfrac{\mu}{k}u_{in} & \textit{for Darcy law} \\ \dfrac{\partial p(x,0)}{\partial x} = -\left(\dfrac{\mu}{k}u_{in} + \beta\rho u_{in}^{\,2}\right) & \textit{for Forchheimer law} \end{cases} \tag{10.49}$$

Initial Condition II

$$\begin{cases} \dfrac{\partial p(x,0)}{\partial x} = -\dfrac{\mu}{k}u_{out} & \textit{for Darcy law} \\ \dfrac{\partial p(x,0)}{\partial x} = -\left(\dfrac{\mu}{k}u_{out} + \beta\rho u_{out}^{\,2}\right) & \textit{for Forchheimer law} \end{cases} \tag{10.50}$$

10.5. Results and discussion

10.5.1. Uniform reservoir

Figure 10.1 shows the concentration profiles at various times for the displacement with uniform frontal velocity. Since a condition of uniform velocity persists, the results are identical for both Darcy and non-Darcy conditions. The numerical results for this case are compared with analytical results as reported by Lake (1989). The results are in excellent agreement for the entire range of dimensionless time. In order to determine the mixing length, the concentration profile for $t^*=0.5$ is recast in Fig. 10.2. In fact, the numerical modeling of the displacement in a finite space domain can be carried out as long as the computation is restricted such that the mixing zone is far from the right hand boundary and remains unaffected by the boundary. In order to study the effect of time on mixing length, Fig. 10.3 is plotted. It shows that as time increases, dispersion takes place with the propagation of the front. Therefore, the mixing length increases. Furthermore, to study the effect of Δx on mixing length, a series of numerical runs are performed as shown in Fig. 10.3. In this case, the grid size is varied in between 1 mm and 2 mm. Although a significant difference is not observed for different Δx, a finer grid size gives closer agreement with analytical solution (Lake, 1989). Since, the improvement is not significant, a small grid number of 1000 is followed in the entire simulation of the paper.

Figure 10.4 indicates that the displacement efficiency increases with time. The efficiency reaches 100% for a dimensionless time (t*) of 1.3. The graph also shows an excellent agreement between the numerical result and the analytical results (Lake, 1989).

Overall, the excellent agreement between numerical and analytical results of Figures 10.1 through 10.4 demonstrates the validation of the numerical displacement model for the linear system as presented in Eq. (10.16). However, for the non-uniform velocity cases, analytical solutions are not available. For these cases of both Darcian and non-Darcian

flow, the displacement, pressure and velocity profiles are discussed in the following sections.

10.5.2. Accumulating reservoir

Figure 10.5 demonstrates the theoretical and numerical prediction of pressure drop with time. For this case, the inlet velocity, u_{in} was 2 *mm/s*, whereas the outlet velocity, u_{out} was set to $0.3u_{in}$. The viscosity was $\mu = 10^{-3}\frac{kg}{ms}$ and permeability, k was $10^{-9}m^2$. For the non-Darcy flow case, the coefficient was set at $\beta = 10^{7}\frac{1}{m}$. The non-Darcy coefficient was used throughout. For all cases, a density, ρ of 1000 m^3/s was used. Figures 10.5, 10.6 and 10.7 (b) show the results obtained for Equations (10.46), (10.47) and (10.48) respectively. It is also to be remembered that the numerical predictions in Figures 10.5 through 10.7 follow the Initial Condition-I described earlier. In Fig. 10.5, both models show that the pressure-drop across the reservoir has two distinct states in time, namely the initial unsteady development state and the finally reached quasi-steady state. During the unsteady state, the pressure drop changes significantly as time increases. Gradually, the reservoir reaches the quasi-steady state when there is almost no change in pressure drop. In addition to numerical predictions, the Darcy and Forchheimer analytical results constructed upon Eq. 10.37 and Eq. 10.46, respectively, are presented by the dotted horizontal lines. Overall, the figure demonstrates that the finally reached quasi-steady numerical results are in excellent agreement with both analytical (Darcy) and semi-analytical (Forchheimer) quasi-steady state results.

The relative pressure distribution along the length of the reservoir for the quasi-steady state is illustrated in Fig. 10.6. The Darcy and Forchheimer relative pressure results are plotted using Equations 10.38 and 10.47, respectively. Both equations demonstrate time-free functions. The numerical plots are also accomplished for both conditions and show excellent agreement with theoretical results. Results also show that the difference in

relative pressure distribution between Darcy and non-Darcy flow is more significant at the inlet and it diminishes gradually as front approaches the outlet boundary. In general, the accumulated reservoir follows a concave parabola in the *p-x* plane as observed in Fig. 10.6.

The velocity distribution at the quasi-steady state in the accumulating reservoir is also studied for Darcy and Forchheimer flow conditions. Figures 10.7(a) and 10.7(b) constitute the theoretical and numerical results for Darcy and Forchheimer conditions respectively. Both graphs begin with a dimensionless velocity of 1 as the left boundary maintains the inlet velocity (u_{in}). Although the numerical accuracy was excellent for the Forchheimer result, little discrepancy is observed for the middle-half of the reservoir between the theoretical and numerical Darcy quasi-steady state results. The numerical results of Figures 10.7(a) and 10.7(b) are presented in Fig. 10.7(c) and it shows that the velocity distribution as predicted by the Forchheimer model is slightly higher than that by the Darcy model. On the contrary, the difference in the velocity profiles between the two models in a radial reservoir system is appreciable (Mustafiz *et al.*, 2006).

It can be added here that if $u_{out} = u_{in}$, the quasi-steady state velocity ($u_{q-s} = u_{out} = u_{in}$) becomes a constant and the relative-pressure curve becomes a straight line (Eq. 10.39) instead of a parabola (Eq. 10.38). Also, Eq. (10.10) and, in turn, Eq. (10.11) are satisfied, indicating that the quasi-steady state collapses assumes a fully steady state. In fact, it is the only case when the quasi-steady state is also the steady state. It is equally true for the non-Darcy Forchheimer flow.

Figure 10.8 describes the performance of the displacement front in a linear accumulating system undergoing Darcy and Forchheimer flow. The figure shows that for all dimensionless time, the front moves slightly faster in case of Forchheimer model than it does for the Darcy model. Figure 10.9 is an alternate presentation of Fig. 10.8, for which dimensionless mixing length is plotted against dimensionless time. It suggests that as

time increases, the mixing length increases. The graph also tells that the mixing length is reasonably longer for the Forchheimer case than that for the Darcy case. It is perhaps due to slight increase in dispersivity, which is assumed to be proportional to the magnitude of velocity (Lake, 1989).

For the overall displacement efficiency, the two different models result in only marginal differences (Fig. 10.10). Theoretically, the efficiency must reach to 1 at the end, which is not the case according to the figure. There is an impact of the boundary condition on the finite domain and therefore numerical calculation is restricted to the region where the mixing zone will remain far from reaching the right boundary. Therefore, within such restriction, as high as 82% displacement efficiency can be achieved for a dimensionless time (t*) of 1 in the case of an accumulating linear reservoir. In fact, it is found to be true in both Darcy and Forchheimer cases. Now, recalling Fig. 10.4, it is noticed that at t*=1.0, the efficiency was as high as 94%. It is quite expected because of the accumulating nature (u_{out}=0.3 u_{in}) of the linear system of Fig. 10.10, while in Fig. 10.4, the condition u_{out}=u_{in} exists.

As previously been discussed that the quasi-steady state results including pressure-drop, relative-pressure and velocity distribution are independent of their prior time history, i.e., they do not depend on the initial condition. To illustrate the flow phenomenon numerically for different initial conditions (here only results of two initial conditions discussed), Figures 10.12 through 10.16 are presented. All these figures apply to the Forchheimer case. For both initial conditions, the flow begins from a steady state, which is evident in Figures 10.11(a) and 10.11(b), for which the pressure values are described by the straight lines in the *p-x* plane. The velocity in the reservoir is lower at Initial Condition I in comparison to that at Initial Condition II. Therefore, according to Eq. (10.49), the reservoir must experience lower pressure gradient when the flow is initiated by Condition I than by condition II. A comparison between the slope of the straight line (at t=0) in Figures 10.11(a) and that of 10.11(b) illustrates that the slope is steeper for Fig.

10.11(b), which is for Initial Condition II. As obvious, the final pressure buildup in the quasi-steady state has a lower value for Initial Condition I than for Initial Condition II (Fig. 10.12). Simply, it means that the transient pressure buildup is closely related to the initial pressure in the reservoir. The relative-pressure profiles (outlet pressure being the reference) corresponding to Figures 10.11 and 10.12 are also plotted in Figures 10.13 and 10.14 respectively. Since a reservoir having Initial Condition I has low initial pressure, the relative-pressure will increase with time and finally reach a steady state as shown in Fig. 10.13 (a). In contrast, when the pressure is high at the beginning as is the case for Initial Condition II, the relative pressure will decrease and finally reach to a steady state.

It is to be noted that if Fig. 10.13(a) is superposed on Fig. 10.13(b), a common curve can be captured on the p-x plane. This curve is shown in Fig. 10.14 and it implies that the final quasi-steady relative-pressure curves resulting from the two initial conditions collapse to a single curve and reveals the fact that the quasi-steady relative-pressure is independent of the initial conditions. Such numerical finding also agrees with the conclusion of the analytical approach.

Figures 10.15(a) and 10.15(b) demonstrate the velocity profiles, which begin from two different directions, under and above the straight line, for Initial Condition I and Initial Condition II respectively. Both figures experience similar time-adjustment process as observed in Figures 10.13(a) and 10.13(b) and finally collapse to each other in the quasi-steady state (Fig. 10.16). Similar to the quasi-steady pressure case, the quasi-steady velocity is independent of the initial conditions.

10.5.3. Depleting reservoir

For the brevity of the paper, only the numerical predictions resulting from Initial Condition I are discussed in this section. In a depleting condition, the outlet velocity is larger than the inlet velocity ($u_{out} = 3.0u_{in}$). Unlike an accumulating reservoir, the

pressure decreases from its initial condition and finally reaches the steady state (Fig. 10.17). Once again, it is applicable to both Darcy and Forchheimer models. However, it is important to note that it takes more time for the reservoir to reach the steady state when non-Darcian (Forchheimer) flow takes place.

The numerical relative-pressure profile is given in Fig. 10.18 for Forchheimer flow in a depleting reservoir. It is observed that the graph is convex in shape, which is consistent with the theoretical analysis. At the quasi-steady state, the relative-pressure profile for Forchheimer flow is compared to that for Darcy flow (Fig. 10.19). It clearly shows that the relative pressure has higher value for Forchheimer flow than that for Darcy flow and the relative-pressure drops more rapidly along the length under non-Darcy conditions than Darcy conditions.

The velocity history in the depleting reservoir is also captured until the quasi-steady is reached (Fig. 10.20). Figure 10.21 shows that the quasi-steady velocities by two models differ only marginally. This in contrast to what is observed for pressure-drops for the same quasi-steady state regime. It shows extra-sensitivity to pressure for the Forchheimer model.

Finally, the displacement fronts for the accumulating, uniform flow and depleting reservoirs are compared in Figures 10.22, 10.23 and 10.24. Fig. 10.22 demonstrates that the displacement front moves slower in an accumulating reservoir and faster in a depleting reservoir than in a reservoir where uniform flow exists. It is also found that the length of the displacement mixing zone is smaller in an accumulating reservoir and larger in a depleting reservoir than that of in a uniform linear flow system (Fig. 10.23).

The linear systems are also compared in terms of displacement efficiency. Figure 10.24 is a combination of the conditions in Figures 10.4 and 10.10 in addition to depleting condition. It shows that a depleting reservoir has the highest displacement efficiency

while the accumulating reservoir has the lowest. The depleting reservoir loses fluid at a higher velocity and, therefore, the displacing fluid has higher displacement ability than it will displace in a uniform or in an accumulating system. An opposite explanation can be attributed to the accumulating system, for which it is difficult to displace the fluid. In addition, it is noted that as t* increases, the effect of depletion becomes more significant on efficiency while the effects are relatively similar in accumulating and uniform systems.

The overall study is equally informative to groundwater research to develop an integrated method of down-hole fracture characterization (Brainerd and Robbins, 2004). In addition to identify water-bearing fractures, they could also measure ambient fracture flow rate and fracture transmissivity by conducting a tracer dilution experiment in fractured bedrock.

10.6. Conclusions

Based on the analytical and numerical work presented in this paper, the following conclusions can be reached:

1) The quasi-steady state pressure-drop, relative-pressure and velocity distribution in both accumulating and depleting linear reservoirs of non-uniform flow are analytically and numerically modeled. An excellent agreement is found between the two models.

2) Pressure-drop and relative-pressure results in the quasi-steady state in a linear reservoir system undergoing non-Darcy flow, show significant variation than their results at the Darcy flow condition. This substantial variation persists in both accumulating and depleting reservoirs of non-uniform flow.

3) The velocity profiles at the quasi-steady state in the same linear system are not affected by the flow type, Darcy or non-Darcy. Such insensitivity is noted in both accumulating and depleting reservoir of non-uniform flow.

4) A numerical uniform flow model is established and compared with the error function solution. The model results, including concentration profile, displacement front mixing length, and displacement efficiency are found to be in excellent agreement with the specified function results.

5) The grid size is found to have insignificant impact on the mixing length of the linear system, for the range studied.

6) The displacement features predicted by Darcy and Forchheimer models demonstrate minor differences.

7) Numerical results show that the tracer front will move slower in an accumulating linear system and faster in a depleting linear system than in a uniform flow system.

8) Accumulation or depletion in a linear system will also affect the length of the tracer mixing zone. Results show that accumulation will reduce the length of the displacement mixing zone of a regular uniform flow system and depletion will increase it.

9) The rate of increase of the overall displacement efficiency in a depleting linear system is higher than that in an accumulating or a uniform linear system.

10.7. Nomenclature

c	compressibility
C, $C1$, $C2$	concentration
c_1, c_2, c_3, c_4, c_5, c_6	constants
D	dispersivity
$f(x)$	general function
i	space position index
k	permeability
L	reservoir length
n	time level index
N	number of x-increment
p, P, p_{in}, p_{out}	pressure, pressure at the inlet boundary and outlet boundaries
q-s	quasi-steady-state
x	Cartesian coordinate
t	calculation time
u	velocity
β	Forchheimer non-Darcy coefficient
ϕ	porosity
Δp	pressure-drop
Δx , Δt	space and time increments
μ	viscosity
ρ	density

10.8. References

Adewale, A. Olalekan, O., Kelani, B. and Abass, I., (2004) Effects of Peclet number on miscible displacement process through the reservoir, SPE 88981, Nigeria Annual International Conference and Exhibition, Abuja, Nigeria, August 2-4

Adler, P. M., (1992) Porous media: geometry and transport, Butterworth-Heinemann, Stoneham, MA, USA

Andrade, J. S., Jr., Costa, U. M. S., Almeida, M. P., Makse, H. A. and Stanley, H. E., (1999) Inertial effects on fluid flow through disordered porous media, Physical Review Letters, vol. 82, no. 26, pp. 5249-5252

Belhaj, H.A., Agha, K.R, Nouri, A.M., Butt, S.D. and Islam, M.R., (2003) Numerical and experimental modeling of non-Darcy flow in porous media, SPE 81037, Proc. SPE Latin American and Caribbean Petroleum Engineering Conference, Port-of-Spain, Trinidad, West Indies, April 27-30

Blick, E.F. and Civan, F., (1988) Porous media momentum equation for highly accelerated flow, SPE 16202, SPE Reservoir Engineering, pp. 1048-1052, August

Brainerd, R. J. and Robbins, G. A., (2004) A tracer dilution method for fracture characterization in bedrock wells, Ground Water, vol. 42, no. 5, pp. 774-780

Choi, I., Cheema, T. and Islam, M. R., (1997) A new dual-porosity/dual permeability model with non-Darcian flow through fractures, Journal of Petroleum Science and Engineering, vol. 17, pp. 331-344

Cvetkovic, V. D., (1986) A continuum approach to high velocity flow in porous media, Transport in Porous Media, pp. 63-97

Coskuner, G. and Hyde, T. C., (1998) Homogeneous equivalents of naturally fractured porous media for miscible fluid displacements, Journal of Petroleum Science and Engineering, vol. 19, pp. 145-157

Couland, O., Morel, P. and Caltagirone, J. P., (1988) Numerical modelling of nonlinear effects in laminar flow through a porous medium, Journal of Fluid Mechanics, vol. 190, pp. 393-407

Darcy, H.P.G., (1856) Les Fontaines Publiques de villle de la Dijon Dalmont, Exposition et Application des Pricipes a Suivre et des Furmules a Emplyer dans les Questions de Distribution d'Eau. Victor Dalmont, Paris

Dullien, F. A. L., (1992) Porous Media: Fluid transport and pore structure, 2nd edition, Academic Press, San Diego, USA

Forchheimer, P., (1901) Wasserbewegung durch Boden ZVDI, vol. 45, pp. 1781

Kocabas, I., (2003) Modeling tracer flow in oil reservoirs containing high permeability streaks, SPE 81429, SPE 13th Middle East Oil Show and Conference, Bahrain, April 5-8

Kocabas, I. and Islam M. R., (2000a) Concentration and temperature transients in heterogeneous porous media, part I: linear transport, Journal of Petroleum Science and Engineering, vol. 26, pp. 211-220

Kocabas, I. and Islam M. R., (2000b) Concentration and temperature transients in heterogeneous porous media, part II: radial transport, Journal of Petroleum Science and Engineering, vol. 26, pp. 221-233

Lake, L. W., (1989) Enhanced oil recovery, Prentice Hall, Englewood Cliffs, NJ, USA

Larson, R. G., (1987) Controlling numerical dispersion by time flux, Society of Petroleum Engineering Journal, March

Ma, H. and Ruth, D., (1997) Physical explanations of non-Darcy effects for fluid flow in porous media, SPE Formation Evaluation, March

Marle, C. M., (1981) Multiphase flow in porous media, Gulf Publishing, Houston, USA

Matthews, C. S. and Russell, D. G., (1967) Pressure buildup and flow tests in wells, Monograph series, SPE, Dallas, USA

Mustafiz, S., Ma, F. and Islam, M. R., (2006) Well test analyses for Darcy and non-Darcy flow using an advanced numerical scheme, Journal of Petroleum Science and Engineering, sent for publication, September

Numbere, D. T. and Erkal, A., (1998) A model for tracer flow in heterogeneous porous media, SPE 39705, SPE Asia Pacific conference on Integrated Modeling for Asset Management, Kuala Lumpur, Malaysia, March 23-24

Peaceman, D. W. and Rachford, Jr. H. H., (1962) Numerical calculation of multidimensional miscible displacement, Society of Petroleum Engineering Journal, Transactions AIME, vol. 228, December

Ruth, D. and Ma, H., (1992) On the derivation of the Forchheimer equation by means of the averaging theorem, Transport in Porous Media, vol. 7, pp. 255

Sahimi, M., (1994) Applications of percolation theory, Taylor &Francis, London, UK

Sahimi, M., (1995) Flow and transport in porous media and fractured rock, VCH, Weinheim, Germany

Stone, H. L. and Brian, P. L. T., (1964) Numerical solution of convective transport problems, American Institute of Chemical Engineering Journal, vol. 9, pp. 681

Van Everdingen, A.F. and Hurst, W., (1949) The application of the Laplace transformation to flow problems in reservoirs, Transactions AIME, vol. 186, pp. 305-324

10.9. Appendices

10.9.1. Appendix A: Figures

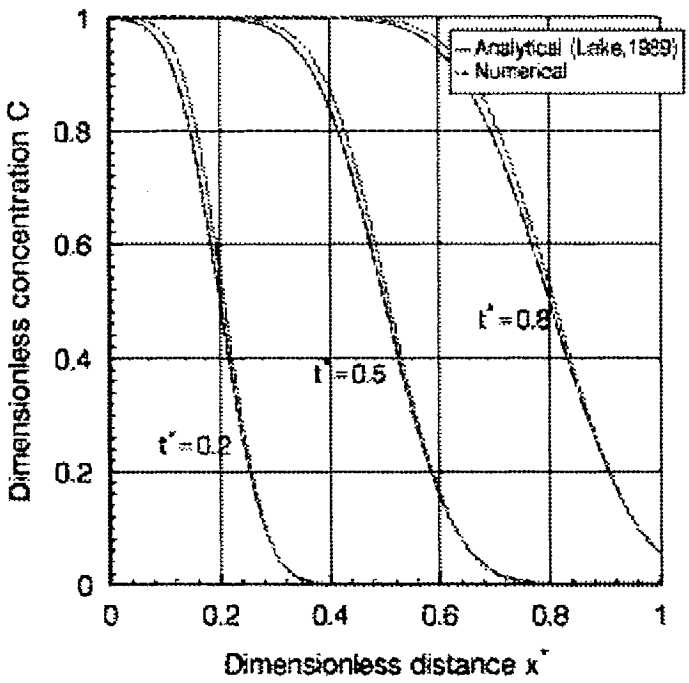

Fig. 10.1. Concentration profile with uniform velocity

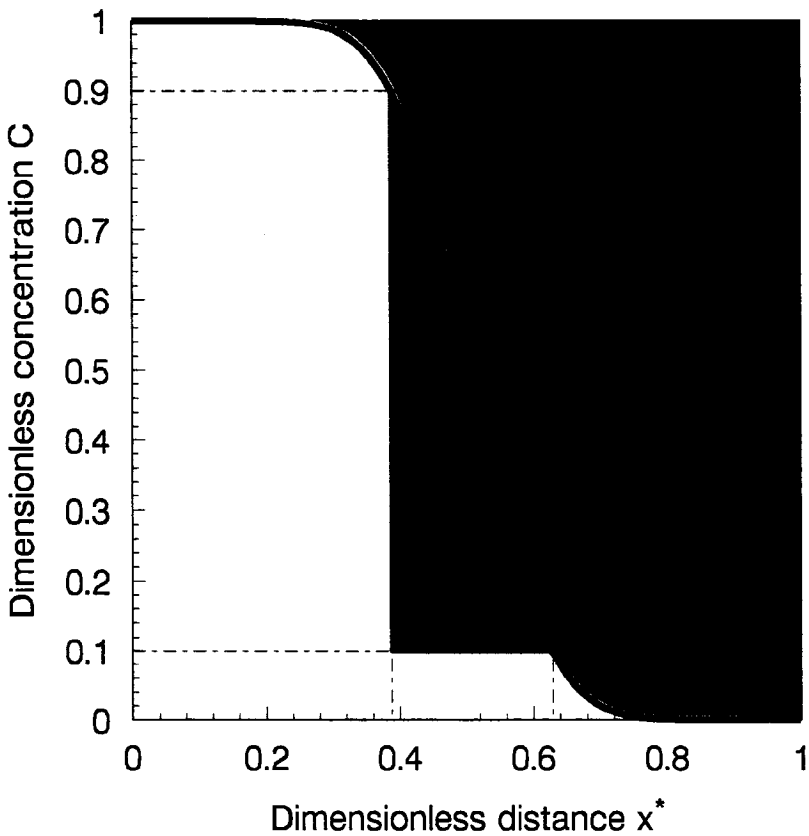

Fig. 10.2. Displacement front and definition of mixing length

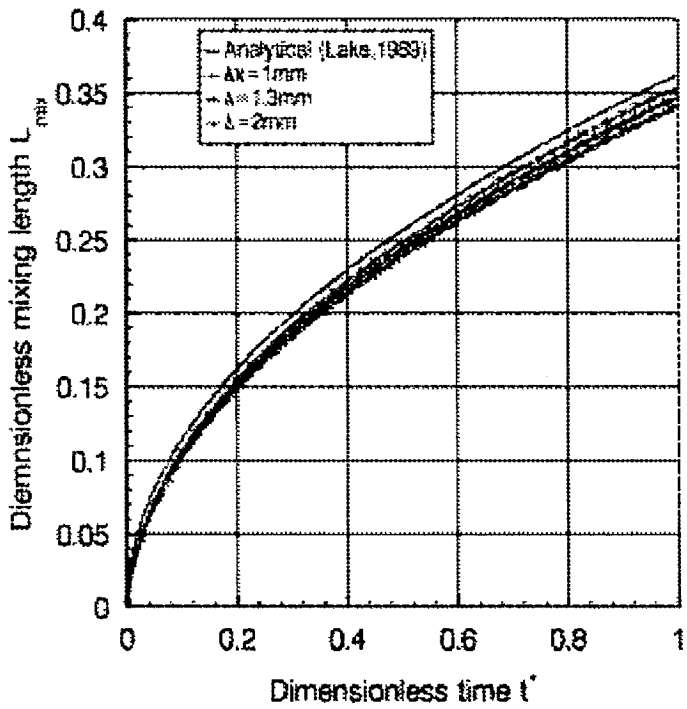

Fig. 10.3. Mixing length with uniform velocity

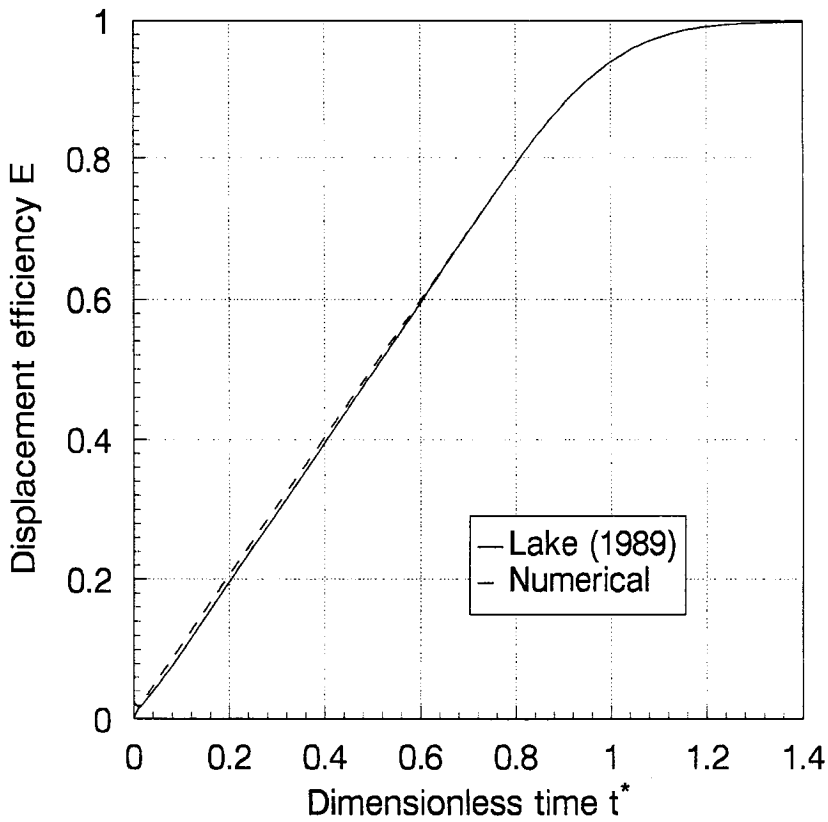

Fig. 10.4. Displacement efficiency with uniform velocity

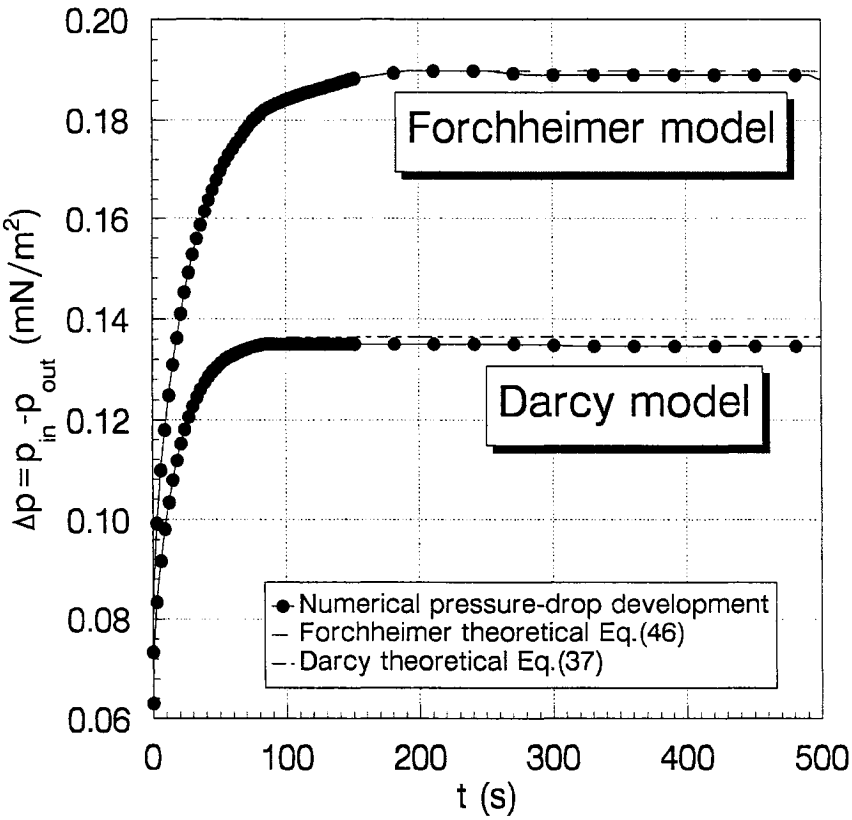

Fig. 10.5. Pressure-drop history in accumulating reservoir

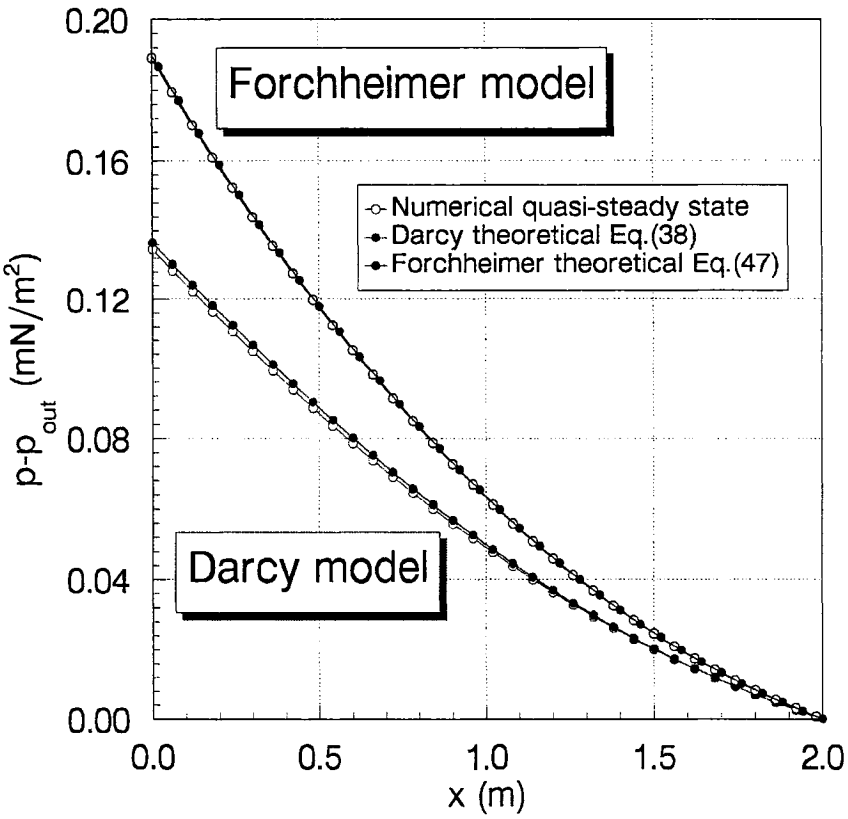

Fig. 10.6. Quasi-steady state relative-pressure distribution in accumulating reservoir

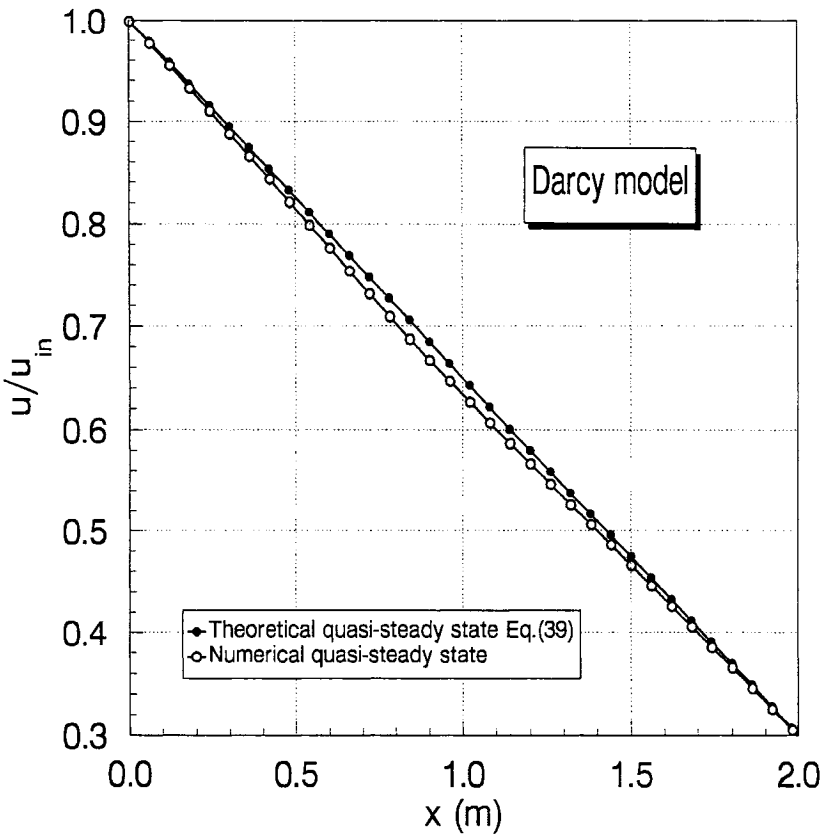

Fig. 10.7(a). Theoretical and numerical quasi-steady state velocity distribution in accumulating reservoir

(Darcy model)

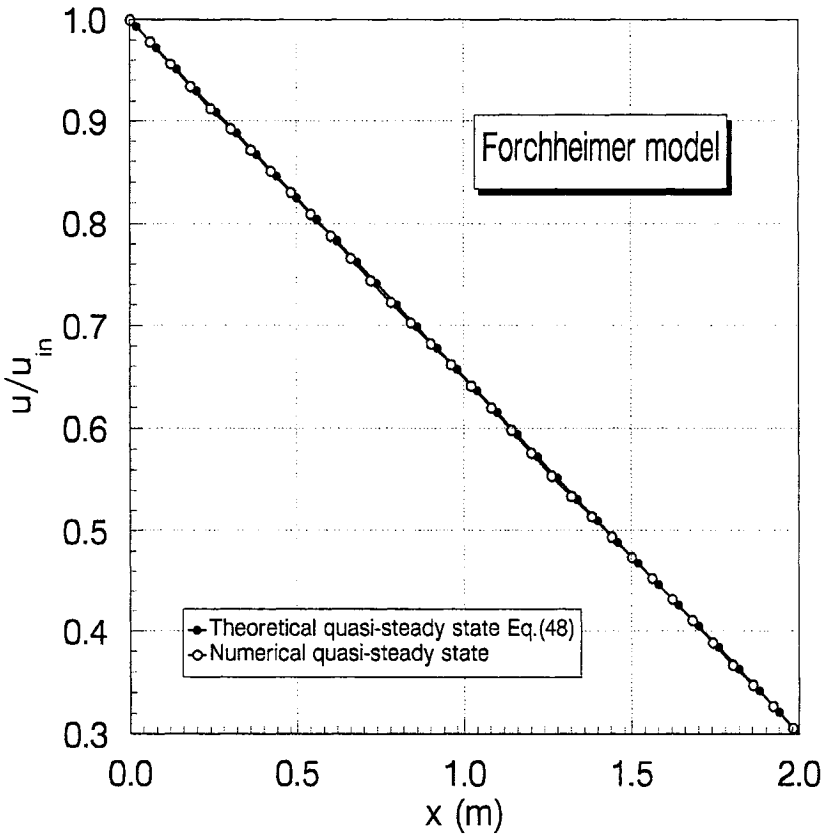

Fig. 10.7(b). Theoretical and numerical quasi-steady state velocity distribution in accumulating reservoir
(Forchheimer model)

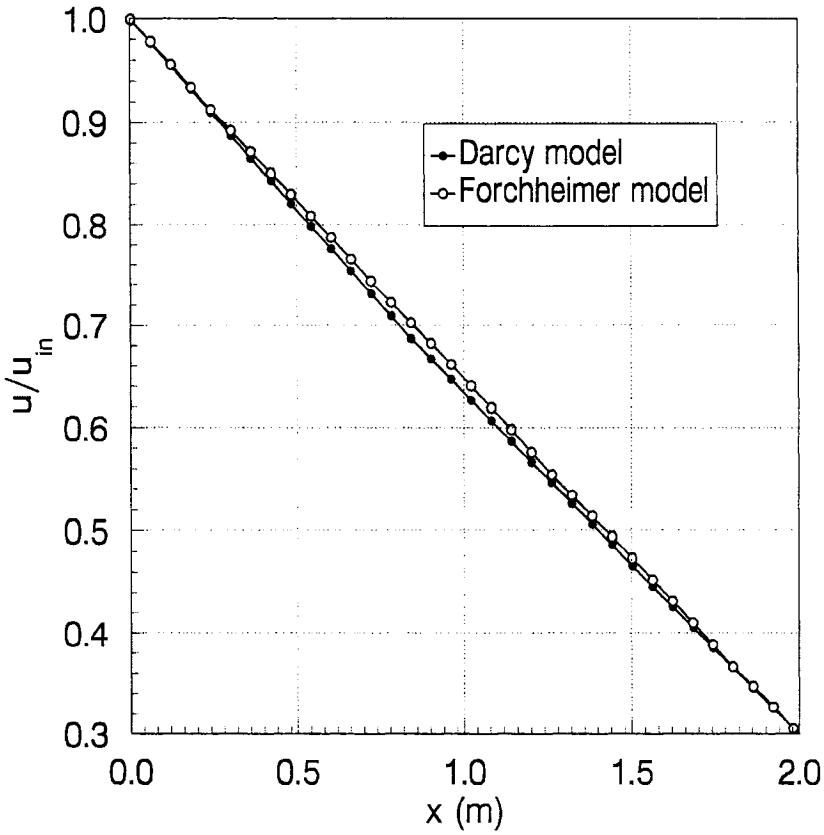

Fig. 10.7(c). Numerical quasi-steady state velocity distribution in accumulating reservoir

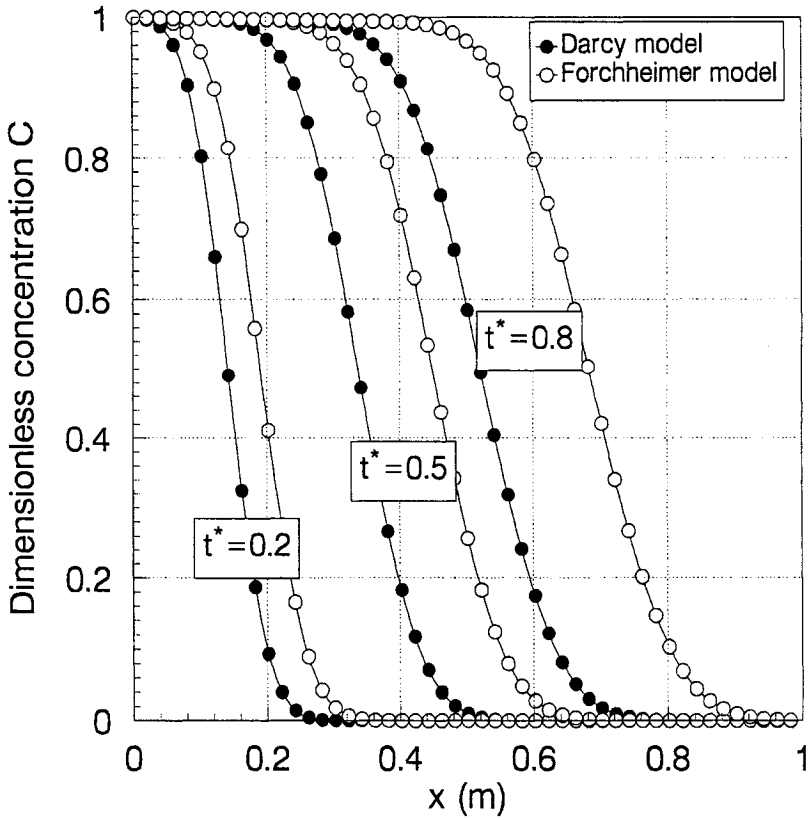

Fig. 10.8. Concentration development in accumulating reservoir

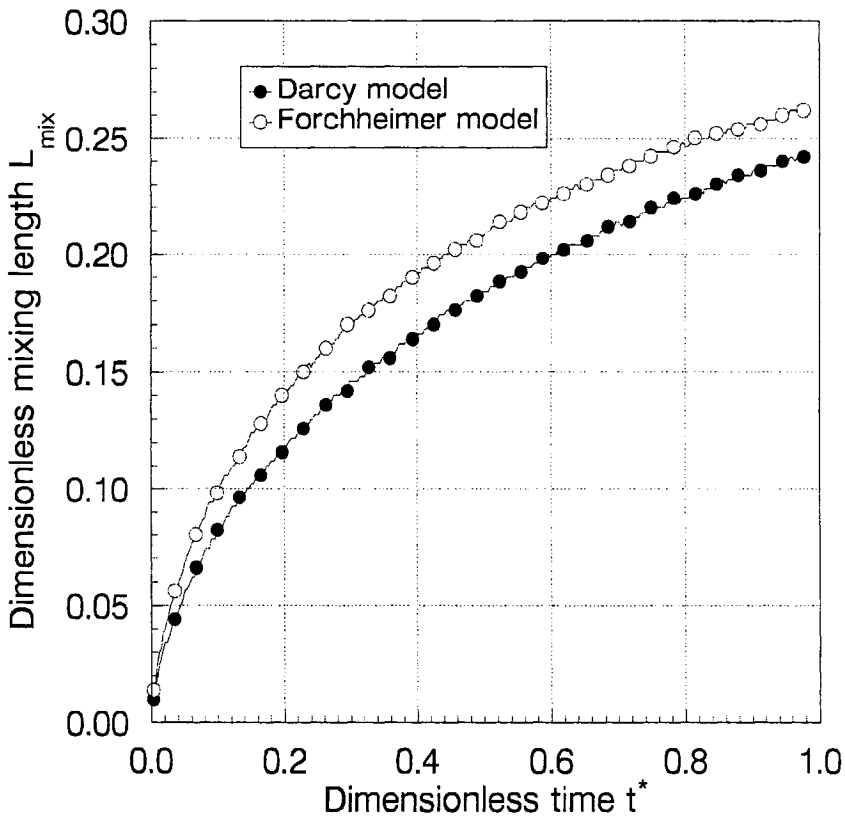

Fig. 10.9. Mixing length in accumulating reservoir

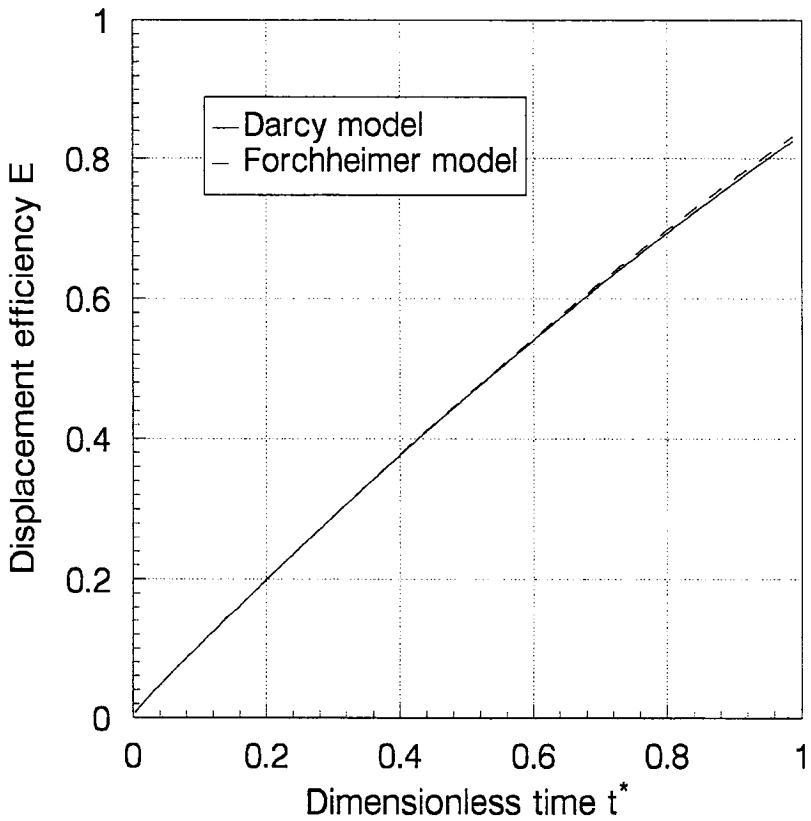

Fig. 10.10. Displacement efficiency in accumulating reservoir

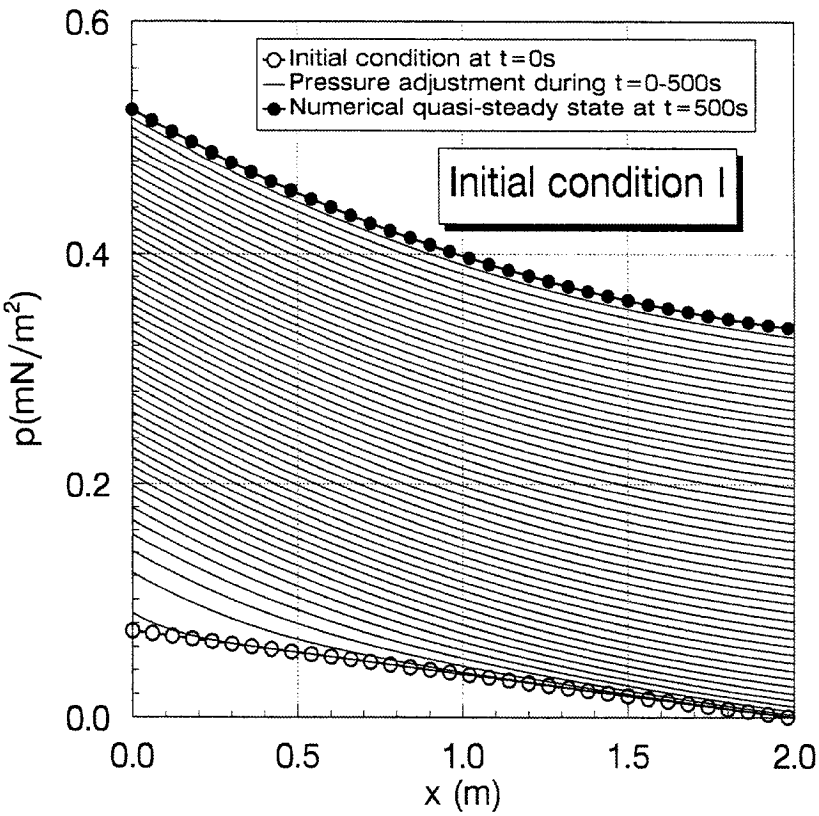

Fig. 10.11(a). Pressure history in accumulating reservoir-initial condition-I

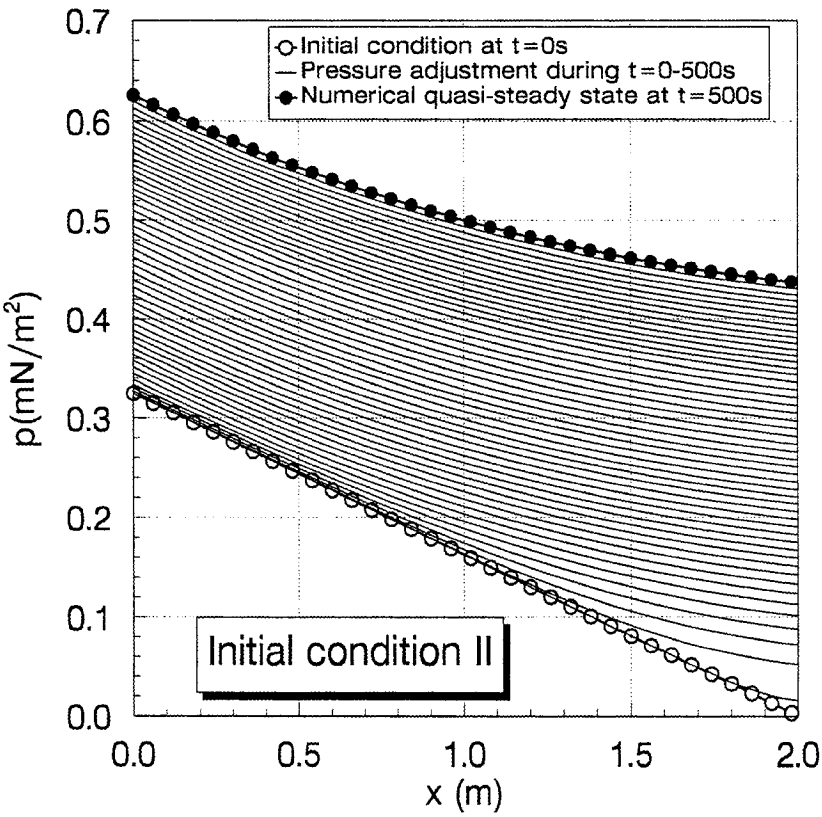

Fig. 10.11(b). Pressure history in accumulating reservoir-initial condition-II

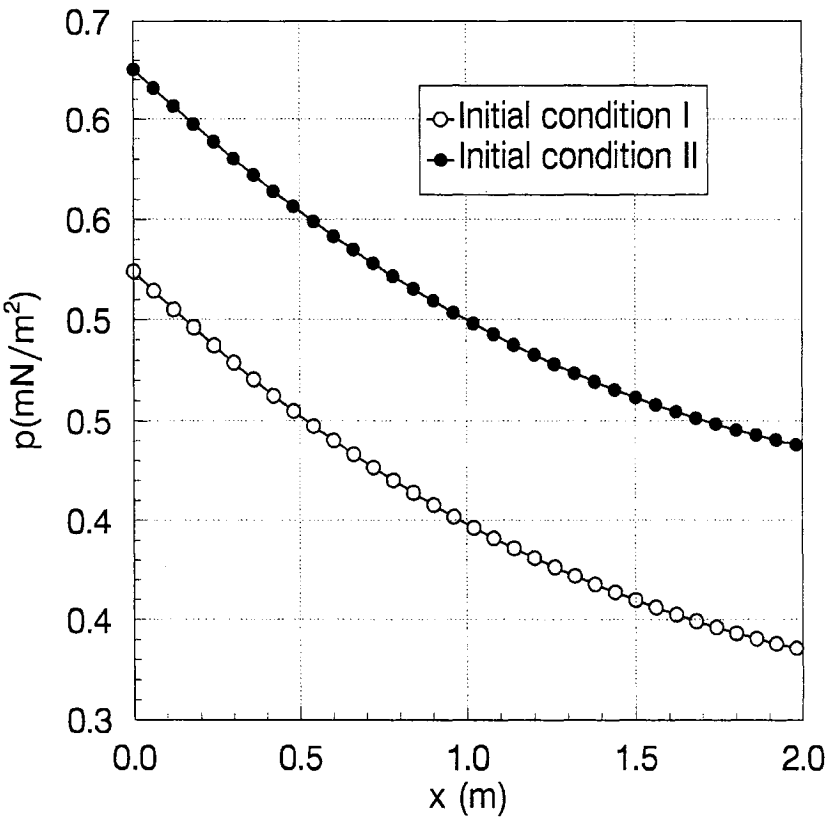

Fig. 10.12. Quasi-steady pressure distribution in accumulating reservoir

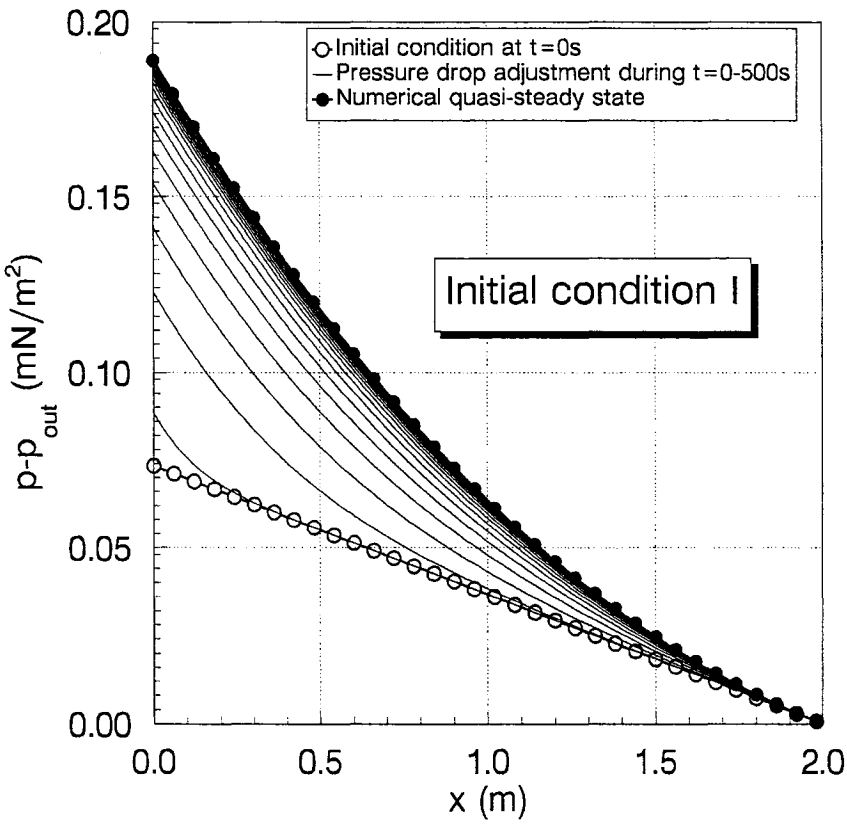

Fig. 10.13(a). Relative-pressure history in accumulating reservoir-initial condition-I

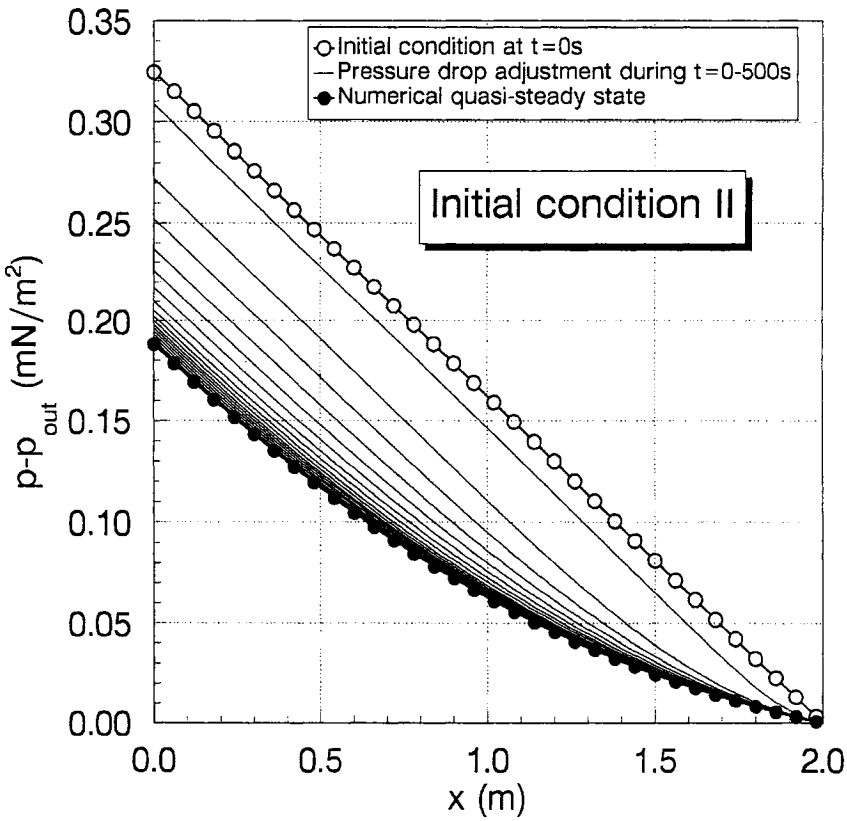

Fig. 10.13(b). Relative-pressure history in accumulating reservoir-initial condition-II

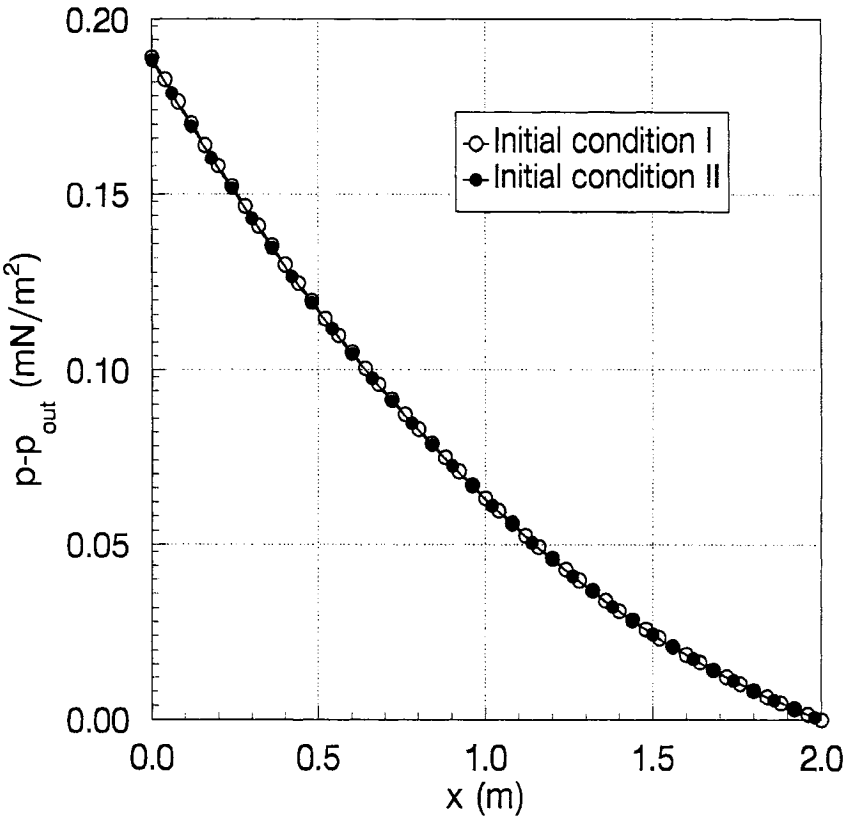

Fig. 10.14. Quasi-steady state relative-pressure distribution in accumulating reservoir

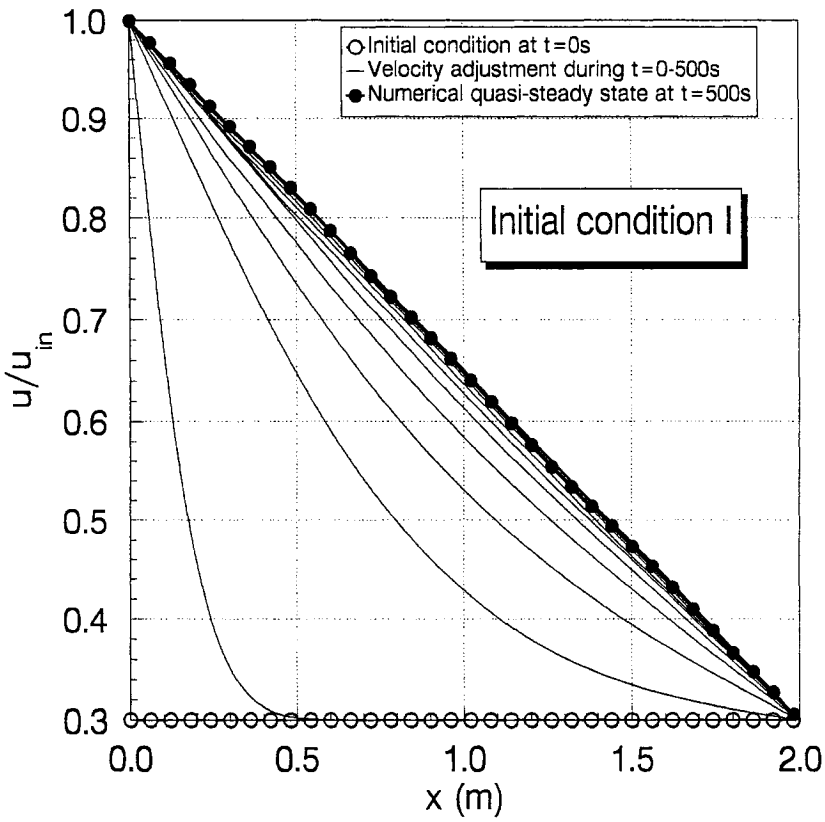

Fig. 10.15(a). Velocity-distribution history in accumulating reservoir-initial condition-I

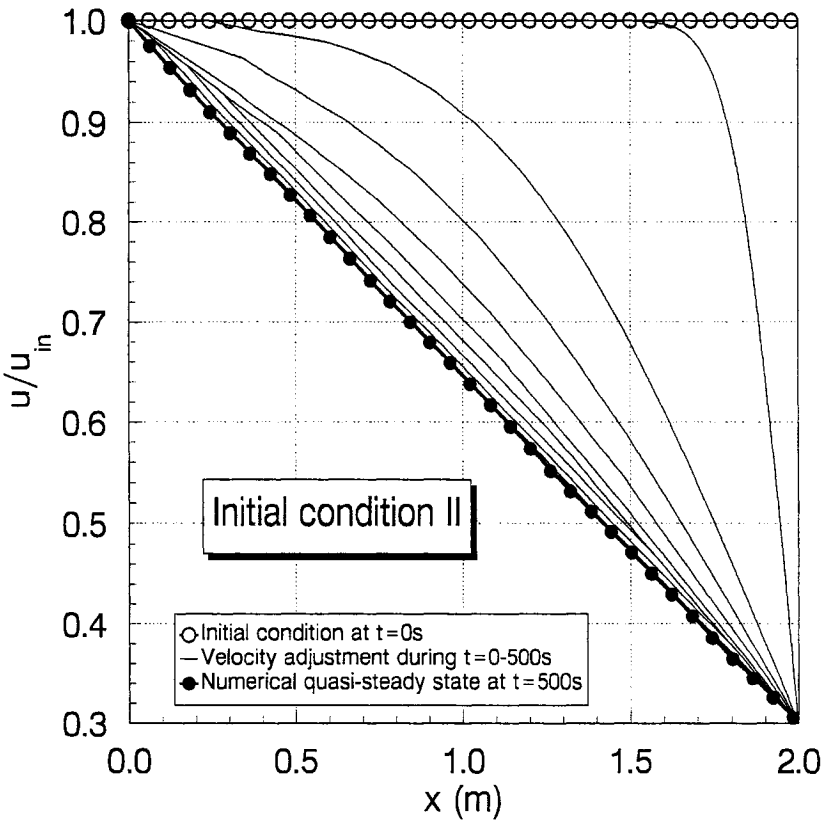

Fig. 10.15(b). Velocity-distribution history in accumulating reservoir-initial condition-II

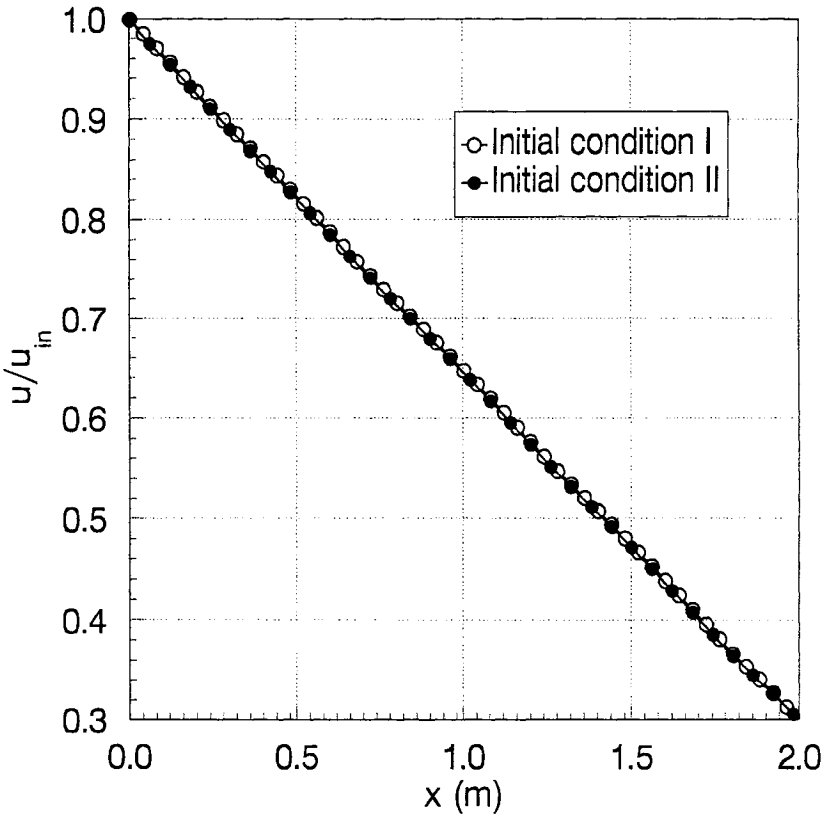

Fig. 10.16. Quasi-steady state velocity distribution in accumulating reservoir

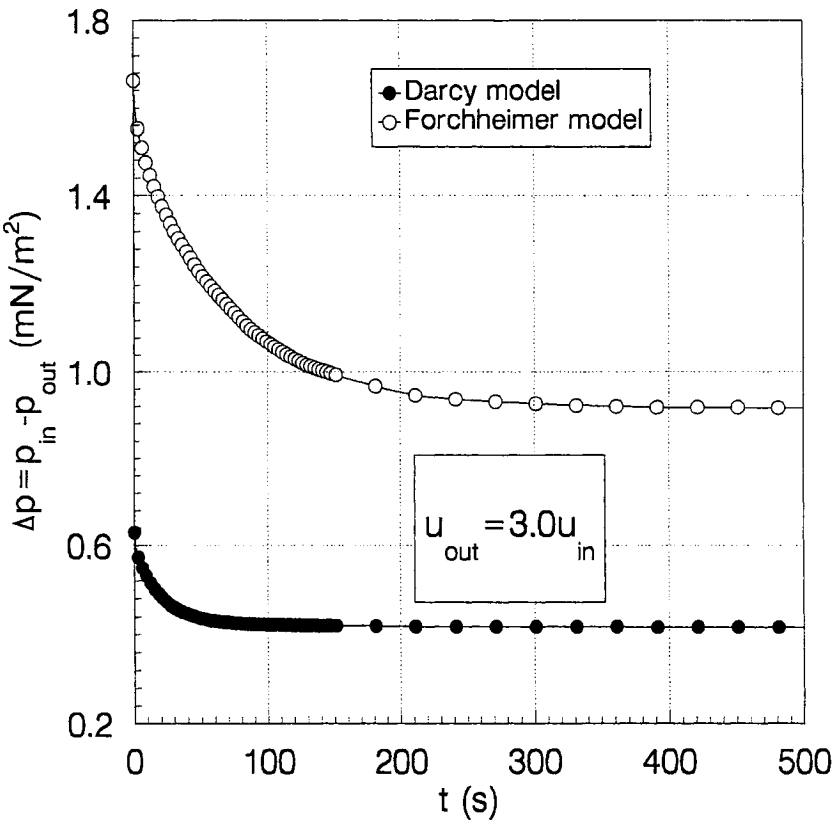

Fig. 10.17. Pressure-drop history in depleting reservoir

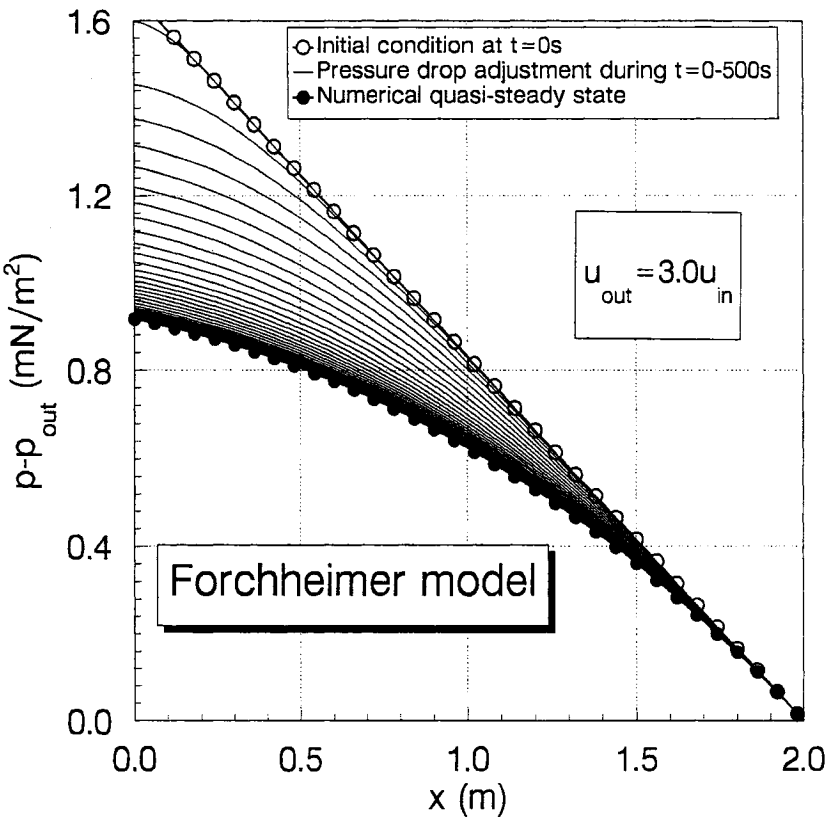

Fig. 10.18. Relative-pressure history in depleting reservoir

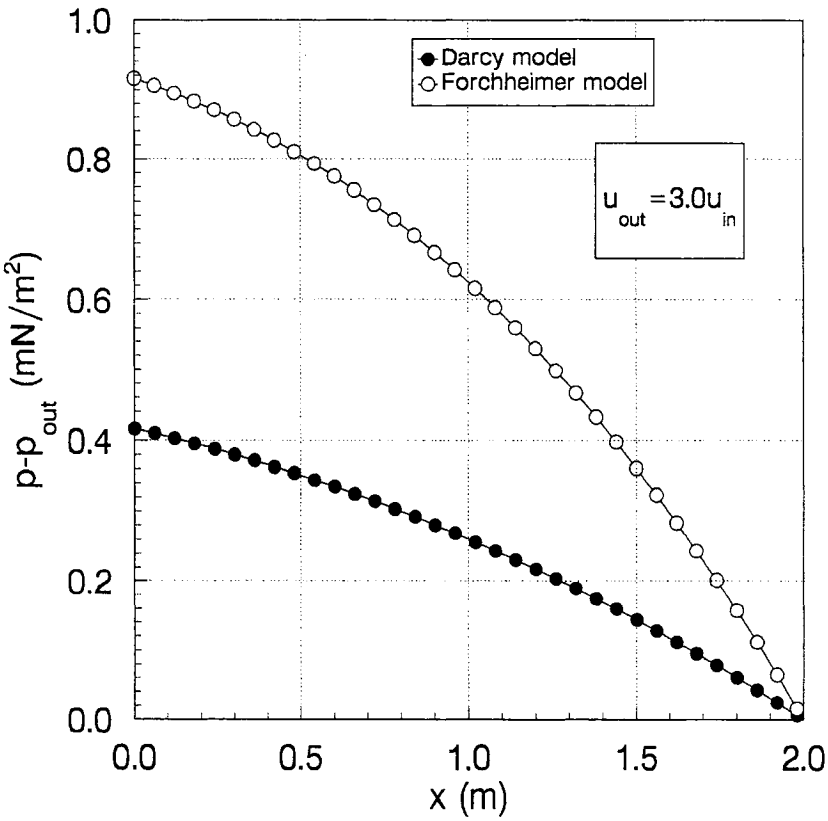

Fig. 10.19. Quasi-steady state relative-pressure distribution in depleting reservoir

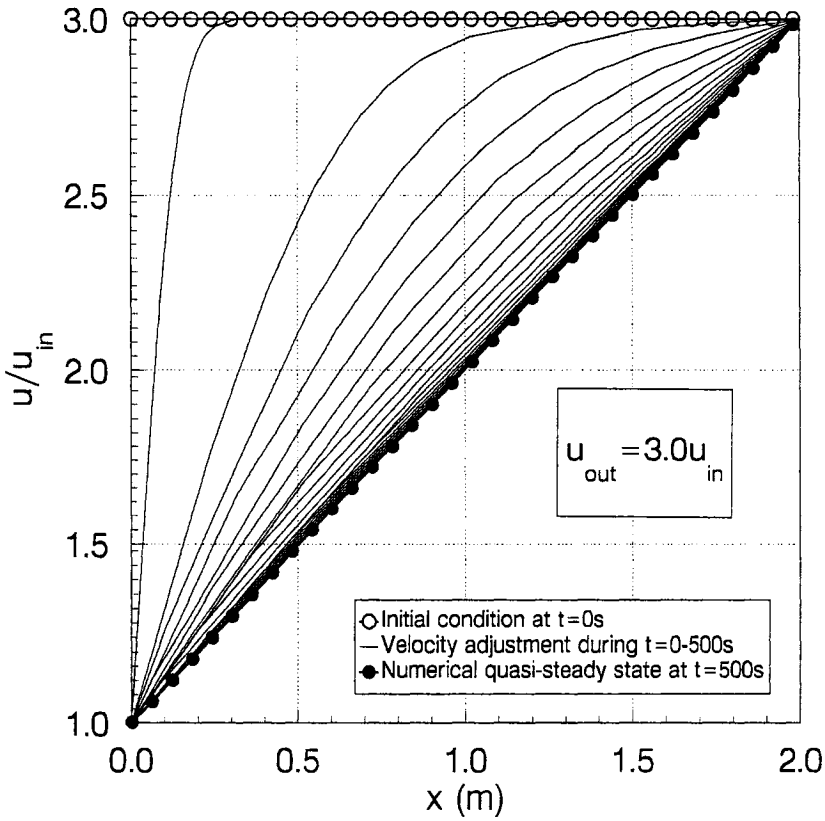

Fig. 10.20. Velocity-distribution history in depleting reservoir

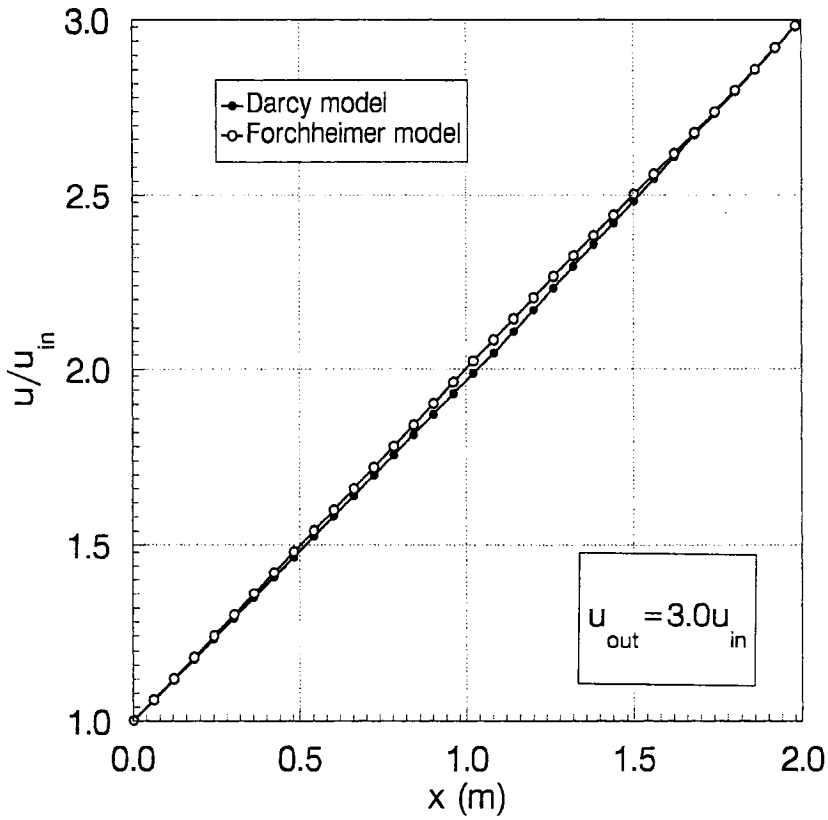

Fig. 10.21. Quasi-steady state velocity distribution in depleting reservoir

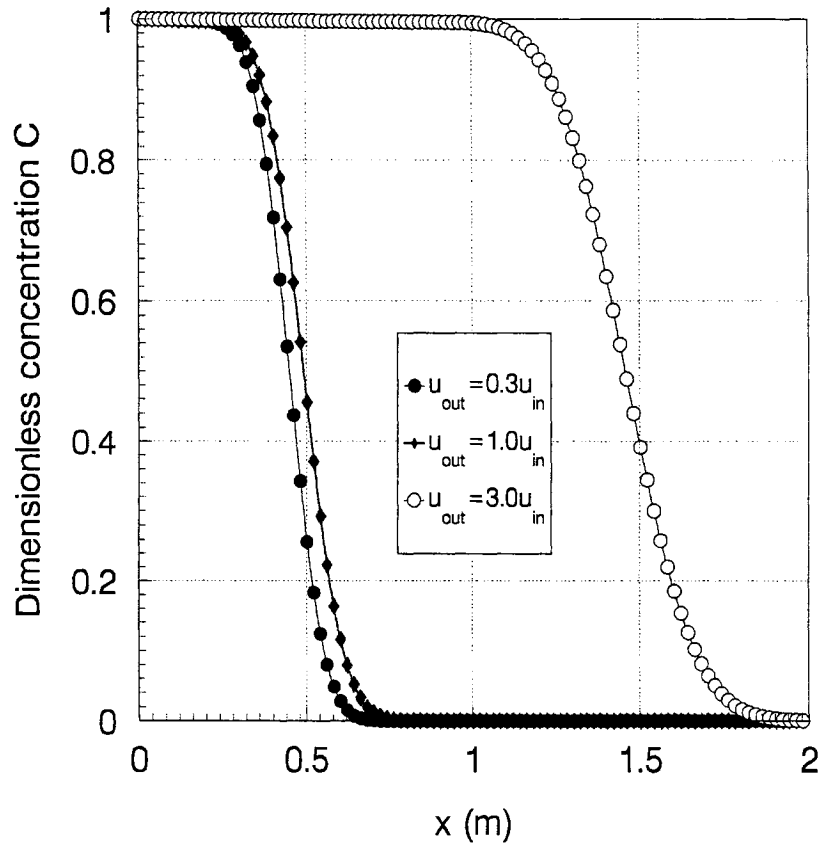

Fig. 10.22. Concentration development in different types of reservoir at t*=0.5

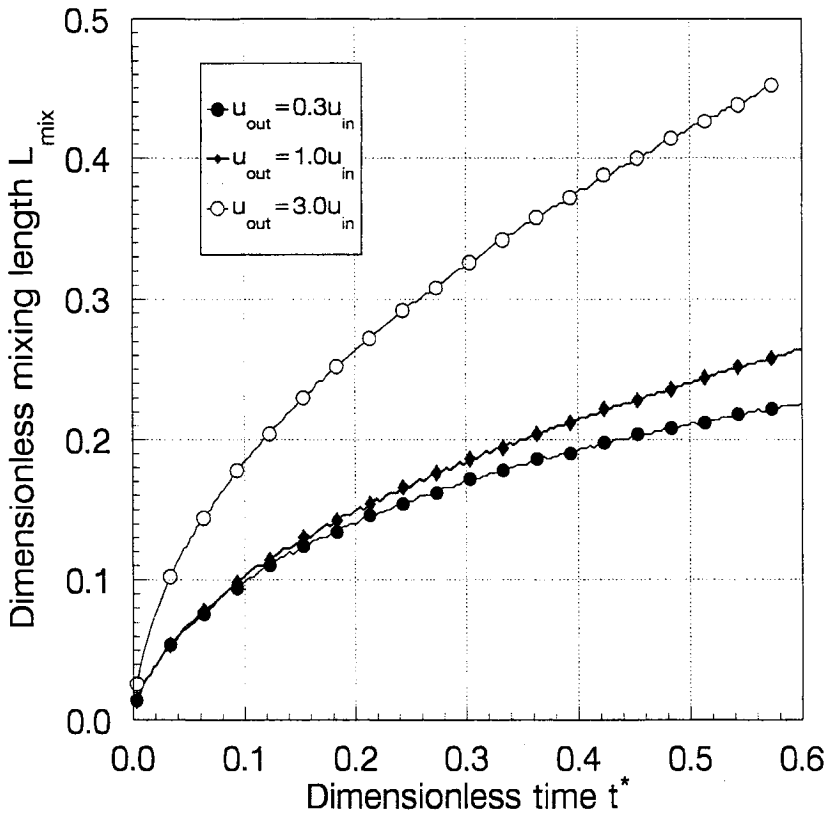

Fig. 10.23. Mixing length profile in different types of reservoir

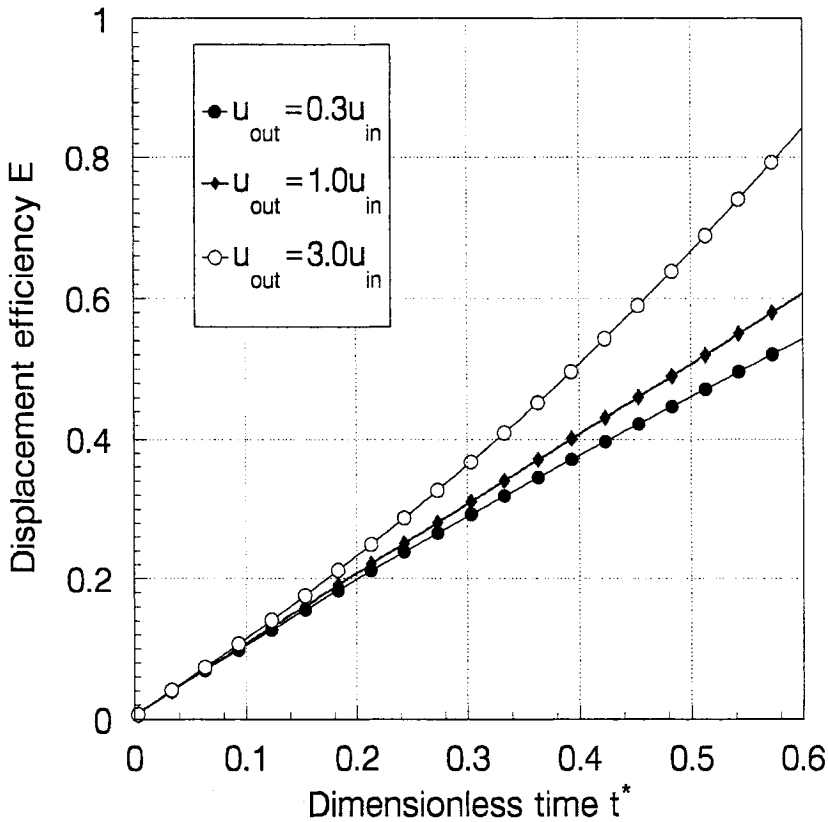

Fig. 10.24. Displacement efficiency in different types of reservoir

Chapter 11

11 THE AREAL SWEEP EFFICIENCY OF THE FIRST CONTACT MISCIBLE DISPLACEMENTS: AN EXPERIMENTAL APPROACH

11.1. Abstract

Solvent flooding using the water alternating gas (WAG) technique is very important for predicting the process performance. This technique has been employed in a number of oil fields. However, little data are available in the literature. Therefore, there is an immense need for the sweep efficiency data resulting from first contact miscible flooding particularly in view of conducting reservoir simulation studies. In this papet, we conducted a series of WAG displacements through glass bead packs. A number of miscible WAG displacement tests were conducted at WAG ratios of 1:1, 1:2 and 2:1. Constant flow rates were used to mask the effects of capillary number on sweep efficiency. Experimental results revealed that the WAG ratio affects the sweep efficiency of the miscible flooding process. In addition, new correlations of areal sweep as function of mobility ratio at various WAG ratios were developed. The data provided can be useful to the oil industry in conducting analytical and numerical modeling studies of miscible WAG processess.

11.2. Introduction

Miscible gas flooding has been widely used as an enhanced oil recovery process in many oil fields around the world. In most oil field applications, the injected gas has a lower viscosity than the reservoir oil. This leads to unfavorable injected gas/reservoir oil mobility ratio and low sweep efficiency. In order to alleviate this problem, the water-

alternating-gas (WAG) process has received considerable interest. Christensen et al. (1998) reviewed some sixty WAG field experiences from the first reported WAG in 1957 in Canada up to new experience in the North Sea. Field experience shows that the WAG process helps decrease the mobility ratio and also reduces the volume of gas required, which improves the economics of the process.

Traditionally, there has been widespread use of the five spot well network in secondary and tertiary recovery operations. The effects of fluid mobility ratio on areal sweep efficiency on breakthrough for a five-spot well pattern was studied by Fay and Prats (1951) as well as Cheack and Menzie (1955) using fluid mapped models; by Armofsky and Ramey (1956) with an electrolytic tank; Bredley et al. (1960) using potentiometer models; and by Dougherty and Sheldon (1961) employing the analytical method. Table 11.1 presents summary of the reported areal sweep efficiency for a five-spot pattern as a function of mobility ratio. The studied system in the previous work was immiscible system. Habermann (1960) studied the effects of miscible slug size that was varied from 10 to 25 percent hydrocarbon pore volume on oil recovery keeping the mobility ratio constant. Habermann (1960) concluded that at high mobility ratio, a miscible slug of 10 percent hydrocarbon pore volume would deteriorate after only a small fraction of the reservoir was swept. Mahaffey et al. (1966) studied the effects of slug size on sweep efficiency by utilizing a five spot pattern of a parallel-plate glass model. Mahaffey (1966) indicated that the presence of a slug increased the sweep efficiency of the oil-solvent system. Lacey et al. (1961) published areal sweepout results for a high pressure (five-spot model), for which propane slugs displaced methane saturated refined crude oil. Lacey (1961) concluded that using Liquid petroleum gas (LPG) slugs of 5% pore volume or less are not effective in increasing oil recovery in horizontal reservoirs.

Stalkup (1983) presented a graphical technique for estimating the optimum WAG ratio from the water-solvent fractional flow. In this method, the water-oil and water-solvent permeabilities were assumed to be the same. In addition, the effects of capillary pressure

on small scale displacement efficiency and the sensitivity of relative permeability as a function of rate (Heaviside et al., 1983; Heaviside et al., 1987) were neglected.

Zekri and Natuh (1992) studied the effects of miscible WAG process on tertiary oil recovery and found that the process did not have any significant effect on total oil recovery in water flooded sandstone oil-wet system. The effects of areal sweep efficiency were not considered in their study since a composite model was employed.

Al-Shuraiqi et al. (2003) investigated the impact of first contact-miscible WAG injection on oil recovery by conducting a series of secondary, miscible WAG displacements through glass bead-packs at WAG ratios of 1:1, 4:1 and 1:4. These laboratory WAG displacements were performed for a range of flow rates in order to investigate the influence of capillary number on recovery efficiency. The results were compared with those obtained from simple miscible injection and water flooding and it was found that the recovery efficiency is a function of rate as well as WAG ratio. Moreover, it was noted that the water-oil and the water-solvent relative permeabilities were not the same for the analogue fluids used, in spite of the fact that the oil and solvent are first contact miscible. Al-Shuraiqi (2003) also commented that the literature lacks sufficient laboratory data regarding WAG displacement efficiency.

Gas enrichment is considered to be one of the most important variables during WAG enriched-gas drives (Solano, 2000; Johns et al., 2003). The optimization of the WAG processes for enriched gas floods above the minimum miscibility enrichment (MME) composition, particularly as a primary recovery method was examined by Johns et al. (2003). In this study, the compositional simulations of x-z cross-sections were conducted to quantify the effects of WAG parameters, numerical dispersion, level of enrichment, heterogeneity on local displacement efficiency and sweep efficiency. One of the most important findings of this study was the richer the gas above the MME, the fewer the number of WAG cycles required for maximum oil recovery at a given WAG ratio. The

increase in recovery as a result of gas enrichments above the MME can be attributed to two facts: a) the density and viscosity of gas increase with enrichment, and in turn, increase the sweep efficiency; b) due to mixing, multicontact miscible flood (MCM) may occur followed the development of two-phase flow. Richer gases have the tendency to mix closer to the locus of the two-phase zone creating a slower as well as smaller lean gas bank, which can increase the sweep efficiency. Interestingly, the continuous slug injection was found to perform better than the WAG process in situations when a) the bottom of the aquifer has the largest permeability layers; b) richer gases are used, and c) the vertical to horizontal permeability ratio is small (Johns et al., 2003).

For miscible displacements, the Hele-Shaw model is believed to adequately represent a porous medium as long as the appropriate scaling rules are applied in its design and operation (Pozzi and Blackwell, 1963; Mahaffey et al., 1966). The radial flow of power-model fluid flow in a Hele-Shaw model developed by Lee and Claridge (1968) is shown in Fig. 11.1. In this study, the areal sweep efficiency of oil displaced by polymer solution was measured in a Hele-Shaw model representing one quarter of a five spot pattern. It was found that the areal sweep at breakthrough was less than what would be if the polymer solution were a Newtonian fluid of comparable average viscosity. However, the areal sweep at later phase of the flood was considerably higher than if polymer had not been added to flood water.

In this paper, the Hele-Shaw type of model filled with glass beads was used. The purpose of this investigation is to provide some additional laboratory data that would be useful to determine the areal sweep efficiency of a WAG process. Three WAG ratios, 1:1, 1:2 and 2:1, with mobility ratios varying from 0.456 to and 45.206 were examined. These examionations are important in finding the relationship between the sweep efficiency and the mobility ratio, and the sweep efficiency and the WAG ratio. A WAG process may affect areal sweep efficiency of a miscible process by alterating relative permeability of the system. In this study, however, the mobility ratios are calculated based on the

assumption that the end-point relative permeabilities of the displacing fluid and the displaced fluid are same, which can be considered a valid assumption for a miscible flow of fluids in a porous system. In other word, the mobility of our systems can be simply calculated using the inverse viscosity ratio.

11.3. Experimental procedure

With an injection well at one corner and a production well at the other corner, Fig. 11.1 represents a symmetry element of one quarter of a completely developed five spot pattern. Glass beads of a fixed mesh number (mesh no. 10) were used in all experimental runs in the model to represent a porous, anisotropic, and homogenous system. In this miscible displacement model, the molecular diffusion is assumed to predominate. The parallel plate spacing was favorably controlled by removing specific amount of thickness from one of the plates leaving the surrounding edges in tact. During the experimental runs, it was observed a spacing of 1.2 cm resulted in minimum mixing. The model area was 412 sq. cm. and the distance between the injection point and the producing point was 28 cm. Tweleve flood experiments were conducted in the laboratory at a constant temperature of 20°C. Primarily, two types of mineral oils were utilized in this study. These oils are called, Oil A and Oil B of which the specifications are shown in Table 11.2 and Table 11.3, respectively. The first six WAG tests were conducted with Oil A and Oil B as the slugs when the mobility ratios were 2.189 and 0.456, respectively. Six displacement runs were conducted with kerosene as the slug at relatively higher mobility ratios of 20.65 and 45.206. Kerosene was considered to be a prototype of Newtonian fluids.

In all experimental runs, the displacements were carried out with colored fluids. A dye, insoluble in oil, was used to color the fluid in order to trace the front and estimate the areal sweep. The production history was obtained by tracing the colored area. A Lucite tube, which was square in its cross section, was placed at the production point of the

system and flow passed through the section. Besides, a light source was placed under the model in order to determine the percentage of displaced (clear) and displacing (colored) area of the model during the experimental runs.

The flooding procedure can be summarized in the following steps:

- The model was throughouly cleaned, dried, and packed completely with glass beads;
- The model was checked for the uniformity of the pore volume;
- The model was saturated with the specific oil (displaced fluid) and the total pore space was estimated based on the amount of fluid injected in the model. Constant hydrostatic head was utilized in the fluid injection process;
- Total pore volume of fluid injection was kept constant for all runs at 20% of the pore volume;
- In the WAG 1:1 tests, 5% pore volume of fluid was injected at each cycle (with equal proportion of water and slug in it) amd the process was repeated for four cycles.
- In the WAG 1:2 tests, a total of 6.666% pore volume of water and 13.333% of solvent was injected.
- In the WAG 2:1 tests, a total of 6.666% pore volume of solvent and 13.333% of water was injected.
- Upon completion of 20% pore volume of water plus solvent injection, flow pattern of different stages were traced on transparency paper.

A number of assumptions underlying all of the displacement runs were invoked. The flow is assumed to be horizontal; permability is assumed constant; no cross flow is in effect, and the effects of gravity force are negligible.

11.4. Results and discussion

Figures 11.2 to 11.13 show the shape of the displacing fluid at the breakthrough point for all experimental runs. These are obtained by tracing different flood front profiles.

In order to determine the effects of WAG ratio on sweep efficiency, three WAG ratios, 1:1, 1:2 and 2:1 were studied in this paper. The effects of WAG ratios are determined for four mobility ratios ranging from 0.456 to 45.206.

Figures 11.2 through 11.4 show the frontal movement for a fixed mobility ratio of 2.189 and at WAG runs of 1:1, 1:2, and 2:1 respectively. A significant difference is observed among the figures. Figure 11.3 shows that the least amount of oil A (displaced fluid) is left in the WAG 1:2 case, while a significant portion of Oil A is trapped in the WAG 1:1 test (Fig. 11.2). The total pore volume of the model was approximately 200 cc. Table 11.4 shows that at a mobility ratio of 2.189, the contacted areas are 300, 322, and 156 cm^2 for WAG ratios of 1:1, 1:2 and 2:1, respectively.

Table 11.4 also shows that a reduction of mobility ratio by five times (mobility ratio of 0.456), resulted in a contact of 316 cm^2 by the solvent for WAG ratio of 1:1, 322 cm^2 for WAG ratio of 1:2 while only 162 cm^2 for WAG ratio of 2:1. The corresponding figures (Figures 11.5 through 11.7) are constructed for WAG ratios of 1:1, 1:2 and 2:1 respectively for mobility ratio of 0.456. In these runs, Oil A was used as the slug while Oil B was the fluid displaced. The white area in these figures represents the unswept fluid (Oil B). A comparison among the figures illustrate that the WAG 1:2 had the least white area while the WAG 2:1 experiences a significant area of undisplaced fluid of Oil B.

Figures 11.8 through 11.13 represent the schematics for displacement runs for which kerosene was used as the slug and Oil B (Figs. 11.8-11.10) and Oil A (Figs. 11.11-11.13)

were the displaced fluids at mobility ratios of 20.65 and 45.206, respectively. Once again, in both sets of Figs. 11.8-11.10 and Figs. 11.11-11.13, the best performance was obtained by using WAG 1:2 (see Fig. 11.9 and Fig. 11.12). The quantitative results of these two sets (Figs. 11.8-11.10 and Figs. 11.11-11.13) also appear in Table 11.4. The table shows that by changing the flood mobility to 20.65 and conducting the experiment at various WAG ratios of 1:1, 1:2 and 2:1, yield an areal invasion of 248 cm^2, 280 cm^2 and 120 cm^2, respectively. If the mobility ratio is further increased from 20.65 to 45.206, the area invaded decreases (200 cm^2, 248 cm^2 and 100 cm^2 for WAG ratios of 1:1, 1:2 and 2:1 respectively).

Figure 11.14 presents the plot of sweep efficiency as a function of WAG ratios. It shows that for all mobility ratios, as the WAG ratio increases from 0.5 (WAG 1:2 tests), the sweep efficiency decreases. The least efficiency is noted for WAG ratio of 2 (WAG 2:1 tests) denoting the fact that the WAG 1:2 is the optimum system.

For a mobility ratio of 0.456, the area sweep efficiencies of WAG ratios of 1:1, 1:2 and 2:1 are 0.79, 0.83 and 0.405 respectively and there is a linear relationship between sweep efficiency and WAG ratio. However, as mobility ratio increases, the relationship between sweep efficiency and WAG ratio does not show a linear relationship, and can be described by a second order polynomial. The calculated areal sweep for a mobility ratio of 2.189 is 0.75, 0.805, and 0.39 for WAG ratios of 1:1, 1:2 and 2:1, respectively. The nonlinear relationship between sweep efficiency and WAG ratio is also evident for tests with other two mobility ratios of 20.65 and 45.206. For a mobility ratio of 20.65, the resulting area sweeps were 0.62, 0.70 and 0.3 for WAG ratios of 1:1, 1:2 and 2:1, respectively while the efficiency dropped to 0.5, 0.62 and 0.25 for the WAG systems of 1:1, 1:2 and 2:1, respectively.

The effects of mobility ratio on areal sweep efficiency at different WAG ratios are plotted in Fig. 11.15. Calculations show that if the mobility ratio is increased from 0.456 to

45.206, the areal sweep efficiency decreases by 33%, 58% and 62% for WAG ratios of 1:2, 1:1 and 2:1 respectively. The relationships between the areal sweep efficiency and the WAG ratio at different mobility ratios and between the areal sweep efficiency and the mobility ratio at different WAG ratios based on the experimental work are given in Table 11.5. This set of equations can be useful in conducting miscible flood performance analyses through analytical and/or numerical models as well as to estimate the sweep efficiency of a changeable mobility system, i.e. the mobility of the system increases or decreases as the miscible flood progresses in the reservoir using WAG methods.

Increasing the mobility ratio from 0.25 to 2.0 results in noticeable decrease in areal sweep efficiency (Table 11.1). However, the effect of the change of mobility ratio on areal sweep efficiency is less pronounced if the optimum WAG scheme (WAG 1:2) is followed for low range of mobility ratios (0.4 to 2.189).

11.5. Conclusions

The following conclusions can be drawn from the results obtained in the present experimental study:

1. The WAG scheme is found to improve the areal sweep efficiency at breakthrough for enclosed five-spot pattern. At any mobiliy ratio in between 0.45 and 45, an increase in WAG ratio from 0.5 to 2.0 is found to lower the areal sweep. Also, at any WAG ratio in between 0.5 and 2.0, an increase in mobility ratio from 0.45 to 45.0 will drop the areal sweep efficiency. The estimations of the areal sweep is possible by utilizing the equations provided in this paper.
2. Of the three WAG schemes (1:1, 1:2 and 2:1), WAG 1:2 was found to be the most efficient scheme.
3. For the range of mobility ratio as low as 0.4 to 2.0, any change in the ratio has less effect on areal sweep efficiency if the water alternating solvent scheme is used.

11.6. References

Al-Shuraiqi, H. S., Muggeridge, A. H., and Grattoni, C. A., (2003) Laboratory investigations of first contact miscible WAG displacement: the effects of WAG ratio and flow rate, SPE 84894, SPE International Improved Oil Recovery Conference in Asia Pacific, Kuala Lumpur, Malaysia, October 20-21

Armofsky d. w., and Ramey, H. J., (1956) Mobility ratio-Its influence on injection or production histories in five-spot water flood, Journal of Petroleum Technology, vol. 8, no. 9, pp. 205-210, September

Bradley H.b., Heller, J.P. and Odeh, A.S., (1961) A potentiometric study of the effects of mobility ratio on reservoir flow patterns, SPE 1585-G, Society of Petroleum Engineering Journal, pp. 125-129, September

Cheek, R.E. and Menzie D.E., (1955) Fluid mapper model studies of mobility ratio, Petroleum Transactions, AIME, vol. 204, pp. 278-281

Christensen, J.R., Stenby, E.H. and Skauge, A., (1998) Review of WAG field experience, SPE 39883, International Petroleum Conference and Exhibition of Mexico, Villahermosa, Mexico, March 3-5

Fay, C.H. and Prats, M., (1951) The application of numerical methods to cycling and flooding problems, Proceedings of the 3rd World Petroleum Congress

Habermann, B., (1960) The efficiency of miscible displacement as a function of mobility ratio, Trans., AIME, vol. 219, p. 264.

Johns, T. R., Bermudez, L., and Parakh, H., (2003) WAG optimization for gas floods

above the MME, SPE 84366, SPE Annual Technical Conference and Exhibition, Denver, Colorado, USA, October 5-8

Lacey, J. W., Faris, J. E. and Brinkman, F. H., (1961) Effect of bank size on oil recovery in the high-pressure gas-driven LPG-bank process, Trans. AIME, vol. 222, p. 806

Lee, K. S., and Claridge, E. L., (1968) Areal sweep efficiency of pseudoplastic fluids in a five-spot Hele-Shaw model, Society of Petroleum engineering Journal, pp. 52-62

Mahaffey, J.L., Rutherford, W.M. and Matthews, C.S., (1966) Sweep efficiency by miscible displacement in a five-spot, Society of Petroleum engineering Journal, vol. 3, p. 73.

Pozzi, A., L., and Blackwell, R. J., (1963) Design of laboratory models for study of miscible displacement, SPE 445, Society of Petroleum Engineering Journal, pp. 28-40, March

Dougherty E. L. and Sheldon, J. W., (1964) The use of fluid-fluid interfaces to predict the behavior of oil recovery processes, SPE 183, SPE Journal, pp. 171-182

Solano, R., (2000) Effect of mixing mechanisms on recovery by enriched-gas injection above the minimum miscible enrichment (MME), Masters thesis, University of Texas at Austin, USA

Stalkup, F.I., (1983) Miscible displacement, Society of Petroleum Engineers Monograph Series, vol. 8, New York, USA, p 75

Zekri, A.Y. and Natuh, A., (1992) Laboratory study of the affects of miscible WAG process on tertiary oil recovery, SPE 24481, Abu Dhabi 5th Petroleum Conference and Exhibition, May 18-20

11.7. Appendices

11.7.1. Appendix A: Tables

Table 11.1. Effect of mobility ratio on areal sweep efficiency at breakthrough Enclosed five-spot pattern (Bradley et al., 1960)

Mobility ratio, M	Potentiometer analyzer Conductive Cloth-Uskon	Electrolytic Tank	Fluid Mapper	X-Ray Shadowgraph	Analytical Calculation
Infinite	62.6[Lee & Claridge]	62.5			
10		64.5	62.7	51.0	
4		65.8	62.0	54.0	45.3[Fay & Prats]
2	66.4	68.0	68.0	60.4	
1	68.8	70.0	71.7	69.8	71.5
0.25	71.6	88.5	78.0	87.0	
0.1	82.2	94.5	82.0	100.0	

Table 11.2. The specification of oil A

Specific gravity @ 60 °F	0.885
API	28.3
Saybolt viscosity @ 100 °F	350
Viscosity, cp @ 20 °C	52.2
Pour point, °F	-10
Flash point, °F	430
Fire point, °F	490
Distillation end point, °F	952

Table 11.3. The specification of oil B

Specific gravity @ 60 °F	0.840
API	36.9
Saybolt viscosity @ 100 °F	70
Viscosity, cp @ 20 °C	25.3
Pour point, °F	+15
Flash point, °F	345
Fire point, °F	420
Distillation end point, °F	844

Table 11.4. Areal sweep for WAG schemes at different mobility ratios

Mobility ratio	WAG	Displaced fluid	Slug	Drive fluid	Total PV, cc	Invaded area, cm^2
0.456	1:1	Oil B	Oil A	Water	205	316
	1:2				210	322
	2:1				205	162
2.189	1:1	Oil A	Oil B	Water	200	300
	1:2				205	322
	2:1				200	156
20.65	1:1	Oil B	Kerosene	Water	210	248
	1:2				220	280
	2:1				200	120
45.206	1:1	Oil A	Kerosene	Water	200	200
	1:2				215	248
	2:1				200	100

Table 11.5. Sweep efficiency as function of mobility ratio (M) or WAG ratio (WR)

Mobility ratio (M) or WAG ratio (WR)		Equation	R^2
M	0.456	$SE = -0.2033(WR)^2 + 0.225(WR) + 0.7683$	1.0
M	2.189	$SE = -0.1667(WR)^2 + 0.14(WR) + 0.7767$	1.0
M	20.65	$SE = -0.1667\ (WR)^2 + 0.15(WR) + 0.6667$	1.0
M	45.206	$SE = -0.2471(WR) + 0.745$	0.99
WR	1:2	$SE = 7E\text{-}05(M)^2 - 0.0076(M) + 0.8278$	0.99
WR	1:1	$SE = 7E\text{-}05(M)^2 - 0.0095(M) + 0.7831$	0.99
WR	2:1	$SE = 7E\text{-}05(M)^2 - 0.0066(M) + 0.4062$	0.99

11.7.2. Appendix B: Figures

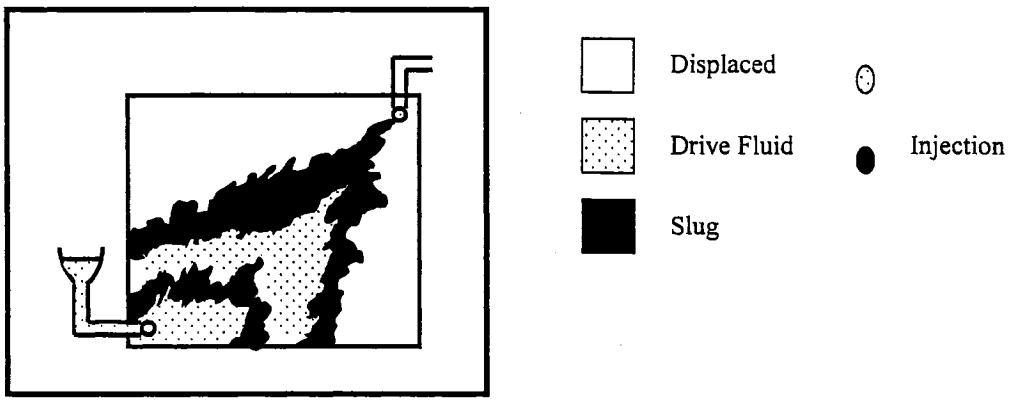

Fig. 11.1. Schematic diagram of the apparatus

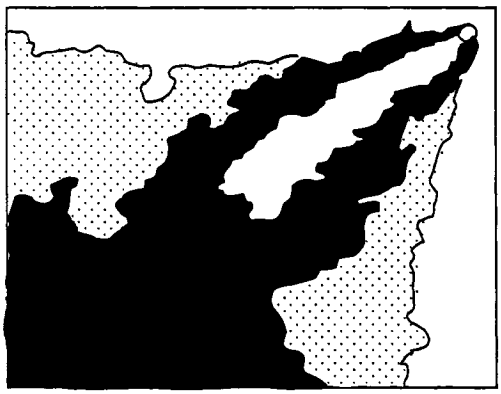

Fig. 11.2. Areal sweep of WAG 1:1 (MR: 2.189)

Fig. 11.3. Areal sweep of WAG 1:2 (MR: 2.189)

Fig. 11.4. Areal sweep of WAG 2:1 (MR: 2.189)

Fig. 11.5. Areal sweep of WAG 1:1 (MR: 0.456)

Fig. 11.6. Areal sweep of WAG 1:2 (MR: 0.456)

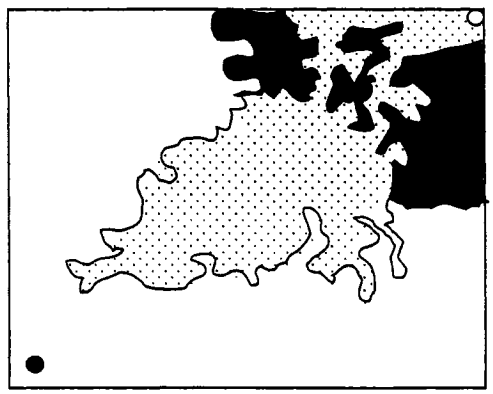

Fig. 11.7. Areal sweep of WAG 2:1 (MR: 0.456)

Fig. 11.8. Areal sweep of WAG 1:1 (MR: 20.65)

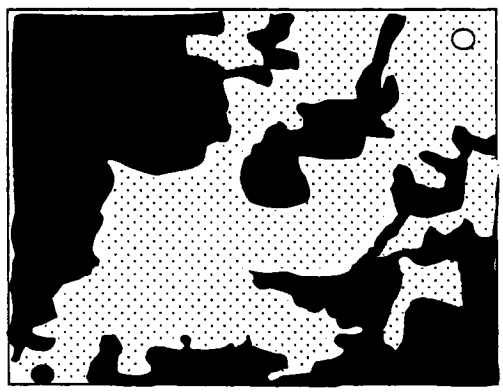

Fig. 11.9. Areal sweep of WAG 1:2 (MR: 20.65)

Fig.11.10. Areal sweep of WAG 2:1 (MR: 20.65)

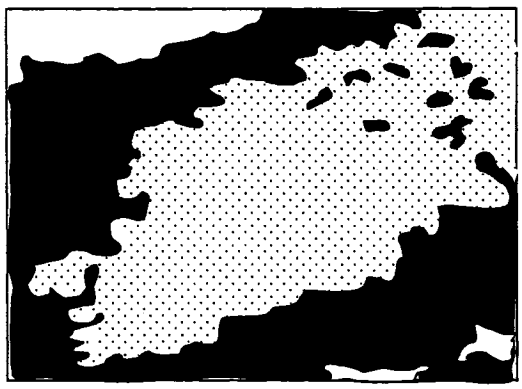

Fig. 11.11. Areal sweep of WAG 1:1 (MR: 45.20)

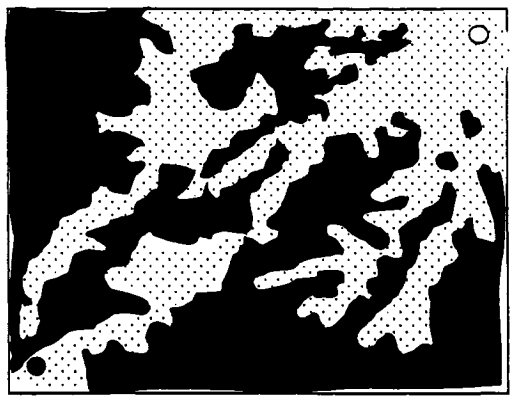

Fig. 11.12. Areal sweep of WAG 1:2 (MR: 45.20)

Fig. 11.13. Areal sweep of WAG 2:1(MR: 45.20)

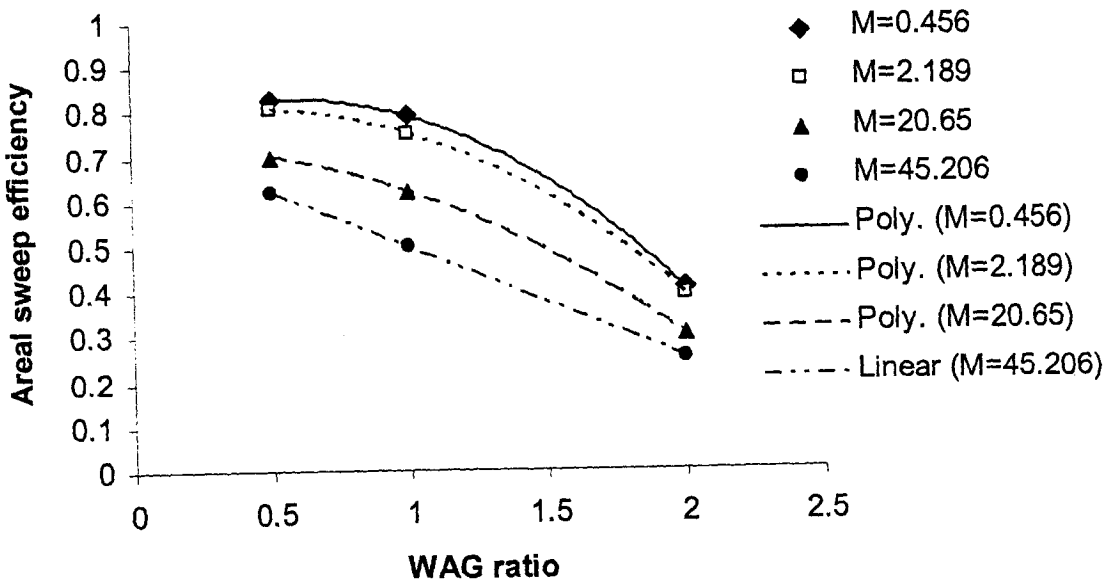

Fig. 11.14. Areal sweep efficiency vs. mobility ratio

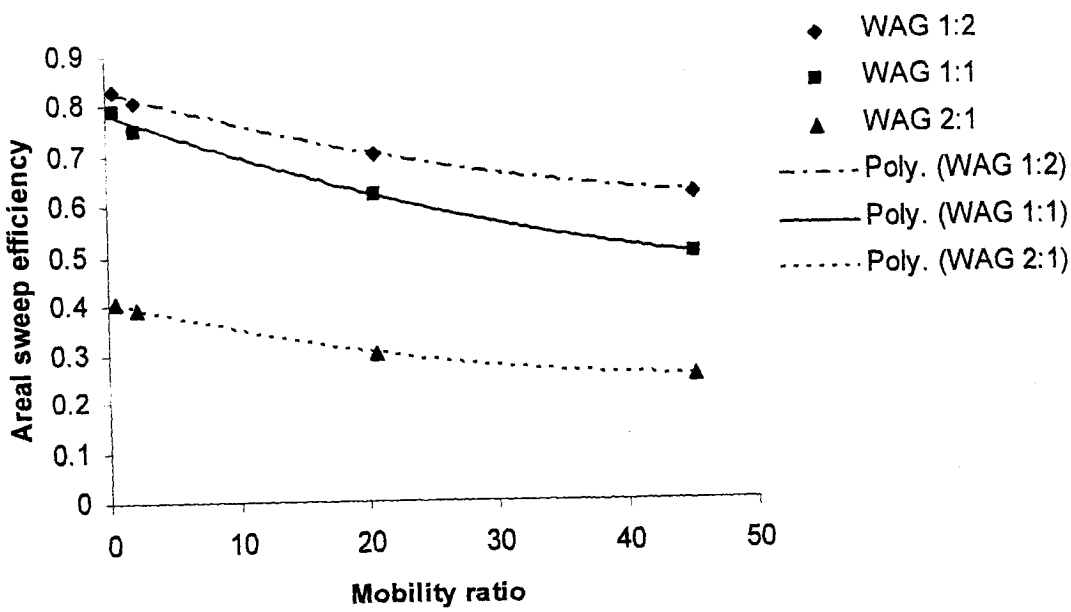

Fig. 11.15. Areal sweep efficiency vs. mobility ratio

Chapter 12

12.1 LASING INTO THE FUTURE: POTENTIALS OF LASER DRILLING IN THE PETROLEUM INDUSTRY

12.1.1. Abstract

The need for a new method of drilling oil and gas wells is immense. Current drilling techniques used were developed at the beginning of the last century. Many problems persist with this method including downtime due to dull bits, the lack of precise vertical or horizontal wells and formation fluid leakage during drilling due to the lack of a seal around the hole. Laser drilling is a new technology that has been proposed as a method to eliminate the current problems while drilling. Although experiments for laser drilling were conducted in the 1960's and 1970's, it is only recently that this research area has been redirected to the oil and gas industry.

This paper reviews the benefits of laser drilling, current laser types and the experimental work that has been conducted. The experimental work conducted thus far is performed with several different lasers such as the US Army's MIRACL and the US Navy's COIL. The data that was generated by these studies was executed on several types of cores including sandstone, limestone and shale. The effect that lasing has on porosity and permeability as well as the effect of saturation and pressure on lasing was determined. The work conducted shows that a great future potential awaits the oil and gas industry with laser drilling.

12.1.2. Introduction

The basic drilling technology currently used by the petroleum industry was developed 100 years ago when rotary drilling surpassed cable tool drilling as the standard method for reaching gas and oil formations. One of the major problems that persist with this method downtime and waste created by drilling mud. As well, when drilling horizontal wells into the formation, theoretically the borehole should be exactly as prescribed by reservoir engineers but it is difficult to achieve such precision with conventional drilling. Additionally, many of the problems associated with drilling occur because the borehole is not sealed and the formation fluid is allowed to seep into it or there is out-flux of drilling fluid into the formation. This can cause many problems such as differential pressure sticking, lost-circulation, swelling and collapse (O'Brien et al., 1999a). As well, the cost of drilling deep wells (20,000 ft) almost doubled between the years of 1979 and 1994 and the cost of drilling offshore between 1974 and 1994 has tripled (Graves and O'Brien, 1998a). The method of laser drilling will eliminate all of the above problems and can offer cost effectiveness by decreasing current drilling times.

Recently, lasers have recently been mentioned as a viable option to improve drilling technologies (Islam and Wellington, 2001). By eliminating the use of a drill bit with laser drilling, the downtime created by drill bits will be drastically reduced and the waste created due to drilling mud will be eliminated. This is especially important in offshore drilling where space limitations hamper operations. In fact, laser drilling can increase penetration rate by greater than 100 times over the conventional rotary drilling methods (Graves and O'Brien, 1999). This can be a tremendous benefit. Lasers can penetrate many different types of rocks including sandstone, limestone and shale (O'Brien et al., 1999a) thus reducing the problems that occur when conventional horizontal drilling is unable to achieve a perfectly straight borehole. As well, lasers may have the ability to melt the rock in a way that creates a ceramic sheath in the wellbore (USDOE, 2002), which would eliminate the problems encountered with formation fluid seepage. Besides,

a significant reduction in drilling cost can be expected with laser application capable of mono-diameter drilling deep into the hole from the surface. Additionally, laser drilling has the potential to be utilized for perforation drilling (Graves and O'Brien, 1998a). A study conducted by the Graves and O'Brien (1998b) for the Gas Technology Institute determined that laser drilling in the oil industry, especially with infrared lasers, is promising due to its excellent heat transfer characteristics. O'Brien et al. (1999a) pointed out that a combination of laser and rotary drilling might be advantageous due to the resulting increase in bit life. The development of downhole laser drilling machines, laser-assisted drill bits, laser-perforation tools, and sidetrack and directional laser drilling devices are all possible with the advancement of laser technology (Gaddy et al., 1998).

12.1.3. Background

The word Laser is an acronym for Light Amplification by Stimulated Emission of Radiation. Basically, lasers convert different forms of energy such as chemical, electrical, heat etc. into energy of light (intense photon). It is a source of electromagnetic coherent radiation where coherency stands for the temporal and spatial phase correlation of the propagation method. Petroleum applications of lasers include temperature measurement inside the wellbore (Woodrow and Drummond, 2001), mud cake thickness measurements (Amanullah and Tan, 2001) and asphaltene remediation in carbonate formations (Zekri et al., 2001). Islam (2001) outlined the application of laser for real-time monitoring and eventual dynamic reservoir management. There are two categories of lasers, Continuous Wave (CW) and Pulse or Repetitive Pulse (RP). Table 12.1.1 lists the various types of high power lasers that are viable for the oil and gas industry (O'Brien et al., 1999b, Graves and O'Brien, 1998a).

The processes of destroying rocks using laser involve the transfer of radiant energy into solids. This transfer is determined by three basic phenomena: reflection, scattering and absorption (Graves and O'Brien, 1998a). Absorption is the process by which heat is

collected by the rock eventually resulting in the destruction of that rock. Scattering is a function of the wavelength and roughness of the surface while the composition of the solid and the planar surface determines the reflection (Gahan et al., 2001). Both scattering and reflection represent the energy that is not absorbed by the rock or the losses in the system. Therefore, the following criteria were outlined by Graves and O'Brien (1998a) for the feasibility of laser drilling:

1. Low reflectivity of rocks resulting in good coupling of laser radiation with rocks
2. Deep penetration of laser energy into rock resulting in volumetric absorption of laser energy
3. Low thermal conductivity of rocks resulting in effective heating.

Physical or chemical changes that may occur in the rock during lasing are determined by rock composition, crystalline lattice structure, porosity, water saturation, hardness, strength, elasticity, laser power density, wavelength, band of radiation absorption and laser pulse length (Batarseh, 2001).

There are many factors in conventional drilling that determine the rate at which the borehole will be created. These factors include the weight-on-bit (WOB), mud circulation rate, rotary speed, hydraulic horsepower bit design and hole size. With laser drilling, this rate may only depend on the delivered power and the hole size (O'Brien et al., 1999a) thus eliminating complexity of current drilling systems.

12.1.4. Experimental review

Experimental work pertaining to laser drilling dates back to the late 1960's and early 1970's (Moavenzadeh et al., 1968; Carstens and Brown, 1971). Moavenzadeh et al. (1968) lased marble and granite to test the lasers ability to weaken the rock. The laser operated at a power output of 750 Watts and the rocks were irradiated for 1, 3, 5, 10, and

30 seconds. Two diameters of beam were applied, 0.3 cm and 3 cm. It was found that the length of lasing time was comparative to the extent of damage. It was also discovered that the damage to the rock was not only surface damage but the laser also had an effect on the interior of the sample. As well, the 0.3 cm diameter beam resulted in more visual damage. Failure tests were conducted and it was determined for granite that has been exposed to lasers for 3 to 5 seconds showed a reduction in strength by 85% and for marble by 100%. Carstens and Brown (1971) used a CO_2 laser to determine its ability to cut rocks. Two different types of tests were run: kerfing and penetration. It was found that all rock types examined, granite, limestone, basalt, dolomite, and concrete, were cut by the laser although the amount of success in granite was hindered by the development of viscous glassy melt. In 1990, Mauer et al. (1990) suggested that laser drilling was not feasible but that was based on the old information provided by the early low powered lasers.

Due to advancements in laser technology, some experimental work on this topic has recently been undertaken. Graves and O'Brien (1998a) conducted an experiment to determine the feasibility of the US Army's MIRACL (Mid Infrared Advanced Chemical Laser) for drilling gas wells. MIRACL is a continuous wave laser with a wavelength of 3.8 μm and a power output of 600 to 1200 kW. Two 9 Darcy dry sandstone samples of twelve by twelve by three were used to drill six inch and two inch diameter holes. The six inch diameter sample was created to determine the amount of rock removed by a full laser beam. The laser was directly pointed at the slab and a 2.5 inch deep hole was created after only 4.5 seconds of exposure. This resulted in the removal of 5.5 pounds of rock and an equivalent rate of penetration (ROP) of 166 ft/hr. The purpose of drilling the two inch diameter drill was to test the lasers ability to drill horizontally for perforation purposes. The output power for this test was 500 kW. The rock was exposed to the laser for 2 seconds and a six inch deep hole was produced during this time. The equivalent ROP for this run was 450 ft/hr. As well after the completion of the experiment, the initial

permeability was compared to the final permeability around the hole and no change was found.

O'Brien et al (1999a) tested various types of cores under various conditions with the US Air Force's Chemical Oxygen-Iodine Laser (COIL). This laser was designed to track and destroy missiles at a range of 31 miles. Since gas wells are drilled to approximately 3 miles this laser was chosen as a welcome candidate. COIL is a continuous wave laser with power levels between 5 and 10 kW and a wavelength of 1.315 μm. For each experimental run, a ¼ in diameter hole was made by 8 seconds of irradiation. Sandstone, limestone, shale, salt and granite were lased and the specific energy (SE) of each run was determined. It was found that the SE ranged from 10 to 40 kJ/cm^3 for 3 different power levels (100%, 50%, 35%) for all types of rock. The salt sample used the least SE for the 100% power level whereas limestone used the least SE for the other power ranges. As well, shale consistently used the greatest amount of SE. Although there is a correlation between the shale samples and SE, many of the samples were taken from different formations so it is very difficult to determine a correlation between SE needed, laser power and rock type. Batarseh (2001) compared the SE to ROP and found that consistently the lower the SE the greater the ROP for seven rock types including sandstone, shale and granite. Gahan et al. (2001) determined that limestone SE values were greater than shale. They concluded that this may be due to the color of the rock and in turn the reflective properties. Since limestone is lighter in color, it is less able to absorb the laser energy. To understand the effect of type of rock materials on SE, short drilling time can be very useful. The ablation of rock depends on the composition of the rock materials (Mauer et al., 1990). Since there are many factors, especially secondary effects that are involved with laser drilling activities, minimization of lasing time can be better indicative of the rock's effect. A longer period usually causes more penetration (depending of the rock type) and after attaining a depth, the purging system can no longer clean the by-products.

Sandstone, limestone, shale, salt and granite; were also lased to determine the effect of beam periodicity, that is continuous wave or chopped wave (O'Brien et al., 1999a). This test results were inconclusive as some chopping resulting in higher SE while others resulted in lower. The authors gave no explanation as to why this might be.

The impact of fluid saturation was studied by O'Brien et al. (1999a) and Batarseh (2001) with Berea Yellow Sandstone. Cores were saturated with fresh water, brine, oil and gas. The effect of saturation test showed that a greater amount of SE was needed to penetrate a saturated core than a non-saturated core but the difference in was not great.

The hole penetration limitations test was performed to determine if hole depth and vapor contamination in the wellbore will have a change on the ROP (O'Brien et al., 1999a). The samples were lased for 3, 6, 9, 12 and 15 seconds and it was found that the greater the exposure time, the greater the SE required. Gahan et al. (2001) also came to this conclusion when they irradiated shale, sandstone and limestone for 0.5, 1.0 and 1.5 seconds with a Nd:YAG pulsed laser. O'Brien et al. (1999a) and Batarseh (2001) cited that plasma screening may be a factor. Plasma screening basically means that a change in the atmospheric conditions inside the rock or in other words the formation of liquid or gas inside the hole. The gas that is formed due to this phenomenon has toxic potentials (Batarseh, 2001). Gahan et al. (2001) concluded that an increase in exposure time allows for the development of melted rock that acts as a barrier, which inhibits the laser from interacting with the virgin face of the rock and consumes laser energy. The greater the percentage of quartz in the rock, the greater the SE required will be due to this melting factor (Batarseh, 2001). Batarseh (2001) observed that different sized holes were created for different types of stones and that glass was found in some rock types such as feldspar and quartz after lasing. Table 12.1.2 summarizes the hole depth and volume obtained for different types of rocks under after 40 s of lasing time. As well, the diameter of the hole, beam shape and geometry also known as fluence may effect the SE required. Gas purging directed at the rock can also affect the SE requirements (O'Brien et al., 1999a). Gahan et

al. (2001) stated that gas purging minimizes the melted material and reduces gas condensation and debris (secondary effects) in the wellbore thus a more accurate SE can be found. The experimental work by Gahan et al. (2001) created a shallow hole whereas the experimental work by Batarseh (2001) involved melted deposits in a deeper hole thus eliminating some of the beneficial effects of gas purging. Hallada et al. (2000) discussed the importance of gas purging and described the function of the purging system. The functions include providing a transparent medium for the laser to pass through, the ability to clean the hole of debris and the ability to move molten rock into fractures to seal them as well as sealing of the wellbore wall. In the sandstone tests performed by Gahan et al. (2001), when the exposure time was increased from 0.5 sec to 1.5 sec, the 1.5 sec sample exhibited a greater SE for pulse repetition rate (W_p) of 400 pulses/sec. However, for a W_p of 200 pulses/sec, an opposite phenomenon was observed. This can be explained by Hallada et al.'s (2000) observations. They compared their test results to that of O'Brien et al.'s (1999b) and found that at the point where SE began to increase the hole depths were similar but the exposure time was not. Thus it was concluded that the main factor in determining efficiency was not exposure time but was the depth of the hole. This conclusion was reiterated when a comparison of depth-drilling speeds and volume-drilling speeds. Therefore, even though the exposure time increased from 0.5 to 1.5 seconds, the hole depth was not sufficient enough to have an effect on SE.

O'Brien et al. (1999a) also studied the hole penetration limitations associated with the effect of confining pressure with Berea Yellow Sandstone and the effect of gas atmosphere with Dry Berea Gray Sandstone. The effect of confining rock stresses test involved stresses applied in the horizontal, vertical and both horizontal and vertical simultaneously. The results showed that the unstressed sample had the lowest SE. Interestingly, the sample with both horizontal and vertical stresses showed lower SE than the samples with just horizontal and vertical. The authors offered no explanation for this and the amount of stress applied was not offered. During the effect of gas atmosphere test the atmosphere was composed of nitrogen and argon gases. The results showed the

nitrogen atmosphere resulted in less energy requirements than argon gas but the difference was only slight.

A comparison between vertical and horizontal shots was made by O'Brien et al. (1999a) in both continuous and chopped waveforms to determine which orientation requires the greatest SE. For the continuous wave, shale was the rock type used and for the chopped wave tests shale, sandstone and limestone were used. In all tests, the vertical shot required more energy than the horizontal shots. The authors gave no explanation for this but it may be because of gravitational effects. The vertical holes can become more easily contaminated with vapors from the laser and rocks whereas with horizontal shooting, the vapor is allowed to escape because gravity is not working against the base of the wellbore.

Gahan et al. (2001) conducted two sets of experiments with Nd:YAG laser. These are initial linear track tests and fixed laser parameter tests. In the linear track test, rectangular samples of Berea Grey sandstone, Frontier shale and Ratcliff limestone were selected. The continuous movement of the slab was followed under a fibre-optic beam with varying beam focal position with respect to the slab surface. This test exhibited different rock-laser reaction zones (areas of identical physical reaction) from the state of melting to scorching. Also, the associated parameters for each zone were determined in achieving the threshold parameters (corresponds to minimum SE). This experiment was also marked with losses during the fibre-optical delivery. The actual delivered power was in the range of 43%-73% of the calculated average power.

The effect of pulse width (W_p) and pulse repetition rate (R) are reported to affect SE (Gahan et al., 2001). An increase in pulse width causes an increase in energy absorption per unit area at a particular intensity. This reduces the SE value. Also, as the pulse width becomes higher there is less time for the samples to cool down raising the heat of the sample. Eventually, thermal stresses are reduced and SE decreases. An increase in pulse

repetition rate also decreased the SE value. Since low R indicates higher cooling time between successive pulses, the rock will cool down with fissure formation and SE will increase. The authors also stated that the dominant feature on SE is the effect of the W_p over R (in a finite range of R, SE drops more for higher W_p). However, this is not a very convincing conclusion since one comparison was made with varying W_p and peak intensity (I).

Batarseh (2001) discussed the effect of lasing on permeability, porosity and elastic moduli. Changes were determined with samples of sandstone, limestone and shale with COIL and as well sandstone with MIRACL. All samples were 5 cm long. It was shown that all samples had an increase in permeability throughout the sample length with the exception of one point. This result differed from Graves and O'Brien (1998a) who found no change in permeability. Due to the thermal conductivity of the rock, it was revealed that there was a permeability change in the stone even where the laser did not come in contact. The size of the hole created was not discussed and therefore the distance between the laser and the permeability change can not be determined from this study. The results of the change in porosity tests showed that the most significant increase was at 2 cm from the top of the sample. This was related to an increase in fractures. The size of the hole created was also not stated for this test. The elastic moduli test showed that Young's moduli, shear moduli, and bulk moduli were reduced for all rock types tested.

12.1.5. Conclusions

The work accomplished so far on laser drilling has resulted in some positive indications. The use of laser technology in petroleum well drilling is a very recent thought. Significant progress has to be made both experimentally and numerically in order to utilize laser techniques to enhance the drilling phase. In addition, detailed studies of changes to reservoir characteristics must be conducted. For example, to what extent will laser drilling create fractures? Experimental results for permeability showed differing

results in that some researchers recorded a change while others did not. Detailed permeability tests should be conduced to determine the exact change in permeability due to lasing. The impact of lasing under different solid-fluid phases present in the reservoir as well as including multiphase flow can be of immense importance to reservoir engineers. Understanding the stress-strain behavior under both confining and lasing conditions remains yet another formidable challenge. Researchers can develop a tri-axial setup with inherent laser source. Even coupling of two types of equipment to represent reservoir conditions will provide one with significant information. As well, health concerns regarding the formation on toxic gases during drilling must be addressed. Numerically, laser drilling is a new topic. Development of a 3-D model describing the drilling phenomenon, along with phase change in porous media, will be a pioneer work in this regard. The result of this challenging research on laser drilling will definitely prove it as the wave of the future.

12.1.6. References

Amanullah, Md. and Tan, C.P., (2001) A field applicable laser-based apparatus for mudcake thickness measurement, SPE 68673, SPE Asia Pacific Oil and Gas Conference and Exhibition, Jakarta, April 17-19

Gaddy, D., Moritis, G. and True, W., (1998) OTC papers highlight technological advancements, Oil & Gas Journal, May 18, p. 46

Gahan, B.C., Parker, R.A., Batarseh, S., Figueroa, H., Reed, C.B. and Xu, Z., (2001) Laser drilling: Determination of energy required to remove rock, SPE 71466, SPE Annual Conference and Exhibition, New Orleans, Louisiana, September 30 –October 3

Graves, R.M. and O'Brien, D.G., (1998a) StarWars laser technology applied to drilling and completing gas wells, SPE 49259, SPE Annual Technical Conference and Exhibition, New Orleans, Louisiana, September 27-30

Graves, R.M. and O'Brien, D.G., (1998b) Targeted literature review: Determining the benefits of StarWars laser technology for drilling and completing natural gas wells, GRI-98/0163, July

Graves, R.M. and O'Brien, D.G., (1999) Journal of Petroleum Technology, February, pp. 50-51

Hallada, M.R., Walter, R.F. and Seiffert, S.L., (2000) High-power-laser rock cutting and drilling in mining, In the proceeding of SPIE, High Power Laser Ablation 2000, vol. 4065-73, New Mexico, USA, April 23-28

Islam, M.R., (2001) Emerging technologies in subsurface monitoring of petroleum reservoirs, SPE 69440, SPE Latin America and Caribbean Petroleum Engineering Conference, Buenos Aries, Argentina, March 25 – 28

Islam, M.R. and Wellington, S.L., (2001) Past, present, and future trends in petroleum research, SPE 68799, SPE Western Regional Conference, Bakersfield, California, March 26-30

Mauer, W.C., Anderson, E.E., Hood, M., Cooper, G. and Cook, N., (1990) Deep drilling basic research, vol. 5, System Evaluations, Final Report, GRI-90/0265.5, June, 5-1

Moavenzadeh, F., McGarry, F.J. and Williamson, R.B., (1968) Use of Laser and Surface Active Agents for Excavation in Hard Rocks, SPE 2240, Fall Meeting of the Society of Petroleum Engineers of AIME, Houston, TX, September 29 - October 2

O'Brien, D.G., Graves, R.M. and O'Brien, E.A., (1999a) StarWars laser technology for gas drilling and completions in the 21st century, SPE 56625, SPE Annual Technical Conference and Exhibition, Houston, TX, October 3-6

O'Brien, D.G., Graves, R.M. and O'Brien, E.A., (1999b) International Society for Optical Engineering, V3614, San Jose, California, vol. 168, January 25-29

U.S. Department of Energy, (2002)
Available:
http://www.fe.doe.gov/oil_gas/drilling/laserdrilling.html [October 7, 2002]

Woodrow, C.K. and Drummond, E., (2001) Heat seeking laser sheds light on Tern, SPE 67729, SPE/IADC Drilling Conference, Amsterdam, February 27 – March 1

Zekri, A.Y., Shedid, S.A. and Alkashef, H., (2001) Use of laser technology for the treatment of asphaltene deposition in carbonate formation, SPE 71457, SPE Annual Technical Conference and Exhibition, New Orleans, Louisiana, September 30 – October 3

12.1.7. Appendices

12.1.7.1. Appendix A: Tables

Table 12.1.1. Laser types and wavelengths

Laser Type	Wavelength, μm	Comments
HF(DF) – Hydrogen Fluoride and Deuterium Fluoride	2.6 – 4.2	A continuous wave (CW) laser. Mid-Infrared Advanced Chemical Laser (MIRACL) is this type
COIL – Chemical Oxygen Iodine Laser	1.315	A continuous wave (CW) laser developed in 1977. It is considered to have the potential to remove drilling and re-completing petroleum problems such as side-tracking, directional drilling or well-control.
CO_2 Laser	10.6	It can be either continuous wave (CW) or repetitive pulsed (RP). The average power is 1 MW. It is durable and reliable although its large wavelength makes it inefficient.
CO Laser	5-6	It can be either continuous wave (CW) or repetitive pulsed (RP). The average power is 200 kW.

Laser Type	Wavelength, μm	Comments
FEL Laser – Free-Electron Laser	Any wavelength	It is a continuous wave (CW) laser. Since it can attain any wavelength, the laser can be adjusted to minimize reflection, scattering and plasma screening.
Nd:YAG – Neodymium: Yttrium Aluminum Garnet	1.06	Operate at a power of 4 kW.
KrF (Excimer) Laser – Krypton Fluoride Excimer	0.248	It is a repetitive pulsed (RP) laser. The maximum average power is 10 kW.

Table 12.1.2. Effect of a CO_2 laser on hole depth and volume after 40 s (Batarseh, 2001)

Hole Depth, cm	Hole Volume, cm^3	Rock
2.5-5.0	1.5-3.0	Limestone, dolomite, marl, travertine, gypsum, anhydrite
2.0-2.5	1.0-1.5	Limonite, granite aplite, liparite, pegmatite, rhyolith, obsidian, tuff, tuffite, agglomerate
1.0-2.0	0.5-1.0	Argillite, clay, kaolinite, mica schist, gneiss sandstone, graywacks, alevrolite
0.5-1.0	0.1-0.5	Quartzite, jasper, siliceous shale, anthracite, boghead
0.1-0.5	<0.1	Graphite shale, eclogite

Chapter 12

12.2 NUMERICAL INVESTIGATIONS OF THE PROSPECTS OF HIGH ENERGY LASER IN DRILLING OIL AND GAS WELLS

12.2.1. Abstract

Lasers are expected to provide a less expensive alternative to conventional machining and have found wide spread use in many industries. However, the physical phenomena involved in many laser applications are not fully understood. A better and more quantitative understanding of the physical mechanisms governing these phenomena will diminish the need for extensive trial and error experiments. Most of the theoretical models available in the literature have dealt with quasi-steady material removal using a continuous wave laser.

This paper presents a numerical model to predict the transient thermal behavior of rocks under the influence of a pulsed laser. A wide range of parameters were considered in this study, the laser powers were varied from 0.1 to 100 kW and the lasing time were varied between 1 sec and to 100 sec. One of the results presented in this paper shows that limestones consume less energy per unit volume of material removed as compared to sandstones. A comparison between the findings of this numerical study and published experimental data is also presented and shows a qualitative agreement. Finally, it is shown that numerical modeling can be useful in scaling up laboratory results to field applications.

12.2.2. Introduction

Lasers are basically devices that convert energy to intense photons. Developments and utilizations of lasers were based on military applications, in so called "Star Wars" programs. However, the commercial application of this technology has been developed not only in the USA but also in Russia and former Soviet Union (Graves and O'Brien, 1998a). The laser technology has become very well known in many fields such as medical, metallurgical and military.

Laser applications in drilling is not a new development and researchers in the mining industry have been active in the enhancement of the performance of tunneling machines by lasers for about three decades. Its real implementation in drilling oil and gas wells is still a dream in the petroleum industry, with the exception of a few laboratory experiments that commenced as recent as 1998.

A limited amount of work has been reported in the literature (Graves and O'Brien, 1998a; O'Brien et al., 1999; Gahan et al., 2001) on the use of laser in drilling oil and gas wells. The results presented are not in a form that can readily be used in practical applications; rather they represent a test of a laser beam to remove rock materials. Graves and O'Brien (1998a) conducted initial laboratory testing using Mid Infrared Advanced Chemical Laser (MIRACL) at the U.S. Army's High Energy Laser Systems Test Facility in New Mexico. Promising results were found in that they claimed that drilling rate of penetration using a laser beam could be increased 100 times over conventional drilling techniques that are currently in use. In 1999, the Chemical Oxygen-Iodine Laser (COIL) - invented by U.S. Air Force in 1977 – ability to penetrate samples of sandstone, limestone, shale, salt, granite and concrete was examined (O'Brien et al., 1999). The samples were exposed to a laser beam at different durations, vertically and horizontally, dry and saturated with water, brine, oil and gas and the results were very encouraging. More recently, in 2001, Gahan et al, conducted another laboratory study to determine the threshold energy, i.e.

the minimum energy required to remove rock materials. They used a pulsed Nd: YAG laser beam of 1.6 KW to penetrate samples of sandstone, limestone and shale. They concluded that each type of rock has a different set of optimal laser parameters to minimize specific energy values.

Modeling of laser drilling, cutting and scribing has been addressed by a number of investigators. Dabby and Paek (1972), Yilbas (1996), Wagner (1974), and Chan and Mazumder (1987) presented a simple one-dimensional drilling model. They reported an interesting observation concerning thermally induced effects due to the usage of high-energy intensities concentrated on a small area. Blackwell (1990) studied this phenomenon and concluded that a metal explosion below the surface occurs due to the effects of these thermal stresses. Balckwell (1990) explained this explosive material removal by stating that the maximum temperature (before the phase change occurs at the exposed surface) lies inside the body because of the heat loss to the surroundings. An analytical solution of 1-D heat conduction with laser energy incident on a metal surface was given by Zubair and Chaudhry (1994; 1996). Modest and others (1990; 1992; 1993) presented a numerical solution to the problem and studied the effects of thermal stresses in ceramic.

This paper addresses the thermal process involved in laser drilling of sandstone and limestone rocks as they represent the most predominantly rock types involved in the process of oil and gas drilling. This study is aimed to develop a numerical simulation model of the fundamental heat transfer and fluid flow phenomena (conduction, melting and vaporization) responsible for material (rocks) removal by laser drilling process. Prediction by the developed model are very encouraging will lead to further research; both experimentally and numerically; in the implementation the use of this technology in the future drilling of oil and gas wells.

12.2.3. Motive for laser drilling

Drilling oil and gas wells is the most expensive operation in the long journey of hydrocarbon production. Tremendous difficulties including mission delays, casualties and injuries as well as high costs are inevitable with the current method of drilling. Many drilling problems occur before running the casing and completing the cement job due to an unsealed borehole. Unsealed boreholes allow the flow of formation fluids into the wellbore or drilling fluids into the formation. Gas kicks, lost circulation, formation damage, borehole swelling, stick pipes, formation fracture and borehole collapse are among the associated problems.

Drilling operations are currently very active. In the U.S alone, over 20,000 wells have been drilled in one year approximated to 9,000 miles penetration (Graves and O'Brien, 1998a). It has been estimated that only 50% of the rig time was actually spent on creating a deeper well, while the other half was spent on rigging-up and down, pulling and lowering the drill string in the hole, casing, cementing, mud conditioning and other operations. The average cost per foot of drilling is currently $388 and the average rate of penetration (ROP) is 22.6 ft/hr. Drilling activities are expected to increase even more with the ever-growing world demand on energy.

The foreseen advantages of laser drilling over the traditional method of drilling based on experience with traditional methods and the limited experimental and numerical research on laser drilling include:

- Increasing rate of penetration dramatically (up to 100 times).
- Significantly reducing rig time, eliminating casing, cementing and bits, and avoiding blowouts and gas kick hazards.
- Cost effective, safe and environmental awareness.

12.2.4. Analysis

In order to develop the mathematical formulation of laser drilling process appropriate for the laser rock interaction, the following assumptions are made:

(a) The laser beam is radially symmetric and is focused on the surface of the rock. The energy flux arriving at a particular location is independent of the distance from the surface on which it impinges.
(b) The convective heat losses from the surface to the environment are treated via an interfacial heat transfer coefficient.
(c) The radiation heat losses from the surface are treated by considering the Stefan-Boltzman law.
(d) Sandstone is assumed to be infinite in all inplane directions. A null heat transfer condition is set up at the lateral boundaries to the modeled domain.
(e) Material removal is assumed to occur only by volatilization, i.e. melt ejections are neglected.
(f) All the thermo-physical properties are assumed to be independent of temperature.
(g) It is assumed that the pulse-on-time is much shorter than the pulse-off-time and therefore all the plasma generated will be extinguished between pulses.
(h) The velocity of the liquid metal inside the hole is neglected and the temperature distribution within the liquid is assumed to be linear.
(i) The incident laser energy is instantly converted into heat at the target material (sandstone) and the laser beam does not penetrate into the sandstone, i.e. the sandstone is assumed to be opaque.

12.2.5. Mathematical formulation

Figure 12.2.1 shows a schematic diagram of the laser drilling (LD) process. A laser beam is incident upon the top surface of the target (rock), which absorbs a fraction of the

incident light energy causing material melting followed by vaporization. The physical process taking place during the material removal are a combination of heat transfer, thermodynamics and fluid flow with a free surface boundary at the liquid-vapor interface (S_{LV}) and a moving boundary condition at the liquid-solid interface (S_{LS}). This kind of problem along with its moving boundary conditions is termed as the Stefan problem.

Laser-rock interaction can be divided into three main stages. The first stage is called the heating-up period where the temperature of the surface is below the melting temperature and therefore no melting or vaporization will occur. The solid absorbs the incident laser energy and, as a consequence, temperature increases with time. The second stage represents the melting stage, which commences as soon as the highest temperature (at the center of the laser beam, i.e. (0,0) reaches the melting point. All the laser energy absorbed during this stage will melt more liquid as well as increasing the liquid temperature. When the highest temperature reaches the vaporization temperature, evaporation will occur at the surface of the liquid and the third stage starts. Since the process of material removal by laser drilling consists of three main stages, an energy balance equation was used for each stage.

12.2.5.1. First Stage: Preheating

This stage can be classified as a pure conduction stage with a convective-radiative boundary condition at the surface. The energy equation used during this stage is the simple heat conduction equation

$$\frac{\partial T}{\partial t} = \frac{k\left[\frac{\partial^2 T}{\partial r^2} + \frac{1}{r}\frac{\partial T}{\partial r} + \frac{\partial^2 T}{\partial y^2}\right] + q_{Laser}}{\rho C_P} \qquad (12.2.1)$$

The thermal penetration depth was evaluated by

$$\delta = \sqrt{\alpha \cdot t} \tag{12.2.2}$$

12.2.5.2. Second Stage: Melting

During this stage, the liquid-surface temperature is below the saturation temperature and, therefore, the liquid-vapor-interface velocity is zero. An energy balance at the solid-liquid interface during this stage is expressed as

$$\frac{\partial S_{SL}}{\partial t} = \frac{\left[K_S \frac{\partial T_S}{\partial y} - K_L \frac{\partial T_L}{\partial y}\right] \cdot \left[1 + \left(\frac{\partial S_{SL}}{\partial r}\right)^2\right]}{\rho \, h_{SL}} \tag{12.2.3}$$

12.2.5.3. Third Stage: Evaporation

Evaporation begins when the liquid-surface temperature reaches the saturation temperature. The mathematical equations involved in this stage are more complicated because the vaporization, melting and conduction equations have to be solved simultaneously. The energy balance at the liquid-vapor interface can be expressed as

$$\frac{\partial S_{LV}}{\partial t} = \frac{\alpha_{abs} q_{Laser,i} - \frac{K_L}{H_{Liq.}}(T_{Sat} - T_m) \cdot \left[1 + \left(\frac{\partial S_{SL}}{\partial r}\right)^2\right]}{\rho \left[h_{LV} + C_{PL}(T_{Sat} - T_m)\right]} \tag{12.2.4}$$

The thickness of the liquid layer is given by

$$\mathbf{H_{Liq.}} = \mathbf{S_{SL}} - \mathbf{S_{LV}} \tag{12.2.5}$$

12.2.5.4. Laser Energy Transfer

There are three main processes by which lasers transfer energy into a rock; Absorption, Reflection and Scattering. In this paper, it is assumed that the laser source is operated in pulse mode only and, therefore the laser power is both a function of space and time. Thus;

$$q_{Laser}(r,t) = I(r) \cdot T(t) \tag{12.2.6}$$

Where I(r) and T(t) are arbitrary functions of space and time, respectively. The laser operating characteristics determines these shape functions. The spatial intensity profile was assumed to take the following Gaussian profile (Bauerle, 2000)

$$I(r) = \frac{2q_0}{\pi R^2} \cdot e^{-2\left(\frac{r}{R}\right)^2} \tag{12.2.7}$$

In addition, the following two phenomena affect the laser energy transfer

- Blackbody radiation: As its temperature rises, the sandstone sample turns into an intense source of radiation. At a high rock temperature over an extended area of heating, a substantial fraction of the incident energy will be emitted back by the surface of the rock as blackbody radiation.

- Plasma screening: High power laser radiation can cause the formation of plasma (ionized gas) over the surface irradiated. The laser plasma reflects, scatters and absorbs the incident laser radiation, preventing energy from reaching the rock face. In this paper, the effects of plasma were not considered.

12.2.6. Numerical Modeling

The governing equations namely, Equations (12.2.1), (12.2.3) and (12.2.4) were solved numerically by using the Crank-Nicholson method in which old and new time temperature values were employed utilizing the iterative implicit method.

A Fortran computer code was developed to solve the above finite difference equations. Figure 12.2.2 gives a simplified flow chart for the solution algorithm employed. The solution procedure starts by calculating the temperature within the solid rock using energy Equation (12.2.1) at all points inside the material. When the highest temperature T(0,0,t) reaches and exceeds the melting temperature, the second stage starts and simultaneous solution of the heat conduction Equation (12.2.1) along with Equation (12.2.3) were carried out to obtain the temperature field as well as the recession velocity of the surface $\left(\frac{\partial S_{SL}}{\partial t}\right)$.

The solution procedure continues as more solid is converted into the liquid phase, and as soon as the maximum temperature in the liquid layer reaches the evaporation temperature, evaporation starts and therefore forming the required keyhole. Table 12.2.1 shows the thermodynamic properties for limestone and sandstone (Graves and O'Brien, 1998b).

12.2.7. Results and discussion

The intensity of laser power incident on the rock surface is the dominant factor in determining the drilling Rate of Penetration (ROP) and the final depth of the drilled hole. Figure 12.2.3 shows the effect of laser power on ROP for both sandstone and limestone. It can be seen that limestones have a higher ROP. This is attributed to the lower melting temperature as well as lower evaporation temperature of limestones. However, at low

laser power levels and owing to the threshold power level, the limestone shows a stagnant period for which increasing power does not increase the ROP. For the sandstone, on the other hand, the ROP increases continuously as power is increased. As laser power is increased, both limestone and sandstone follow very similar linear and parallel paths.

Studying the effect of lasing time can further manifest the effect of laser power on the drilling speed. This effect is presented in Figure 12.2.4 for limestones and sandstones under two different laser power levels. It is evident that there is a rapid decrease in drilling speed as the lasing time increases up to 25 seconds. Increasing the lasing time beyond this point does not seem to have a noticeable effect on ROP. This is attributed to the fact that more lasing time means more laser interaction with the rock, resulting in a more penetration depth and subsequent higher energy losses. This is particularly true at low levels of laser power.

Figure 12.2.5 shows the total depth of the drilled hole as a function of lasing time. However the effect of plasma formation and gases in the lased hole, which is expected to increase the energy losses, was not considered in this study.

For the purpose of obtaining the energy requirements and the optimum drilling speed for different materials, the specific energy requirements were calculated for both materials. The specific energy was calculated as the ratio between the incident flux of laser power and the drilling speed. The results for the specific energy requirements are given in Figure 12.2.6. It is evident that with an increase in power there is an increase in specific energy for fixed lasing times.

Figure 12.2.7 shows a comparison between specific energy required to penetrate a sandstone rock sample and that required to penetrate limestone when laser power intensity and lasing time were kept constant. From the figure one can see that more specific energy is consumed when lasing sandstone than limestone.

Predictions of the numerical model presented in this paper have been compared to documented experimental data (O'Brien et al., 1999), Figure 12.2.8 demonstrates such comparison in terms of specific energy consumption to penetrate sandstone and limestone samples as predicted numerically and tested experimentally. Figure 12.2.9 compares numerical and experimental results of depth of hole drilled in sandstone and limestone rocks. It clearly shows that the numerical model prediction of energy consumption per unit volume of rock removed is higher than what the experimental results suggested. Moreover, for the same energy consumption the numerical model predicted less depth drilled of key hole, this is attributed to the assumption of neglecting the melt expulsion process imposed in the numerical model. This assumption is valid knowing that in reality as the hole becomes deeper, the chance to remove melt rocks out of the hole as a melt is not foreseen; rather any removal is expected to be by vaporization process. It is not practical to assume other means of rock melt removal and evaporation seems to be the only effective process for any material removal. This indeed will result in higher energy consumption (compare 20-40 kJ/cm^3 to 3-6 kJ/cm^3). Field applications, therefore, should give results closer to the numerical predictions reported in this study.

12.2.8. Conclusions

A numerical simulation model describing the transient thermal behavior of limestone and sandstone rocks under the influence of laser radiation has been developed. Considering the results of this model for each set of circumstances, the following conclusions were drawn:

- Using laser technology in drilling oil and gas wells is very feasible considering the efficiency of the process and its impact on the economics, drilling time and environmental aspects supported by both prediction of numerical modeling and experimental data.

- Although, in this study only sandstone and limestone has been considered, other types of rock are expected to behave in the same manner.
- Rate of penetration can be increased dramatically by increasing laser power for both sandstone and limestone. Although the rate of increase is about the same, it seems that sandstone consumes slightly more power than limestone.
- Numerical predictions show greater energy consumption and less ROP when compared to published experimental data. This is due to the intentional assumption that rock removal out of the drilled hole is due to only vaporization process. The contribution from the melting process, which may take place, is neglected.
- Effect of rock fluid saturation on ROP and energy consumption has not been addressed in this study; future investigation is required to cover this aspect.

12.2.9. References

Bauerle, D., (2000) Laser Processing and Chemistry, 3rd edition, Springer, Heidelberg

Blackwell, B. F., (1990) Temperature profile in semi-infinite body with exponential source and convective boundary condition, ASME, Transactions, Journal of Heat Transfer, vol. 112, August, pp. 567-571

Chan, C. L. and Mazumder, J., (1987) One-dimensional steady-state model for damage by vaporisation and liquid expulsion due to laser-material interaction, Journal of Applied Physics, vol. 62, pp. 4579 - 4596

Chaudhry, M. A., and Zubair, S. M., (1994) On a pair of functions useful in heat conduction problems, International Communications in Heat and Mass Transfer, vol. 21, no. 5, p. 673-681

Dabby, F. W. and Paek, U., (1972) High-intensity laser-induced vaporization and explosion of solid material, IEEE Journal of Quantum Electronics, vol. QE-8, no. 2, pp. 106-111

Gahan, B.C., Parker, R.A., Batarseh, S., Figueroa, H., Reed, C.B. and Xu, Z., (2001) Laser drilling: Determination of energy required to remove rock, SPE 71466, SPE Annual Conference and Exhibition, New Orleans, Louisiana, September 30 –October 3

Graves, R.M. and O'Brien, D.G., (1998a) StarWars laser technology applied to drilling and completing gas wells, SPE 49259, SPE Annual Technical Conference and Exhibition, New Orleans, Louisiana, September 27-30

Graves, R. M. and O'Brien, D. G., (1998b) Targeted literature review: Determining the benefits of StarWars laser technology for drilling and completing natural gas wells, GRI-98/0163, July

O'Brien, D.G., Graves, R.M. and O'Brien, E.A., (1999) StarWars laser technology for gas drilling and completions in the 21st century, SPE 56625, SPE Annual Technical Conference and Exhibition, Houston, TX, October 3-6

Ramanathan, S. and Modest, M. F., (1990) Effects of variable thermal properties on evaporative cutting with a moving CW laser, ASME Heat Transfer in Space Systems, vol. HTD–135, pp. 101–108

Ramanathan, S. and Modest, M. F., (1992) CW laser drilling of composite ceramics, Proceedings of ICALEO '91, Laser Materials Processing, vol. 74, pp. 305-326, San Jose, CA

Roy, S., and Modest, M. F., (1993) CW laser machining of hard ceramics-Part I: Effects of three-dimensional conduction and variable properties and various laser parameters, International Journal of Heat and Mass Transfer, vol. 36, no. 14, pp. 3515–3528

Wagner, R. E., (1974) Laser drilling mechanics, Journal of Applied Physics, vol. 45, pp. 4631-4637

Yilbas, B. S., (1996) Experimental investigation into CO_2 laser cutting parameters, Journal of Materials Processing Technology, vol. 58, no. 2-3, pp. 323-330

Zubair, S. M and Chaudhry, M. A., (1996) Heat conduction in a semi-infinite solid due to time-dependent laser source, Journal of Heat and Mass Transfer, vol. 39, no. 14, p. 3067-3074

12.2.10. Appendices

12.2.10.1. Appendix A: Table

Table 12.2.1. Thermodynamic properties of rocks used in the numerical model (Graves and O'Brien, 1998b)

Property	Sandstone	Limestone
Melting Temperature, °C	1540	1260
Vaporization Temperature, °C	2200	2000
Latent Heat of Melting, kJ/cm^3	4.5	
Latent Heat of Vaporization, kJ/cm^3	30	

12.2.10.2. Appendix B: Figures

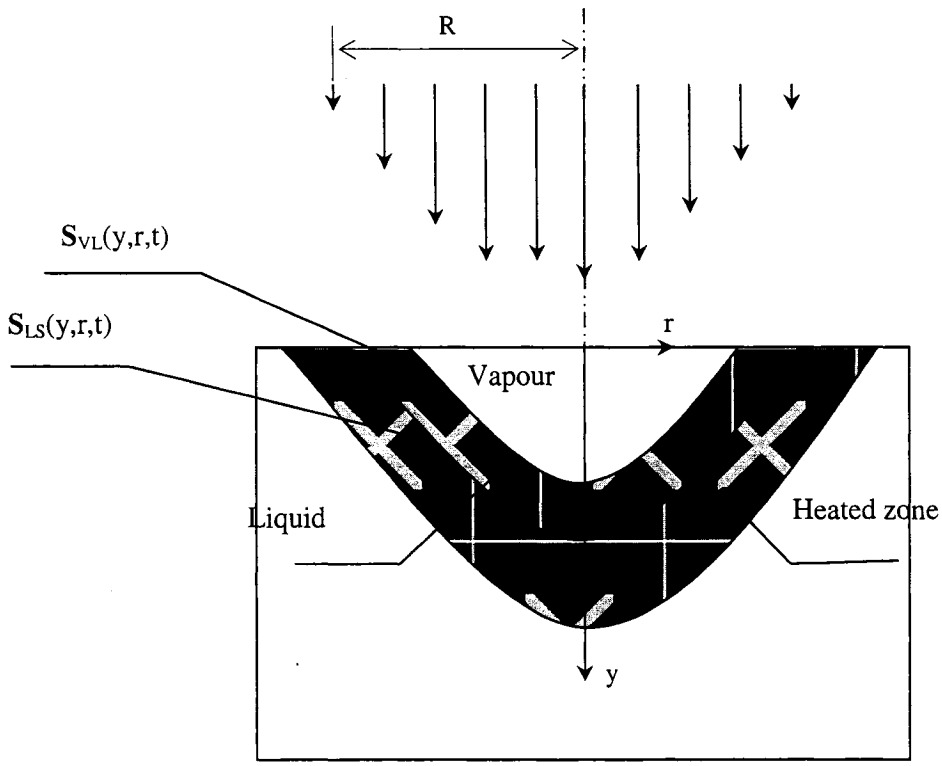

Figure 12.2.1. Physical model of Laser Drilling (LD) process

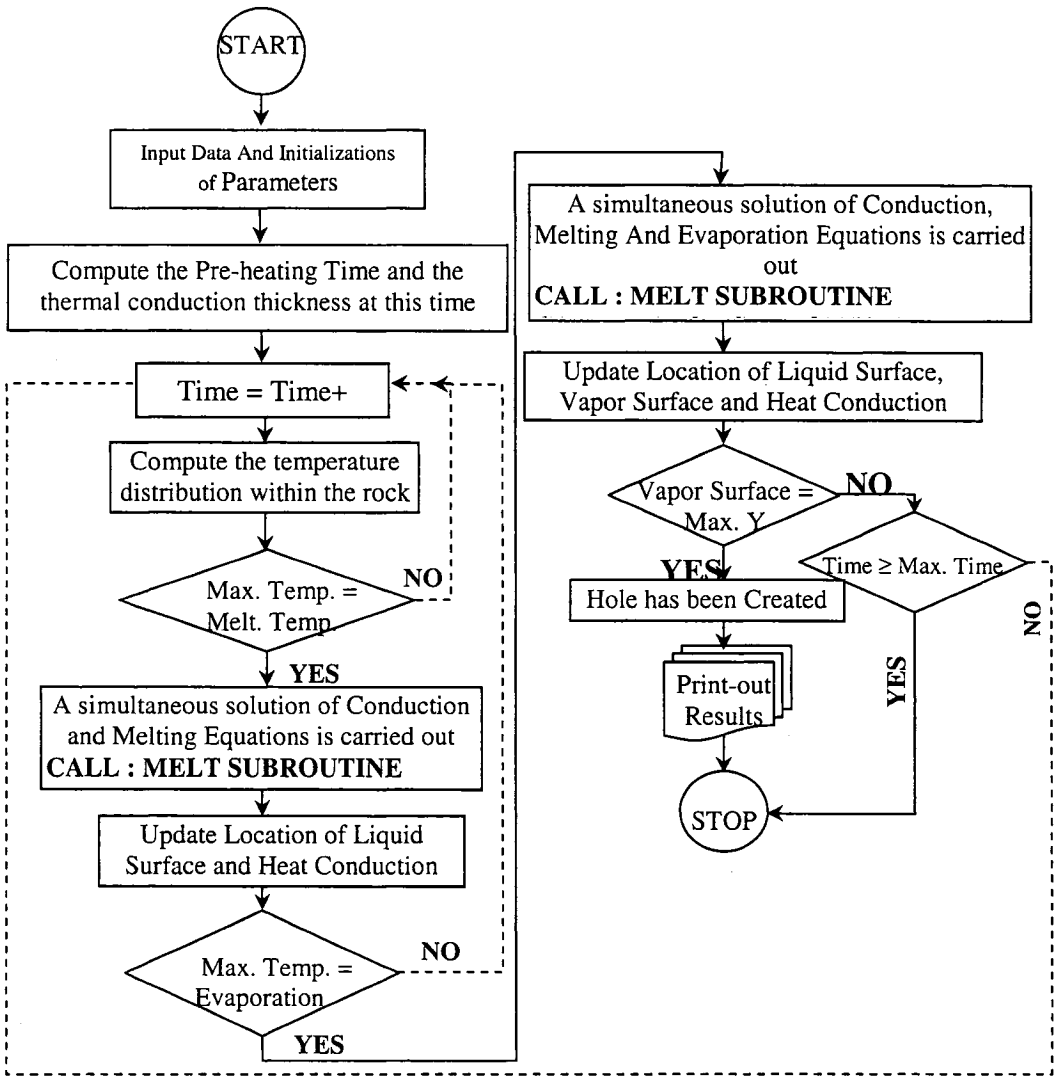

Figure 12.2.2. Flow Chart for the algorithm

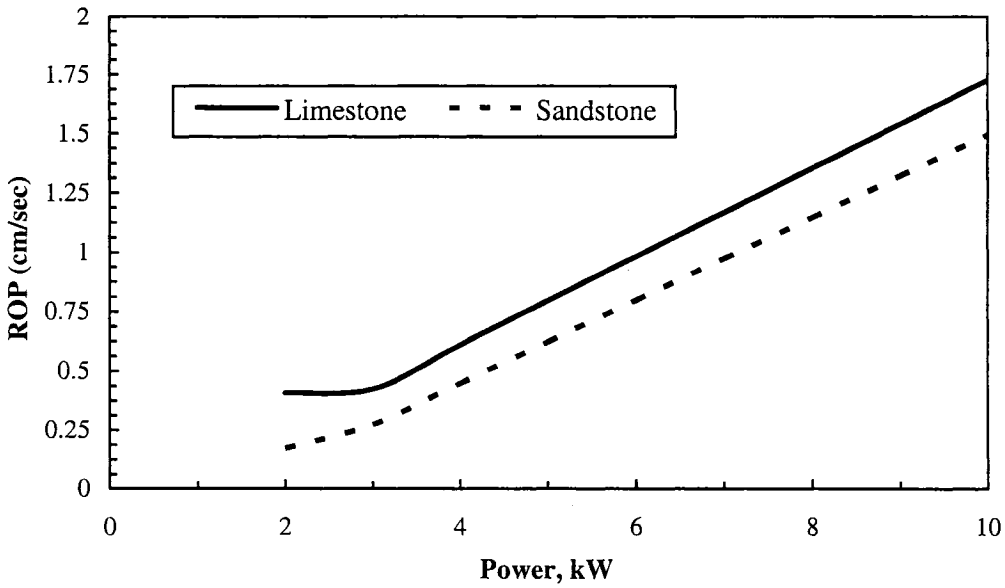

Figure 12.2.3. Effect of Laser Power on Drilling Rate of Penetration, ROP (cm/sec) for 8 seconds lasing time.

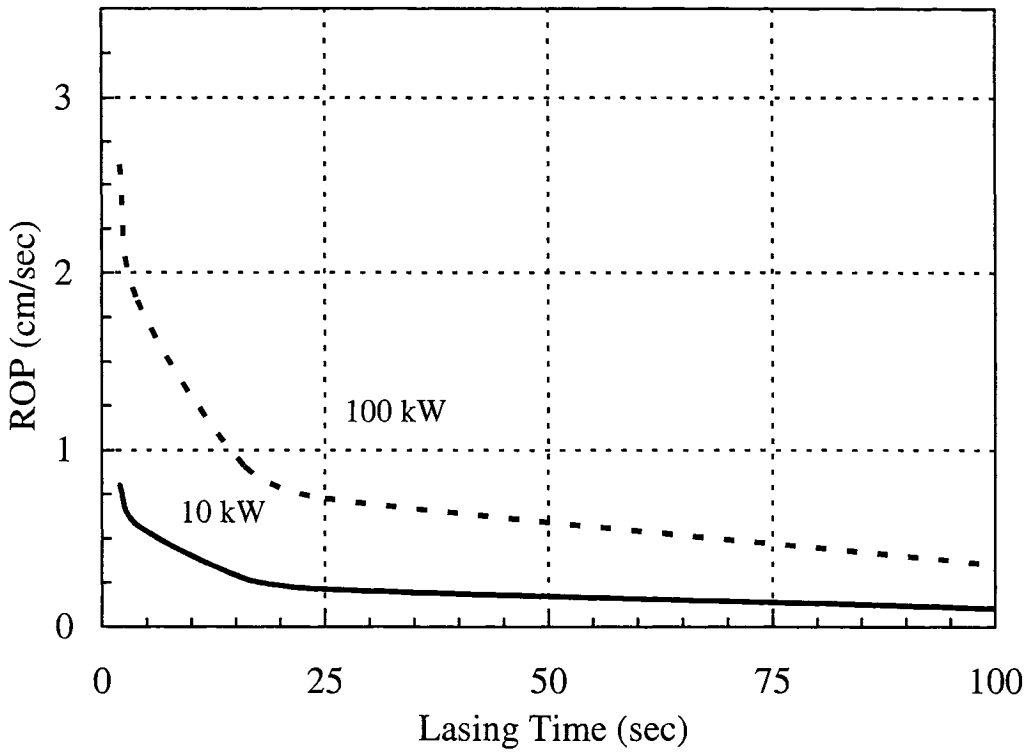

(a) Sandstone

Figure 12.2.4. The effect of lasing time on drilling Rate of Penetration

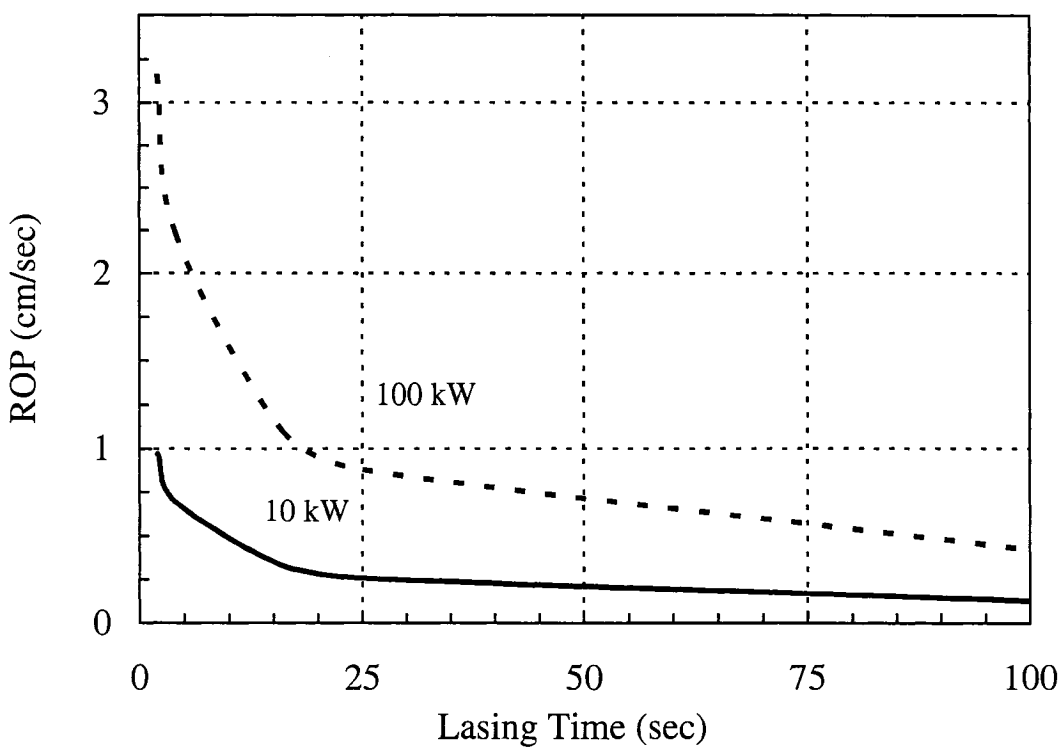

(b) Limestone

Figure 12.2.4. The effect of lasing time on drilling Rate of Penetration

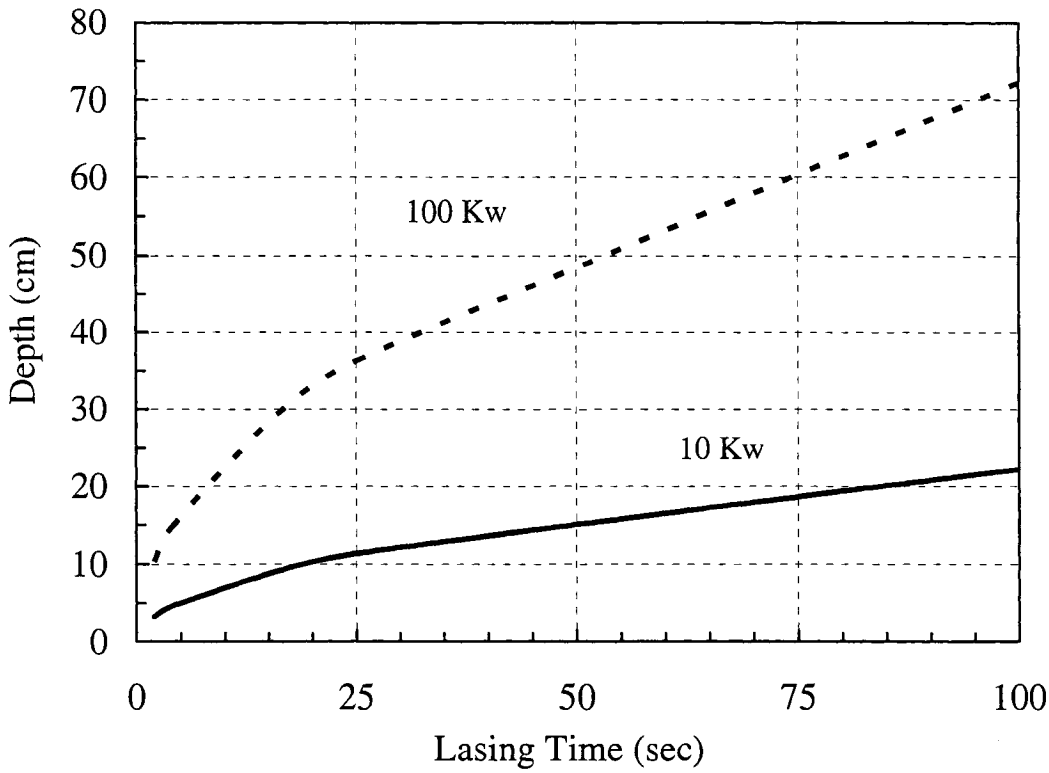

(a) Sandstone

Figure 12.2.5. The effect of lasing time on the final depth of drilled hole

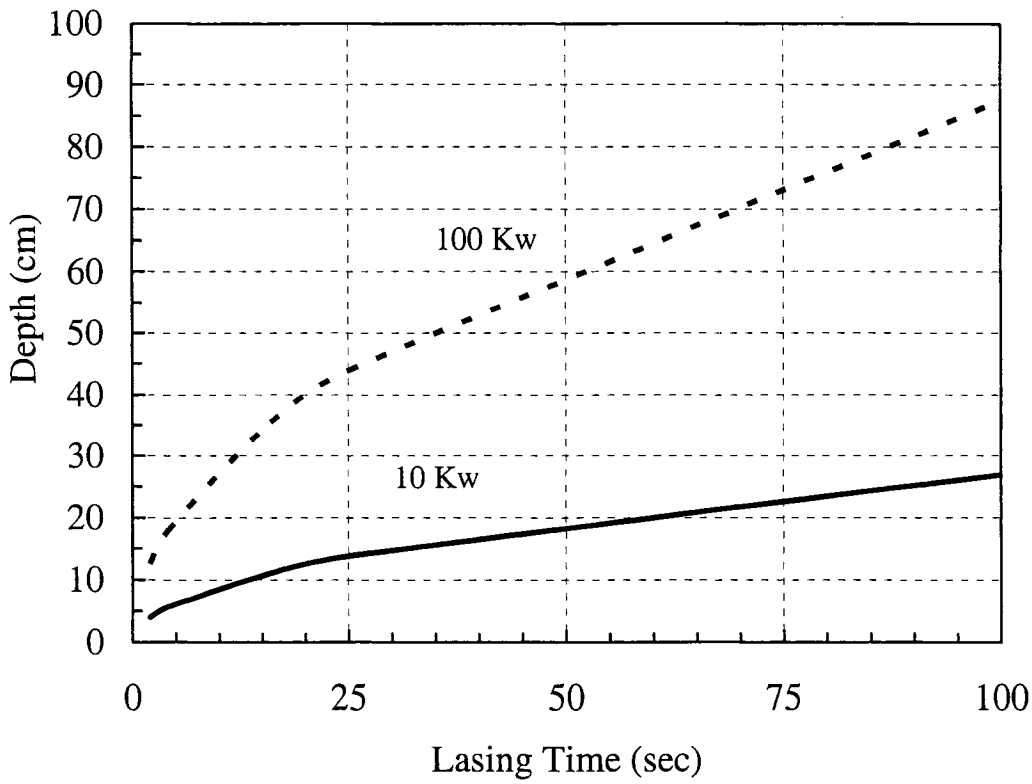

(b) Limestone

Figure 12.2.5. The effect of lasing time on the final depth of drilled hole

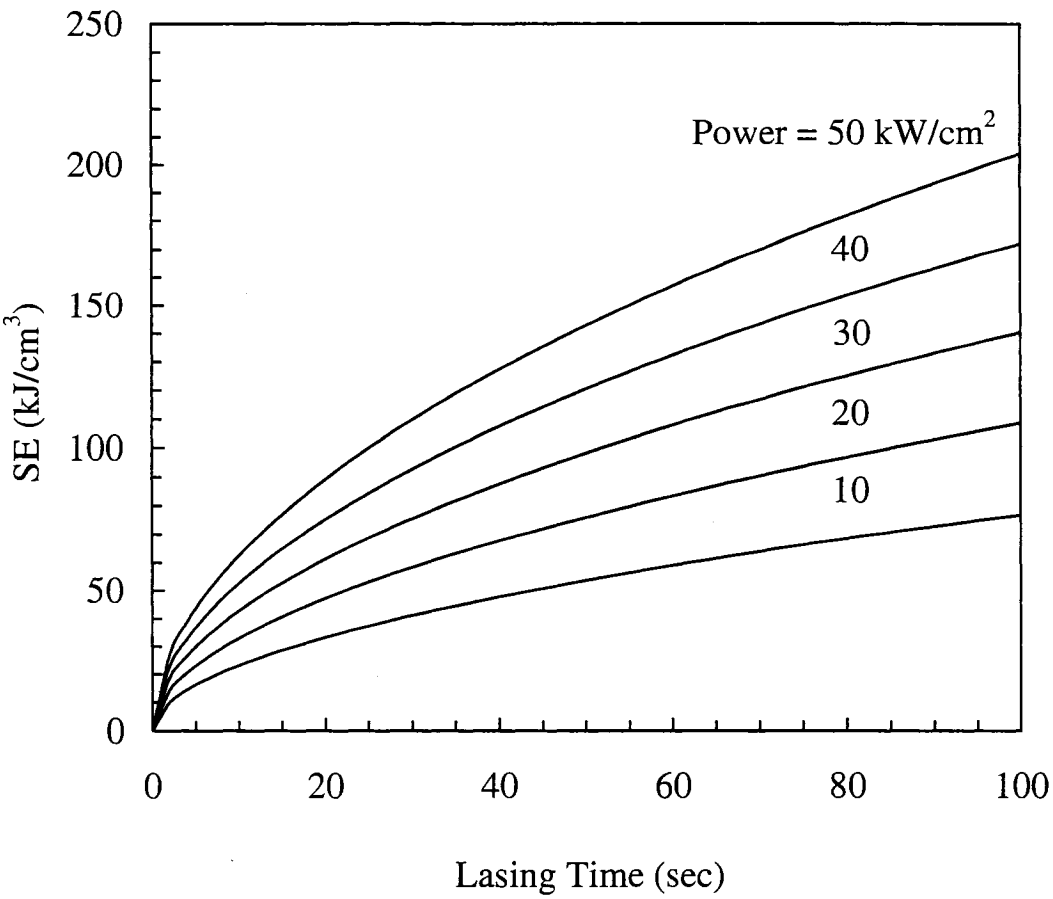

Figure 12.2.6. The variation of Specific energy with lasing time under different incident laser power intensity -- for Sandstone

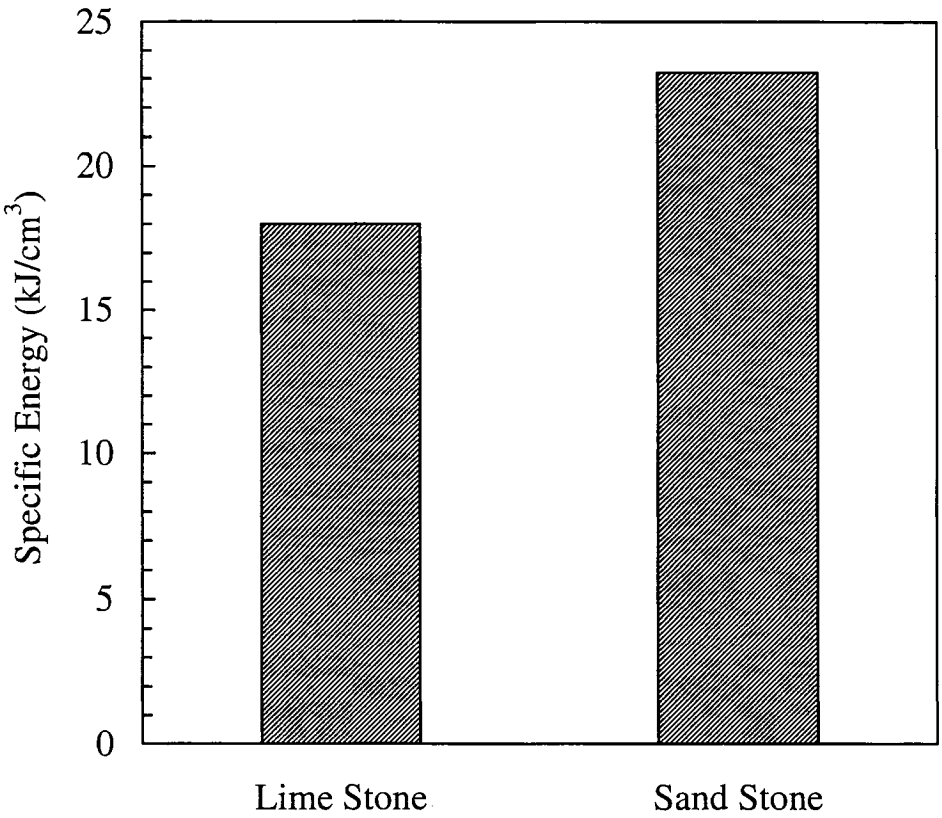

Figure 12.2.7. Specific Energy Requirement, for a laser power intensity of 10 kW/cm^2 and 10 seconds lasing time

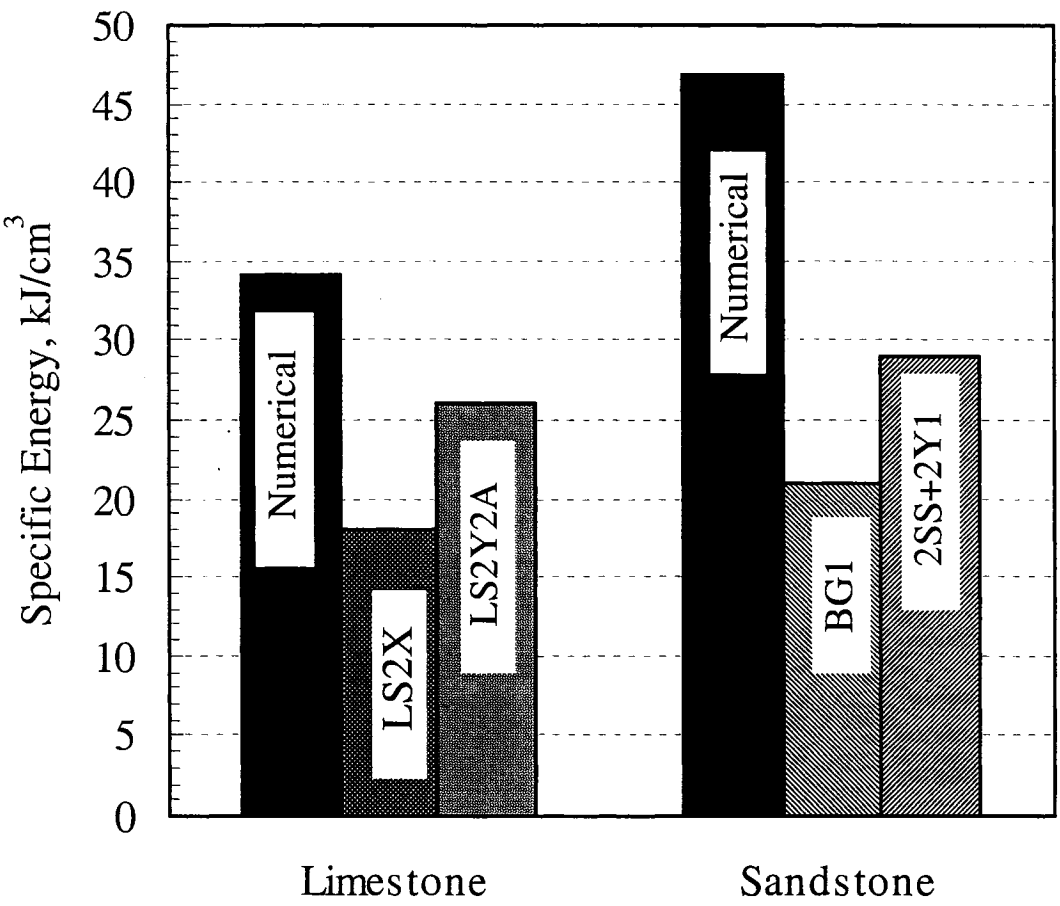

Figure 12.2.8. Comparison between the predicted specific energy consumption and that obtained experimentally

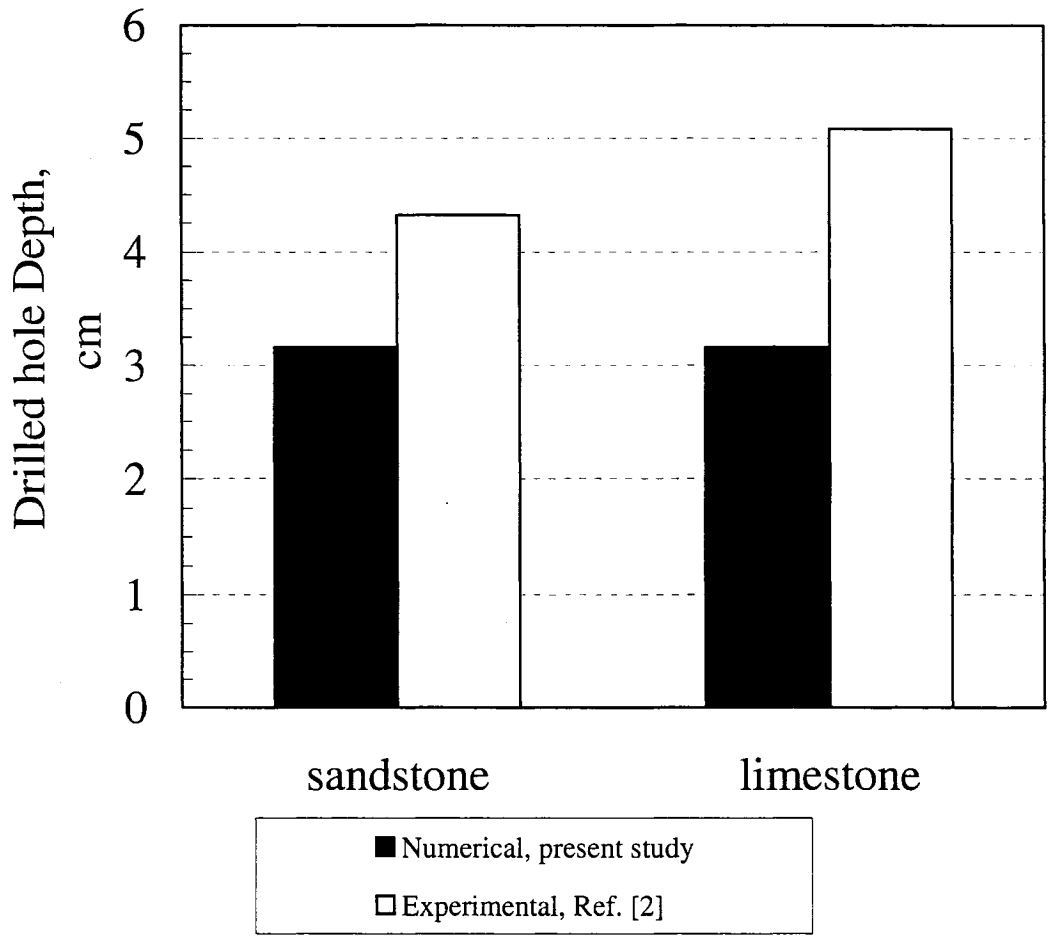

Figure 12.2.9. Comparison between estimated and experimentally documented final depth of hole drilled

Chapter 13

13 THE EFFECT OF IRRADIATION ON IMMISCIBLE FLUIDS FOR INCREASED OIL PRODUCTION WITH HORIZONTAL WELLS

13.1. Abstract

Oil recovery using horizontal wells gives an undeniable benefit to the petroleum industry. One of the problems of using this method is that the wells can plug due to pressure and temperature changes. The components of crude oil such as asphaltene and paraffin wax can precipitate in the horizontal section of the well causing a loss of productivity and profit. Microwave or irradiation has been proposed to remove these precipitates remotely.

The effect of microwaves on crude oil properties has been studied and a numerical model is presented to gain an understanding of the effect of the rise in temperature. These results include temperature increases for various concentrations of crude oil, and paraffin wax under different exposure times. The effect that different media (bentonite and gypsum) has on the temperature of these components has also been studied. By understanding the temperature rise, one can determine the effect that irradiation will have on oil production. Overall, the agreement between experimental and numerical results was acceptable.

13.2. Introduction

Horizontal wells have many applications worldwide. By utilizing horizontal wells in offshore applications, the number of platforms that need to be constructed can be reduced. This is also a benefit in SAGD applications in Northern Alberta where

environmental concerns restrict land use. During horizontal well production particles such as asphaltenes, paraffin wax and fines can precipitate out of the crude oil and stick to the wellbore causing a decrease in tubular radius. The same problem prevails in pipeline transportation. Paraffin precipitation is a strong function of temperature changes but asphaltene precipitation is not greatly affected. It has been shown that an increase in pressure can increase the precipitation of wax whereas an increase in pressure decreases the likelihood of asphaltene precipitation (Pan *et al.*, 1997). The amount of asphaltene precipitation can be affected by CO_2 injection, miscible flooding, pH shift, mixing of crude streams, well stimulation and shear (Islam, 1995). Temperature changes in the crude oil may increase or decrease the likelihood of asphaltene precipitation depending on the situation (Firoozabadi, 1999).

Microwave irradiation has been utilized in various areas of the the petroleum industry (Stanley, 2001; Vega, 2002; Honarpour, 1996; Rogers *et al.*, 1988; Ashton *et al.*, 1994). Ferri and Uthe (2001) and Gunal and Islam (2000) discussed the use of microwave irradiation as a mobilization tool. Ferri and Uthe (2001) developed a technique to remediate hydrocarbons from surface formations and groundwater. Microwave irradiation can be utilized to decrease or eliminate the collection of these particles by maintaining particle suspension which will save the industry with a decrease in costly shut downs (Bjorndalen and Islam, 2004). This paper explores the effect of microwave irradiation on crude oil, water and on one of the critical precipitant, paraffin.

13.3. Experimental setup and procedure

The Samsung Mini-Chef MW101OC microwave was used for the microwave tests. The running frequency is 60 Hz and the output power is 120V. The temperature probe was the Greenlee THH-500 Non-Contact Infrared Thermometer. Santa Barbara Crude Oil was supplied by Caleb Brett, Dartmouth, N.S.

Four samples of distilled water mixed with varying percentages (1%, 5%, 10% and 50%) of crude oil or paraffin oil were prepared. The combined volume of each sample was 50 ml. The samples were placed in the microwave for a total of 80 seconds and the temperature reading was recorded at a time interval of 10 seconds. For the media test the same quantity of liquid and method was used. An amount of 5g of either bentonite or gypsum was added to the sample.

13.4. Numerical model

The modeling of microwave irradiation as applied in the petroleum industry has seldom been attempted. Bjorndalen et al. (2003a) discussed double diffusive phenomena under microwave irradiation for petroleum industry purposes. A numerical model for petroleum fluids based on the heat conduction equation with special attention to heat transfer models at the gas/liquid interface has been developed by Bjorndalen et al. (2003b) and further explanation of the model can be found there. This study further applies this model to immiscible petroleum mixtures as well as mixtures of solids and fluids.

Temperature rise due to irradiation can be calculated using the following heat conduction equation:

$$\frac{\partial T}{\partial t} = \frac{k}{\rho C_p}\left[\frac{\partial^2 T}{\partial x^2} + \frac{\partial^2 T}{\partial y^2}\right] + \frac{Q'}{\rho C_p} \tag{13.1}$$

The Heat Generation Term (Q') is defined as:

$$Q' = \boldsymbol{P}\,\delta x \delta y \delta z \tag{13.2}$$

The value of the total dissipated power ($\boldsymbol{P}$) for water is given by Desai *et al.* (1992).

Equation (13.1) is discretized using the finite difference scheme of Barakat and Clark (1966). Figure 13.1 illustrates the boundary conditions that were assumed for this study. The height of the fluid is 2.4 cm and the width is 5.0 cm. The distance between nodal points was taken as 0.1 cm. The top boundary, where there is an interface between the respective petroleum liquid and the air, was calculated by:

$$\frac{\partial T}{\partial y} = aT^2 + bT \tag{13.3}$$

where a and b are heating parameters. It is important to note that the value of 'a' and 'b' are specific to the liquid/gas system and is also a function of pressure. Because this study was performed under atmospheric pressure conditions, the pressure dependence form was not included. For field applications, however, such dependence must be included. This can be done by using the equation of state and then assigning appropriate values of 'a' and 'b', based on both pressure and temperature values.

This paper explores the percent volume averaged method to calculate heating parameter values for a mixture. That is, that the mixture is considered to be homogeneous. Although this is not the case, the prediction using this method can result in close matches to the heterogeneous mixtures. The overall value for a binary fluid system of crude oil and water can be calculated by using the following equation:

$$X_{w/o} = P_w.X_w + P_o.X_o \tag{13.4}$$

where $X_{w/o}$ is the parameter in question for water-crude oil mixture, P_w represents the percent fraction of water in water-crude oil mixture, X_w is the heating parameter in question for pure (100%) water system, P_o represents the percent fraction of crude oil in water-crude oil mixture, and X_o is the heating parameter in question for pure (100%)

crude oil system. This method was used to determine the mixture values of a, b, ρ, k and C_p. It is to be noted that when an overall value of a particular parameter for the mixture is calculated, the same parameter for the pure cases should be used. For instance, in cases of pure (100%) water and pure (100%) crude oil, the suggested values for 'a' are -0.07 and 0.99, respectively (Bjorndalen et al., 2003b). Now, if a solution contains 5% crude oil, 95% of 0.99 and 5% of -0.07 would be summed up to calculate the value for 'a' for the mixture. Similarly, the value for other parameters for the mixture can be calculated.

Table 13.1 lists the homogeneous parameters for the various fluids (Bjorndalen et al., 2003b).

13.5. Results and discussion

The results for the homogeneous cases can be found in Bjorndalen et al. (2003b). Figures 13.2 shows the numerical and experimental data for 1% crude oil and 99% water using the homogeneous method described above. This graph shows a reasonable agreement between experimental and numerical results. The experimental data shows that the temperature increases until 60 seconds and then becomes fairly constant. This shows that after 60 seconds the water phase of the water-oil mixture has reached a boiling point and the temperature is the steam temperature.

Figures 13.3 and 13.4 illustrate the temperature rise in 5% crude oil in water and 10% crude oil in water. The results are very similar to those reported in Figure 13.2 in that the numerical model with the homogeneous mixture theory predicts the experimental results. As well, Figure 13.4 shows the same temperature increase as Figure 13.2. Figure 13.3 does not show the same trend but the experimental data after 80 seconds has just reached approximately 370 K. This would indicate that the boiling point had not been reached yet at the termination of the experiment. This could be due to improper placement of the

beaker in the microwave. It may also be due to the interaction between the crude oil and water. If the crude oil were mixed with water in a stable emulsion form during this run, the crude oil would have acted as a cooling phase which would not allow water to reach a boiling point.

Figure 13.5 illustrates that at 50% crude oil and 50% water, the model significantly overestimates the temperature rise. This may be due to the fact that crude oil droplets act as storage sites for heat. The experimental results here are similar to those obtained for the 5% crude oil run. Therefore, as the concentration of crude oil increases, more heat is absorbed by the solution and the temperature at the surface does not increase as rapidly. Figures 13.6 and 13.7 show similar results for paraffin oil and water. A several methods could be approached to solve this. Firstly, another term, which will be a function of concentration of crude oil or paraffin oil, can be plugged into the equation. Secondly, the values of 'a' and 'b' can be adjusted for the discrepancy and a correlation can be developed based on this. The second option is explored in Figure 13.8 where new values of 'a' and 'b' results in a better prediction.

Similarly, this can be done for paraffin oil. The value of 'a' is 2 and the value of 'b' is -546. Figure 13.9 shows how 'a' and 'b' vary with concentration of crude oil. The linear shape at low concentrations of crude oil is due to the assumption that the mixture is homogeneous. The maximum point 'a' values (presented by dotted line) represents 50% crude oil. This is where the crude oil is storing the heat generated by the microwave and the temperature increase is less. The experimental results are a measure of both the storage and the water which is at a lower temperature due to the crude oil storage. It can be said that the crude oil is acting as a cooling agent for water. At lower amounts of crude oil, the effect is less pronounced than the previous cases. At 100% the thermometer measures the heat storage of the crude oil and there is no water available for cooling. This is why the value of 'a' decreases to 100%. The inverse can be said for the value of 'b'. Figure 13.9 shows that when the oil content increases from 50% to 100%,

'b' increases from -645 to -195. A similar method can be used to find the values for paraffin oil. It should be noted that there is limited amount of data for percentages of crude oil between 50% and 100% and the evaluation for the values of 'a' and 'b' at these intervals may be crude to some extent, although the trend is self evident.

Figure 13.10 shows that small amounts of solids do not affect the increase in temperature rise. The exception is Figure 13.11 where gypsum has a large effect (significant discrepancy between experimental and numerical) on the temperature rise in 100% crude oil. This is similar when comparing these results to 100% paraffin oil with gypsum and 100%, 2.5% ashpaltene with toluene results (Bjorndalen, 2002). However, this figure also illustrates that by adjusting the 'b' parameter a better prediction can be made. As well, with an increase in the amount of gypsum (Figure 13.12), the temperature dependence becomes less pronounced. This is also similar to that of other fluids examined by Bjorndalen (2002). Hence the value of 'b' changes drastically from 0 to 5g and less drastically from 5g to 50g.

13.6. Conclusions

A numerical and experimental study has been performed on the temperature rise of immiscible fluids when microwave irradiation is applied. Based on this study, the following conclusions can be made:

- The heterogeneous mixture can be assumed to be a homogeneous mixture for mixtures that are high in water content. This assumption can be made for mixtures of up to 10% of crude oil. When considering other mixtures this percentage may increase or decrease.

- The model introduced by Bjorndalen et al. (2003b) has been examined for immiscible petroleum mixtures. A new value for the suggested heating parameters 'a' and 'b'

was introduced for mixtures of 50% oil and 50% water. These parameters, 'a' and 'b' exhibit a maximum and minimum value, respectively. This demonstrates that the crude oil acts as a heat storage fluid and does not allow the water to rise to a greater temperature. These values can be used as a guiding tool for mixtures of other composition.

- The homogeneous model can also be used to predict the temperature rise of the mixture with small amount of bentonite since bentonite enhances the thermal conductivity of the mixture.

- The homogeneous model cannot be used for so-called inert solids. A new value of the parameter of 'b' was determined for an increasing weight of gypsum in crude oil. As the weight increases, the effect that the solid has on the fluid becomes less important. These values can be used as a guiding tool for other fluids with solids.

13.7. Nomenclature

a	Heating Parameter
b	Heating Parameter
C_p	Specific Heat (J/kgK)
k	Thermal Conductivity (J/Kms)
P_w	Percent Fraction of Water in Water-Crude Oil Mixture
P_o	Percent Fraction of Crude Oil in Water-Crude Oil Mixture
Q'	Heat Generation Term
T	Temperature (K)
t	Time (s)

x Space in the Horizontal Direction (m)

X_o Heating Parameter for Pure (100%) Crude Oil System

X_w Heating Parameter for Pure (100%) Water System

$X_{w/o}$ Heating Parameter for Water-Crude Oil Mixture

y Space in the Vertical Direction (m)

z Space (m)

13.8. References

Ashton, S. L., Cutmore, N. G., Roach, G. J., Watt, J. S., Zastawny, H. W. and McEwan, A. J., (1994) Development and trial of microwave techniques for measurement of multiphase flow on oil, water and gas, SPE 28814, SPE Asia Pacific Oil & Gas Conference, Melbourne, Australia, November 7-11

Barakat, H. Z. and Clark, J. A., (1966) On the solution of the diffusion equations by numerical methods, Transactions ASME, Journal of Heat Transfer, vol. 88, pp. 421-427

Bjorndalen, N. and Islam, M.R., (2004) The effect of microwave and ultrasonic irradiation on crude oil during production with a horizontal well, Journal of Petroleum Science and Engineering, vol. 43, pp. 47-60

Bjorndalen, N., Agha, K. R. and Islam, M. R., (2003a) Numerical and experimental study of double diffusive phenomena under microwave irradiation, 31st Annual Conference of the Canadian Society for Civil Engineering, Moncton, NB, GCR-479, June 4-7

Bjorndalen, N., Mustafiz, S., and Islam, M. R., (2003b) Numerical modeling of petroleum fluids under microwave irradiation for improved horizontal well performance, International Communications in Heat and Mass Transfer, vol. 30, no. 6, pp. 765-774

Bjorndalen, N., (2002) Irradiation techniques for improved performance of horizontal wells, MASc Thesis, Dalhousie University, Halifax, Canada

Desai, R. A., Lowery, A. J., Christopoulos, C., Naylor, P., Blashard, J. M. V. and Gregson, K., (1992) Computer modeling of microwave cooking using the transmission line model, IEEE Proceedings-A, vol. 139, no. 1, pp. 30-38

Ferri, R. P. and Uthe, M. T., (2001) Hydrocarbon remediation using microwave, SPE 66519, SPE/EPA/DOE Exploration and Production Environmental Conference, San Antonio, Texas, February 26-28

Firoozabadi, A., (1999) Thermodynamics of Hydrocarbon Reservoirs, McGraw-Hill, New York, Chapter 5

Gunal, O. G. and Islam, M. R., (2000) Alteration of asphaltic crude rheology with electromagnetic and ultrasound irradiation, Journal of Petroleum Science and Engineering, vol. 26, pp. 263-272

Honarpour, M. M., Huang, D. D. and Al-Hussainy, R., (1996) Simultaneous measurements of relative permeability, capillary pressure, and electrical resistivity with microwave system for saturation monitoring, SPE 30540, SPE Annual Technical Conference & Exhibition, Dallas, TX, October 22-25

Islam, M. R., (1995) Potential of ultrasonic generators for use in oil wells and heavy crude oil/bitumen transportation facilities, Chapter 7, Asphaltenes: Fundamentals and Applications, E.Y. Sheu and O.C. Mullins (eds.), Plenum Press, New York

Pan, H., Firoozabadi, A. and Fortland, P., (1997) Pressure and composition effect on wax precipitation: Experimental data and model results, SPE 36740, SPE Production and Facilities, vol. 12, no. 4, pp. 250-258, November

Rogers, W. J., Eubank, P. T., Hall, K. R. and Holste, J. C., (1988) Microwave technique for phase behavior studies of petroleum and natural gas mixtures, SPE 17770, SPE Gas Technology Symposium, Dallas, TX, June 13-15

Stanley, R. K., (2001) Methods and results of inspecting coiled tubing and line pipe, SPE 68423, SPE/IcoTA Coiled Tubing Roundtable, Houston, TX, March 7-8

Vega, C., Delgardo, M. and Vega, B., (2002) Treatment of waste-water/oil emulsions using microwave radiation, SPE 74167, SPE International Conference on Health, Safety and Environment in Oil and Gas Exploration and Production, Kuala Lumpur, Malaysia, March 20-22

13.9. Appendices

13.9.1. Appendix A: Table

Table 13.1. Parameter values (Bjorndalen et al., 2003b)

Liquid	Parameter					
	Density (Kg/m^3)	**Thremal Conductivity (J/Kms)**	**Specific Heat (J/KgK)**	**Heat Generation Term**	***a***	***b***
Water	1000	0.6	4180	0.00000065	-0.07	140
Crude Oil	730	0.15	2250	0.00000065	0.99	-195
Paraffin Oil	800	0.13	2093	0.00000065	3.46	-1000

13.9.1. Appendix B: Figures

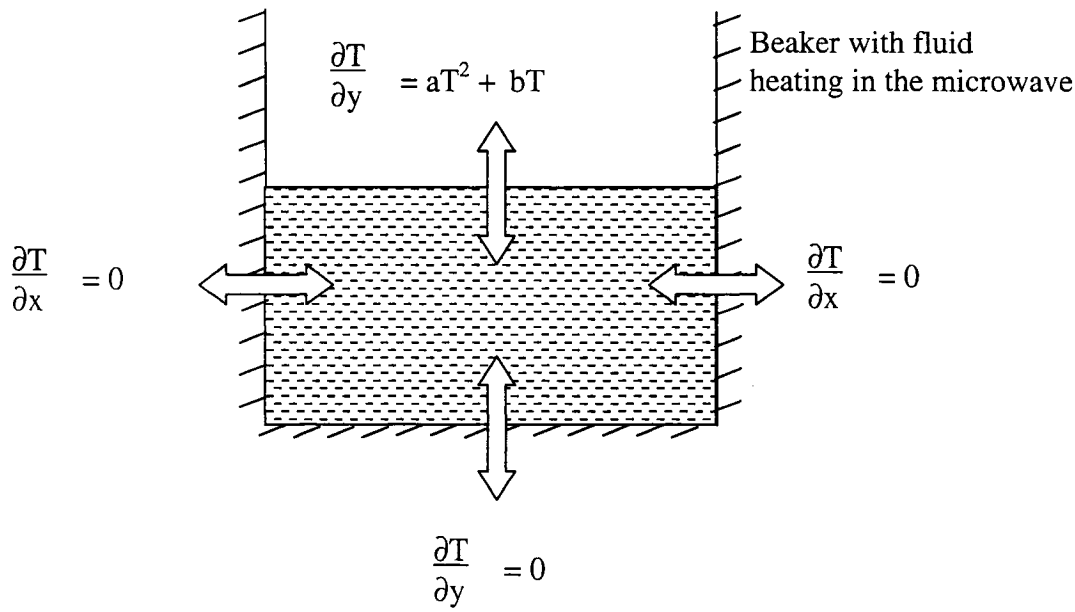

Fig. 13.1. Boundary conditions of beaker heating in the microwave (Bjorndalen et al., 2003b)

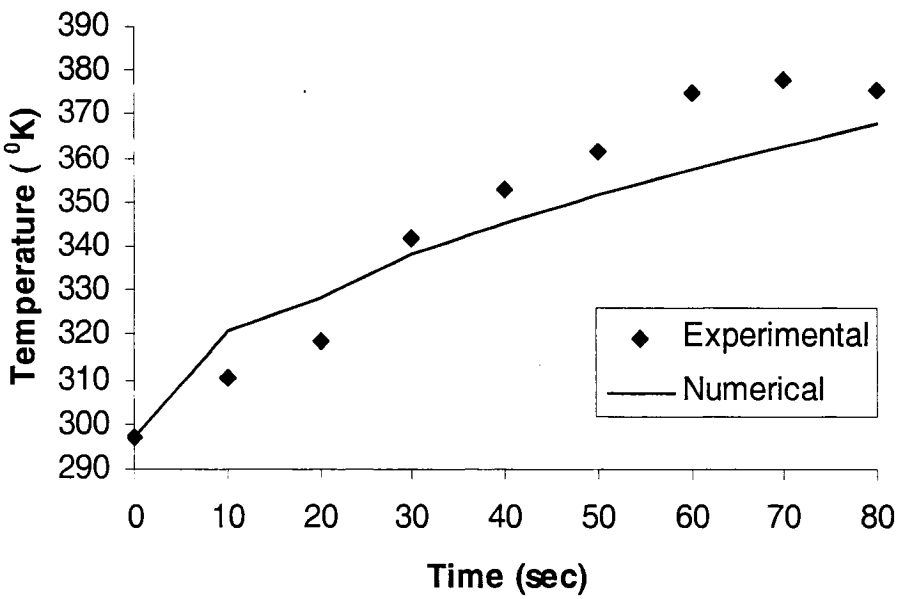

Fig. 13.2. Comparison of numerical and experimental data of 1% crude oil and 99% water heating under irradiation

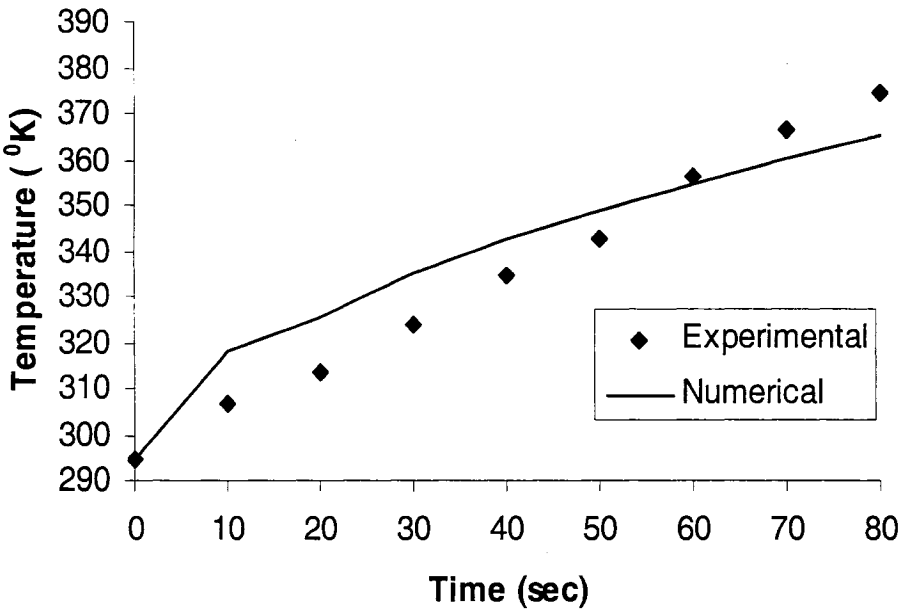

Fig. 13.3. Comparison of numerical and experimental data of 5% crude oil and 95% water heating under irradiation

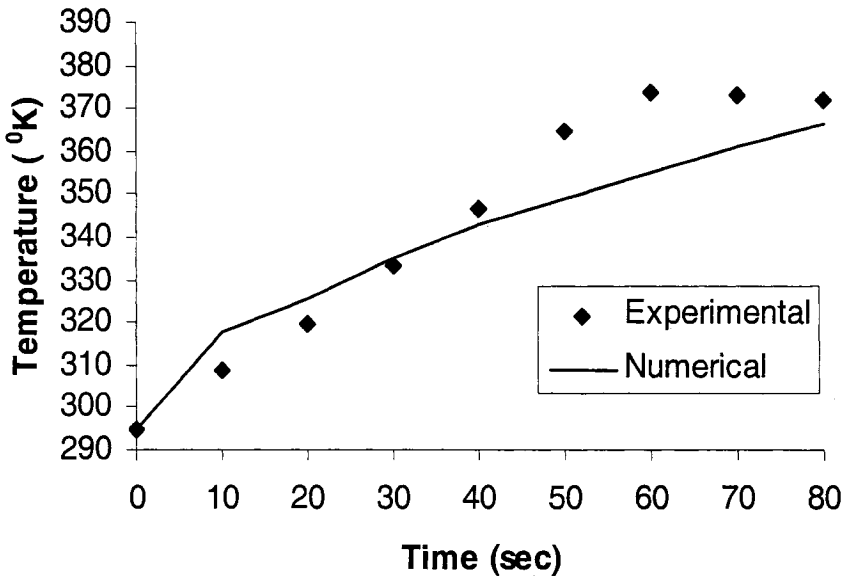

Fig. 13.4. Comparison of numerical and experimental data of 10% crude oil and 90% water heating under irradiation

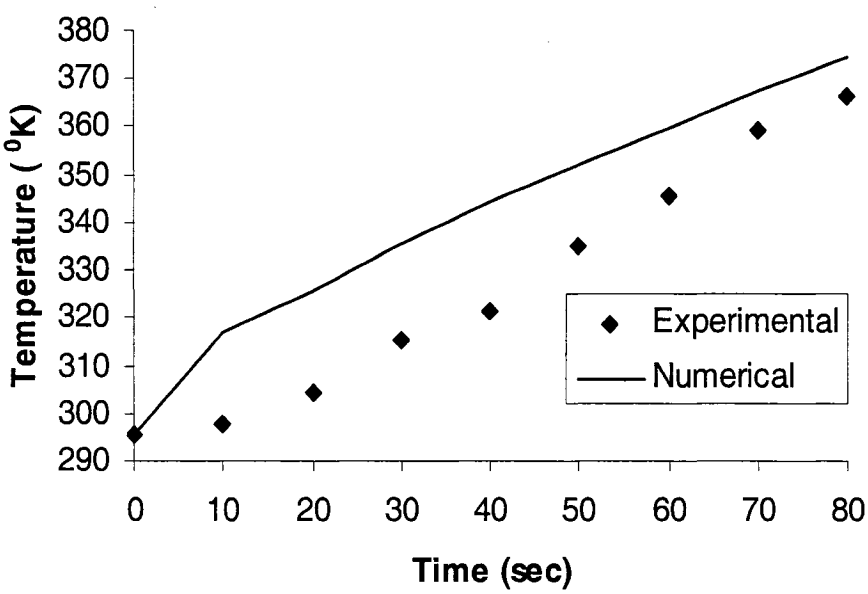

Fig. 13.5. Comparison of numerical and experimental data of 50% crude oil and 50% water heating under irradiation

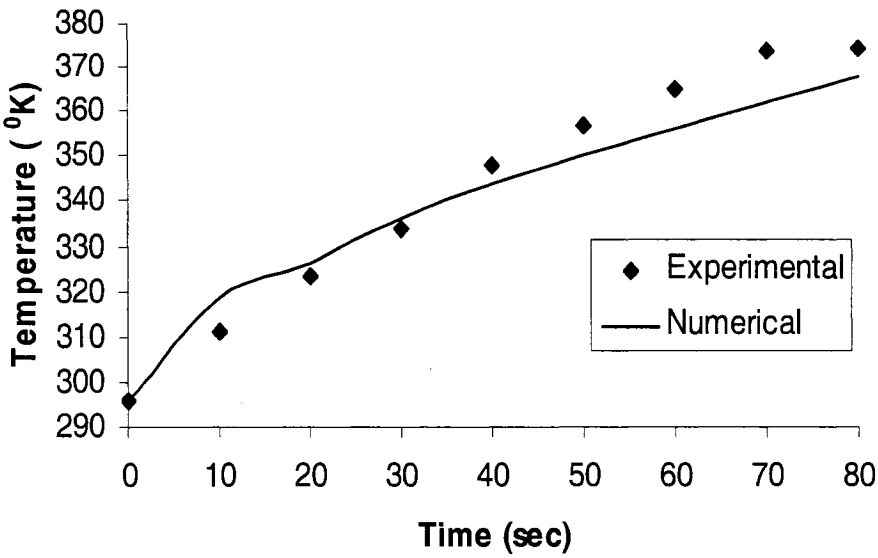

Fig. 13.6. Comparison of numerical and experimental data of 3% paraffin oil and 97% water heating under irradiation

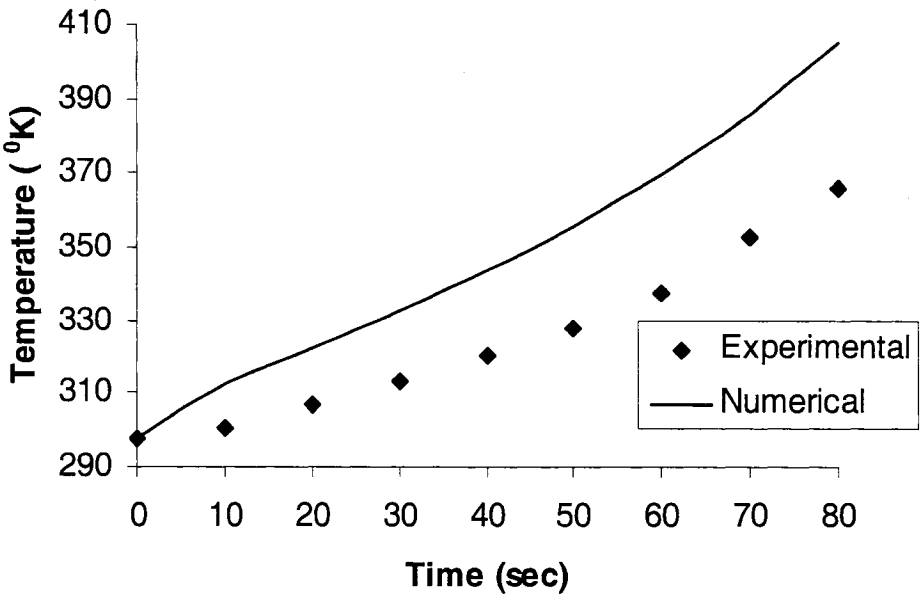

Fig. 13.7. Comparison of numerical and experimental data of 50% paraffin oil and 50% water heating under irradiation

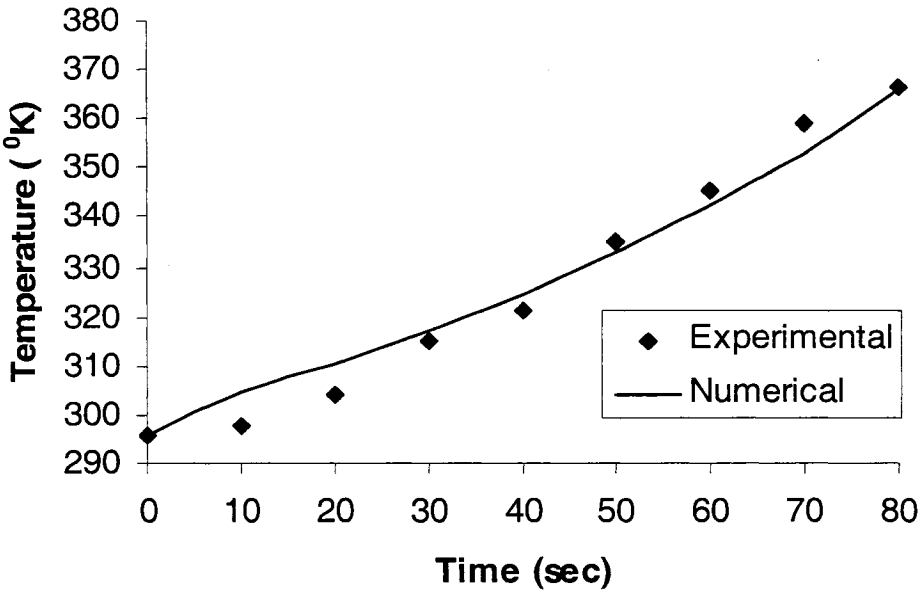

Fig. 13.8. Comparison of numerical and experimental data of 50% crude oil and 50% water heating under irradiation (adjusted a, b)

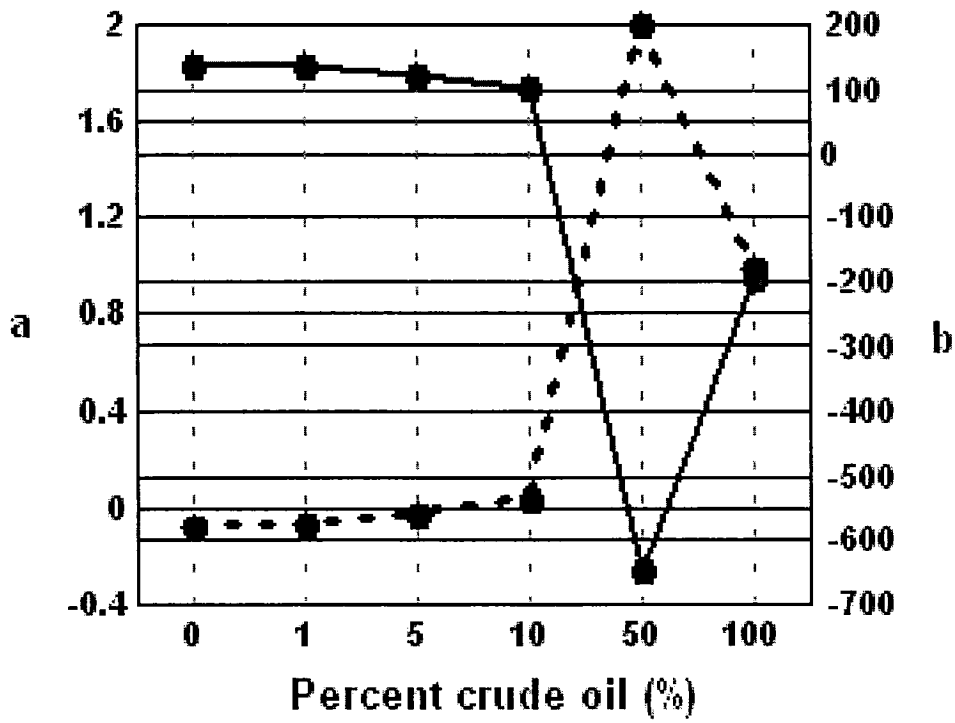

Fig. 13.9. Heating parameters (a , b) as a function of crude oil content

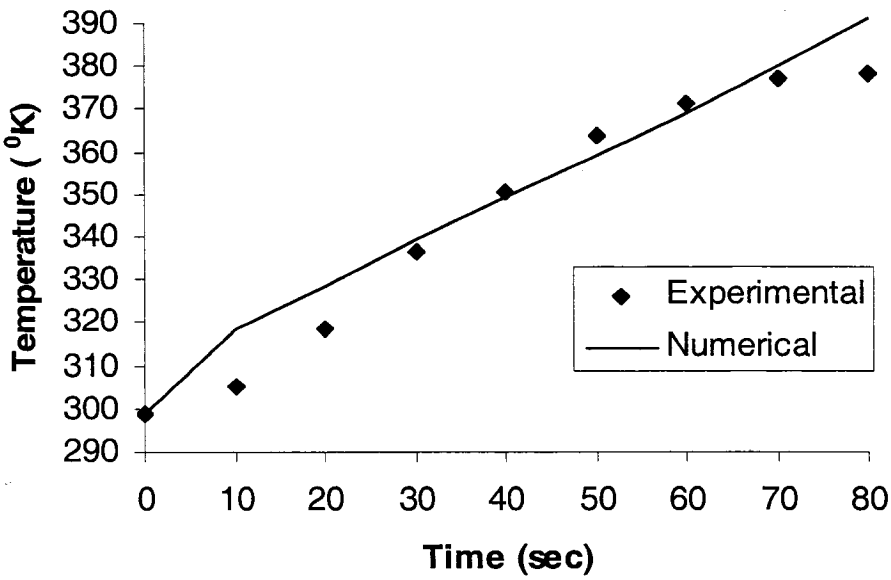

Fig. 13.10. 100% crude oil and 5 g of bentonite in 50 ml of fluid

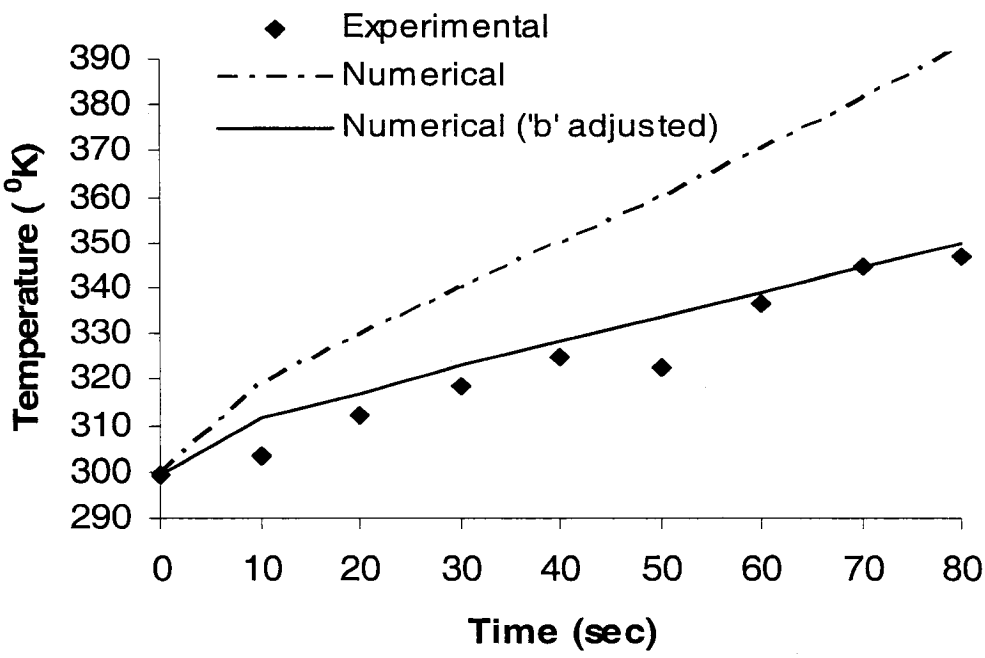

Fig. 13.11. 100% crude oil and 5 g of gypsum in 50 ml of fluid

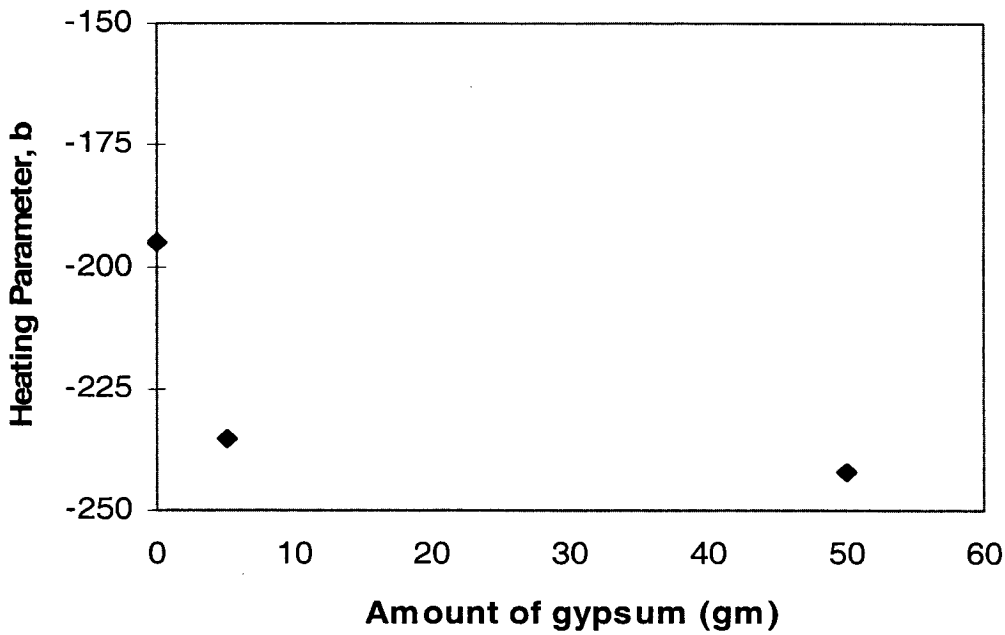

Fig. 13.12. Effect of amount of gypsum on 100% crude oil heating under irradiation

Chapter 14

14 GENERAL DISCUSSION

At this point, it is evident that the previous chapters have presented research results that are related to modeling of certain complex phenomena such as the issue of nonlinearity, existence of multiple solutions, behavior of reservoir fluids under microwave irradiation, laser technology for the purpose of drilling for improved fluid production, the effects on non-Darcy flow in well-test analyses and displacement study, water-alternate-solvent scheme, solution of nonlinear waterflood problems through advanced mathematical scheme etc. The following brief discussion reemphasizes the objectives and achievements of this dissertation.

In Chapter 2, the state-of-the-art of reservoir simulation is reviewed. Also identified are the important features of an ideal reservoir simulator. This chapter gives a flavor of what needs to be done in the short-term and in the long-term in order to keep up with the demands of the information age. It is discussed that reservoir simulators have to do more than number crunching tools if one has to make decisions based on knowledge. In the information age, it has become possible and necessary to include socioeconomic considerations along with novel computational tools in a comprehensive reservoir simulator.

In Chapter 3, the calculation of interblock geometric factors and bulk volume of blocks in radial-cylindrical coordinates for both block-centered grid and point-distributed grid require the estimation of the location in the r-direction of pressure points, block boundaries for transmissibility calculations and block boundaries for bulk volume calculations. Since such block boundaries in the r-direction are not important in interpreting simulation results, new and simple equations are presented in this

dissertation. These equations are useful to calculate interblock geometric factors and bulk volume of blocks for both block-centered grid and point-distributed grid. In these equations, one observes that the knowledge of logarithmic spacing constant (α_{lg}) and logarithmic spacing constant (α_{lg}) and radius of pressure points (r_i), which are very easy to obtain, can be used to calculate interblock geometric factor and the bulk volume.

The above mentioned equations are needed in the formulation step of fluid flow equations. However, the use of these equations is only a part of the task of formulating the reservoir fluid flow equations. In a single phase fluid flow system, the pressure value is sought after, whereas in presence of two or three phases, e.g., oil-water, oil-gas, oil-water-gas, both saturation and pressure values are required to obtain. Now the manner the fluid flow equations are solved, involves linearization at some point of the mathematical manipulation. Linearization is done in order to facilitate solutions of the governing equations that are invariable non-linear in their complete form.

In Chapter 4 (Section 4.1), the effects of linearity in the fluid flow equations are discussed. The investigation is limited to single phase fluid flow only. The linearization is imposed on the equations in two ways: linearization in formulation of fluid flow equations and linearization in computation. The discussion also covers the effects of interpolation functions and formulation, time interval, number of gridblocks, permeability variation, spatial and transient pressure distribution using different interpolation functions, CPU time etc. It is noted that no major discrepancy results between the pressure values obtained through original formulation and approximate formulation at different time steps, although the difference gradually increases with increasing time. The discrepancy is much more noticeable when the cubic spline is applied to approximate the variation of viscosity and formation volume factor with pressure. In another study, the interpolation in viscosity and formation volume factor by linear and cubic spline methods did not exhibit a significant difference in results of transient pressure values irrespective of original or linear formulation of equation. However, it is noted that if a

continuous function is used for interpolation, pressure values in the gridblocks can be overestimated.

Chapter 4 (Section 4.1) also highlights the effect of time step in a study when cubic spline and linearization techniques are used for interpolation and formulation respectively. With original formulation, the predicted pressure values for a 4-month time step exhibits a maximum relative error of only 0.01%. However, with linearization imposed in formulation, the relative error is found to increase with increasing time step (up to almost 8%). In a separate study, when permeability among gridblocks is varied, the final pressures in the gridblocks deviate from the pressures predicted assuming constant permeability all along the reservoir.

The effect of number of gridblocks on transient pressure profiles is found in another study with original formulation for equations and cubic spline as interpolation technique being followed. An increased number of gridblocks resulted in lower pressure values, which, however did not change with further increase in number of gridblocks.

In Chapter 4 (Section 4.1), a method is followed to obtain possible multiple solutions for pressure at any gridblock in the reservoir. This method basically branches out solutions from a solution. Although this investigation could not give us meaningful multiple results, it shows that mathematically the existence of multiple solutions is entirely possible.

The dissertation also examines the treatment of constant pressure boundary condition. This boundary condition is particularly chosen as the present simulation practice shows some biasness to the point-distributed grid system in treating this condition. In Chapter 4 (Section 4.2), we notice that such preference given to point-distributed grid system is not necessary in the '*engineering approach*' as found through examples of incompressible and slightly compressible fluid flow.

In Chapter 5, the search for multiple solutions is continued on several polynomials and simultaneous equations of two variables, which are considered to be the model cases for natural phenomena. Here we also obtain multiple solutions, although some solutions are not readily recognized as meaningful or even 'real'. It is important to note that these numbers are not deemed meaningful or real as per today's knowledge. It can be argued that as Science progress further toward intangibles, these numbers will reveal meanings that are currently buried under the blanket of Science of tangibles.

In Chapter 6, a relatively new mathematical technique, the Adomian decomposition method (ADM), is applied to solve several nonlinear partial differential equations including the Burgers equation, the Korteweg-de Vries (KdV) equation and the Klein-Gordon (KG) equation. During the solution process of each of these equations, the numerical result is approximated by truncating the series solution to a finite number. It is found that the accuracy of the solutions of these equations using ADM is affected by the number of series solution terms and the solutions appear acceptable for a small value of the independent variables. It is also noted that the ADM solution may be susceptible to instability as spatial or time variables are increased.

In Chapter 7, the Adomian decomposition method is applied to the classic, nonlinear Buckley-Leverett problem. The saturation-distance profile obtained through the decomposition technique is significant with regard to no occurrence of unrealistic multiple saturation points or development of shock fronts. The evaluation of saturation through recursion method is limited up to four terms, because with four terms the convergence of the series solution takes place. The decomposition technique is also applied to diffusivity equations, and the formulation of it is presented in Chapter 8 followed by an example.

Both Darcy and non-Darcy flow in a radial system with no-flow at the outer boundary and constant rate production from a single well are investigated in Chapter 9. During

Darcy flow condition, pressure analyses are conducted for unsteady state and quasi-steady state both analytically and numerically. The analytical solution in the quasi-steady state suggests two distinct contributions to pressure analyses: pressure decline in the reservoir with time at a constant rate, which is exclusively a time dependent function, and the contribution from the function of space (r) in the reservoir determining the production. Numerically the quasi-steady state pressure-time slope is found to be in excellent agreement with the theoretical prediction. The quasi-steady pressure difference is also found to be within 2% variation between theoretical and numerical predictions. This study also utilizes a numerical scheme, which demonstrates excellent accuracy with an advanced numerical model reported to be Δx^4 and Δt^4 accurate, as well as to the analytical solution of quasi-steady state velocity profile along reservoir radius. The analytical solution to quasi-steady state velocity along reservoir radius also points out that the profile is dependent on $\left(r - \frac{r_o^2}{r} \right)$.

In Chapter 9, the non-Darcy flow is presented through Forchheimer model and the numerical studies show that the linear relationship between pressure drop in the quasi-steady state and production velocity diminishes with increasing velocity and pressure drop becomes significantly higher than that predicted by Darcy's model. The quasi-steady Forchheimer velocity is also found to be higher than that predicted by Darcy model. There is also an indication in the quasi-steady velocity profile that under the no-flow at the external boundary and constant production in the inner boundary conditions, it may be possible to find a critical distance at which the difference between the Darcy and Forchheimer quasi-steady velocity is the highest.

The Darcy and non-Darcy conditions are included in another study in the dissertation (Chapter 10). In this chapter, a theoretical and numerical laboratory scale study for fluid flow through a reservoir under steady state, accumulating and depleting conditions are conducted. During steady state, the pressure profile does not vary with time whether

Darcy or Forchheimer equations are followed. Displacement features including concentration, mixing length and displacement efficiency in the steady and uniform flow condition are numerically modeled and found to be in excellent agreement with their analytical solutions. It is further noted that as grid size becomes finer, the numerical prediction approximates better to the analytical solutions.

The derived equations for Darcy and Forchheimer flow regarding transient pressure profile in the quasi-steady period are similar to the quasi-steady flow equations described in Chapter 9. In Chapter 9, the equations are in the radial coordinate system while in Chapter 10, they are in the Cartesian coordinate system. Both theoretical and numerical studies confirm that the quasi-steady Forchheimer-pressure drop is significantly higher than the Darcy-pressure drop. The theoretical and numerical quasi-steady differential pressures are also found to be in excellent agreement to each other. Under the accumulating condition, the quasi-steady velocity profile along reservoir length shows insignificant difference between the Forchheimer result and Darcy result. The numerical study also shows that the Forchheimer model predicts longer mixing length due to increased dispersion at any time than Darcy model.

In a separate numerical study on depleting reservoir, it is noted that it takes more time for the reservoir to reach the steady state if non-Darcy flow conditions prevails. In addition, the differential pressure is found to drop more significantly along the length of the reservoir in a non-Darcy state than in a Darcy state. The depleting reservoir also exhibits insignificant differences in quasi-steady velocities between Darcy and Forchheimer models; however, the Forchheimer model particularly shows more sensitivity to pressure change in the same quasi-steady condition. Numerical studies confirm that the front will move slower in an accumulating reservoir than in a depleting reservoir, which leads to larger displacement mixing area in depleting reservoir than accumulating reservoir.

Further displacement results based on an experimental study of first contact miscible displacement are reported in Chapter 11. The investigation of using two different types of oil either as slug or displaced fluid and kerosene as slug in some experimental runs, the water-alternating-gas (WAG) scheme is found to increase the sweep efficiency. The mobility ratio and the water-alternating-gas ratio are also found to affect areal displacement efficiency and some empirical relationships are provided in this chapter to calculate the sweep efficiency. The experimental results are useful for future works considering the fact there are not many data available in the literature.

The prospects of laser drilling are discussed in Chapter 12 (Section 12.1) of the dissertation. The review on laser technology, its types and their potentials, and also the discussion on experimental work conducted with MIRACL and COIL on sandstone, limestone and shale show that that laser technology can be the wave of future drilling and appealing to oil and gas industries.

The numerical study on laser drilling in Chapter 12 (Section 12.2) reveals that limestone experiences higher rate of penetration than sandstone and the drilling speed decreases as lasing time increases. However, at some lasing period, there is no appreciable decrease in drilling speed and it is found to be true in both sandstone and limestone samples. Besides, it is numerically shown that with as lasing time increases, the hole created by laser beam, increases its depth and the use of a more powerful laser will create higher depth provided the sample is exposed to same lasing time. The study also demonstrates that the energy required to remove per unit volume of sandstone is higher than that of limestone.

The dissertation also presents experimental and numerical models for microwave irradiation on immiscible fluids, i.e., crude oil-water and paraffin oil-water mixtures. In Chapter 13, the numerical model predicts transient temperature profiles with reasonable accuracy to experimental results. The values of microwave heating parameters, 'a' and

'b' for petroleum mixtures of equal proportion (1:1 oil-water ratio) are newly assigned. The models also reasonably match experimental findings for immiscible mixtures in presence of small amount of bentonite. However, the model does not show close agreement to experimental results of mixtures in presence of gypsum. These results the need for developing mathematical models that are based on composition of the rock.

Chapter 15

15 GENERAL CONCLUSIONS

From the results and discussion presented in the previous chapters, it can be concluded that the primary and secondary specific objectives outlined in Chapter 1 are achieved.

The following conclusions are in support of the above claim:

1. The discussion on some of the most important topics related to petroleum reservoir simulation, e.g., 3D imaging with comprehensive reservoir models, modelling of coupled fluid flow and geomechanical stress, modeling fluid flow under thermal stress, remote sensing and monitoring, dynamic characterization tool, virtual reality, intelligent reservoir management etc. delineate the latest advancements and also future scopes in reservoir simulation. It is concluded that in the Information Age, it has become possible and necessary to include all the salient features of the Science of Intangibles (previously known as social science and hard science) if a reservoir simulator is to be reliable.

2. The equations for interblock geometric factors and bulk volumes in both block-centred grid and point-distributed grid systems for single-well simulation developed in this dissertation are new, simple and explicit. They are useful for improving reservoir simulation performance of a mathematical model.

3. The linearization in formulation is found to have more pronounced effect than that caused by the linearization during numerical evaluation in single phase fluid flow.

4. Pressure dependent properties such as fluid viscosity and formation volume factor are found to have weak nonlinear effects in single phase fluid flow.

5. The treatment of Dirichlet type (constant pressure) boundary condition through engineering approach alleviates the present practice of giving preference to the point-distributed grid system over the block-centred grid system.

6. Any natural phenomenon may have multiple solutions, the number of which depends on the degree of nonlinearity of the equation. However, some solutions may not be readily recognizable as meaningful or even 'real'. However, as more intangible meanings are revealed in the future, this conclusion is likely to change.

7. A relatively new mathematical technique, the Adomian decomposition method (ADM) is introduced to nonlinear reservoir engineering problems such as the Buckley-Leverett equation. The technique is also further investigated to solve several other partial differential equations such as the Burgers equation, the Korteweg-de Vries equation and the Klein-Gordon equation. The model is found useful for solving non-linear equations without invoking linearity during the solution process.

8. The Buckley-Leverett equation is solved first time by the Adomian decomposition method by maintaining the nonlinear dependence of capillary pressure on saturation. The solution confirms that frontal shock is not an accurate portrayal of the displacement process. This close to exact solution also avoids unrealistic multiple saturation values.

9. Numerical models show that the pressure drop predicted by the Forchheimer model is almost same as that predicted by the Darcy model when the production velocity is kept low. However, an increase in velocity results in increasing pressure difference predicted by the models.

10. Numerical studies reveal that the pseudo-steady velocity as predicted by Forchheimer model is higher than that predicted by Darcy model everywhere in a reservoir under the influence of constant production and no-flow outer boundary conditions. Also, the high velocity region near the wellbore is much more prone to non-Darcy effects and careful considerations need to be given to this area in production scheme.

11. The results provided by the upwind technique instead of central difference approximation in the convective term of the convection-diffusion equation and the time forward scheme are comparable enough to the results predicted by a state-of-the-art scheme. Therefore, the difficulty of having an analytical solution of the Forchheimer model can be overcome by using similar advanced numerical scheme.

12. A linear reservoir experiencing non-Darcy flow is found to show significant variation in pressure drop than that result at Darcy flow during the quasi-steady state. Such significant variation is also noted for reservoirs either accumulating or depleting fluids.

13. The frontal movement in a linear reservoir undergoing accumulation of fluids is faster for Forchheimer model than for Darcy model. The mixing length is also reasonably longer for the Forchheimer case than that for the Darcy case.

14. The numerical study shows that the front moves slower in an accumulating reservoir and faster in a depleting reservoir than in a reservoir, in which uniform flow takes place. Accumulation and depletion of fluid in the reservoir are also found to affect the length of the tracer mixing zone by reducing and increasing the length, respectively.

15. The displacement efficiency rate of a depleting linear system is found to be increasingly higher than that in an accumulating or a uniform reservoir.

16. New correlations of areal sweep efficiency as a function of mobility ratio at water-alternating-gas (WAG) ratios in the range of 0.5 to 2 and as a function of water-alternating-gas (WAG) ratio at mobility ratios in the range of 0.4 and 40 are developed from the results of a number of miscible displacement tests. Generally, the efficiency is found to decrease with an increase in mobility ratio as well as with an increase in WAG ratio.

17. The WAG scheme of 1:2 is found to be the most efficient scheme for the miscible tests conducted in a WAG ratio range of 0.5 to 2.0.

18. Laser technology is reviewed as a potential and novel option in drilling oil and gas wells. While this technology has great potential, more advanced numerical models should be in place before a field design can be completed.

19. The numerical study on laser drilling shows that sandstone consumes more energy than limestone per unit volume of material removed. It is also found that the rate of penetration increases significantly as laser power increases.

20. The numerical results of specific energy consumption during laser drilling are found to be higher than the experimental data. The drilled hole-depths in sandstone and limestone samples as predicted by the numerical models are less than the experimental results.

21. An experimental and numerical model is given on the temperature rise in immiscible fluids, i.e., water and crude oil, when exposed to microwave irradiation. Reasonable accuracy is observed in the temperature profiles between the experimental and numerical results.

22. The results of microwave heating parameters for oil-water mixture in equal proportion (50% oil and 50% water) indicate that crude oil may act as a cooling agent for water during irradiation.

In future, the microwave study can be extended to determine the effect of irradiation on oil production in horizontal wells. The research can also make it possible of setting up a microwave demulsification unit, which can be applied to treat oil sludge generated during the pretreatment of the exhausted lubricating oil re-refinery.

Concluding remarks

The dissertation also fulfills the global objectives to a great extent. This dissertation shows that the use of laser technology in drilling can be tremendously beneficial in terms of time-saving as well as reduction of cost. The use of microwave can be helpful to remove plugging problems and can save millions of dollars by eliminating conventional practices of cleaning. The study of nonlinearity can lead to predicting reservoirs with much more accuracy than ever, which in turn will have significant impact on economy. Perhaps the nonlinearity has more pronounced effects in multiphase system, a subject of interest for future studies. The use of advanced mathematical method such as the Adomian decomposition technique has answered decade-long questions of shock-front in the Buckley-Leverett profiles. Perhaps the answers of many other unknown avenues of petroleum engineering topics are to be discovered through implementation of more advanced science and mathematics and innovative technologies. In future, we may find some answers of uncertainty if the mysteries of multiple solutions and complex numbers are answered. The answers of knowledge, i.e., truth are perhaps unmasking these questions.

Chapter 16

16 COMPLETE REFERENCES

Abdeh-Kolahchi, A., Satish, M.G., Ketata, C. and Islam, M.R., (in press) Sensitivity analysis of genetic algorithm parameters in groundwater monitoring network optimization for petroleum contaminant detection, International Journal of Risk Assessment and Management

Aboudheir, A., Kocabas, I. and Islam, M.R., (1999) Improvement of numerical methods in petroleum engineering problems. Proc. of the IASTED International Conference on Applied Modeling and Simulation, Cairns, Australia, September 1-3

Abou-Kassem, J.H., Farouq Ali, S.M., and Islam, M.R., (2006) Petroleum reservoir simulation: A basic approach, Gulf Publishing Company, Houston, 445 p.

Abou-Kassem, J. H., Osman, M. E., Mustafiz, S. and Islam, M. R., (in press) New simple equations for interblock geometric factors and bulk volumes in single-well simulation, Petroleum Science and Technology

Adewale, A. Olalekan, O., Kelani, B. and Abass, I., (2004) Effects of Peclet number on miscible displacement process through the reservoir, SPE 88981, Nigeria Annual International Conference and Exhibition, Abuja, Nigeria, August 2-4

Adjedj, B., (1999) Application of the decomposition method to the understanding of HIV immune dynamics, Kybernetes, vol. 28, no. 3, pp. 271-283

Note: Any previous chapter that has the 'References' section include only references related to that particular chapter. Chapter 16 is the collection of all references of this dissertation.

Adler, P. M., (1992) Porous media: geometry and transport, Butterworth-Heinemann, Stoneham, MA, USA

Adomian, G., (1984) A New approach to nonlinear partial differential equations, Journal of Mathematical Analysis and Applications, vol. 102, pp. 420-434

Adomian, G., (1986) Nonlinear stochastic operator equations, Academic Press, San Diego

Adomian, G., (1989) Nonlinear stochastic systems theory and applications to physics, Kluwer Academic Publishers, MA

Adomian, G., (1994) Solving frontier problems of physics: The decomposition method, Kluwer Academic Publishers, Dordrecht

Adomian, G. and Adomian, G.E., (1984) A Global method for solution of complex systems, Journal of Mathematical Modelling, vol. 5, pp. 521-568

Adomian, G., Cherruault, Y. and Abbaoui, K., (1996) A nonperturbative analytical solution of immune response with time-delays and possible generalization, Mathematical and Computer Modelling, vol. 20, no. 10, pp. 89-96

Ali, M.A. and Islam, M.R., (1998) The effect of asphaltene precipitation on carbonate-rock permeability: an experimental and numerical approach, SPE Production and Facilities. SPE 50963, vol. 13, no. 3, pp. 178-183

Al-Shuraiqi, H. S., Muggeridge, A. H., and Grattoni, C. A., (2003) Laboratory investigations of first contact miscible WAG displacement: the effects of WAG ratio and

flow rate, SPE 84894, SPE International Improved Oil Recovery Conference in Asia Pacific, Kuala Lumpur, Malaysia, October 20-21

Amanullah, Md. and Tan, C.P., (2001) A field applicable laser-based apparatus for mudcake thickness measurement, SPE 68673, SPE Asia Pacific Oil and Gas Conference and Exhibition, Jakarta, April 17-19

Andrade, J.S., Jr., Costa, U.M.S., Almeida, M.P., Makse, H.A. and Stanley, H. E., (1999) Inertial effects on fluid flow through disordered porous media, Physical Review Letters, vol. 82, no. 26, pp. 5249-5252

Araktingi, U. G. and Orr, F. M., Jr. (1993) Viscous fingering in heterogeneous porous media, SPE Advanced Technology Series, vol. 1, no. 1, pp. 71-80, October

Armofsky d. w., and Ramey, H. J., (1956) Mobility ratio- its influence on injection or production histories in five-spot water flood, Journal of Petroleum Technology, vol. 8, no. 9, pp. 205-210, September

Ashton, S.L., Cutmore, N.G., Roach, G.J., Watt, J.S., Zastawny, H.W. and McEwan, A.J., (1994) Development and trial of microwave techniques for measurement of multiphase flow on oil, water and gas, SPE 28814, SPE Asia Pacific Oil & Gas Conference, Melbourne, Australia, November 7-11

Aziz, K. and Settari, A., (1979) Petroleum reservoir simulation, Applied Science Publishers, London, UK

Baade, H.W., Lopez-Portillo, G.M., and Guillermo, F., (1990) Texas International Law Journal, vol. 25, no.3, 381-387

Barakat, H.Z. and Clark, J.A., (1966) On the solution of the diffusion equations by numerical methods, Transactions ASME, Journal of Heat Transfer, vol. 88, pp. 421-427

Basu, A. and Islam, M.R., (1996) Instability in a combined heat and mass transfer problem in porous media, Chaos, Solitons & Fractals, vol. 7, no. 1, pp. 109-123.

Basu, A., Mustafiz, S., Bjorndalen, N., Rahaman, S. and Islam, M.R., (2006) A comprehensive approach for modeling sorption of lead and cobalt ions through fish-scales as an adsorbent, Chemical Engineering Communications, vol. 193, pp. 580-605

Batarseh, S., (2001) Application of laser technology in the oil and gas industry: An analysis of high power laser-rock interaction and its effect of altering rock properties and behavior, PhD dissertation, Colorado School of Mines, 192 p.

Bauerle, D., (2000) Laser Processing and Chemistry, 3rd edition, Springer, Heidelberg

Bear, J., (1972) Dynamics of Fluids in Porous Media. Dover, New York: American Elsevier

^Belhaj, H.A., Agha, K.R, Butt, S.D. and Islam, M.R., (2003a) Simulation of non-Darcy flow in porous media including viscous, inertial and frictional effects, SPE 84879, Proc. 2003 SPE International Improved Oil Recovery Conference, Asia Pacific, Kuala Lumpur, Malaysia, October 20-21

+Belhaj, H.A., Agha, K.R, Butt, S.D. and Islam, M.R., (2003b) A comprehensive numerical simulation model for non-Darcy flow including viscous, inertial and convective contributions, SPE 85678, Proc. 27th Annual SPE International Technical Conference and Exhibition, Abuja, Nigeria, August 4-6

^ (2003a) in Chapter 9

+ (2003c) in Chapter 9

^Belhaj, H. A., Agha, K. R, Nouri, A. M., Butt, S. D. and Islam, M. R., (2003) Numerical and experimental modeling of non-Darcy flow in porous media, SPE 81037, Proc. SPE Latin American and Caribbean Petroleum Engineering Conference, Port-of-Spain, Trinidad, West Indies, April 27-30

Belhaj, H.A., Mousavizadegan, S.H., Ma, F. and Islam, M.R., (2006) Three-dimensional permeability utilizing a new gas-spot permeameter, SPE 100428, SPE Gas Technology Symposium, Calgary, May 15-17

Bentsen, R.G., (1978) Conditions under which the capillary term may be neglected, Journal of Canadian Petroleum technology, vol. 17, no. 4, pp. 25-30

Biazar, J., Babolian, E. and Islam, R., (2004) Solution of the system of ordinary differential equations by Adomian decomposition method, Applied Mathematics and Computation, vol. 147, pp. 713-719

Biazar, J. and Ebrahimi, H., (2005) An approximation to the solution of hyperbolic equations by Adomian decomposition method and comparison with characteristics method, Applied Mathematics and Computation, vol. 163, pp. 633–638

Biazar, J. and Islam, R., (2004) Solution of wave equation by Adomian decomposition method and the restrictions of the method, Applied Mathematics and Computation, vol. 149, pp. 807-814

Biazar, J. and Islam, M.R., (in press) The Adomian decomposition method for the solution of transient energy equation in rocks subjected to laser irradiation, International Journal of Science and Technology

^ (2003b) in Chapter 9; (2003) in Chapter 10

Bjorndalen, N., (2002) Irradiation techniques for improved performance of horizontal wells, MASc Thesis, Dalhousie University, Halifax, Canada

[+]Bjorndalen, N., Agha, K.R. and Islam, M.R., (2003) Numerical and experimental study of double diffusive phenomena under microwave irradiation, 31st Annual Conference of the Canadian Society for Civil Engineering, Moncton, NB, GCR-479, June 4-7

Bjorndalen, N. and Islam, M.R., (2004) The effect of microwave and ultrasonic irradiation on crude oil during production with a horizontal well, Journal of Petroleum Science and Engineering, vol. 43, pp. 47-60

[^]Bjorndalen, N., Mustafiz, S. and Islam, M.R., (2003) Numerical modeling of petroleum fluids under microwave irradiation for improved horizontal well performance, International Communications in Heat and Mass Transfer, vol. 30, no. 6, pp. 765-774

Bjorndalen, N., Mustafiz, S. and Islam, M.R., (2005) The effect of irradiation on immiscible fluids for increased oil production with horizontal wells, ASME International Mechanical Engineering Conference and Exposition, Orlando, Florida, USA, November 6-11

Blackwell, B. F., (1990) Temperature profile in semi-infinite body with exponential source and convective boundary condition, ASME, Transactions, Journal of Heat Transfer, vol. 112, August, pp. 567-571

Blick, E.F. and Civan, F., (1988) Porous media momentum equation for highly accelerated flow, SPE 16202, SPE Reservoir Engineering, pp. 1048-1052, August

[+] (2003a) in Chapter 13

[^] (2003b) in Chapter 13

Bokhari, K., (2003) Experimental and numerical modeling of viscous fingering in liquid-liquid displacement, MASc thesis, Department of Chemical Engineering, Dalhousie University

Bokhari, K. and Islam, M.R., (2005) Improvement in the time accuracy of numerical methods in petroleum engineering problems – A new combination, Energy Sources, vol. 27, no. 1-2, 45-60

Bokhari, K., Mustafiz, S. and Islam, M.R., (2006) Numerical modeling of viscous fingering under combined effects of thermal, solutal and mixed convection in liquid-liquid miscible displacements, Journal of Petroleum Science and Technology, accepted for publication, May

Bradley H.b., Heller, J.P. and Odeh, A.S., (1961) A potentiometric study of the effects of mobility ratio on reservoir flow patterns, SPE 1585-G, Society of Petroleum Engineering Journal, pp. 125-129, September

Brainerd, R.J. and Robbins, G.A., (2004) A tracer dilution method for fracture characterization in bedrock wells, Ground Water, vol. 42, no. 5, pp. 774-780

Buckley, S.E. and Leverett, M.C., (1942) Mechanism of fluid displacement in sands, Trans. AIME, vol. 146, pp. 187–196

Carstens, J.P. and Brown, C.O., (1971) SPE 3529, 46th Annual Fall Meeting of SPE, New Orleans, Louisiana, October 3-6

Chalaturnyk, Rick, and Scot, J. D., (1995) Geomechanics issues of steam assisted gravity drainage, paper SPE 30280, presented at the International Heavy Oil Symposium held in Calgary, AB, Canada, June 19-21

Chan, C. L. and Mazumder, J., (1987) One-dimensional steady-state model for damage by vaporisation and liquid expulsion due to laser-material interaction, Journal of Applied Physics, vol. 62, pp. 4579 - 4596

Chappelear, J.E. and Hirasaki, G.J., (1976) A model of oil/water coning for two-dimensional areal reservoir simulation, Society of Petroleum Engineering Journal, vol. 16, no. 2, pp. 65-72

Chaudhry, M. A., and Zubair, S. M., (1994) On a pair of functions useful in heat conduction problems, International Communications in Heat and Mass Transfer, vol. 21, no. 5, pp. 673-681

Cheek, R.E. and Menzie D.E., (1955) Fluid mapper model studies of mobility ratio, Petroleum Transactions, AIME, vol. 204, pp. 278-281

Cheema, T.J. and Islam, M.R., (1995) A new modeling approach for predicting flow in fractured formations, In: El-Kady (Editor), Groundwater Models for Resources Analysis and Management, Lewis Publishers, Boca Raton, FL, pp. 327-338

Chen, H. Y., Teufel, L.W., Lee, R. L., (1993) Couple fluid flow and geomechanics in reservoir study-I, theory and governing equations, paper SPE 30752, paper presented at the SPE annual technical conference and exhibition, Dallas, USA., October

Choi, I., Cheema, T. and Islam, M.R., (1997) A new dual-porosity/dual permeability model with non-Darcian flow through fractures, Journal of Petroleum Science and Engineering, vol. 17, pp. 331-344

Christensen, J.R., Stenby, E.H. and Skauge, A., (1998) Review of WAG field experience,

SPE 39883, International Petroleum Conference and Exhibition of Mexico, Villahermosa, Mexico, March 3-5

Christie, M. A., (1989) High resolution simulation of unstable flows in porous media, SPE Reservoir Engineering, vol. 4, pp. 297-304

Christie, M. A. and Bond, D. J., (1987) Detailed simulation of unstable processes in miscible flooding, SPE Reservoir Engineering, vol. 2, pp. 514-522

Coates, D. E, and Kirkaldy, J. S., (1971) Morphological stability of alpha-beta phase interfaces in the Cu- Zn- Ni system at 775 C , Metallurgy Transactions, vol. 2, no. 12, pp. 3467-3477, December

Cole, J.D., (1951) On a quasi-linear parabolic equations occurring in aerodynamics, Quarterly of Applied Mathematics, vol. 9, pp. 225-236

Coriell, S.R., McFadden, G.B., Sekerka, R.F.and Boettinger W.J., (1998) Multiple similarity solutions for solidification and melting, Journal of Crystal Growth, vol. 191, pp. 573-585

Coskuner, G. and Hyde, T.C., (1998) Homogeneous equivalents of naturally fractured porous media for miscible fluid displacements, Journal of Petroleum Science and Engineering, vol. 19, pp. 145-157

Couland, O., Morel, P. and Caltagirone, J. P., (1988) Numerical modelling of nonlinear effects in laminar flow through a porous medium, Journal of Fluid Mechanics, vol. 190, pp. 393-407

Courant, R., Isaacson, E. and Rees, M., (1952) On the solution of nonlinear hyperbolic

differential equations by finite differences, Communications on Pure and Applied Mathematics, vol. 5, pp. 243-249

Craft, B.C. and Hawkins, M.F., (1991) Applied petroleum reservoir engineering, 2nd edition, Prentice Hall PTR, Englewood Cliffs, NJ

Cvetkovic, V.D., (1986) A continuum approach to high velocity flow in porous media, Transport in Porous Media, pp. 63-97

Dabby, F. W. and Paek, U., (1972) High-intensity laser-induced vaporization and explosion of solid material, IEEE Journal of Quantum Electronics, vol. QE-8, no. 2, pp. 106-111

Darcy, H.P.G., (1856) Les Fontaines Publiques de villle de la Dijon Dalmont, Exposition et Application des Pricipes a Suivre et des Furmules a Emplyer dans les Questions de Distribution d'Eau. Victor Dalmont, Paris

Debnath, L., (2005) Nonlinear partial differential equations for scientists and engineers, 2nd edition, Boston: Birkhäuser

Deeba, E. Y. and Khuri, S. A., (1996) A decomposition method for solving the nonlinear Klein-Gordon equation, Journal of computational physics, vol. 124, pp. 442-448

Desai, R.A., Lowery, A.J., Christopoulos, C., Naylor, P., Blashard, J.M.V. and Gregson, K., (1992) Computer modeling of microwave cooking using the transmission line model, IEEE Proceedings-A, vol. 139, no. 1, pp. 30-38

Dougherty E. L. and Sheldon, J. W., (1964) The use of fluid-fluid interfaces to predict the behavior of oil recovery processes, SPE 183, SPE Journal, pp. 171-182

Dullien, F.A.L., (1992) Porous Media: Fluid transport and pore structure, 2nd edition, Academic Press, San Diego, USA

Dung, H.T. and Piracha, A.L., (2000) Journal of Energy and Development, vol. 25, no. 1, pp. 47-70

Editorial, (1996) Watching the world: tangible benefits of virtual reality, Oil & Gas Journal, vol. 94, no.13, p. 30

El-Sayed, S.M. and Abdel-Aziz, M.R., (2003) A comparison of Adomian's decomposition method and wavelet-Galerkin method for solving integro-differential equations, Applied Mathematics and Computation, vol. 136, pp. 151-159

Emmanuel, A.S. and Cook, G.W., (1974) Pseudorelative permeability for well modeling, Society of Petroleum Engineering Journal, vol. 14, no. 1, pp. 7-9

Ertekin, T., Abou-Kassem, J. H., and King, G. R., (2001) Basic applied reservoir simulation, SPE textbook series, vol. 7, 406 p., SPE: Richardson, TX

Eugene, Y., (1993) Application of the decomposition method to the solution of the reaction-convection-diffusion equation, Applied Mathematics and Computation, vol. 56, pp. 1–27

Farouq Ali, S.M., (1994) Elements of reservoir modeling and selected papers, Course notes: Petroleum engineering, Mineral engineering department, The University of Alberta

Fay, C.H. and Prats, M., (1951) The application of numerical methods to cycling and flooding problems, Proceedings of the 3rd World Petroleum Congress

Fayers, F.J., and Sheldon, J.W., (1959) The effect of capillary pressure and gravity on two-phase fluid flow in a porous medium, Transactions AIME, vol. 216, pp. 147-155

Feature, (1997) Caution expressed over industry optimism on 4D seismic technology, First Break, vol. 15, no. 2, p. 51

Ferri, R.P. and Uthe, M.T., (2001) Hydrocarbon remediation using microwave, SPE 66519, SPE/EPA/DOE Exploration and Production Environmental Conference, San Antonio, Texas, February 26-28

Finley, J.R., Pinter, J.D., and Satish, M.G., (1998) Automatic model calibration applying global optimization techniques, Journal of Environmental Modeling and Assessment, vol. 3, no. 1-2, pp. 117-126

Firoozabadi, A., (1999) Thermodynamics of Hydrocarbon Reservoirs, McGraw-Hill, New York, Chapter 5

Forchheimer, P., (1901) Wasserbewegung durch Boden ZVDI, vol. 45, pp. 1781

Gaddy, D., Moritis, G. and True, W., (1998) OTC papers highlight technological advancements, Oil & Gas Journal, May 18, p. 46

Gahan, B.C., Parker, R.A., Batarseh, S., Figueroa, H., Reed, C.B. and Xu, Z., (2001) Laser drilling: Determination of energy required to remove rock, SPE 71466, SPE Annual Conference and Exhibition, New Orleans, Louisiana, September 30 –October 3

Graves, R.M. and O'Brien, D.G., (1998a) StarWars laser technology applied to drilling and completing gas wells, SPE 49259, SPE Annual Technical Conference and Exhibition, New Orleans, Louisiana, September 27-30

Graves, R.M. and O'Brien, D.G., (1998b) Targeted literature review: Determining the benefits of StarWars laser technology for drilling and completing natural gas wells, GRI-98/0163, July

Graves, R.M. and O'Brien, D.G., (1999) Journal of Petroleum Technology, February, pp. 50-51

Guellal, S. and Cherruault, Y., (1995) Application of the decomposition method to identify the distributed parameters of an elliptical equation, Mathematical and Computer Modelling, vol. 21, no. 4, pp. 51-55

Gunal, O.G. and Islam, M.R., (2000) Alteration of asphaltic crude rheology with electromagnetic and ultrasound irradiation, Journal of Petroleum Science and Engineering, vol. 26, pp. 263-272

Habermann, B., (1960) The efficiency of miscible displacement as a function of mobility ratio, Trans., AIME, vol. 219, p. 264.

Hallada, M.R., Walter, R.F. and Seiffert, S.L., (2000) High-power-laser rock cutting and drilling in mining, In the proceeding of SPIE, High Power Laser Ablation 2000, vol. 4065-73, New Mexico, USA, April 23-28

Hettema, M., Papamichos, E. and Schutjens, P., (2002) Subsidence delay: Field observations and analysis, Oil and Gas Science and Technology, Rev. IFP, vol. 57, no. 5, pp. 443-458

Hickernell, F. J. and Yortsos, Y. C., (1986) Linear stability miscible displacement processes in porous media in the absence of dispersion, Studies in Applied Mathematics, vol. 74, pp. 93-115

Hojka, K., Dusseault, M.B. and Bogobowicz, A.D., (1993) Analytical solutions for transient thermoplastic stress fields around a wellbore during fluid injection into permeable media, Journal of Canadian Petroleum Technology, vol. 32, no. 4, pp. 49-57

Holmgren, C.R. and Morse, R.A., (1951) Effect of Free gas saturation on oil recovery by waterflooding, Trans., AIME, vol. 192, pp. 135-140

Honarpour, M.M., Huang, D.D. and Al-Hussainy, R., (1996) Simultaneous measurements of relative permeability, capillary pressure, and electrical resistivity with microwave system for saturation monitoring, SPE 30540, SPE Annual Technical Conference & Exhibition, Dallas, TX, October 22-25

Hossain, M.E., Ketata, C., Khan, M.I. and Islam, M.R., (in press) Flammability and individual risk assessment for natural gas pipelines, International Journal of Risk Assessment and Management

Hovanessian, S.A., and Fayers, F.J., (1961) Linear water flood with gravity and capillary effects, Society of Petroleum Engineering Journal, March, pp. 32-36

Howarth, R.B. and Winslow, M.A., (1994) Energy use and CO_2 emissions reduction: Integrating pricing and regulatory policies, Energy – The International Journal, vol 19, pp. 855-867

Islam, M.R., (1993) Route to chaos in chemically enhanced thermal convection in porous media, Chemical Engineering Communications, vol. 124, pp. 77-95

Islam, M.R., (2000) Energy State of the Art 2000, Ed. C.Q. Zhou, Int. Sci. Serv., Charlottesville, VA, 21 pp.

Islam, M.R., (2001a) Emerging technologies in monitoring of oil and gas reservoirs, SPE paper no. 68804, proc. SPE Western Regional Conference, Bakersfield, California, March 26-30

[+]Islam, M.R., (2001b) Emerging technologies in subsurface monitoring of petroleum reservoirs, SPE 69440, SPE Latin America and Caribbean Petroleum Engineering Conference, Buenos Aries, Argentina, March 25 – 28

Islam, M.R. (2006a) Comprehensive mathematical modelling of horizontal wells, paper no. 69, Proc. of the 2nd European Conference on the Mathematics of Oil Recovery, Latitudes Camargue, Arles, France, September 11-14

[^]Islam, M.R., (2006b) Computing for the information age, Proc. of the 36th International Conference on Computers and Industrial Engineering, Keynote speech, Taipei, Taiwan, June 20-23

Islam, M.R., Chakma, A. and Nandakumar, K., (1990) Flow transition in mixed convection in a porous medium saturated with water near 4C, Canadian Journal of Chemical Engineering, vol. 68, pp. 777-785

Islam, M.R. and Nandakumar, K., (1986) Multiple solution for buoyancy-induced flow in saturated porous media for large Peclet numbers, Transactions ASME Journal of Heat Transfer, vol.108, no. 4, pp. 866-871

Islam, M.R. and Nandakumar, K., (1988) Mixed convection heat transfer in porous media in the non-Darcy regime, Canadian Journal of Chemical Engineering, vol. 66, no. 1, pp. 68-74

[+] (2001) in Chapter 12.1

[^] (2006) in Chapter 5

Islam, M.R. and Nandakumar, K., (1990) Transient convection in saturated porous layers with internal heat sources, International Journal of Heat and Mass Transfer, vol. 33, no. 1, pp. 151-161

Islam, M.R. and Wellington, S.L., (2001) Past, present, and future trends in petroleum research, SPE 68799, SPE Western Regional Conference, Bakersfield, California, March 26-30

Islam, M.R. and Zatzman, G.M., (2006) Emulating nature in the information age, Chemcon-06, 59th Annual Conference of the Indian Chemical Engineering Congress, Gujarat, December 27-30

Johns, T. R., Bermudez, L., and Parakh, H., (2003) WAG optimization for gas floods above the MME, SPE 84366, SPE Annual Technical Conference and Exhibition, Denver, Colorado, USA, October 5-8

Joseph, G.G., (2000) The crest of the peacock: Non-European roots of mathematics, Ed. 2, Penguin Books, London

Ketata, C., Satish, M., Islam, M.R., (2005a) Knowledge-based optimization of rotary drilling system, Proceedings of 2005 International Conference on Computational and Experimental Engineering and Science, Hyderabad, India, December 1-6

Ketata, C. Satish, M., Islam, M.R., (2005b) Stochastic evaluation of rock properties by sonic-while-drilling data processing in the oil and gas industry, Proceedings of 2005 International Conference on Computational and Experimental engineering and Science, Hyderabad, India, December 1-6

Ketata, C. Satish, M.G., and Islam, M.R., (2006a) The Meaningful zero, Proceedings of 36th Conference on Computer and Industries, June, Taiwan

Ketata, C. Satish, M.G., and M.R. Islam, (2006b) Cognitive work analysis of expert systems design and evaluation in the oil and gas industry, Proceedings of 36th Conference on Computer and Industries, June, Taiwan

Ketata, C., Satish, M.G., Islam, M.R., (2006c) The meaningful infinity, International Conference on Computational Intelligence for Modelling, Control and Automation-2006, Sydney, Australia, November 29–December 1

Ketata, C., Satish, M.G. and Islam, M.R., (2006d) Multiple Solution Nature of Chaos Number-Oriented Equations, International Conference on Computational Intelligence for Modelling, Control and Automation-2006, Sydney, Australia, November 29–December 1

Khan, M.I. and Islam, M.R., (2006) True sustainability in technological development and natural resources management, Nova Science Publishers, NY, USA

Khan, M.I. and Islam, M.R., (in press[1]) A handbook on sustainable oil and gas operations, Gulf Publishing Company, TX

Khan, M.I. and Islam, M.R., (in press[2]) Technological analysis and quantitative assessment of oil and gas development on the Scotian Shelf, Canada, International Journal of Risk Assessment and Management

Khan, M.I., Lakhal, S.Y., Satish, M., and Islam, M.R., (in press) Towards achieving sustainability: application of green supply chain model in offshore oil and gas operations, International Journal of Risk Assessment and Management

Kim, K.S. and van Stone, R.H., (1995) Hold time crack growth analysis at elevated temperatures, Engineering Fracture Mechanics, vol. 52, no. 3, pp. 433-444

Kocabas, I., (2003) Modeling tracer flow in oil reservoirs containing high permeability streaks, SPE 81429, SPE 13th Middle East Oil Show and Conference, Bahrain, April 5-8

Kocabas, I. and Islam M.R., (2000a) Concentration and temperature transients in heterogeneous porous media, part I: linear transport, Journal of Petroleum Science and Engineering, vol. 26, pp. 211-220

Kocabas, I. and Islam M.R., (2000b) Concentration and temperature transients in heterogeneous porous media, part II: radial transport, Journal of Petroleum Science and Engineering, vol. 26, pp. 221-233

Lacey, J. W., Faris, J. E. and Brinkman, F. H., (1961) Effect of bank size on oil recovery in the high-pressure gas-driven LPG-bank process, Trans. AIME, vol. 222, p. 806

Laffez, P. and Abbaoui, K., (1996) Modelling of the thermic exchanges during a drilling: resolution with Adomian's decomposition method, Mathematical and Computer Modelling, vol. 23, no. 10, pp. 11-14

Lake, L.W., (1989) Enhanced oil recovery, Prentice Hall, Englewood Cliffs, NJ, USA

Lakhal, S., H'mida, S., and Islam, M.R., (in press) Green supply chain parameters for a Canadian petroleum refinery company, International Journal of Environmental Technology and Management

Larson, R.G., (1987) Controlling numerical dispersion by time flux, Society of Petroleum Engineering Journal, March

Lee, J., (2002) Well Testing, SPE textbook series, vol. 1, SPE, Richardson, TX

Lee, K. S., and Claridge, E. L., (1968) Areal sweep efficiency of pseudoplastic fluids in a five-spot Hele-Shaw model, Society of Petroleum Engineering Journal, pp. 52-62

Li, D. and Engler, T.W., (2002) Modeling and simulation of non-Darcy flow in porous media, SPE 75216, SPE/DOE Improved Oil Recovery Symposium, Tulsa, OK, April 13-17

Liu, SW. and Ramirez, W.F., (1994) Optimal control of three-dimensional steam flooding process, Journal of Petroleum Science and Engineering, vol. 11, pp. 137-154

Ma, H. and Ruth, D., (1997) Physical explanations of non-Darcy effects for fluid flow in porous media, SPE Formation Evaluation, March

MacDonald, R.C. and Coats, K.H., (1970) Methods for numerical simulation of water and gas coning, Society of Petroleum Engineering Journal, vol. 10, no. 4, pp. 425-436

Mahaffey, J.L., Rutherford, W.M. and Matthews, C.S., (1966) Sweep efficiency by miscible displacement in a five-spot, Society of Petroleum engineering Journal, vol. 3, p. 73

Marle, C.M., (1981) Multiphase flow in porous media, Gulf Publishing, Houston, USA

Matthews, C.S. and Russell, D.G., (1967) Pressure buildup and flow tests in wells, Monograph Series: SPE, Dallas, USA

Mauer, W.C., Anderson, E.E., Hood, M., Cooper, G. and Cook, N., (1990) Deep drilling basic research, vol. 5, System Evaluations, Final Report, GRI-90/0265.5, June, 5-1

Maugis, P.; Hopfe, W.D.; Morral, J.E.; Kirkaldy, J.S., (1996) Degeneracy of diffusion paths in ternary, two-phase diffusion couples, Journal of Applied Physics, vol. 79, no. 10, pp. 7592-7596

Merle, H.A., Kentie, C.J.P., van Opstal, G.H.C. and Schneider, G.M.G., (1976) The Bachaquero study - A composite analysis of the behavior of a compaction drive/solution gas drive reservoir, SPE Journal of Petroleum Technology, pp. 1107-1115, September

Mishra, S., and DebRoy, T., (2005) A computational procedure for finding multiple solutions of convective heat transfer equations, Journal of Physics D: Applied Physics, vol. 38, pp. 2977–2985

Moavenzadeh, F., McGarry, F.J. and Williamson, R.B., (1968) Use of Laser and Surface Active Agents for Excavation in Hard Rocks, SPE 2240, Fall Meeting of the Society of Petroleum Engineers of AIME, Houston, TX, September 29 - October 2

Moisses, D.E., Miller, C. A. and Wheeler, M. F., (1989) Simulation of miscible viscous fingering using a modified method of characteristic: effect of gravity & heterogeneity, SPE 18440, 10th Symposium on Reservoir Simulation, Houston, TX, February 6-8

Mufti, A.A., Tadros, G., and Jones, P.R., (1997) Field assessment of fibre-optic Bragg grating strain sensors in the Confederation Bridge, Canadian Journal of Civil Engineering, vol. 24, no. 6, pp. 963–966

Mustafiz, S., (2002) A novel method for heavy metal removal from aqueous streams, MASc Thesis, Dalhousie University, Canada

[+]Mustafiz, S., Biazar, J. and Islam, M.R., (2005a) An Adomian decomposition solution to the modified Brinkman model (MBM) for a 2-dimensional, 1-phase flow of petroleum fluids, Proc. CSCE 33rd Annual Conference, Toronto, Canada, June 2-4

[^]Mustafiz, S., Biazar, J. and Islam, M.R., (2005b) Formulation of two-phase, two-dimensional non-linear PDE's as applied in well testing, proceeding of the 1st International Conference on Modeling, Simulation and Applied Optimization, Sharjah, UAE, February 1-3

Mustafiz, S. and Islam, M. R., (2005) Adomian decomposition of two-phase, two-dimensional non-linear PDEs as applied in well testing, Proc. 4th International Conference on Computational Heat and Mass Transfer, Paris-Cachan, May 17-20

Mustafiz, S. and Islam, M. R., (2006) The state-of-the-art of reservoir simulation, Petroleum Science and Technology, accepted for publication, August

Mustafiz, S., Ma, F. and Islam, M. R., (2006) Well test analyses for Darcy and non-Darcy flow using an advanced numerical scheme, Journal of Petroleum Science and Engineering, submitted for publication, September

[*]Mustafiz, S., Mousavizadegan, H., and Islam, M.R., (2006a) The effects of linearization on solutions of reservoir engineering problems, Journal of Petroleum Science and Technology, accepted for publication, July, 17 pg.

Mustafiz, S., Mousavizadegan, H., and Islam, M.R., (2006b) Adomian decomposition of Buckley-Leverett equation with capillary effects, Journal of Petroleum Science and Technology, submitted for publication, August

[+] (2005) in Chapters 2 and 7

[^] (2005) in Chapter 8

*(2006) in Chapters 5 and 7

Naami, A.M., Catania, P., and Islam, M.R., (1999) Numerical and experimental modeling of viscous fingering in two-dimensional consolidated porous medium, CIM paper no. 118, CIM conference, Regina, October

Nixon, D., (1989) Occurence of multiple solutions for the TSD-Euler equation Source: Acta Mechanica, vol. 80, no. 3-4, pp. 191-199

Nolen, J.S. and Berry, D.W., (1972) Tests of the stability and time step sensitivity of semi-implicit reservoir simulation techniques, Transactions AIME, vol. 253, pp. 253-266

Nouri, A., Vaziri, H. and Islam, M.R., (2002) A new theory and methodology for modeling sand production, Energy Sources, vol. 24, no. 11, pp. 995-1008

Nouri, A., Vaziri, H., Kuru, E. and Islam, R., (2006) A Comparison of Two Sanding Criteria in Physical and Numerical Modeling of Sand Production, Journal of Petroleum Science and Engineering, vol. 50, pp. 55-70

Numbere, D.T. and Erkal, A., (1998) A model for tracer flow in heterogeneous porous media, SPE 39705, SPE Asia Pacific conference on Integrated Modeling for Asset Management, Kuala Lumpur, Malaysia, March 23-24

^O'Brien, D.G., Graves, R.M. and O'Brien, E.A., (1999a) StarWars laser technology for gas drilling and completions in the 21st century, SPE 56625, SPE Annual Technical Conference and Exhibition, Houston, TX, October 3-6

O'Brien, D.G., Graves, R.M. and O'Brien, E.A., (1999b) International Society for Optical Engineering, V3614, San Jose, California, vol. 168, January 25-29

^ (1999) in Chapter 12.1

Pan, H., Firoozabadi, A. and Fortland, P., (1997) Pressure and composition effect on wax precipitation: Experimental data and model results, SPE 36740, SPE Production and Facilities, vol. 12, no. 4, pp. 250-258, November

Panawalage, S.P., (2002) The solution of an inverse problem in reservoir permeability, Masters Thesis, Dalhousie University, Halifax, Canada

Peaceman, D.W. and Rachford, Jr. H. H., (1962) Numerical calculation of multidimensional miscible displacement, Society of Petroleum Engineering Journal, Transactions AIME, vol. 228, December

Pedrosa, Jr., Oswaldo, A. and Aziz, K., (1986) Use of hybrid grid in reservoir simulation, SPE 13507, SPE Reservoir Engineering, vol. 1, no. 6, pp. 611-621

Powers, D.L., (1979) Boundary value problems, 2nd edition, Academic Press, New York

Pozzi, A., L., and Blackwell, R. J., (1963) Design of laboratory models for study of miscible displacement, SPE 445, Society of Petroleum Engineering Journal, pp. 28-40, March

Rahman, M. A., Mustafiz, S., Biazar, J., Koksal, M. and Islam, M. R., (in press) Investigation of a novel perforation technique in petroleum wells - perforation by drilling, Journal of the Franklin Institute

Rahman, M., (1995) Water Waves: Relating Modern Theory to Advanced Engineering Practice, Oxford University Press Inc., New York

Rahman, H., Wasiuddin, N. M., Islam, M. R., (2003) Experimental and numerical modeling studies of arsenic removal with wood ash from aqueous streams, The Canadian Journal of Chemical Engineering, vol. 82, no. 5, pp. 968-977

Ramanathan, S. and Modest, M. F., (1990) Effects of variable thermal properties on evaporative cutting with a moving CW laser, ASME Heat Transfer in Space Systems, vol. HTD–135, pp. 101–108

Ramanathan, S. and Modest, M. F., (1992) CW laser drilling of composite ceramics, Proceedings of ICALEO '91, Laser Materials Processing, vol. 74, pp. 305-326, San Jose, CA

Rogers, W.J., Eubank, P.T., Hall, K.R. and Holste, J.C., (1988) Microwave technique for phase behavior studies of petroleum and natural gas mixtures, SPE 17770, SPE Gas Technology Symposium, Dallas, TX, June 13-15

Roy, S., and Modest, M. F., (1993) CW laser machining of hard ceramics-Part I: Effects of three-dimensional conduction and variable properties and various laser parameters, International Journal of Heat and Mass Transfer, vol. 36, no. 14, pp. 3515–3528

Ruth, D. and Ma, H., (1992) On the derivation of the Forchheimer equation by means of the averaging theorem, Transport in Porous Media, vol. 7, pp. 255

Saghir, M.Z., Chaalal, O. and Islam, M.R., (2000) Experimental and numerical modeling of viscous fingering, Journal of Petroleum Science and Engineering, vol. 26, no. 1-4, pp. 253-262

Saghir, M. Z. and Islam, M. R., (1998) Double diffusive and marangoni convection in a multi-cavity system, International Journal of Heat and Mass Transfer, vol. 41, no. 14, pp. 2157-2174

Saghir, M.Z. and Islam, M.R., (1999) Viscous fingering during miscible liquid-liquid displacement in porous media, International Journal of Fluid Mechanics Research, vol. 26, no. 4, pp. 215-226

Saghir, M.Z., Vaziri, H. and Islam, M.R., (2001) Heat and mass transfer modeling of fractured formations, Journal of Computational Fluid Dynamics, vol. 15, no. 4, pp. 279-292

Sahimi, M., (1994) Applications of percolation theory, Taylor &Francis, London, UK

Sahimi, M., (1995) Flow and transport in porous media and fractured rock, VCH, Weinheim, Germany

Sarma, P., Durlofsky, L.J., Aziz, K. and Chen, W.H., (2006) Efficient real-time reservoir management using adjoint-based optimal control and model updating, Computational Geosciences, vol. 10, pp. 3-36

Sattar, M.A. and Islam, M.R., (1993) Flow instability in a large aspect ratio porous medium with an internal heat source, Chaos, Solitons & Fractals, vol. 3, no. 2, pp. 149-169

Shapiro, R., Zatzman, G.M., Mohiuddin, Y., (in press) Towards understanding the science of disinformation, Journal of Nature Science and Sustainable Technology

Solano, R., (2000) Effect of mixing mechanisms on recovery by enriched-gas injection above the minimum miscible enrichment (MME), Masters thesis, University of Texas at Austin, USA

Stalkup, F.I., (1983) Miscible displacement, Society of Petroleum Engineers Monograph Series, vol. 8, New York, USA, p 75

Standenes, S., (1995) Seismic monitoring – a tool for improved reservoir management, SEISMIC 95, London

Stanley, R.K., (2001) Methods and results of inspecting coiled tubing and line pipe, SPE 68423, SPE/IcoTA Coiled Tubing Roundtable, Houston, TX, March 7-8

Stickey, D.C., (1993) New forces in international energy law: A discussion of political, economic, and environmental forces within the current international energy market, Tulsa Journal of Comparative and International Law, vol. 1, no. 1, p. 95.

Stone, H.L. and Brian, P.L.T., (1964) Numerical solution of convective transport problems, American Institute of Chemical Engineering Journal, vol. 9, pp. 681

Tan, C. T. and Firoozababdi, A., (1995) Theoretical analysis of miscible displacement in fractured porous media by a one-dimensional model: part I – theory, Journal of Canadian Petroleum Technology, vol. 34, no. 2, pp. 17-27

Tan, C. T. and Homsy, G. M., (1986) Stability of miscible displacement in porous media: rectilinear flow, Physics of Fluids, vol. 29, p. 3549-3556

Tan, C. T. and Homsy, G. M., (1988) Simulation of non-linear viscous fingering in miscible displacement, Physics of Fluids, vol. 33, no. 6, pp. 1330-1338

Tchelepi, H. A., Rakotomalala, N., Orr, F. M., Salin D., and Woumeni, R., (1993) Dispersion, permeability heterogeneity, and viscous fingering: acoustic experimental observations and particle tracking simulations, Physics of Fluids A, vol. 5, no. 7, pp. 1558-1574

Terwilliger, P.L., Wilsey, L.E., Hall, H.N., Bridges, P.M. and Morse, R.A., (1951) An experimental and theoretical investigation of gravity drainage performance, Trans. AIME, vol. 192, pp. 285-296

Tidwell, V.C., and Robert, J.G., (1995) Laboratory investigation of matrix imbibition from a flow fracture, Geophysical Research Letters, vol. 22, pp. 1405-1408

Tiscareno-Lechuga, F., (1999) A sufficient condition for multiple solutions in gas membrane separators with perfect mixing, Computers and Chemical Engineering, vol. 23, no. 3, pp. 391-394

Tortike, W.S. and Farouq Ali, S.M., (1987) A framework for multiphase nonisothermal fluid flow in a deforming heavy oil reservoir, SPE 16030, 9th SPE symposium on reservoir simulation, San Antonio, TX, February 1-4

Ucan, S. and Civan, F., (1996) Simultaneous estimation of relative permeability and capillary pressure for non-Darcy flow-steady state, SPE 35271, Mid-Continent Gas Symposium, Amarillo, TX, April 26-30

U.S. Department of Energy, (2002)
Available:
http://www.fe.doe.gov/oil_gas/drilling/laserdrilling.html [October 7, 2002]

Van Everdingen, A.F. and Hurst, W., (1949) The application of the Laplace transformation to flow problems in reservoirs, Transactions AIME, vol. 186, pp. 305-324

Vaziri, H.H., Xiao, Y., Islam, R. and Nouri, A., (2003) Numerical modeling of seepage-induced sand production in oil and gas reservoirs, Journal of Petroleum Science and Engineering, vol. 36, pp. 71-86

Vega, C., Delgardo, M. and Vega, B., (2002) Treatment of waste-water/oil emulsions using microwave radiation, SPE 74167, SPE International Conference on Health, Safety and Environment in Oil and Gas Exploration and Production, Kuala Lumpur, Malaysia, March 20-22

Waggoner, J. R., Castllo, J. L., and Larry, W. L., (1992) Simulation of EOR processes in stochastically general permeable media, SPE 21237, SPE Formation Evaluation, pp. 173-180, June

Wagner, R. E., (1974) Laser drilling mechanics, Journal of Applied Physics, vol. 45, pp. 4631-4637

Wazwaz, A.M., (1999) A reliable modification of Adomian decomposition method, Applied Mathematics and Computation, vol. 102, pp. 77-86

Wazwaz, A.M., (2001) A new algorithm for calculating Adomian polynomials for nonlinear operators, Applied Mathematics and Computation, vol. 111, no. 1, pp. 33–51

Wazwaz, A.M., (2001) Construction of solitary wave solutions and rational solutions for the KdV equation by Adomian decomposition method, Chaos, Solitons and Fractals, vol. 12, no. 12, pp. 2283-2293

Wazwaz, A.M. and El-Sayed, S.M., (2001) A new modification of Adomian decomposition method for linear and nonlinear operators, Applied Mathematics and Computation, vol. 122, no. 3, pp. 393-405

Wit, A., and Homsy, G. M., (1997) Viscous fingering in periodically heterogeneous porous media, II, Numerical simulation, Journal of Chemical Physics, vol. 107, no. 22

Woodrow, C.K. and Drummond, E., (2001) Heat seeking laser sheds light on Tern, SPE 67729, SPE/IADC Drilling Conference, Amsterdam, February 27 – March 1

Yilbas, B. S., (1996) Experimental investigation into CO_2 laser cutting parameters, Journal of Materials Processing Technology, vol. 58, no. 2-3, pp. 323-330

Zaman, M., Agha, K.R. and Islam, M.R., (2006) Laser based detection of paraffin in crude oil samples: Numerical and experimental study, Petroleum Science and Technology, vol. 24, no. 1, pp. 7-22

Zaman, M., Bjorndalen, N. and Islam, M.R., (2004) Detection of precipitation in pipelines, Petroleum Science and Technology, vol. 22, no. 9-10, pp. 1119-1141

Zatzman, G.M., and Islam, M.R., (in press[1]) Natural gas pricing, in Mokhatab, S., Speight, J.G., and Poe, W.A., editors, Handbook of natural gas transmission and processing, Elsevier Inc.

^Zatzman, G.M. and Islam, M.R., (in press[2]) Economics of intangibles: Nova Science Pulisher, NY, USA

^ (in press) in Chapter 5

Zekri, A.Y. and Natuh, A., (1992) Laboratory study of the affects of miscible WAG process on tertiary oil recovery, SPE 24481, Abu Dhabi 5th Petroleum Conference and Exhibition, May 18-20

Zekri, A.Y., Shedid, S.A. and Alkashef, H., (2001) Use of laser technology for the treatment of asphaltene deposition in carbonate formation, SPE 71457, SPE Annual Technical Conference and Exhibition, New Orleans, Louisiana, September 30 – October 3

Zekri, A.Y., Mustafiz, S., Chaalal, O. and Islam, M.R., (2006) The effects of thermal shock on homogenous and fractured carbonate formation, Journal of Petroleum Science and Technology, submitted for publication

Zimmerman, W. B. and Homsy, G. M., (1991) Non-linear viscous fingering in miscible displacement with an-isotropic dispersion, Physics of Fluids A, vol. 3, no. 8, pp. 1859-1872, August

Zimmerman, W. B. and Homsy, G. M., (1992) Three-dimensional viscous fingering: a numerical study, Physics of Fluids A, vol. 4, no. 9, pp. 1901-1914, September

Zubair, S. M and Chaudhry, M. A., (1996) Heat conduction in a semi-infinite solid due to time-dependent laser source, Journal of Heat and Mass Transfer, vol. 39, no. 14, p. 3067-3074